

This dissertation has been
microfilmed exactly as received

69-12,928

BAUERLE, George Louis, 1934-
SURFACE AND CATALYTIC EFFECTS IN HIGH
PRESSURE OXIDATION OF METHANE.

The University of Oklahoma, Ph.D., 1969
Engineering, chemical

University Microfilms, Inc., Ann Arbor, Michigan

THE UNIVERSITY OF OKLAHOMA

GRADUATE COLLEGE

SURFACE AND CATALYTIC EFFECTS IN
HIGH PRESSURE OXIDATION OF METHANE

A DISSERTATION

SUBMITTED TO THE GRADUATE FACULTY

in partial fulfillment of the requirements for the

degree of

DOCTOR OF PHILOSOPHY

BY

GEORGE LOUIS BAUERLE

Norman, Oklahoma

1969

SURFACE AND CATALYTIC EFFECTS IN
HIGH PRESSURE OXIDATION OF METHANE

APPROVED BY

C. M. Sheppard

H. T. Jenkins

K. E. Starling

V. K. Wilson

Darrel H. Harden

DISSERTATION COMMITTEE

ABSTRACT

The influence of surface-to-volume ratio on the ignition delay and product distribution of a reacting fuel-rich mixture of methane and oxygen was investigated. Surface-to-volume ratio was varied from 3.5 to $5.5(10)^5$ cm^2/cm^3 ; pressure was varied from 100 to 750 atm; and temperature was varied from 294 to 363°C in the investigation. Methane-to-oxygen ratio was nominally a value of 10 (molar).

Concentration-temperature-time histories were obtained at various conditions of pressure, temperature, and time. Unlike oxidation at low pressures, in which explosion can occur only at the coincident points of maximum usage of oxygen and maximum in formaldehyde concentration, explosion at high pressures can occur well after the above-mentioned maxima. Thermal acceleration due to exothermic termination reactions is felt to be responsible for the possible interval between maximum depletion rate of oxygen and the thermal maximum.

Over approximately the same range of conditions, ignition delay and product distribution were studied with the oxidation process heterogeneously catalyzed. Catalysts included silica-alumina (natural and synthetic), silica-

magnesia, cobalt molybdate, and nickel oxide. Nickel catalyst initiated the reaction without presence of an induction delay; rapid oxidation to carbon dioxide and water occurred. In general, the other catalysts shortened ignition delay, but an inductive reaction was observed. Product distribution was influenced by catalytic activity, with cobalt molybdate, in particular, appearing to enhance aldehyde production.

A brief feasibility study was made of the photocatalytic ignition of the 10/1 methane-oxygen mixture using formaldehyde, acetone, and acetaldehyde as initiators. A mercury-quartz radiation source was used. Pressure was varied from 119 to 340 atm and the temperature range was 23 to 273°C. In general, methane oxidation did not occur, and oxygen was used only in formation of products of the initiator. Methane formation was, in fact, indicated with acetaldehyde initiation.

ACKNOWLEDGMENTS

The author expresses his sincere appreciation to his advisory committee, Dr. C. M. Sliepcevich, Dr. H. T. Hashemi, Dr. K. E. Starling, Dr. C. P. Colver, and Dr. D. G. Harden, for their interest, direction, and assistance during this graduate program.

A special vote of thanks is due to Dr. J. L. Lott, who provided countless beneficial suggestions during the course of this work and who undertook the unenviable task of advisement in assembling the manuscript of this dissertation.

Mr. J. Bryan and Mr. B. Farid assisted in the analytical and operational work throughout the experimental program; their efforts are gratefully acknowledged.

The efforts of Mrs. Joyce Meyer and Mr. T. Booker, who handled the graphical work, and Mrs. Ruth Kempton and Miss Connie Ellender, who typed the manuscript, are appreciated.

The author expresses a great measure of appreciation to North American Rockwell Corporation for the educational opportunity they provided, for allowing an extended leave of absence, and for the financial assistance they gave. In particular, the author thanks Mr. F. G. Rizzardi, the North

American Rockwell Fellowship Administrator for his interest,
confidence, and assistance during these three years.

George Louis Bauerle

TABLE OF CONTENTS

	Page
LIST OF TABLES	ix
LIST OF ILLUSTRATIONS	xi
Chapter	
I. INTRODUCTION	1
II. THEORETICAL CONSIDERATIONS	4
General Aspects	
Free Radicals and Chain Reactions	
Review of General Mechanism of	
Hydrocarbon Oxidation	
Ignition Delay and Induction Time	
Activation Energy of the Oxidation	
Reaction	
The Effect of Surfaces and Catalysts	
Photocatalytic Oxidation of Methane	
III. REVIEW OF WORK IN OXIDATION OF METHANE	52
The Homogeneous Reaction	
Activation Energy of the Oxidation	
Reaction	
The Effect of Surfaces and Catalysts	
IV. EXPERIMENTAL EQUIPMENT	103
Feed Section	
Compression Section	
Reactor	
Product Collection System	
Photocatalytic Equipment Modification	
High Pressure Test Cell	

TABLE OF CONTENTS (Cont'd)

Chapter	Page
V. EXPERIMENTAL PROCEDURE.	125
Feed Stock Formulation	
Intermediate Compression	
Reactor Operation	
Photochemical Reaction Studies	
VI. ANALYTICAL EQUIPMENT AND PROCEDURE.	131
Chromatographic Equipment Used	
Analytical Procedure	
Chemicals Used	
VII. RESULTS AND DISCUSSION.	143
VIII. CONCLUSIONS	254
NOMENCLATURE.	258
LITERATURE.	261
APPENDICES	
A. Experimental Results.	267
B. Rates of Chain Reactions and Energy Considerations	280
C. Determination of Factors for the Benedict-Webb-Rubin Equation of State	290
D. Method of Reference Curves for Order Determination	293
E. Chromatographic Calibration Curves. .	295

LIST OF TABLES

Table	Page
1. The Variation of the Maximum Rate of Hydrocarbon Oxidation with Concentration of Hydrocarbon and Oxygen at Different Temperatures	59
2. The Variation of the Maximum Rate of Methane Oxidation with Concentrations of Methane and Oxygen at Different Temperatures	60
3. Values of E of the Oxidation Reaction of Methane	85
4. The Reaction Orders at 500°C and Activation Energies on the Range 462.5-525°C.	91
5. Reaction Orders at 650°C and Activation Energies on the Range 575-675°C.	92
6. The Variation of W_{max} and $[HCHO]_{max}$ with Treatment of the Reaction Vessel	98
7. The Composition of Products at the End of the Oxidation Reaction of Butane-No Catalyst.	100
8. Liquid Phase Oxidation of Butane in a Solvent.	101
9. Test Conditions.. . . .	145
10. Feed-Stock Compositions.	145
11. Properties of Alumina Additives.	155
12. Surface/Volume Ratio of Various Reactor Systems.	155

Table	Page
13. Apparent Order of Non-Explosive Tests During Period of Rapid Usage of Oxygen.	209
14. Results of Nickel-Catalyzed Reactions.	241
15. Operating Voltage of Hg Lamp as Function of Temperature	247
16. Photoinitiation Feasibility Tests.	248
17. Photochemical Test Reactants and Products	249
A-1. Experimental Test Parameters and Outlet Product Compositions	268
A-2. Yield of Products as Percentages of Reacted Methane and Oxygen	274
C-1. BWR Constants for Methane and Oxygen for Use at Elevated Pressures.	292

LIST OF ILLUSTRATIONS

Figure	Page
1. Time-Temperature-Concentration History of Oxidation at 150 atm	25
2. Reaction Rate as Function of Time and Pressure	28
3. Variation of Rate with Reactant Depletion	28
4. Reaction Rate as Function of Time for Normally-Branched and Degenerately- Branched Reactions	34
5. Kinetics of Methane Oxidation and Accumulation of Reaction Products for the Mixture $\text{CH}_4 + 2\text{O}_2$ at 472°C and 235 mm Hg Pressure in an HF -Treated Vessel . . .	62
6. Effect of Temperature on Ignition Delay	69
7. Effect of Residence Time on Methanol Yield at Various Pressures	71
8. Effect of Residence Time on Total Oxygenated Liquid Product Yield at Various Pressures . .	72
9. Trend in Methane Conversion with Increasing Pressure	73
10. A Comparison of the Reaction Rates of Methane Oxidation in Vessels with Differently Treated Surfaces	89
11. Process Flow Diagram of Feed and Compression Sections	104
12. Process Flow Diagram of Reaction and Product Collection Systems	105

Figure	Page
13. Thermowell and Head Closure Assembly	112
14. Plug-end Closure.	113
15. Reactor Heater Schematic	115
16. Pressure Measurement Circuit	119
17. Mercury-Quartz Lamp Design	122
18. High-Voltage Lead-Through Assembly	123
19. Chromatographic Equipment Used for Analyses	132
20. Ignition Delay as Function of Temperature at Various Pressures	148
21. Pressure Correction Factor for Ignition Delay. .	150
22. Pressure-Corrected Ignition Delay as Function of Temperature.	153
23. Graphical Determination of Surface Factor. . . .	157
24. Surface Factor for Correction of Ignition Delays.	158
25. Ignition Delay Corrected for Pressure and Surface Effects as Function of Temperature . .	160
26. Ignition Delay as Function of Maximum Temperature for Non-Explosive Tests.	164
27. Ignition Delay as Function of Maximum Temperature for Explosive Tests.	166
28. Ignition Delay Using Kao-Spheres Catalyst. . . .	168
29. Ignition Delay Using Cobalt Molybdate Catalyst .	169
30. Ignition Delay Using Silica-Alumina Catalyst . .	170
31. Ignition Delay Using Silica-Magnesia Catalyst. .	171
32. Reaction History at 367 atm, 306.5°C, and S/V of 3.5 cm ⁻¹	177

Figure	Page
33. Reaction History ₁ at 367 atm, 312.3°C, and S/V of 3.5 cm ⁻¹	178
34. Reaction History at 470 atm, 303.5°C, and S/V of 3.5 cm ⁻¹	179
35. Reaction History at 490 atm, 304.6°C, and S/V of 3.5 cm ⁻¹	180
36. Reaction History at 381 atm, 316°C, and S/V of 3.5 cm ⁻¹	181
37. Reaction History at 475 atm, 307.9°C, and S/V of 3.5 cm ⁻¹	182
38. Reaction History at 367 atm, 312.6°C, and S/V of 7.3 cm ⁻¹	183
39. Reaction History at 380 atm, 317.2°C, and S/V of 7.3 cm ⁻¹	184
40. Reaction History ₁ at 433 atm, 312.6°C, and S/V of 7.3 cm ⁻¹	185
41. Reaction History ₁ at 680 atm, 308.8°C, and S/V of 7.3 cm ⁻¹	186
42. Reaction History at 483 atm, 315°C, and S/V of 13.4 cm ⁻¹	187
43. Reaction History at 374 atm, 314.7°C, and S/V of 13.4 cm ⁻¹	188
44. Reaction History ₁ at 368 atm, 318.2°C, and S/V of 545 cm ⁻¹	189
45. Reaction History ₅ at 368 atm, 324.6°C, and S/V of 5.5(10) ⁵ cm ⁻¹	190
46. Reaction History at 374 atm, 331°C, and S/V of 5.5(10) ⁵ cm ⁻¹	191
47. Determination of Order by Method of Reference Curves	208
48. Influence of Residence Time on Ratio: (CO + CO ₂ + HCHO)/CH ₃ OH.	213

Figure	Page
49. Actual and Calculated Values of Maximum Formaldehyde Mole Fraction at Non-Explosive Conditions.	219
50. Carbon Monoxide/Carbon Dioxide Ratio as Function of Residence Time.	222
51. Reaction History at 375 atm, 327°C, and S/V in Excess of $5(10)^5 \text{ cm}^{-1}$ with Kao-Spheres Catalyst	227
52. Reaction History at 150 atm, 337°C, and S/V in Excess of $5(10)^5 \text{ cm}^{-1}$ with Kao-Spheres Catalyst	228
53. Reaction History at 476 atm, 314.5°C, and S/V in Excess of $5(10)^5 \text{ cm}^{-1}$ with Kao-Spheres Catalyst	229
54. Reaction History at 680 atm, 303.1°C, and S/V in Excess of $5(10)^5 \text{ cm}^{-1}$ with Silica- Alumina Catalyst	232
55. Reaction History at 367 atm, 320.3°C, and S/V in Excess of $5(10)^5 \text{ cm}^{-1}$ with Silica- Magnesia Catalyst.	233
56. Reaction History at 680 atm, 308.6°C, and S/V in Excess of $5(10)^5$ with Cobalt Molybdate Catalyst	234
57. Reaction History at 476 atm, 309.2°C, and S/V in Excess of $5(10)^5 \text{ cm}^{-1}$ with Cobalt Molybdate Catalyst	235
58. Reaction History at 367 atm, 318.4°C, and S/V in Excess of $5(10)^5 \text{ cm}^{-1}$ with Cobalt Molybdate Catalyst	236
59. Oxygen Concentration as a Function of Time with Nickel Catalyst.	243
60. Initial Rate of Oxygen Depletion as a Function of Temperature for Nickel- Catalyzed Oxidation.	245
61. Initial Rate of Oxygen Depletion as a Function of Reciprocal Temperature for Nickel-Catalyzed Oxidation	246

Figure	Page
B-1 Activation Energy and Heat of Reaction	286
E-1 Chromatographic Calibration Curve for Oxygen and Nitrogen.	296
E-2 Chromatographic Calibration Curve for Carbon Monoxide.	297
E-3 Chromatographic Calibration Curve for Carbon Dioxide	298
E-4 Chromatographic Calibration Curve for Formaldehyde	299
E-5 Chromatographic Calibration Curve for Methanol	300
E-6 Chromatographic Calibration Curve for Methyl Formate	301
E-7 Chromatographic Calibration Curve for Ethanol.	302
E-8 Chromatographic Calibration Curve for Formic Acid.	303
E-9 Chromatographic Calibration Curve for Acetic Acid.	304

CHAPTER I

INTRODUCTION

During the last half century or more, extensive investigation into the characteristics of combustion of methane has been made. The great interest in this reaction has been due, from an academic standpoint, to the existence of methane as the simplest organic fuel and, from a practical standpoint, to the preponderance of methane in natural gas.

Little success was obtained in early studies in formulating a mechanism of combustion which adequately described the oxidation over even small ranges of conditions until the introduction of chain theories. Early chain mechanisms involved stable molecules, but the likelihood of consecutive and concurrent reactions was established. The introduction of the concept of free radicals greatly accelerated research effort in combustion processes. However, even radical chain mechanisms did not describe adequately the experimental results until the discovery was made that several types of ignition and combustion exist with many hydrocarbons.

A single mechanism for combustion of methane had not existed up to 1965, as shown by recent high-pressure

studies conducted at the University of Oklahoma. Prior to that time, it was generally felt that methane undergoes only one mode of oxidation; with higher hydrocarbons, at least three modes exist, generally separated into temperature ranges. It now appears certain that methane also exhibits mechanistic changes in oxidation in view of recent high pressure work. Initial investigations at elevated pressures have been divided into two main categories: (1) product distribution analyses in non-isothermal oxidation leading to explosion, and (2) isothermal batch reaction in the slow induction mode of oxidation. Complete histories of the decay of reactants, build-up of products and increase of temperature with time had not been made at pressures exceeding 150 atm.

Practically no investigations of the effect of surfaces and heterogeneous catalysts have been made at elevated pressure. Further, photo-initiation techniques have been reserved to subatmospheric pressures or, at the most, to total pressures not far above atmospheric.

The objectives of this study were: (1) to investigate the effect of surface-to-volume ratio on the rate of oxidation and product distribution, (2) to determine if the product distribution could be altered by introduction of heterogeneous catalysts. (3) to provide time-temperature-species histories for non-isothermal oxidation at elevated

pressures and (4) to investigate the feasibility of photo-initiation at elevated pressures.

Experiments were conducted over the pressure range 100 to 750 atm, with a variation in temperature of 280° to 375°C. A nominal methane-oxygen volumetric mixture ratio of 10 was used in all tests. Surface-to-volume ratio was varied from 3.5 to 13.4 cm⁻¹ by addition of steel packing and up to 550,000 cm⁻¹ by addition of various grades of alumina pellets. The effect of catalytic surfaces was investigated by addition of the following heterogeneous materials: (1) silica-alumina, (2) silica-magnesia, (3) Kaolin, (4) cobalt molybdate, and (5) nickel oxide. A brief investigation of photo-initiation was conducted at pressures from 100 to 340 atm using acetaldehyde, acetone, and formaldehyde as initiators. Temperature in this latter phase of study was varied from 23° to 273°C.

CHAPTER II

THEORETICAL CONSIDERATIONS

General Aspects

It has been well established that hydrocarbon oxidation in the vapor phase takes place by a chain mechanism involving free radicals. In general, oxidation of all hydrocarbons shows features which can be explained only by chain mechanisms.

Exact descriptions of the chemical reactions taking place in oxidation of even the simplest organic fuel, methane, have not been possible due to the large number of consecutive and concurrent reactions taking place. The theoretician, in general, usually lists all the possible reactions and then must establish the likelihood of one over the other. Without quantitative information describing the chronology of product formation and reactant depletion, this selection of alternative steps cannot be made and a complete understanding of hydrocarbon oxidation is impossible.

As a rule, hydrocarbons are felt to exhibit three modes of oxidation. Up to about 325°C most hydrocarbons will oxidize at a rate which increases with temperature. Somewhere

between 350° and 400°C a phenomenon, first observed by Pease (54), occurs; over a short temperature interval, the rate actually decreases with temperature (i.e., a negative temperature coefficient is observed). Finally, at all temperatures above a certain point, the rate of reaction again increases with temperature. It has been established that the negative temperature coefficient occurs to some degree with all hydrocarbons which exhibit the low temperature mode of oxidation, but the low pressure results of oxidation of methane, benzene, and ethylene indicate that they oxidize only by a single mechanism. However, recent experimental work by Lott (35) and Hardwicke (26) show that methane can indeed exhibit two regimes of oxidation.

The low temperature regime is usually characterized by the formation of aldehydes, ketones, and alcohols, in addition to the gaseous carbon oxides and water. In the high temperature regime, products corresponding to cracking and dehydrogenation reactions occur. The zone in which negative dependence of rate on temperature is observed represents, as far as products are concerned, a transition between the low and high temperature regimes. Because no olefinic structure corresponding to the methane skeleton is possible, it would seem intuitive that methane should oxidize only by a low temperature mechanism. Methane, however, has been thought to oxidize by a high temperature mechanism only because of the temperature range necessary to effect its oxidation (40).

Lott (35) observed, in his study of product distribution in the batch oxidation of methane under fuel-rich conditions, what appeared to be a change in mechanism at about 476 atm. He also observed the cool flame phenomenon at 3200 atm and 262°C. Vanpee (71) also reported cool flames in oxidation of methane at 800 mm Hg pressure and 500°C. Some investigators attributed cool flame production to a transition between low and high temperature mechanisms. It may well be that the mechanistic change at 476 atm. and the cool flame production were indications of a transition between modes of oxidation.

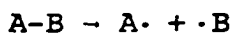
It will be shown later that almost all previous work in the field of hydrocarbon oxidation has been limited to moderate pressures, and the great bulk of that work limited to atmospheric and subatmospheric experimentation. Because of the elevated temperatures necessary to oxidize methane at near-atmospheric pressures, it is not surprising that methane was thought to undergo only one mode of oxidation.

The discussion which follows will present a review of chain theory, as applicable to the present study, an outline of the aspects of the various modes of oxidation of hydrocarbons, and finally, the applicability of the general theories to methane oxidation.

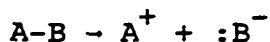
Free Radicals and Chain Reactions

A free radical is defined as an atom or group of atoms with an unpaired electron (56). Typical examples of

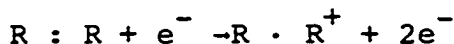
free radicals are the chlorine atom ($:\ddot{\text{Cl}}\cdot$, or, simply, $\text{Cl}\cdot$) or a group of atoms such as the methyl radical ($\text{H}:\overset{\text{H}}{\underset{\text{H}}{\text{C}}}\cdot$ or $\text{CH}_3\cdot$). This latter entity is one of the radicals taking part in methane oxidation. The free, unpaired electron is shown as a dot. The radicals depicted above are in a neutral state since they have lost none of the valence electrons. A chemical compound, AB, can cleave in two ways:



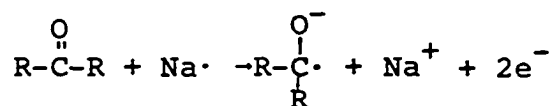
or



The first case shows the symmetrical rupture of a bond, producing radicals; in the second case, one group asymmetrically kept both bond electrons resulting in formation of ions. A third case, a combination of both examples above, can arise when a stable compound is depleted one or more electrons.



or



In these examples, radical ions are formed, showing that radicals need not in all cases be neutral.

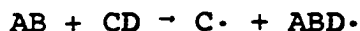
The convention followed here will be to show radicals in the form, $\text{R}\cdot$, and ions as R^+ or R^- . It is also understood that symmetrical cleavage refers to the acceptance by each

molecular portion of one of the previously shared electrons and not necessarily to the size or identity of the molecular "halves."

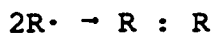
Radicals enter into three types of reactions: formation of radicals, transference of identity, and destruction of radicals. The formation and destruction of radicals are basically opposite processes in concept. Generally, radicals are formed in pairs:



or



and destroyed in pairs:



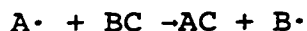
or



The transference reactions are the steps, arising in all overall reactions involving radicals, that give the process a chain nature. That is, the number of radicals does not normally change (a special case called chain branching will be discussed later), but the identity of the radical or the active site is changed. Four types of transfer or propagation reactions occur: (1) atom transfer, (2) addition reaction, (3) fragmentation and (4) rearrangement.

Examples of the various propagation steps are given below and the nature of the mechanisms are self-evident.

1. Atom transfer



Examples in practice are hydrogen or halogen abstractions.

2. Addition

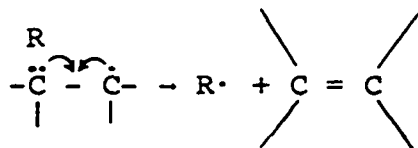


In general, $AB\cdot$ is more stable than $A\cdot$.

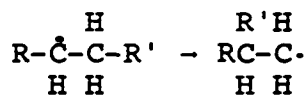
3. Fragmentation



An example of this process is β -scission of a hydrocarbon chain molecule, in which a pair of electrons is in a β position with respect to a radical electron, and the radical splits to give an olefin and another radical, e.g.:

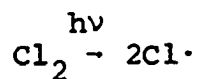
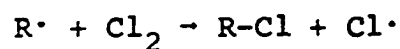
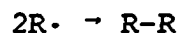
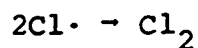


4. Rearrangement



In this case, the chain center (radical) is maintained, but the exact form is altered.

The overall mechanism in a chain process always includes the steps of initiation, propagation, and termination. These steps can be shown, for example, in the photo-initiated chlorination of a hydrocarbon, R-H.

InitiationPropagationTermination

In general, a cross termination reaction, which in the above example leads to formation of R-Cl, is always favored over homogeneous termination if alternative steps are energetically similar.

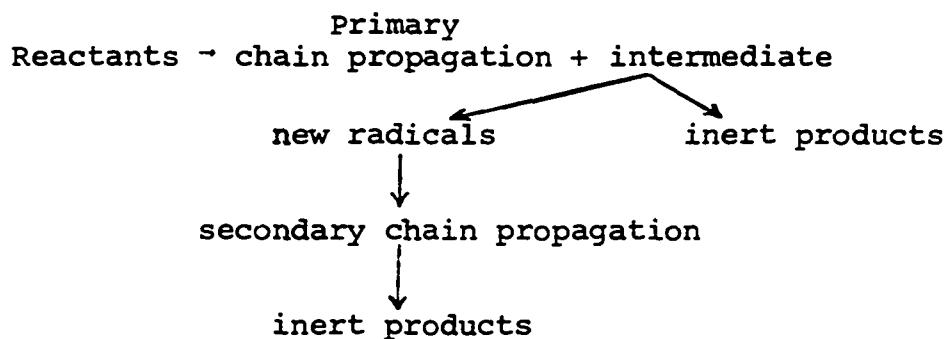
Another important process connected with chain propagation is the phenomenon of chain branching. This type of reaction is associated with flames and explosions. The number of free radicals is actually increased in at least one of the propagation steps. An example of a branching reaction is:



If the rate of branching is greater than the rate of termination of the chain, it can be shown that the concentration

of active centers (radicals) and the rate of reaction increase as the reaction proceeds. Complete termination is not possible until depletion of the reactants has occurred or equilibrium has been reached. In some cases, the build-up in rate is auto-accelerating, leading to explosion.

In 1933, Semenov (64) extended the concept of chain branching. It was observed that a series of homogeneous reactions proceeded in the same manner as auto-accelerating branched-chain reactions but at a very slow rate. He did not accept the theory that the usual branching reactions occur at this very slow rate in view of the high activity and short lifetimes of radicals. Instead, he proposed that a moderately stable, intermediate molecular product builds up through action of the primary chain and disappears by the simultaneous processes of creation of new chain centers and formation of inert products. The overall scheme can be shown as:



The theory of degenerate branching, as the Semenov concept is named, explains the existence of induction periods and subsequent auto-catalytic reactions commonly observed in

hydrocarbon oxidation. Although the concept is well accepted today, the identity of the intermediate responsible for chain branching in the low temperature oxidation regime of hydrocarbons is in dispute. In the high temperature regime, formaldehyde is generally accepted as the intermediate (32,49,71,77).

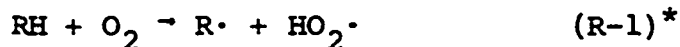
Review of General Mechanism of Hydrocarbon Oxidation

In this section, the mechanism of hydrocarbon oxidation will be reviewed. In particular, the individual steps of initiation, propagation, branching, and termination will be outlined.

As temperature is increased, some mechanistic changes in the oxidation occur. These changes are discussed in the sub-sections describing the occurrence of cool flames and the region of negative temperature dependence on the rate of oxidation.

Initiation Reaction

Because thermal dissociation of a hydrocarbon is not appreciable at low temperatures, the initiation step in hydrocarbon oxidation is generally accepted to be a radical-producing reaction between the hydrocarbon and oxygen:



*In this text, reactions will be numbered R-X, while mathematical equations will be arranged numerically in sequence.

Because of the relatively high endothermic heat of reaction involved (ca. 55 kcal/mole), this step is necessarily slow. Most authors assume, as a next step, that oxygen reacts readily with alkyl radicals with a very low activation energy to form an alkyperoxy radical



Small and Ubbelohde (68) estimated reaction R-2 to be exothermic by about 46 kcal/mole. It is thought that $RO_2\cdot$ is formed in a highly excited state, momentarily possessing the exothermic energy (40).

The radicals formed from the fuel molecule can decompose, add to oxygen, or isomerize. For alkyl molecules, the course depicted by reactions R-1 and R-2 are generally assumed. At low temperatures reaction R-2 in which $R\cdot$ refers to alkyl radicals, appears to be of the third order and more exactly should be written:

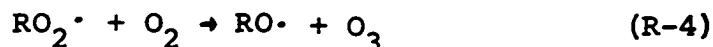


Propagation Steps

The chain is continued in a series of propagation reactions of the form



One propagation reaction suggested for hydrocarbon oxidation is

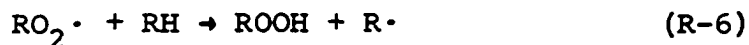


Ozone is extremely reactive with hydrocarbons:

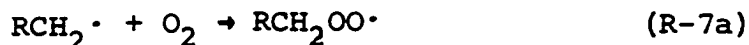


Reactions R-4 and R-5 would present rapid branching at high temperatures. Minkoff and Tipper (43) discounted the likelihood of occurrence of reactions R-4 and R-5 in view of the results of Sleppy and Calvert (67), who detected no traces of ozone in the flash photolysis of azomethane.

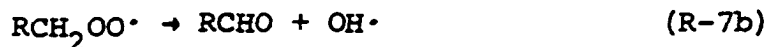
The $\text{RO}_2\cdot$ radicals can react with additional hydrocarbon to form a peroxide and an alkyl radical:



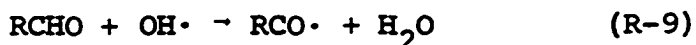
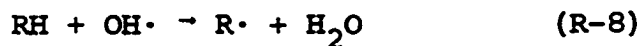
The alkyl radical can react with oxygen, as shown in reaction R-2, giving a peroxy radical



which can subsequently dissociate to form an aldehyde and a new radical.

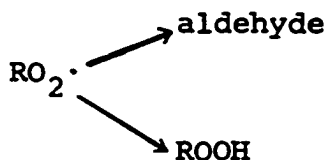


The hydroxyl radical ($\text{OH}\cdot$) can also enter into a series of non-branching reactions such as:



Branching Reactions

The reactions of $\text{RO}_2\cdot$ radicals give rise to two alternative branching schemes, involving aldehydes and peroxides.



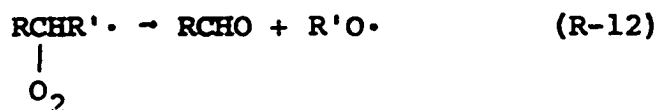
There has been considerable controversy concerning which of these intermediates is responsible for degenerate branching. Fission of the peroxygen bond gives rise to two radicals; the alkoxy radical ($\text{RO}\cdot$) and the hydroxy radical ($\text{OH}\cdot$):



The action of $\text{OH}\cdot$ has been shown in combination with RH . The $\text{RO}\cdot$ radical can also react with the hydrocarbon giving an alcohol and an alkyl radical:

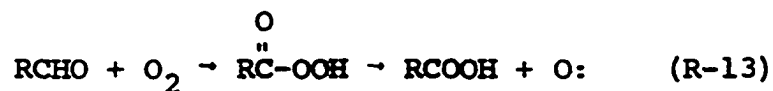


Medley and Cooley (40) presented an objection to the formation of hydroperoxides occurring in every case of initial attack on the hydrocarbon on the grounds that branching would be too intense and induction periods not observable. Lewis and von Elbe (34) suggested only minimal formation of hydroperoxide and simultaneous formation of a carbonyl compound and an alkoxy radical, e.g.:



Reaction R-7b is a special case of reaction R-12.

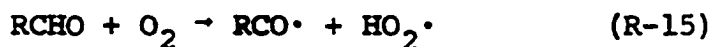
Although there is no evidence that oxygen atoms are formed, Norrish (32,49) suggested that the branching sequence involves the formation of an oxygen atom through a peracid:



with the oxygen atom reacting with hydrocarbon:



A similar sequence could be the direct oxidation of the aldehyde by molecular oxygen



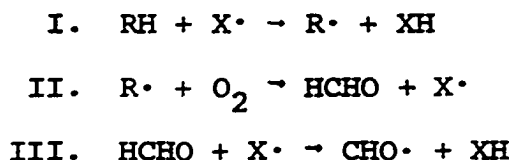
Activation energies of about 23 kcal/mole have been estimated for reaction R-15; its competitor, reaction R-1, is

endothermic in the order of 50 kcal/mole. Since the reverse to reaction R-15 involves only radicals, the activation energy is very close to the heat of reaction and reaction R-15 should predominate. On this basis, aldehydes are considered to be the more plausible branching agent in the oxidation of hydrocarbons. Ridge (57) concluded that all data favor the role of formaldehyde as the major contributor to degenerate branching in both the low and high temperature regimes. It has been observed that a branching reaction can still be made to occur at conditions not favoring the existence of peroxides (43).

The induction period observed in the slow oxidation of hydrocarbons can be explained on the basis of the branching agents. Only small portions of the hydrocarbon react with oxygen during the induction period; the major portion is consumed in the propagation steps which lead to formation of the branching agent and, possibly, oxides of carbon. The concentration of both the aldehydes and the hydroperoxides closely parallels the rate of reaction. At some relatively high concentration of the branching agent, a rapid propagation reaction occurs to form oxygenated products.

It has been observed that the maximum formaldehyde concentration formed in the oxidation of several fuels is proportional to fuel concentration and not to oxygen concentration (79,25,39,7). This result indicates that the radicals

present attack either the fuel, leading toward production of formaldehyde, or the formaldehyde itself, oxidizing it in a non-branching manner. As an example, one can consider the scheme:



where $\text{X}\cdot$ denotes a chain carrying radical such as $\text{OH}\cdot$ or $\text{HO}_2\cdot$ (hydroperoxy radical).

The predominant radical which most often takes the role of $\text{X}\cdot$ in the oxidation of methane has been concluded to be $\text{OH}\cdot$ by McConkey and Wilkinson (38). They also reviewed the energetics of the steps I, II, III. A discussion follows in the next chapter, dealing with methane in particular, in which the logic of McConkey and Wilkinson will be shown. The prediction that radicals oxidize formaldehyde in a non-branching manner suggests that molecular oxygen must be involved in the branching step (reaction R-15).

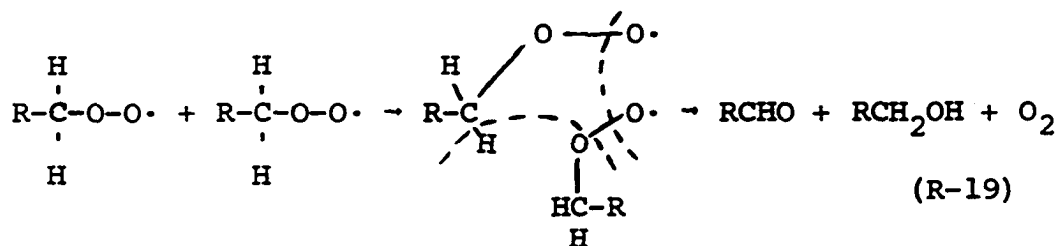
Termination Reaction

Termination reactions have already been shown schematically as the literal opposite of initiation steps. In general, the termination steps for hydrocarbon oxidation are accepted to be:



In oxygen-rich systems, reactions of $R\cdot$ and $RO_2\cdot$ radicals with oxygen should predominate over reactions R-16 and R-17 with almost all termination due to reaction R-18. In fuel-rich situations, all three alternatives are likely.

Russell (59) suggested an interesting possibility involving the formation of a six-membered ring which subsequently splits to give an alcohol, oxygen, and a carbonyl compound (aldehyde or ketone). The scheme, a form of reaction R-18, is:



Because production of products from two $RO_2\cdot$ radicals involves activation energies of 2 kcal/mole or less (75), while the usual hydrogen-abstraction route for $RO_2\cdot$ radicals involves higher energies, reaction R-19 is considered to be possible at high concentrations of $RO_2\cdot$ radicals.

High Temperature Mechanism

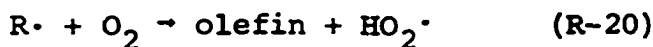
Methane has been frequently referred to as a hydrocarbon which is oxidized only in a high-temperature mechanism.

The reason is apparently based on the fact that, until recently, methane could not be caused to oxidize below about 400°C.

Not all of the characteristics of the high temperature region will be pertinent to methane oxidation. The region is generally characterized by products formed through oxygen-sensitized cracking and dehydrogenation reactions. This group must, in the case of methane, lead to formation of hydrogen. Few investigators have reported production of hydrogen in slow oxidation; their works will be reviewed in the next chapter. In the high temperature region, higher hydrocarbons decompose to olefins and lower hydrocarbons with the oxygenated liquid products being made in decreasing amounts.

Region of Negative Temperature Coefficient

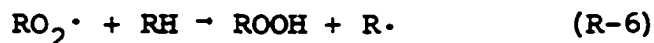
Oxidation of most hydrocarbons is characterized by a region, usually between 325° to 450°C, in which a slight increase in temperature corresponds to a decrease in overall reaction rate. It has been suggested that the region is only one of transition between the low and high temperature regions and that competition between cracking and chain branching occurs:



Satterfield and Reid (62) showed that the difference in the activation energies of reaction R-20 and R-2 ($E_{20} - E_2$) is about 19 kcal/mole and that the steric factor ratio (P_{20}/P_2) is about 4,000,000. This ratio shows that the probability of association via reaction R-2 is very small; at the same time, the higher activation energy for reaction R-20 causes this reaction to predominate as temperature increases. Thus, branching via hydroperoxides and aldehydes is suppressed at some temperature level.

Robertson (58) showed that olefin formation is suppressed at higher pressures, indicating that reaction R-2 is of higher order than reaction R-20. Third body effects have already been shown to be adequate explanations for some pressure effects (see reaction R-2a).

Medley and Cooley (40) showed that the general consensus of most writers is that alkyl radicals larger than methyl do not need a third body for association with oxygen because the liberated energy of association can be distributed among many modes of vibration. They suggested that the pressure suppression of olefin formation can be explained if it is assumed that reactions leading to an oxygenated product involve the formation of an intermediate hydroperoxide molecule. Competition is then between reactions R-21 and R-6:



This set then gives the necessary lower order for olefin formation.

Cool Flames and Periodicity

The appearance of cool flames in the oxidation of hydrocarbons, in which a pale blue luminescence of periodic nature is observed, can be explained by a chain mechanism. This phenomenon has been observed for almost all hydrocarbons larger than methane with regularity. Vanpee (71) was the first to observe the cool flame phenomenon in methane oxidation although a pre-ignition glow had been observed by others (22). Only Lott (35) has observed the effect with methane at high pressures. Excited formaldehyde molecules have been widely accepted as the cause of cool flames, the formation of which must come from purely radical reactions since a high energy of excitation is required. As many as five cool flames have been observed before the depletion of reactants (32).

Norrish (32,49) explained the periodic nature by supposing that self-heating drives the reaction into the negative temperature region where the branching reactions are quenched. It is possible that the explanation of Norrish may be too broad in that periodicity can also be explained by merely considering a multi-step process in the formation and depletion of the excited formaldehyde molecules. If, as has been observed, formaldehyde is formed with only a

slight increase in temperature and if the secondary reactions are also exothermic and have an activation energy larger than the formation step, depletion of the intermediate will occur with energy release and subsequent periodicity (61).

Other writers consider organic peroxides as the intermediate responsible for cool flames. Bardwell and Hinshelwood (5) reported a sharp depletion of peroxides immediately behind the flame front and the complete absence of the phenomenon under conditions not conducive to peroxide formation.

Newitt and Thornes (48) observed that cool flames always originate in the center of a vessel, implying that production of cool flames must involve a balance between heat production and ability of the vessel to dissipate the energy. A decrease in vessel diameter or packing the vessel suppressed cool flame production (32); these latter observations can also be easily explained by the above implication of Newitt's observation.

Frank-Kamenetskii (17) proposed two mechanisms explaining periodic processes in combustion. One was derived strictly from kinetic considerations and the second involved both kinetic and thermal considerations. Frank-Kamenetskii admitted that his two-intermediate product theory, although agreeing closely with some observations including the variation in frequency of periodicity with initial reactant concentration, did not

fully explain the vessel diameter effect or the fact that pulsation frequency was independent of total pressure. He concluded that thermal effects must also be introduced in his scheme. He and Salnikov (18) proposed a two-step process involving an intermediate product, which considered the thermokinetic effect and ably explained both oscillatory and stable periodic oxidation processes.

Ignition Delay and Induction Time

The fuel-rich methane-oxygen reaction under non-isothermal batch conditions is characterized by the existence of several periods during which the overall reaction experiences mechanistic changes. The terms induction period, ignition delay, reaction time and residence time, having been used interchangeably by several authors, must be defined.

As an illustration, the appearance of a typical reaction temperature history of Newitt and Haffner (46) is shown in Figure 1. Species concentrations are also shown in the figure. Admission of reactants to a reactor, unless performed extremely slowly, causes some temperature rise due to adiabatic compression.

At some point, because the driving force for gas flow decreases as filling progresses, the rate of the heating due to compression becomes less than the rate of heat dissipation to the walls and temperature passes through a maximum. If filling continues for a substantial time after the maximum has been passed, and if inlet gas

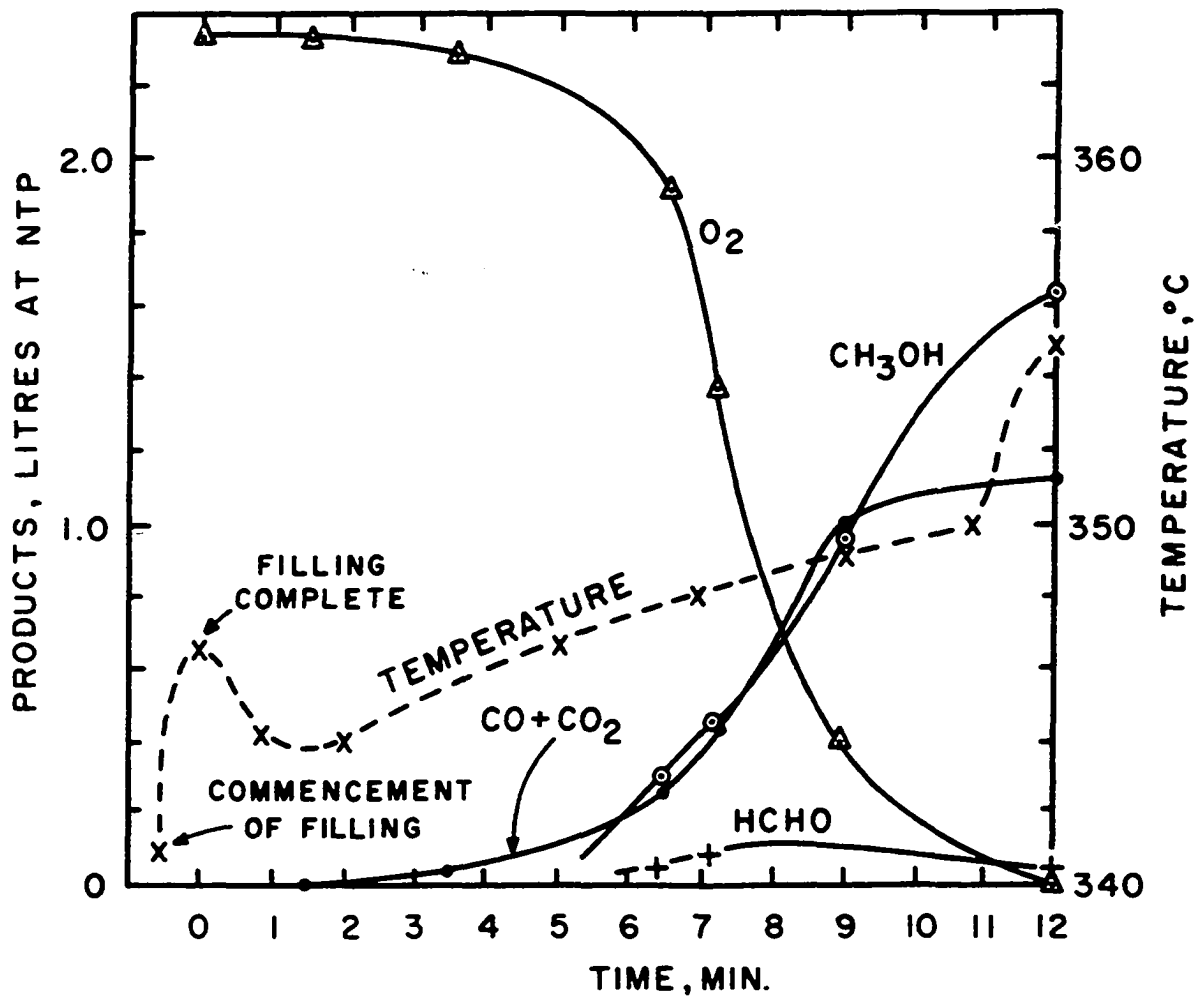


Figure 1. Time-Temperature-Concentration History of Oxidation at 150 ATM (From Ref. 46).

is at a significantly lower temperature than the gas already in the reactor, temperature in the reactor may, in fact, fall below the set-point temperature. In Newitt and Haffner's work, temperature fell to about the initial point after passing through a maximum.

Induction time has been variously defined as the time from start of fill to the instant of: (1) temperature rise from the minimum, (2) start of auto-acceleration or rapid change in slope of the temperature-time (or pressure-time) curve, (3) maximum rate of temperature (or pressure) change, or (4) peak of the temperature (or pressure) curve. Other authors have defined induction times to begin at the point filling is completed and to end at any of the above points. Still others considered the shape of the reactant concentration curves in their definition. Semenov (63) considered induction time to be the period during which concentration change cannot be detected. This definition must vary with each individual analytical method. Conceivably, if an extremely sensitive analytical technique could be developed, Semenov's induction times would be non-existent. Some authors considered induction period as time to the point that the reactants experience maximum rate of reaction. The definition of Semenov for induction time will be used here.

Ignition delay, although called induction time by some, has been more uniform in definition than induction time. The conventions have been limited to three cases:

(1) time to start of auto-acceleration, (2) time to maximum rate of temperature rise, and (3) time to maximum temperature. Because the time at maximum rate of temperature rise coincides very closely with time to maximum temperature when true ignition or explosion occurs, little error is introduced by defining ignition time as being from end of fill to maximum temperature. In cases in which explosion does not occur (due to depletion of oxygen), the time period to maximum temperature is perhaps best called merely a residence time. However, because residence time, by convention, also applies to total length of time a given reactant is allowed to remain in a reactor, the term ignition delay in the remainder of this discussion will refer to the time from end of fill to the temperature maximum.

The problem of whether or not a reaction mixture undergoing moderate self-heating or auto-acceleration will proceed from mere temperature increase to explosion has been considered by Semenov (63), Shtern (66) and Frank-Kamanetskii (17).

Qualitatively, if it is assumed that at some critical reaction rate, w_{cr} , explosion always occurs, rate-time curves for several reactions proceeding at various pressures might be shown as in Figure 2. Explosion is seen to occur in reactions 1 and 2 with delays t_1 and t_2 , respectively. Delay t_3 is the longest possible delay during which explosion can occur. However, the reaction rate itself

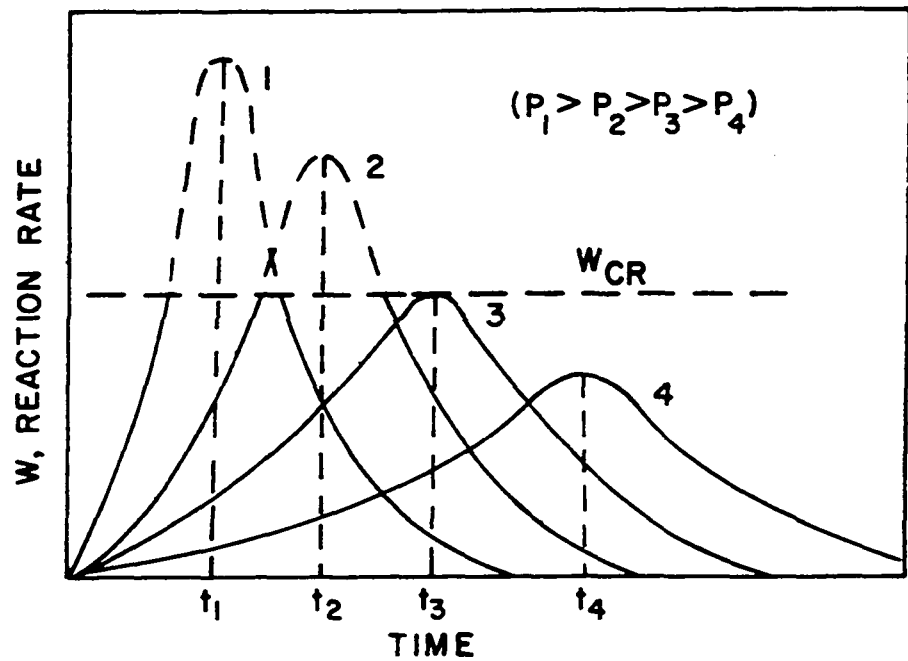


Figure 2. Reaction Rate as Function of Time and Pressure.

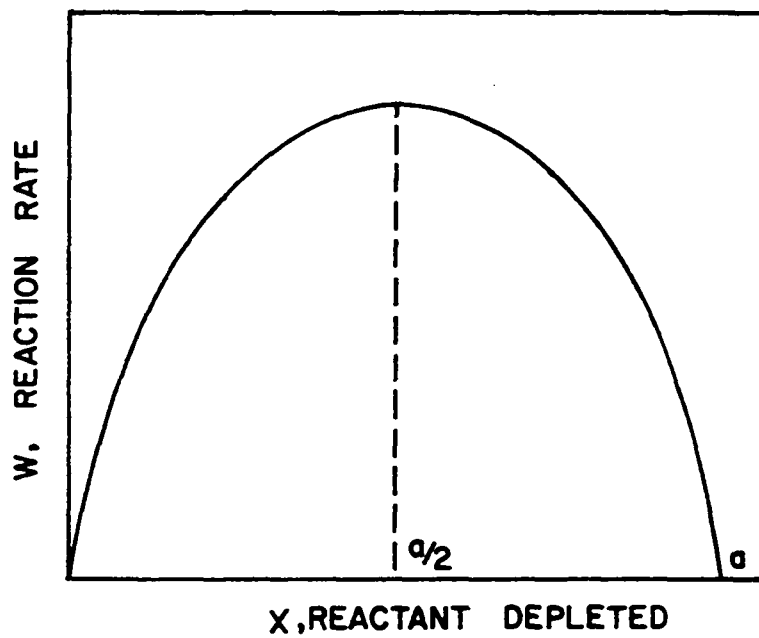


Figure 3. Variation of Rate with Reactant Depletion.

can proceed through a maximum even under sub-explosive conditions as shown in curve 4.

Semenov (63) showed that the rate of reaction, w , leading to the maximum can be represented by a function of the form

$$w = \frac{dx}{dt} = \phi x + n_0 \quad (1)$$

where n_0 is the number of final or intermediate products produced per second per unit volume, x is the amount of reactant depleted, ϕ is a constant, and t is time. Upon integration from zero time ($x_0 = 0$), equation 1 becomes

$$x = \frac{n_0}{\phi} (e^{\phi t} - 1) \quad (2)$$

Differentiation of equation 2 with respect to time gives

$$\frac{dx}{dt} = n_0 e^{\phi t} \quad (3)$$

If ϕ is not a constant, but decreases during reaction due to depletion of reactants, i.e.,

$$\phi = \phi_0 (a-x) \quad (4)$$

where a is the maximum amount of reactant depleted, the curve of initial rate versus time then will be as depicted in Figure 2 up to the maximum of each curve, and the rate as

a function of x will be of the shape shown in Figure 3. The maximum in rate occurs at one-half depletion of reactant (if n_0 is very small) due to the parabolic function derived upon substituting equation 4 into equation 1. Semenov determined x , in his analysis, as a function of t assuming constant ϕ ; he then inserted the expression describing the variation in ϕ with x (equation 4).

The more rigorous technique of integrating equation 1 after substitution of equation 4 leads to a far more complicated expression for rate as a function of depletion; however, it can still be shown that rate as a function of reactant depletion and time will have the general shapes shown in Figures 2 and 3.

In a chain reaction, the rate of reaction is equal to the rate of chain propagation if the rate of chain initiation is negligible in comparison with the rate of propagation. Denoting by w the rate of reaction, a the kinetic coefficient of chain propagation, and n the concentration of active centers:

$$w = a n \quad (5)$$

In isothermal chain reactions, explosion can occur due to buildup of active chain centers. Denoting the kinetic coefficients of branching and termination by f and g , respectively, the rate of change of active centers is given by:

$$\frac{dn}{dt} = w_0 - gn + fn \quad (6)$$

where w_0 is the chain initiation reaction rate. For unbranched chain reactions the last term disappears, leaving

$$\frac{dn}{dt} = w_0 - gn \quad (7)$$

Upon integration, assuming n is zero at zero time, one obtains

$$n = \frac{w_0}{g} (1 - e^{-gt}) \quad (8)$$

For large t , the second term is much smaller than unity, giving

$$n = w_0/g \quad (9)$$

Substituting equation 9 into equation 5 yields

$$w = an = aw_0/g \quad (10)$$

Since the values of a , w_0 and g are about constant for a given reaction, it can be seen that the rate of an unbranched chain reaction remains constant. The development assumes that sufficient time has elapsed after the start of reaction that active centers have reached their stable concentration (see Appendix B for discussion of stationary-state analysis).

The rate of an isothermal branched chain reaction is also described by equation 5:

$$w = an \quad (5)$$

and the rate of appearance of active centers is again given by equation 6, but the branching coefficient, f , is retained:

$$\frac{dn}{dt} = w_0 - gn + fn \quad (6)$$

Integrating, assuming $n = 0$ at $t = 0$, one obtains

$$n = \frac{w_0}{g-f} (1 - e^{-(g-f)t}) \quad (11)$$

There are now two possibilities: $g > f$ and $g \leq f$. When $g > f$, the rate (or probability) of chain breaking is greater than the rate (or probability) of chain branching. Then for large t , the exponential can be neglected giving

$$n = \frac{w_0}{g-f} \quad (12)$$

Thus, even for branched chain reactions under the condition, $g > f$, the reaction remains stationary.

If, however, $g \leq f$, implying branching is more probable than chain breaking, the reaction can accelerate. If $g = f$, the rate of change of concentration of n becomes

$$\frac{dn}{dt} = w_0 \quad (13)$$

Then

$$n = w_0 t \quad (14)$$

and

$$w = an = aw_0 t \quad (15)$$

The reaction rate increases linearly with time and ceases to be stationary.

If $g < f$, equation 11 can be arranged giving

$$n = \frac{w_0}{f-g} (e^{(f-g)t} - 1) \quad (16)$$

and the rate equals

$$w = an = \frac{aw_0}{f-g} (e^{(f-g)t} - 1) \quad (17)$$

For large t , unity is negligible in comparison with the exponential and

$$w = \frac{aw_0}{f-g} (e^{(f-g)t}) = Ae^{\phi t} \quad (18)$$

Thus, since f is larger than g , the reaction auto-accelerates with time until reactant depletion halts it.

In degenerate-branching systems, where the branching occurs very slowly due to dissociation or reaction of a

stable molecular intermediate, equation 18 still applies.

The amount of consumed reactant, x , is in either case

$$x = N_e \bar{\phi} t \quad (19)$$

where N can be shown to be equal to $aw_0/(f-g)^2$.

Semenov (63) stated that degenerate-branching reactions always, and non-steady branching reactions sometimes, proceed without occurrence of isothermal chain explosions. The apparent contradiction with equations 18 and 19 is explained by the fact that $\bar{\phi}$ does not remain constant during the entire reaction.

In degenerate-branching reactions, considerable reactant must be consumed before a definite reaction level, w_{cr} , is reached. Figure 4 shows schematically the difference between normally and degenerately branched chain reactions.

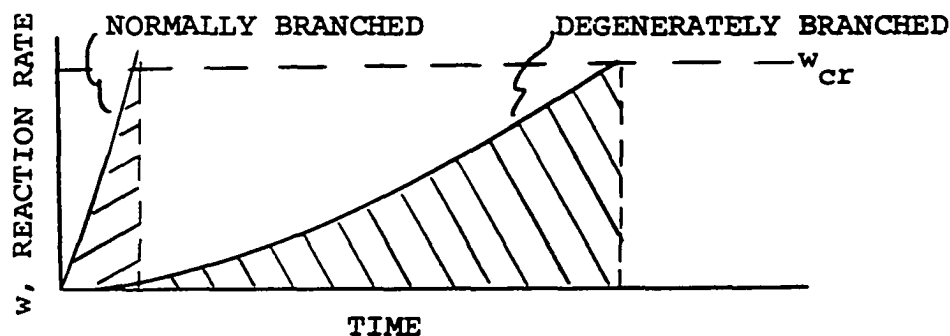


Figure 4. Reaction Rate as Function of Time for Normally Branched and Degenerately Branched Reactions.

The area under the curve is indicative of the amount of reactant consumed. Degenerate-branching frequently depletes

the supply of unreacted material to the point that explosion cannot occur.

The degenerate-branching reaction can reach explosive rates thermally, however. If the reaction is exothermic, it is possible that heat evolution can at certain times exceed heat dissipation and produce a "thermal avalanche." Heat is then simultaneously the cause and effect of explosion.

Degenerate-branching reactions follow the law given above

$$w = A e^{\phi t} \quad (18)$$

At the instant the heat balance is destroyed,

$$w_{cr} = A e^{\phi t} = \text{constant}, \quad (20)$$

which, if A is constant, leads to

$$\phi t = \text{constant} \quad (21)$$

where t is the time to explosion.

Semenov (63) showed ϕ to be of the form

$$\phi = k P^n e^{-E/RT} \quad (22)$$

where k is a proportionality constant, P is the pressure, n is a constant which depends on the reaction under consideration, E is the activation energy, R is the gas constant

and T is the absolute temperature. At constant pressure, substituting equation 22 into equation 21, rearranging, and taking the logarithm yields

$$\log t = \frac{A}{T} + B \quad (23)$$

with

$$A = E/R \quad (23a)$$

and

$$B = \log \left(\frac{\text{constant}}{kP^n} \right) \quad (23b)$$

Similarly, at constant temperature and variable pressure

$$\log t = C - n \log P. \quad (24)$$

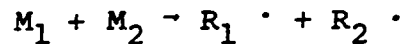
with

$$C = \log \left(\frac{\text{constant}}{k e^{E/RT}} \right) \quad (24a)$$

It can be seen that a semi-logarithmic plot of ignition delay versus $1/T$ and a log-log plot of ignition delay and pressure should result in straight lines. Because the expressions above hold for both thermal and chain explosions, the relationships cannot determine the mechanism, but they can be used for correlation or determination of an overall activation energy.

Activation Energy of the Oxidation Reaction

A complicated chain reaction consists of many consecutive and concurrent individual reactions. Each of these steps can be described by a rate equation. For instance, an initiation reaction of the form:



has a descriptive rate equation:

$$w = Ae^{-E/RT} [M_1][M_2] \quad (25)$$

where A is the frequency factor, E is the activation energy, and the brackets represent concentration.

Experimental investigation of any single reaction occurring in a chain process involves considerable difficulty. At times, initiation and termination steps can be followed individually in isolated systems, but in general, molecule-radical reactions cannot be studied by themselves.

Semenov (64) considered a large amount of data in suggesting an empirical relationship for prediction of activation energies of molecule-radical reactions. He proposed the empirical equation:

$$E = 11.5 - 0.25 |q| \quad (26)$$

where $|q|$ is the absolute value of the thermal effect of the reaction for exothermic reactions; for an endothermic reaction he proposed:

$$E = 11.5 + 0.75 |q| \quad (27)$$

Semenov's derivation assumes homogeneous reactions in the gas phase.

Through the use of the quasi-stationary theory, the overall activation energy of a complete chain sequence can be calculated if the activation energies of the individual steps are known. In the case of degenerate-branching systems, all radicals are considered at steady concentration, and the branching agent is assumed at variable concentration. By solving the set of simultaneous equations describing the rate of appearance of active centers, the entire system can be represented in terms of the concentration of the branching agent (see Appendix B). The overall reaction then can be described in terms of the concentration of the branching agent and the initial reactants.

In general, the rate of the branching step (in degenerate branching, radicals are products, but not reactants) can be studied individually. Then the overall reaction rate can be represented by an expression based on only the initial reactant concentrations. For instance, the overall mechanism of Semenov (64) can be reduced to a single rate equation of the form:

$$-\frac{d[\text{CH}_4]}{dt} = Ae^{-46000/RT} [\text{CH}_4]^2[\text{O}_2] \quad (28)$$

This result agrees with data taken at about 235 mm Hg and 423-513°C.

Measurement of overall activation energy necessarily involves the observation of some variable which is dependent on the reaction rate. Karmilova, Yenikolopyan, and Nalbandyan (31) showed that activation energies for the inductive oxidation of methane, estimated by determining the variation of pressure increase, consumption of oxygen, consumption of methane, accumulation of water, and accumulation of carbon monoxide, all give (when plotted versus 1/T) activation energies of the order 41.5 to 43.0 kcal/mole. They also showed that the induction period, when plotted versus 1/T, results in a straight line with a slope equal to 18,100 (E = 36.0 kcal/mole).

The development presented in the section dealing with ignition delay showed that induction time or ignition delay should be a logarithmic function of 1/T. It can be shown that the slope of such a function should be an approximation of the activation energy of the overall reaction.

For the oxidation of methane, consider a rate equation of the form

$$-\frac{d[O_2]}{dt} = Ae^{-E/RT} [O_2]^n [CH_4]^m \quad (29)$$

where [] represents concentration, t is time, A is the frequency factor, E is the activation energy, R is the gas constant, T is absolute temperature, and n and m are the orders of the reaction with respect to oxygen and methane, respectively. Assuming a fuel-rich condition, for which $[CH_4]$ is approximately constant throughout the reaction, ignition delay can be defined as:

$$t = -\frac{1}{A} e^{E/RT} [CH_4]^{-m} \int_{[O_2]_i}^{[O_2]_f} \frac{d[O_2]}{[O_2]^n} \quad (30)$$

where the subscripts i and f refer to initial and final concentrations of oxygen. If the integral is approximately constant, it can be seen that a plot of $\log t$ versus $1/T$ should result in a straight line with slope E/R .

In the program of Karmilova et al. (31), the maximum rate of depletion and formation of the various species were considered. In this case, assuming constant initial concentrations, the rate equation given as equation 29 would become:

$$-\left\{ \frac{d[O_2]}{dt} \right\}_{\max} = Ae^{-E/RT} [O_2]^n [CH_4]^n = Ke^{-E/RT} \quad (31)$$

where K is a constant. A plot of the logarithm of maximum rate versus $1/T$ will give a straight line with slope $-E/R$.

It can be seen that several methods of estimating the overall activation energy are available. For a given initial concentration (held constant while T is varied), it must be mentioned that activation energy determination by use of ignition delays is most subject to error of the various methods unless final concentration is not a strong function of temperature.

The Effect of Surfaces and Catalysts

Surface effects cannot be generalized for all reactions. Each particular reactant system must be evaluated individually for meaningful mechanisms. Surfaces which are inactive for one reaction can be extremely active through physical processes such as adsorption and, perhaps, even catalytic in nature for still others. However, almost all observations dealing with changes in surface activity for a given reaction can be explained by chain mechanisms.

Chain theory is used to explain another phenomenon: the marked effect upon reaction rates by addition of insignificant amounts of certain substances. For instance, substances such as formaldehyde, acetaldehyde, nitrogen peroxide, iodine, and water are known to decrease the induction

period in methane oxidation under some conditions while the same materials can, under other conditions, retard the reaction (10, 11). Acceleration is caused by greater ability of the additive to initiate chain carriers, while retardation is caused by the ability of additives to react with free radicals to form less active radicals or inert products.

The effect of surfaces or heterogeneous catalysts on chain reactions is due to identical general considerations. Some surfaces can accelerate an overall reaction due to increased initiation rates, while others can be effective destroyers of radicals, resulting in shorter chain lengths.

Some surfaces can be classified as effective destroyers of free radicals. Acidic surfaces, for instance, are known to convert $\text{HO}_2\cdot$ radicals to hydrogen peroxide and, subsequently, to hydroxyl radicals ($\text{OH}\cdot$) (38).

In general, most investigators have found that high surface-to-volume ratios in the reactor lead to decreased reaction rates in the oxidation of hydrocarbons. It appears that surface inhibiting effects are more pronounced than effects due to enhanced initiation.

Because the intermediates formed in gas-phase hydrocarbon oxidation are more easily oxidized than the original fuel, catalysis in this field has been used generally in the sense that lower reaction temperatures can be employed. Extreme care must be exercised to prevent extension of oxidation steps which would cause the reaction to go toward

complete conversion to water and carbon dioxide. Catalysts, as such, are not used in this field to drive the reaction to a higher degree of completion.

It is possible that catalysis will enable oxidation processes to be conducted at sufficiently low temperatures that products not found at elevated temperatures are formed. The appearance of these products may be due to avoidance of thermal degradation or intermediate dissociation reactions.

In liquid phase oxidation of hydrocarbons some degree of reaction control and selectivity is afforded. It has been reported that use of metallic catalysts in the liquid-phase oxidation of butane leads to higher selectivity when compared with the very diverse mixture of products obtainable through vapor-phase oxidation (40). It is likely that stability of intermediates at lower temperatures can alter the normal branching steps.

Shtern (66) pointed out that it is not possible to alter the relative proportion of the branching agents in hydrocarbon oxidation through catalysis. This group of branching agents includes aldehydes and peroxides. However, he assumed constant activation energies and reaction constants over a wide range of conditions in his analysis. If any of the individual steps involve species which are selectively absorbed on the catalyst, a change in the activation energy

for the step is possible. Although Shtern cited experimental evidence that his assertion is true in comparing the catalytic and non-catalytic oxidation of methane under identical conditions, it cannot be concluded that catalytic activity that enables the reaction to proceed at far lower temperatures will not result in altered product distribution.

The stable end products of oxidation, methanol and the organic acids, are formed in non-branching steps. The yield of these products, formed through termination processes, should be variable through alteration of surface conditions. These products should be formed in large quantity if the amount of hydrocarbon entering the reaction can be increased.

Several catalytic materials are felt to be of interest in the high pressure oxidation of methane. Two specific types of catalysts have properties considered to be influential in the reaction process. These general classes are hydrogenation catalysts and oxidation catalysts.

Strong acid catalysts are able to donate and re-absorb protons. This mobilization of protons can be beneficial to hydrogen transfer (which is the mechanism of a majority of the steps in hydrocarbon oxidation) and alkylation. Included in this category are silica-magnesia and silica-alumina. A commercially available silica-alumina is Kao-spheres, marketed by Houdry Process and Chemical Co., manufactured from naturally occurring clay.

Synthetic silica-alumina and silica-magnesia, and natural kaolin clays, are also used for cracking operations. Cracking normally converts high molecular weight oils to gasoline fractions. With methane, due to the ability to absorb and desorb protons, there is a possibility that selective production of methyl radicals can be made.

Oxidation catalysts are frequently made of metals of group VIII of the periodic table and of transition metals and their oxides. The activity of the oxides is related to the ability of the material to donate and re-absorb oxygen. The pure metal catalysts exhibit activity related to their ability to bond chemically with free electrons or radicals with an unpaired electron. Nickel, copper, platinum, vanadium and manganese are included in this group.

An exceptionally active catalyst in this latter group is cobalt molybdate. This material is reported by a major manufacturer (Houdry) to be very useful for hydrogenation of organic materials which contain impurities that would poison nickel catalysts.

Photocatalytic Oxidation of Methane

Oxidation of methane depends on the rate and quantity of free radicals generated in an endothermic initiation step. For each pressure level, there is a temperature below which the initiation step is insufficiently rapid to provide the necessary buildup in radicals at rates

in excess of the chain termination steps. It would seem likely that lower temperatures of reaction could be observed in methane oxidation if free radicals could be supplied by some external process.

The field of photochemistry provides three methods for maintenance of controllable environments for investigation of mechanisms and product distributions. These distinct fields are: (1) photolysis of the primary reactants, generating radicals and/or excited molecules, (2) photolysis of an initiator, present in the reaction mixture in minute quantity, resulting in radicals usually observed in thermal processes, and (3) photosensitization of an inert additive, generating excited molecules which can, in turn, transfer absorbed energy to the primary reactants.

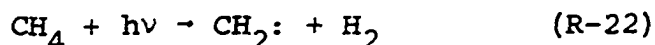
There are several advantages which make photochemical processes attractive. The most important of these is the possibility of raising the electronic energy of a molecule to a specified level by selection of wavelength. It is possible to increase energy without altering rotational and translational contributions, a process which is impossible through thermal excitation. Further, excitation of only select molecules can be made.

Selectivity enables production of products which are possibly not formed in significant quantity at elevated temperatures because equilibrium yields of certain products

can suffer at these elevated temperatures. In addition, thermal excitation can cause many unwanted reactions to take place as energy is raised from a low level to a higher level. Proper selection of wavelength enables quantum jumps in energy without traversing intermediate levels.

In hydrocarbon oxidation, generation of radicals which react readily with the primary reactants, leading toward production of stable intermediates, is desired. Both peroxides and aldehydes, known to be intermediates responsible for degenerate branching, may be produced in greater quantities at lower temperatures through the use of photolysis.

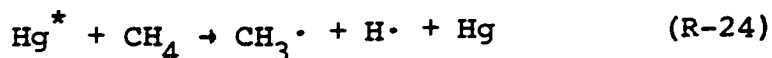
Methane absorbs radiation below 1400 Å., producing the diradical $\text{CH}_2\cdot$ and hydrogen:



The intense ultraviolet light necessary for the above dissociation presents considerable problems in practicality.

Because of constructional problems, the solution of which was not felt to be practical in this short section of study, only wavelengths produced by standard mercury vapor-quartz discharge lamps were considered. The characteristic wavelength for this type of lamp is 2537Å. Initiators accepting this radiation were sought.

Mercury vapor is known to absorb radiation at 2537Å. The following reactions can then occur:



where Hg^* is an excited mercury atom.

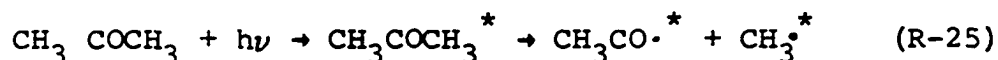
Mercury thus assumes the role of catalyst. Even though removal of hydrogen from methane involves energy of only 104 kcal/mole (24), and light of 2537Å wavelength would provide 113 kcal/mole (more than enough to cause dissociation), inability of methane to absorb in this range precludes dissociation. The energy, carried by mercury atoms in an excited state, transfers to methane molecules upon collision. The additional 9 kcal/mole show up as heat.

Mixed with oxygen, exposure of a methane/mercury mixture to 2537Å radiation can lead to a variety of reactions. Mercury vapor is capable of sensitizing the decomposition of water, ethanol, and acetone and can lead also to ozonolysis of oxygen. With mixtures of hydrogen and oxygen, mercury vapor is able to lead to production of hydrogen peroxide. It follows that with methane, quantities of both CH_3OOH and H_2O_2 should be produced.

Another method of possible initiation of methane oxidation at low temperatures is the introduction of a substance sensitive to radiation, which decomposes into radicals normally present in thermal oxidation. The most efficient initiators used in photolysis are usually organic peroxides. Dimethyl peroxide or methylhydroperoxide would

seem logical choices. However, instability of these materials presents handling problems.

Acetone is known to decompose over a wide range of wavelengths in the ultraviolet. Only 70 kcal/mole are required to break a C-C bond in acetone, resulting in an excess of 13-14 kcal/mole at 3130Å. The primary step is felt to be (12):

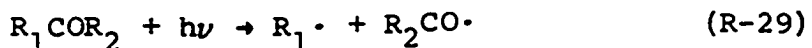
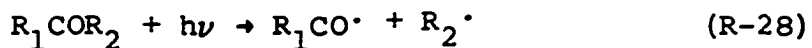
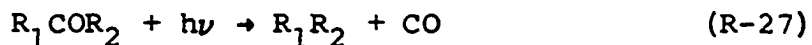


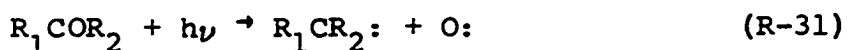
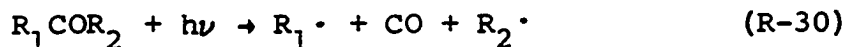
where the asterisk denotes an excited state. The excess energy is sufficient to dissociate the acetyl radical to a methyl radical and carbon monoxide.



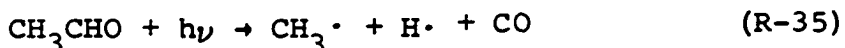
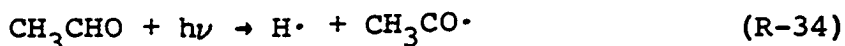
In absence of oxygen, methyl radicals lead to formation of ethane. With oxygen, $\text{CH}_3\cdot$ radicals can produce formaldehyde. If methane is also present, methylhydroperoxide may be produced (see mechanism on page 77). Thus, the chain mechanism for oxidation of methane can be initiated.

Carbonyl groups, known to absorb in the near ultraviolet, are present also in aldehydes. Noyes and Leighton (53) presented the possible modes of dissociation of aldehydes and ketones by the following reactions.

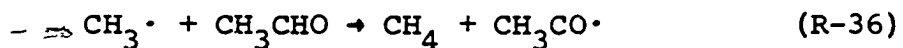




When considering wavelengths in the near ultraviolet, reaction R-31 can be discounted; because of the energy involved (160 kcal/mole), wavelengths shorter than 1900A would be required. The four remaining generalized reactions become, for acetaldehyde:



The following products of the photochemical decomposition of acetaldehyde have been observed by various investigators: CH_4 , H_2 , CO , $(CH_3CO)_2$, and an unknown polymer. Since ethane has been observed among the products, methyl radicals must react with acetaldehyde to give methane and an acetyl radical.



The acetyl radical decomposes to methyl radicals and carbon monoxide



or dimerizes to biacetyl.

Dissociation of formaldehyde, at wave lengths shorter than 2750A, yields hydrogen atoms. If the overall reaction below is also the primary process, no chains are possible:



If, however, a chain process occurs,



A convenient source of radicals is thus provided.

CHAPTER III

REVIEW OF WORK IN OXIDATION OF METHANE

The Homogeneous Reaction

Just as there has been controversy over which intermediate is the true source of degenerate chain branching in the general theory of oxidation of hydrocarbons, there have been many theories put forth pertaining to the characteristics of methane oxidation. The controversy over mechanism is by no means limited to recent times; disagreement dates back over half a century, long before modern chain theory was formulated. Several of the earlier schemes used as mechanistic explanations were the hydroxylation, peroxidation, aldehyde formation and dehydrogenation theories. Shtern (66) described these schemes in chronological detail.

After chain theory ideas were first formulated in the late 1920's, experimenters lost little time in assembling again into opposing schools of thought and the controversy continued. For a few years, workers were mainly involved in attempting to correlate, with the new chain theory, the vast amount of data previously assembled. Later, sophisticated experiments were designed to prove or disprove the ideas which evolved in this brief "academic" period. Some of the more pertinent experimentation and the mechanistic theories

that evolved will be described. An excellent chronology of this period has been presented by Shtern and will not be repeated here in great detail.

At atmospheric pressure, methane does not undergo appreciable oxidation below 400°C. Carbon monoxide and water are the major products. Other products, especially oxygenated liquid species, are produced at elevated pressures, with the minimum reaction temperature varying inversely with pressure.

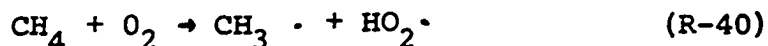
All workers report the existence of an induction period during which little pressure change occurs. At the end of this time period, pressure and temperature (in adiabatic systems) have been seen to rise exponentially to a maximum. Rate of pressure change then falls to zero as the reactants are depleted.

The importance of the role of formaldehyde was suspected by several workers. Bone and Gardner (11) noted that formaldehyde concentration appears to parallel closely the rate of change of pressure. These authors noted that addition of formaldehyde shortens the induction period. Norrish and Foord (50) reported similar results. Norrish (49) also saw that excess formaldehyde (over that present in its usual maximum concentration) causes the reaction to proceed at an abnormally fast rate until formaldehyde concentration falls to its normally observed maximum value, at which time the reaction returns to its normal rate.

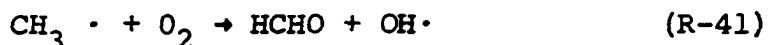
von Elbe (70) listed the important characteristics which must be explained in any oxidation scheme for methane:

(a) reaction is initiated by formaldehyde made from methane and oxygen, (b) new chain carriers must be made from formaldehyde, (c) additional formaldehyde must be made from the chain carriers and methane, and (d) formaldehyde is destroyed by chain carriers.

There is no disagreement over the initiation step:



Formaldehyde can be formed by a reaction between a methyl radical and oxygen.



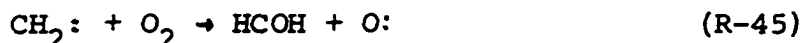
The reaction of formaldehyde in a degenerate branching step is a center of controversy. Lewis and von Elbe (34) suggested the branching step to be:



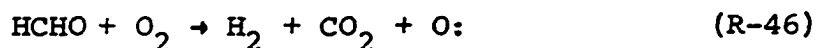
Norrish (49), however, suggested that oxygen atoms formed from performic acid are involved:



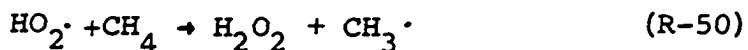
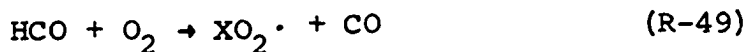
where $\text{O} \cdot$ is an oxygen diradical. He further assumed that reaction of the oxygen diradical occurs by



Norrish later partially refuted the mechanism and supposed that two monoradicals, $\text{OH}\cdot$ and $\text{H}\cdot$, are formed and only one diradical is involved:



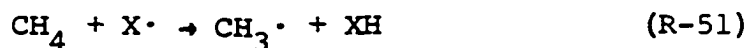
Walsh and co-workers (13,28) supposed that degenerate branching involves the $\text{HO}_2\cdot$ radical in the scheme:



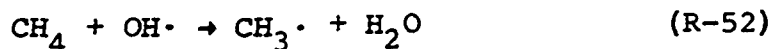
where X is oxygen or a free radical.

Egerton, Minkoff and Salooja (15) showed that all three of the branching mechanisms given thus far may be valid, depending on the condition of the surface of the reactor. For instance, if the surfaces destroy $\text{HO}_2\cdot$ radicals, reactions R-37 or R-38 can predominate, but with inactive surfaces, reactions R-43 to R-45 are also feasible.

Medley and Cooley (40) showed that, regardless of the chain center formed in the branching step, new chains are formed by:

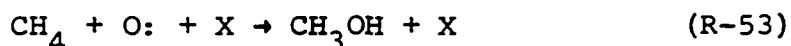


where $X\cdot$ is the chain center formed in the branching step ($OH\cdot$, $HO_2\cdot$, $O\cdot$, etc.). In the primary chain, the same general reaction is assumed, where X is the $OH\cdot$ radical:



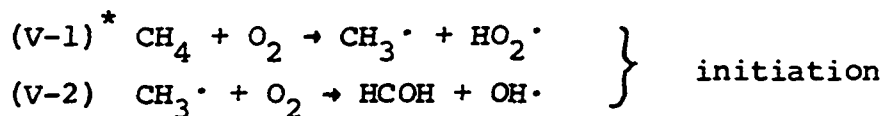
Many authors have presented mechanisms for the oxidation of methane. Notable contributions have been the works of Norrish (49), Lewis and von Elbe (34), Yenikolopyan (79) and Semenov (63).

Norrish's scheme involved the production of oxygen and hydrogen atoms. Because of the lack of detection of hydrogen in non-explosive tests, most later writers opposed Norrish's scheme. Norrish, however, recognized the importance of the production of methanol at elevated pressures. His scheme for production of methanol involved the oxygen diradical:

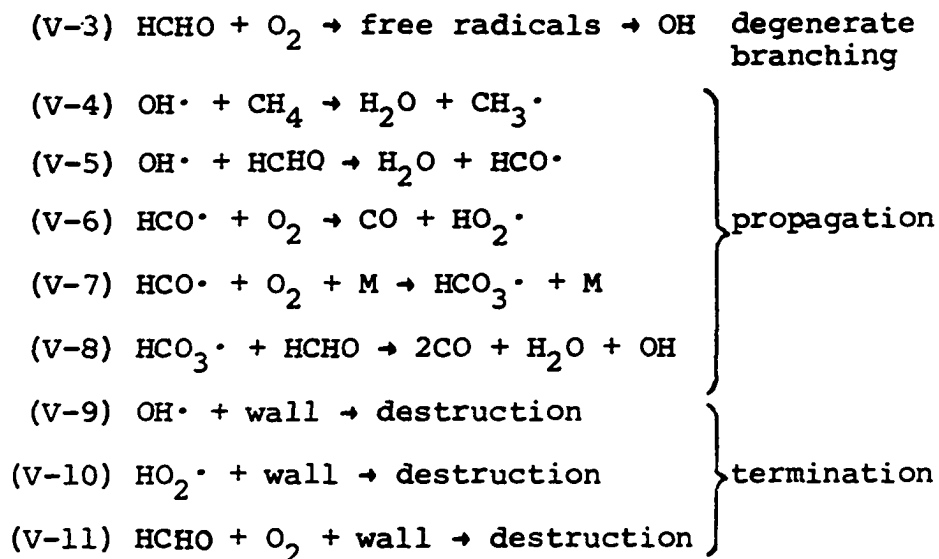


where X is a third body such as oxygen, methane, or an inert gas. A mole-reducing step was shown to explain the beneficial effect of pressure.

A complete scheme for the slow oxidation of methane at low pressures was proposed by Lewis and von Elbe (34).

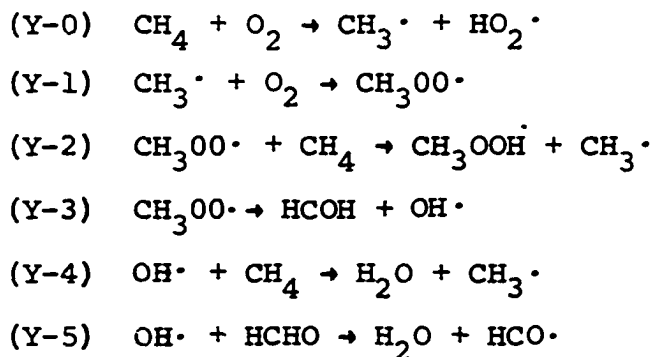


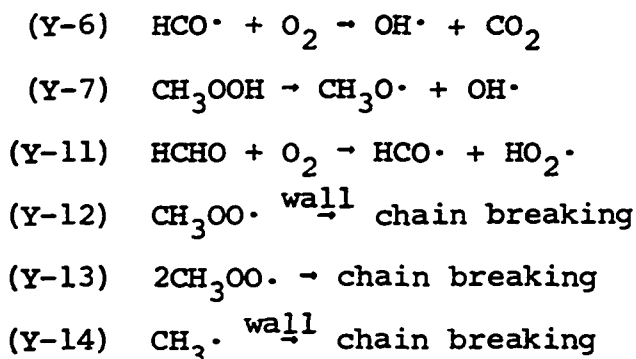
*In this text, complete mechanisms will be identified by a letter prefix denoting the author.



Production of carbon dioxide was not listed in the mechanism. Formation of carbon dioxide was considered by Lewis and von Elbe to be due to additional oxidation of carbon monoxide. Reaction V-3 is not specified in detail, but the degenerate branching step leading to the hydroxy radical is presented in general.

Yenikolopyan (79) proposed a mechanism for low pressure oxidation which he felt fully explained experimental observations. The numbering scheme is that of Yenikolopyan; his general scheme for alkyl hydrocarbons has been reduced to apply only to methane.





An interesting aspect is the production of the methyl peroxy radical ($\text{CH}_3\text{OO}\cdot$) as an intermediate in the formation of formaldehyde. Yenikolopyan, in the incorporation of this step, provided for the production of methylhydroperoxide which, he supposed, provided a second branching step (Y-7). Yenikolpyan computed the order of reaction with respect to the initial reactants by using the method of steady-state concentrations and by neglecting those reactions that he felt to be unlikely over certain temperature ranges. He obtained the results given in Table 1. The reported temperatures are indicative of general reaction temperatures for higher hydrocarbons; with methane, the temperature ranges of Table 1 are low by 50 to 100°C. What is of interest, instead, is the trend in reaction orders as temperature is varied.

The orders in Table 1 might be compared with the orders determined experimentally by several workers, as reported by Shtern (66) and shown in Table 2. The trend, with increasing temperatures, in the progression from low to high order with respect to oxygen and from high to low orders with respect to methane, is seen.

TABLE 1

THE VARIATION OF THE MAXIMUM RATE OF HYDROCARBON
OXIDATION WITH CONCENTRATION OF HYDROCARBON
AND OXYGEN AT DIFFERENT TEMPERATURES
(From Ref. 66)

$w_{\max} \sim [RH]:$	liquid phase, branching via ROOH according to reaction Y-7 (reaction Y-11 neglected), chain breaking by means of the quadratic destruction of ROO according to reaction Y-13 (reactions Y-12 and Y-14 neglected).
$w_{\max} \sim [RH]^2:$	gaseous phase up to 300°, branching via ROOH according to reaction Y-10 (reaction Y-11 neglected), chain breaking by means of the linear destruction of ROO according to reaction Y-12 (reactions Y-13 and Y-14 neglected).
$w_{\max} \sim [RH][O_2]:$	gaseous phase around 300° and higher, branching via HCHO according to reaction Y-11 (reaction Y-7 neglected), chain breaking by means of the linear destruction of ROO according to reaction Y-12 (reactions Y-13 and Y-14 neglected)
$w_{\max} \sim [RH][O_2]:$	gaseous phase from 300° to 500°, transition region, branching via HCHO according to reaction Y-11 (reaction Y-7 neglected), chain breaking by means of destruction of ROO and R according to reactions Y-12 and Y-14 (reaction Y-13 neglected).
$w_{\max} \sim [RH][O_2]^2:$	gaseous phase above 500°, branching via HCHO according to reaction Y-11 (reaction Y-7 neglected), chain breaking by means of linear destruction of R according to reaction Y-14 (reaction Y-12 and Y-13 neglected).

TABLE 2.

THE VARIATION OF THE MAXIMUM RATE OF METHANE OXIDATION
WITH CONCENTRATIONS OF METHANE AND OXYGEN
AT DIFFERENT TEMPERATURES.
(From Ref. 66)

Tem- per- ature °C	Vessel	Order of reaction with respect to methane $n\text{CH}_4$	Order of reaction with respect to oxygen $n\text{O}_2$
376	Pyrex	2.3	0.5
416	Pyrex	2.0	0.5
467	Clean vessel	1.6	1.0
480	--	2.0	1.0
500	Quartz, treated by heating	2.4	1.0--1.6
570	--	1.4	2.4
617	--	0.11(?)	2.5
650	Quartz, treated by heating	0--0.7	2.3--2.7
666	--	--0.14	3.8
750	--	-0.4 +0.4	2--2.4

Yenikolopyan was unable to obtain a mechanism which explained the independence of maximum rate and hydrocarbon concentration, or the inhibiting effect of hydrocarbons, both of which occur at high temperatures. Experimentally, Yenikolopyan confirmed the role of formaldehyde as the degenerate branching agent over the range 400°-450°C. He and his co-workers (31) established the production of hydrogen peroxide, which, however, he did not specify in his earlier mechanism.

Figure 5 shows some experimental results of Yenikolopyan and others (31) for oxygen-rich combustion at 472°C and 235 mm Hg total pressure. The exponential rise in peroxide concentration has also been corroborated by Egerton, Minkoff and Salooja (15), while the flatter shape for the formaldehyde curve was observed by both groups. This result led Minkoff and Tipper (43) to conclude that both hydrogen peroxide and formaldehyde are important to branching above 450°C.

Semenov (63) introduced a radical-chain mechanism in 1958, which more adequately described methane oxidation at low pressures. He incorporated the experimental findings of several workers, notably Yenokolopyan et al. (31), in his scheme by including the formation of hydrogen peroxide. Until very recently, the scheme was considered by many as the mechanism best explaining the results observed in methane oxidation at low pressures. The mechanism is:

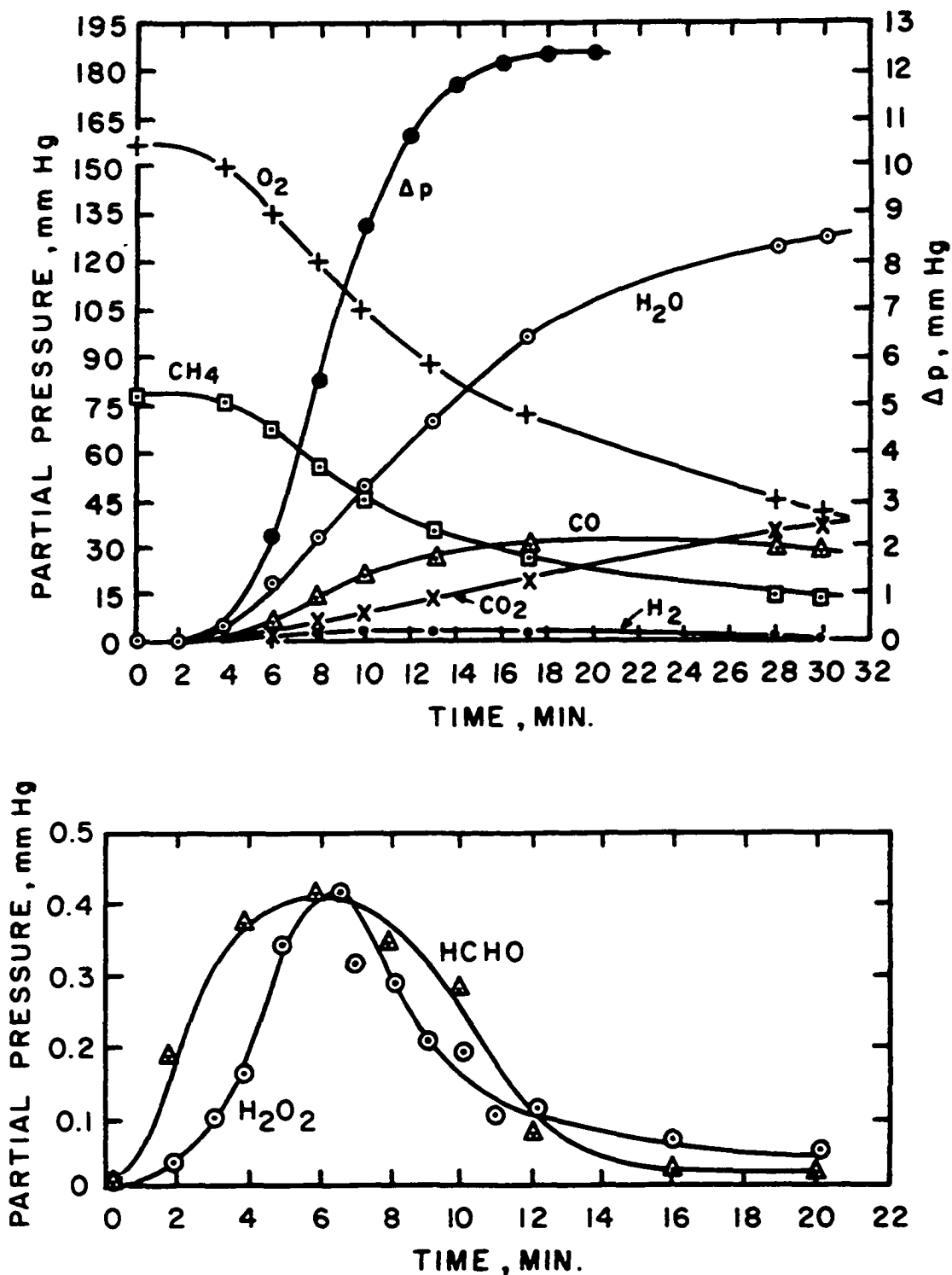
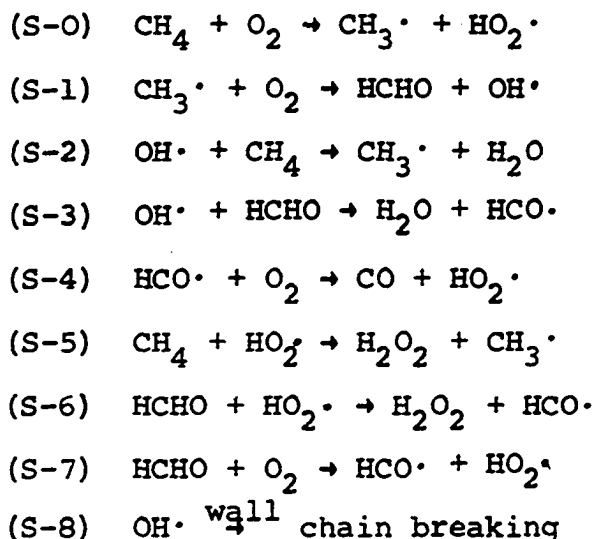


Figure 5. Kinetics of Methane Oxidation and Accumulation of Reaction Products for the Mixture $\text{CH}_4 + 20_2$ at 472°C and 235 mm Hg Pressure in an HF-Treated Vessel. (From Ref. 31.)



It should be noted that the mechanism applies only at low pressures and at temperatures low enough that formation of carbon dioxide is not considered.

Semenov did not consider the production and subsequent branching of methylhydroperoxide but he did account for the experimentally observed production of hydrogen peroxide. He did not, however, propose a scheme predicting the destruction of hydrogen peroxide, nor the formation of methanol at higher pressures.

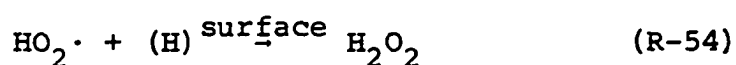
Minkoff and Tipper (43) recently assumed the identical reactions, but they considered that termination occurs by heterogeneous destruction of $\text{HO}_2\cdot$ radicals rather than $\text{OH}\cdot$ radicals. Both mechanisms, when subjected to stationary-state analysis, give:

$$w_{\max} \sim [\text{CH}_4]^2 [\text{O}_2] \quad (32)$$

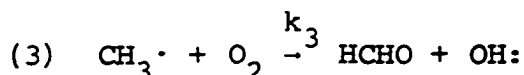
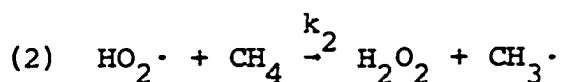
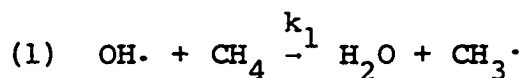
This result is in agreement with the orders predicted by Yenokolopyan for temperatures of 300°C and above and at

low pressures in the general oxidation and hydrocarbons.

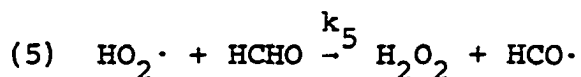
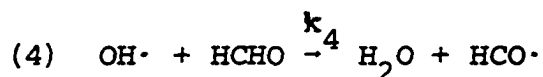
McConkey and Wilkinson (38) conducted oxidations in a fluidized-bed, continuous flow reactor in which the walls were made acidic in nature. They felt that the $\text{OH}\cdot$ radical must be the chain carrier involved in view of the theory that $\text{HO}_2\cdot$ radicals will heterogeneously combine in branching steps by:



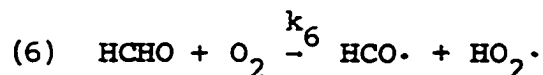
They supposed, as have others, that methane is oxidized to formaldehyde by (where the k_i are rate constants):



and that formaldehyde produced is oxidized further by the same radicals:

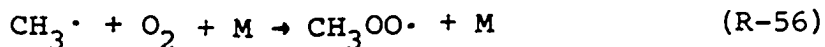


and more slowly by:

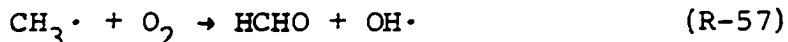


Norrish (49), in the scheme mentioned earlier, included the formation of methanol as a termination step between methane and oxygen atoms. This termination step was mole-reducing to account for the enhanced formation of methanol at elevated pressures. Shtern (66) presented arguments that the scheme of Norrish is unlikely in view of considerations involving bond energies and reaction heat effects. He, instead, lent strong support to the mechanism of Semenov.

The formation of methanol was considered by Medley and Cooley (40) who proposed that a methyl peroxy radical ($\text{CH}_3\text{OO}\cdot$) is formed in a ternary reaction at high pressures:



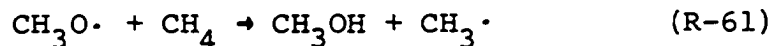
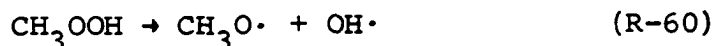
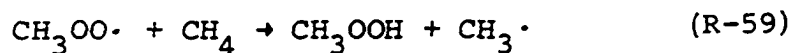
in preference to the reaction generally accepted at lower pressures:



It can be seen that isomerization and dissociation of $\text{CH}_3\text{OO}\cdot$ will give formaldehyde and the $\text{OH}\cdot$ radical by:

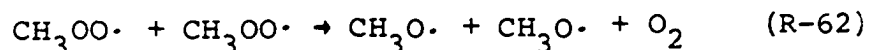


It is assumed that at low pressures, the $\text{CH}_3\text{OO}\cdot$ radical dissociates immediately, excluding the peroxide radical from other steps. Medley and Cooley showed the possibility of formation of an intermediate, methylhydroperoxide, and the subsequent formation of methanol by:



Steps R-56 through R-60 were also suggested by Yenikolopyan, but he did not show the formation of methanol as in reaction R-61. He did, however, predict formation of alcohols in the oxidation of higher hydrocarbons.

Vaughan and co-workers (6) proposed, as an alternative method for production of $\text{CH}_3\text{O}\cdot$ radicals, the interaction of $\text{CH}_3\text{OO}\cdot$ radicals:



with the subsequent production of methanol, as before.

Lott (35) studied the oxidation of very fuel-rich methane/oxygen mixtures in batch reactors up to 13,600 atm. At pressure up to 3,400 atm, experiments were performed under nearly adiabatic conditions.

In addition to verifying the formation of methanol, Lott discovered several products not detected in significant amount in earlier works. These products included methyl formate and formic acid. In his non-isothermal tests, Lott measured ignition delays and product distribution under widely varying conditions.

Figure 6, summarizing some of Lott's data, shows the effect of temperature on ignition delay with a fuel/oxidizer molar ratio of 10. Included in the plot are

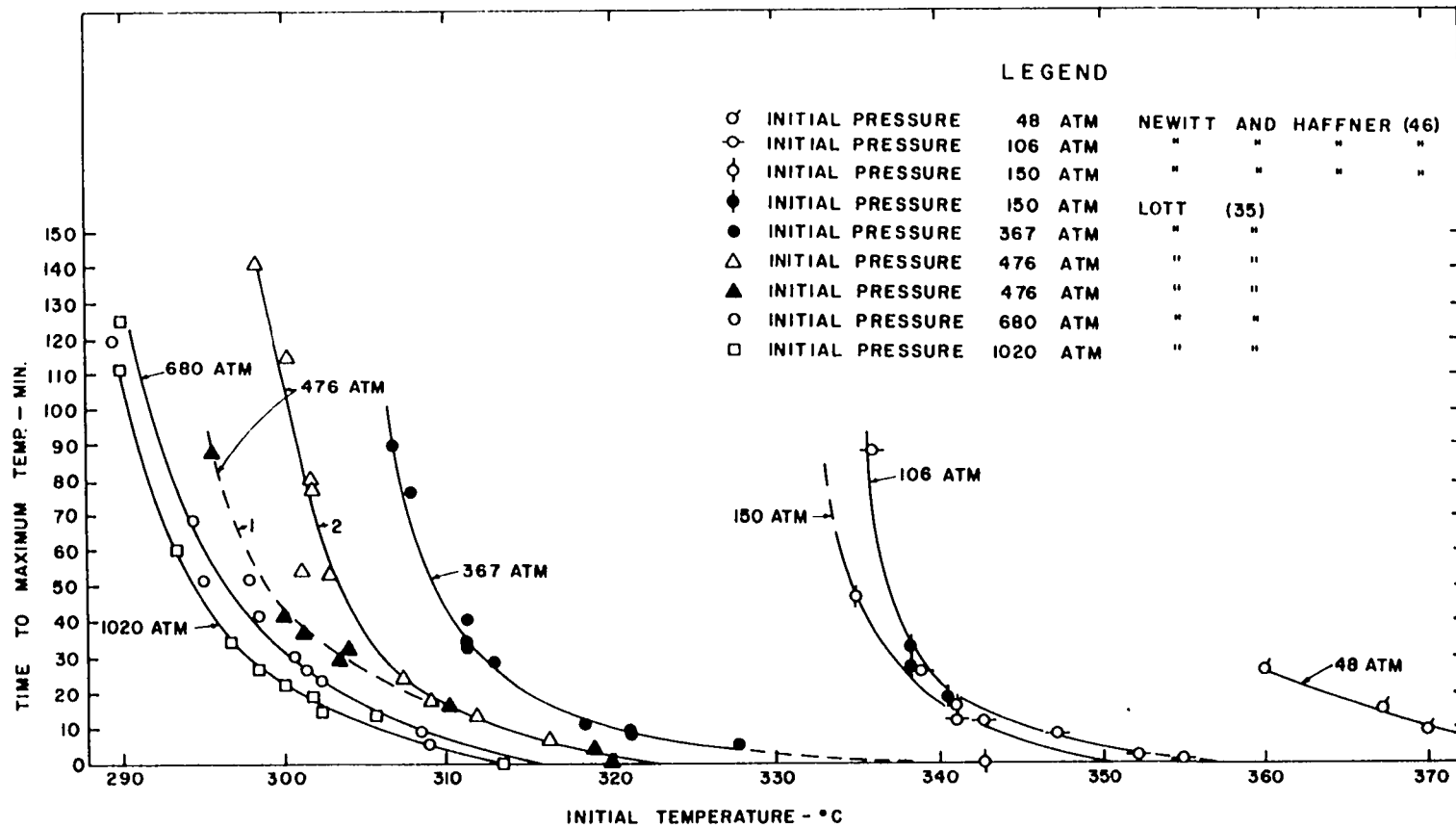
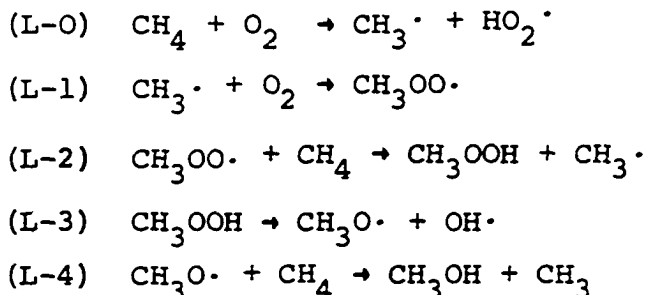


Figure 6. Effect of Temperature on Ignition Delay.
 (From Lott (35) reproduced by permission.)

points of Newitt and Haffner (46). Other data of Lott and Lott and Sliepcevich (36) are presented in Figures 7 through 9. Of interest is the apparent decrease in methanol yield at about 680 atm as shown in Figure 7. Lott attributed this trend to the shift in equilibrium slightly toward formic acid and methyl formate production at the expense of methanol. Overall liquid products show no reversal at elevated pressures (Figure 8).

In his isothermal tests, Lott reported a reduction in methane conversion with increasing pressure up to about 6800 atm., and then a slow increase in conversion up to the limit of his experimental program (Figure 9). He reported considerable "aging" of his reactor; auto-acceleration occurred at 3,400 atm and 250°C, while auto-acceleration was not observed at 9,400 atm and 250°C. The runs were conducted in order of increasing pressure. The drop in conversion could reflect a decrease in activity with a gradual "conditioning" effect allowing the expected pressure enhancement to overcome the aging process at 6,800 atm.

Lott proposed the following mechanism for oxidation of methane based on his high pressure study:



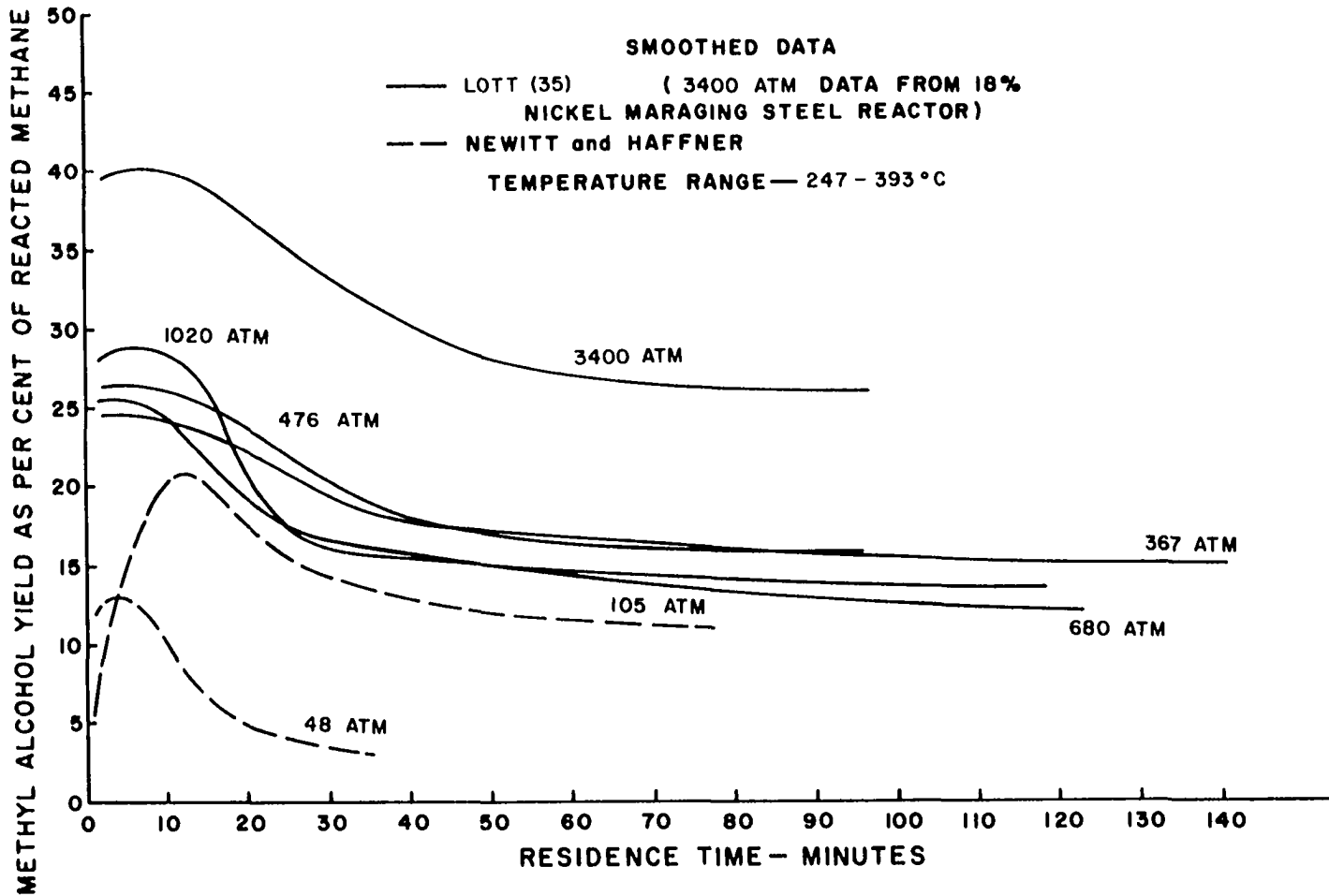


Figure 7. Effect of Residence Time on Methanol Yield at Various Pressures. (From Lott and Sliepcevic (36) reproduced by permission.)

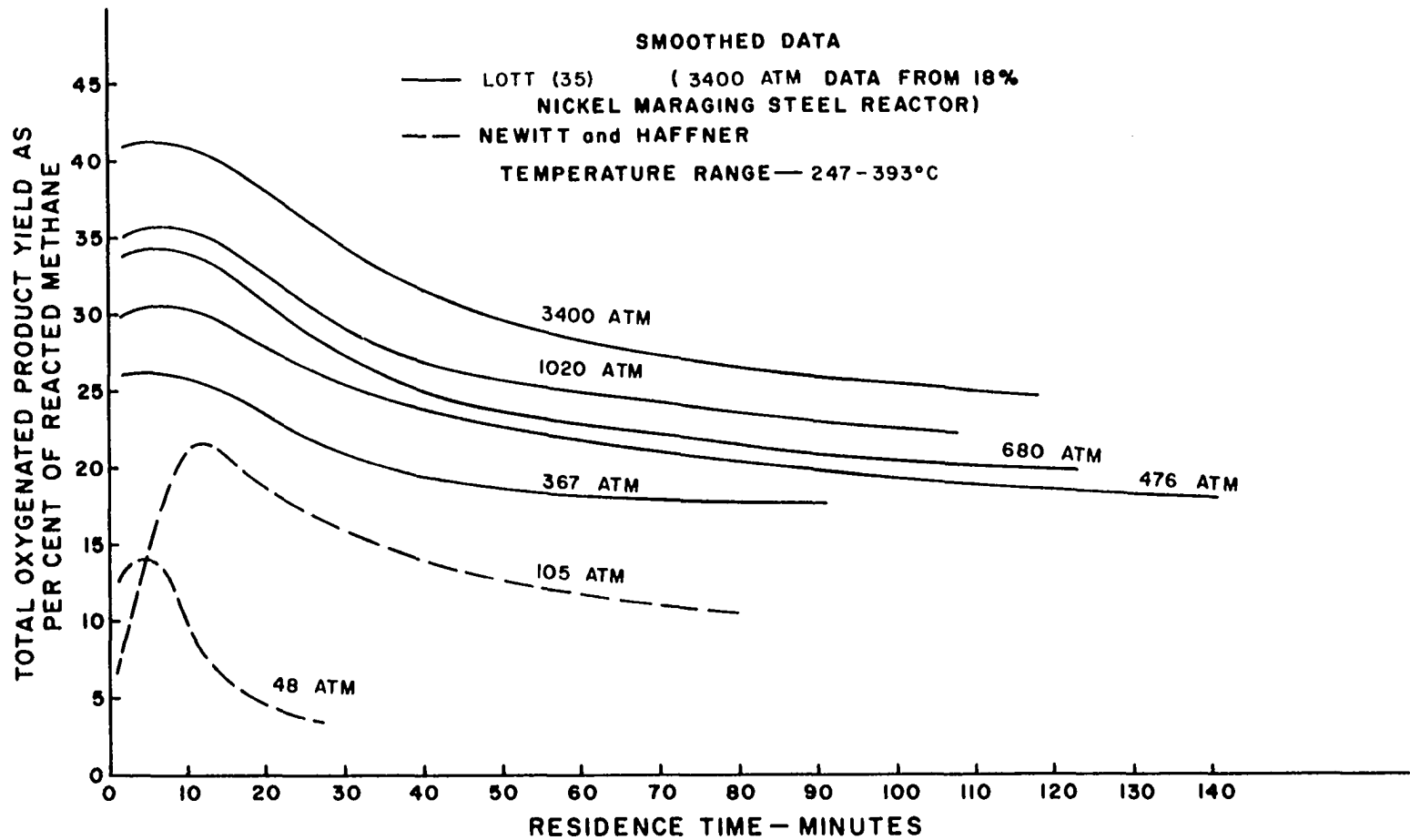


Figure 8. Effect of Residence Time on Total Oxygenated Liquid Product Yield at Various Pressures. (From Lott and Sliepceovich (36) reproduced by permission.)

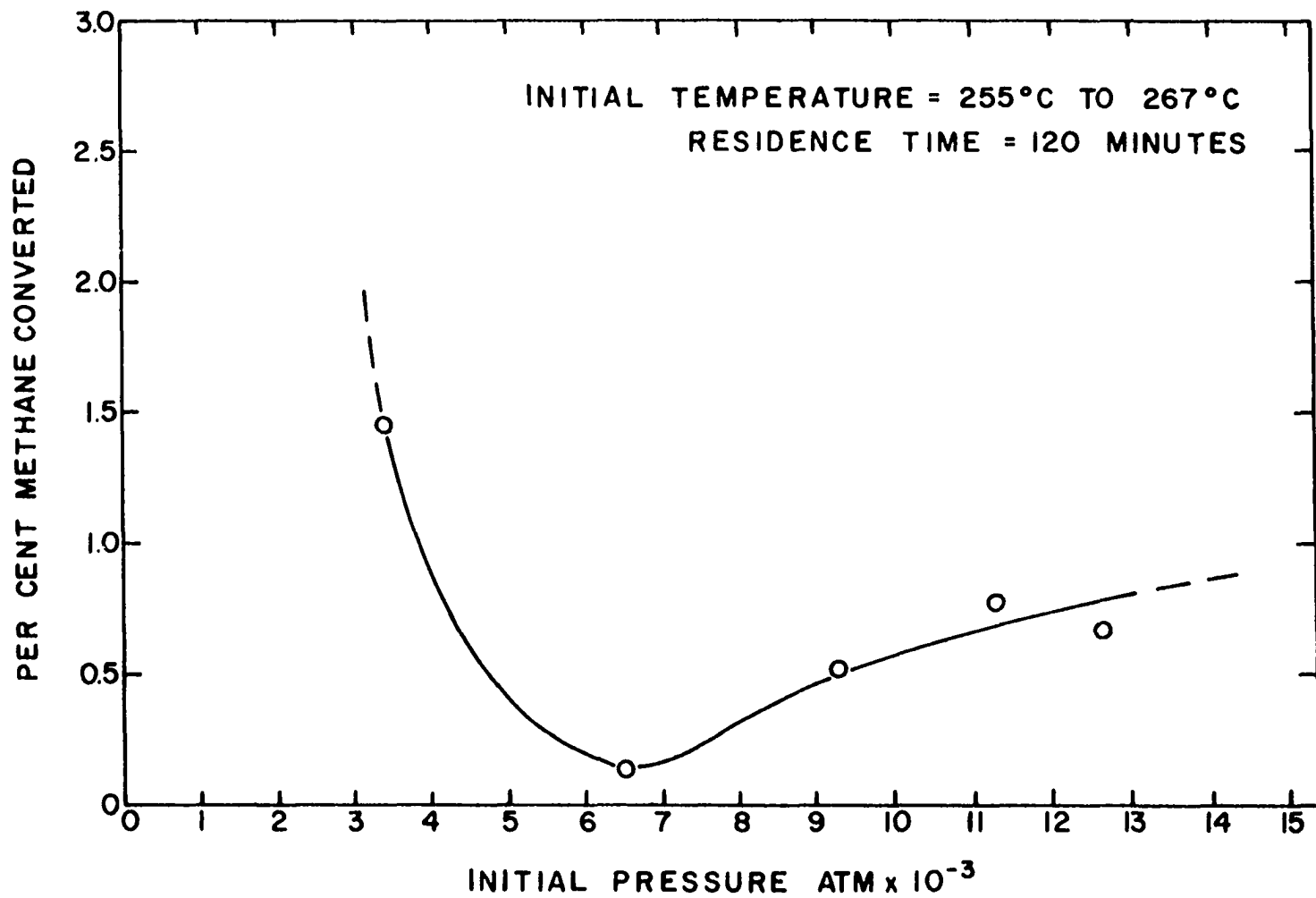


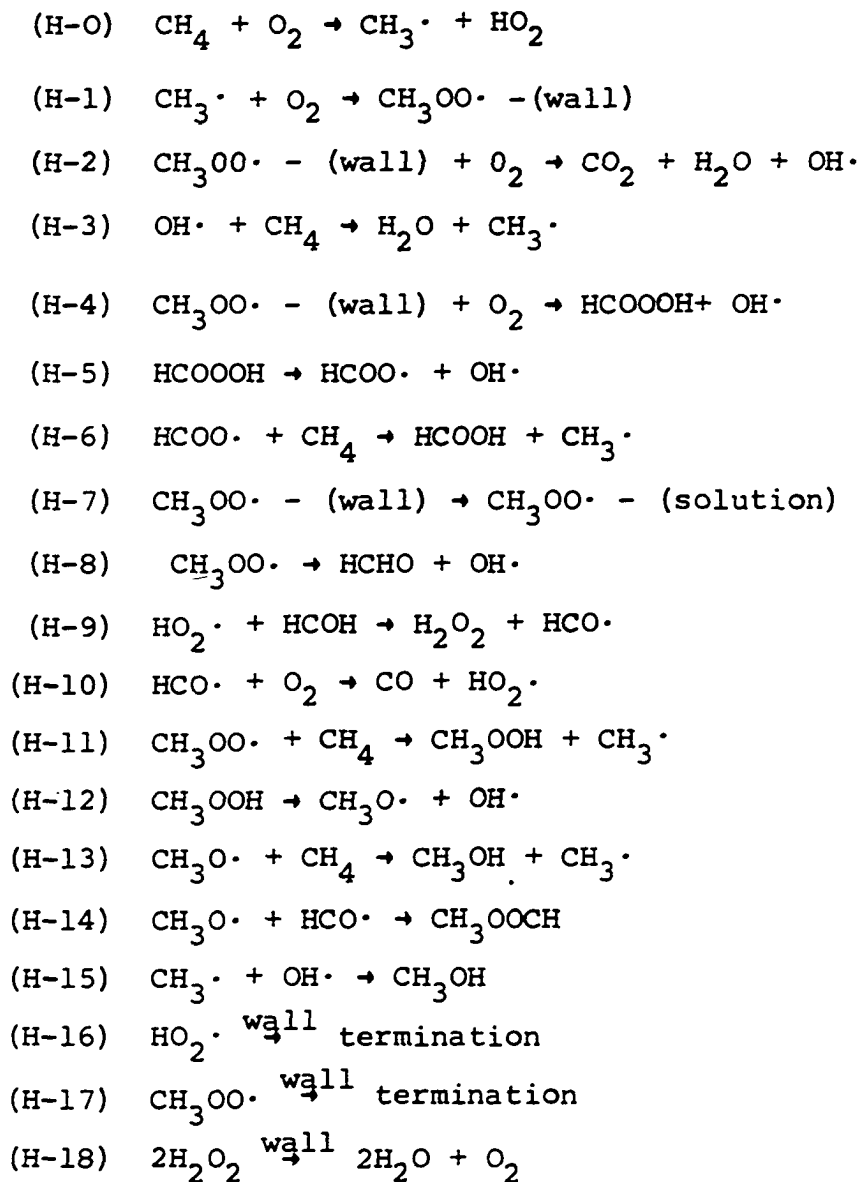
Figure 9. Trend in Methane Conversion with Increasing Pressure. (From Lott and Sliepcevich, Ref. 36, Reproduced by Permission.)

- (L-5) $\text{CH}_3\text{OO}\cdot \rightarrow \text{HCHO} + \text{OH}\cdot$
 (L-6) $\text{OH}\cdot + \text{CH}_4 \rightarrow \text{H}_2\text{O} + \text{CH}_3\cdot$
 (L-7) $\text{OH}\cdot + \text{HCHO} \rightarrow \text{H}_2\text{O} + \text{HCO}\cdot$
 (L-8) $\text{HCHO} + \text{O}_2 \rightarrow \text{HCO}\cdot + \text{HO}_2\cdot$
 (L-9) $\text{HCO}\cdot + \text{O}_2 \rightarrow \text{HO}_2\cdot + \text{CO}$
 (L-10) $\text{HO}\cdot \xrightarrow{\text{wall}}$ chain breaking
 (L-11) $\text{CH}_3\text{OO}\cdot \xrightarrow{\text{wall}}$ chain breaking

In comparison with the mechanism of Semenov (63), several similarities are apparent. The initiation step L-0 is identical. Lott's reactions L-1 and L-5 combine into Semenov's reaction S-1: the peroxide radical is thought to be preserved for a more lengthy period at elevated pressure. Lott did not, however, stipulate a third order for reaction L-1 as did Medley and Cooley (40). The major differences between Lott's and Semenov's mechanisms appear in the reactions involving CH_3OOH and $\text{CH}_3\text{O}\cdot$. These latter steps were also suggested by Medley and Cooley. No reactions were considered by Lott involving hydrogen peroxide.

Hardwicke (26) performed tests with a nominal 10/1 methane-oxygen mixture at pressures up to 5,400 atm under isothermal conditions. He studied the effects of residence time and temperature on product distribution. It was found that carbon dioxide was formed in some tests long before the presence of carbon monoxide was detected. The conclusion was that carbon monoxide, carbon dioxide and methanol are all made by different mechanisms. Hardwicke

also thought that the methyl peroxy radical $\text{CH}_3\text{OO}\cdot$ was important at high pressures. His overall mechanism, incorporating these findings, is as follows:



where $\text{CH}_3\text{OO}\cdot - (\text{wall})$ represents a complex at the wall.

While Lott considered the formation of methyl formate to be a molecular reaction between methanol and formic acid, Hardwicke suggested chain production of the

ester (reaction H-14). Hardwicke also considered the possibility of formation of methanol from methyl and hydroxy radicals (reaction H-15).

Hardwicke considered reactions H-0 through H-8 as predominant up to 285°C. To make his scheme consistent with a high-temperature mechanism, he suggested the methyl peroxide radical can be complexed at the wall. Assuming the attachment point to be the oxygen end of the molecule, he suggested the complete destruction of the molecule is due to attack by additional oxygen on the methyl end of the complexed radical, with a small amount of performic acid produced (reactions 2 and 4). Because of the delay in observed formation of carbon monoxide, free $\text{CH}_3\text{OO}\cdot$ radicals were considered to be only available for production of formaldehyde (via reaction H-8) after the finite period of time it takes for the radicals to occupy all available wall sites.

At 285°C reactions H-9 and H-10 become important. At these temperatures, Hardwicke observed early production of carbon monoxide. Reactions H-11 through H-13 were thought to be important, based on trends observed in forming methanol. The remaining steps are termination reactions.

Hardwicke's reaction H-9 and Lott's reaction L-7 consider attack on formaldehyde by two different chain carriers. Since neither detected peroxide in the reaction products, there may be no basis for selecting the route

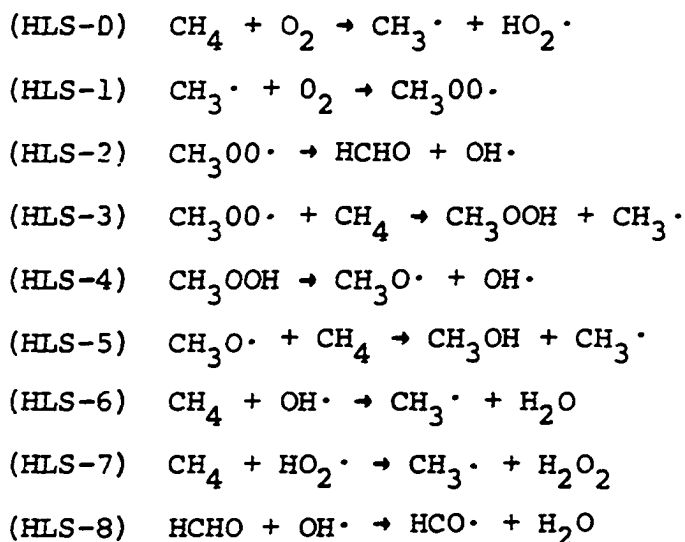
which produces H_2O_2 . Hardwicke also omitted direct attack of oxygen on formaldehyde on the basis that the reaction is not competitive with radical attack.

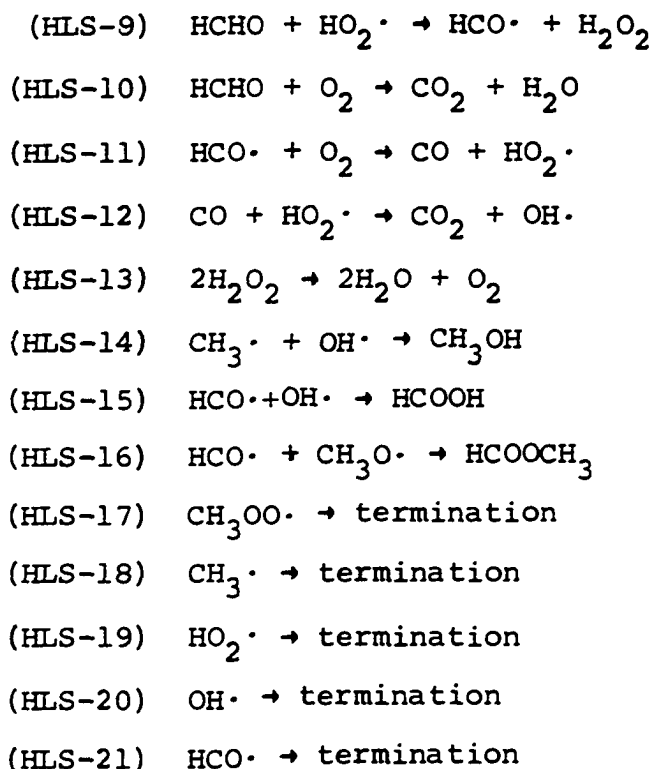
Hardwicke calculated overall reaction rates according to an equation of the form:

$$w = - \frac{d[\text{O}_2]}{dt} = k [\text{CH}_4]^m [\text{O}_2]^n \quad (34)$$

His data correlated with $m = 2$ and $n = -2$. He obtained an overall activation energy for oxidation of 40-60 kcal/mole. The orders imply an inhibiting effect due to oxygen.

Hardwicke, Lott and Sliepcevich (27) later re-evaluated all data taken under high pressure conditions in various studies at the University of Oklahoma and collaborated on a revision of the individual mechanisms of Hardwicke and Lott. A mechanism explaining the differences observed between low and high pressure oxidation of methane was suggested by the authors:

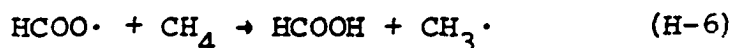




Hardwick's original suggestion that the methyl peroxy radical ($\text{CH}_3\text{OO}\cdot$) is complexed at the wall and that adsorption processes determine the induction time was abandoned. In its place was substituted the premise that $\text{CH}_3\text{OO}\cdot$ is sufficiently stable at elevated pressures for simultaneous attack by methane and decomposition into formaldehyde and $\text{OH}\cdot$ radicals to occur. The attack of $\text{HO}_2\cdot$ radicals on carbon monoxide was also included.

The authors considered the formation of hydrogen peroxide directly from methane and $\text{HO}_2\cdot$ to be significant (reaction HLS-7). They also considered reaction of formaldehyde to occur with $\text{OH}\cdot$, $\text{HO}_2\cdot$, and oxygen.

Hardwicke originally considered the formation of formic acid to be a chain propagation step:

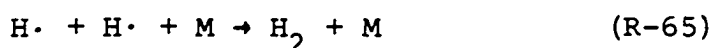
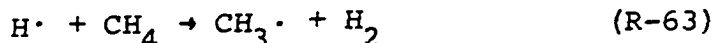


whereas, in the above mechanism, he and his co-authors have altered the scheme in favor of a termination reaction between $\text{OH}\cdot$ and $\text{HCO}\cdot$ (reaction HLS-15). Reaction HLS-10 was included to explain the early appearance of carbon dioxide.

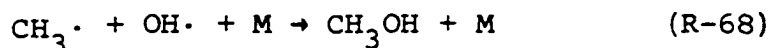
A significant experimental observation in the isothermal tests was that the ratio of the sum of concentrations of formaldehyde, carbon monoxide, and carbon dioxide to that of methyl alcohol was of the order of 24. In non-isothermal tests, in which the heat production exceeded surface dissipation, the ratio dropped to about 5. These low values were experienced regardless of the extent of adiabatic temperature rise. Since theoretical considerations dictate that methyl hydroperoxide should decrease with temperature, all methanol cannot be produced through reaction HLS-5 via HLS-2, HLS-3, and HLS-4. The termination step (reaction HLS-14) was thus included.

This latter termination step, resulting in the production of methanol, is in accord with the mechanism of Melvin (41). In his work, Melvin explosively reacted methane and air at pressures up to 110 atmospheres and at such high temperatures that very short ignition delays were observed. Relatively large amounts of hydrogen and ethane were produced; traces of other hydrocarbons, including n-butane, iso-butane and 1,3-butadiene, were

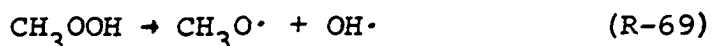
also produced. During the period of fast explosive pressure rise, hydrogen atoms were suggested as being influential in the mechanism. Melvin suggested that oxygen-sensitized pyrolysis produces hydrogen atoms which enter a series of steps:



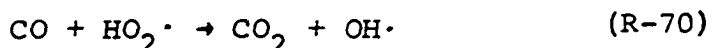
An activation energy of 20 to 25 kcal/mole was measured during initial stages of explosion, which is close to the activation energy for the branching process between hydrogen atoms and oxygen in the explosion peninsula between the first and second limits as measured by Nalbandyan (44) and by Alyea and Frost (3). During the ignition delay period, Melvin observed relatively little change in rate due to oxygen concentration. As explosion is initiated, the order with respect to oxygen jumps to two. Melvin observed an increase in methanol concentration as the oxygen level was decreased. Because of the above branching step producing hydroxyl radicals ($\text{OH}\cdot$), the availability of these latter chain carriers should increase leading to the reaction:



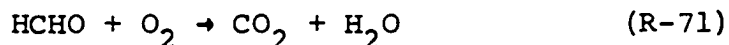
as represented in a second order scheme by Hardwicke, Lott and Sliepcevich (27). In their scheme, it is likely that an abundance of OH· radicals might occur through destruction of methyl hydroperoxide:



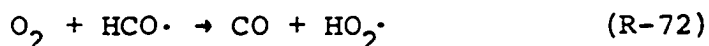
or the sudden attack on carbon monoxide by HO₂· radicals



The second step is probably not predominant because the data of Hardwicke did not show a sharp decrease in carbon monoxide as the reaction became adiabatic. A general increase in both carbon monoxide and carbon dioxide was seen, however, which implies the simultaneous attack of oxygen on formaldehyde, as in the low pressure scheme:



with a reaction between oxygen and HCO· radicals,



to complete the cycle. These steps are included in the mechanism of Hardwicke, Lott and Sliepcevich (see page 77) as reactions HLS-10 through HLS-14. Carbon monoxide concentration in the explosive or non-isothermal regime would undergo relatively little change if reactions HLS-11 and HLS-12 are of approximately equal rates and carbon dioxide could build up through reactions HLS-10 and HLS-12.

Hardwicke, Lott and Sliepcevich (27) determined the isothermal rate of reaction at very fuel-rich (10:1) conditions. An overall rate equation of the form:

$$-\frac{d[O_2]}{dt} = k [O_2]^{-2} \quad (35)$$

was found to correlate data from 1000 atm to 6600 atm. An activation energy of 42.9 kcal/mole was determined.

Newitt and Haffner (46) pointed out that from simple stoichiometric and thermodynamic considerations, methanol production should be favored at elevated pressures. They considered the complete reactions:

- (1) $2CH_4 + O_2 \rightarrow 2CH_3OH + \dots 2 \times 29,730 \text{ cal.}$
- (2) $2CH_3OH + O_2 \rightarrow 2HCHO + 2H_2O + \dots 2 \times 20,640 \text{ cal.}$
- (3) $2HCHO + O_2 \rightarrow 2HCOOH + \dots 2 \times 81,540 \text{ cal.}$

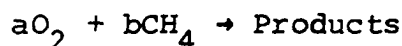
They concluded the above because methyl alcohol and formic acid are formed with a contraction in volume and formaldehyde involves an expansion. Hence, increase in pressure favors survival of alcohol and acid at the expense of formaldehyde. The mechanism lent strong support to the hydroxylation theory of Bone et al.* More recent works, as stated earlier, have shown that methyl alcohol is not made in significant quantity until the onset of explosion.

*See the excellent chronicle of the efforts of Bone and his co-workers in Ref. (66).

energy to be 44-46 kcal/mole. Yenikolopyan's work was done at 235 mm Hg initial pressure and temperatures from 423° to 513°C.

Other workers have found various values for activation energy. Table 3 summarizes some of these works. It is interesting to note that the activation energy appears to increase as temperature is reduced. If there is no direct effect of pressure on the activation energy, high pressure oxidation performed at low temperatures should then show a high activation energy.

Assuming a general, overall reaction of the form:



The reaction rate is given by

$$\text{Rate} = -\frac{1}{a} \frac{d[O_2]}{dt} = -\frac{1}{b} \frac{d[CH_4]}{dt} \quad (37)$$

The individual depletions are given by

$$-\frac{d[O_2]}{dt} = k_1 [O_2]^a [CH_4]^b \quad (38)$$

and

$$-\frac{d[CH_4]}{dt} = k_2 [O_2]^a [CH_4]^b \quad (39)$$

Thus, $k_2 = \frac{b}{a} k_1$, and activation energies are identical in describing rate equations based on either initial reactant.

It has been shown that an exponential relationship theoretically exists between induction time and $1/T$ or between ignition delay and $1/T$. Melvin (41) showed that

TABLE 3

VALUES OF E OF THE OXIDATION REACTION OF METHANE

Hydro-carbon	E kcal/mole	Temperature Range °	Mixture	Reaction Vessel	
CH ₄	92	423--447	2CH ₄ +O ₂	Quartz	
	46	420-490	CH ₄ +2O ₂	Quartz, "old"	
	51*				
	40	475-500	2CH ₄ +O ₂	Quartz, HF treated	
	25	500-525	2CH ₄ +O ₂	Ditto	
	43	625-675	CH ₄ +O ₂	"	
	65	462-500	2CH ₄ +O ₂	Quartz, heat treated	
	57	600-675	2CH ₄ +O ₂	Ditto	
	Decreases from 65 at 475° to 50 at 525°		475-525	2CH ₄ +O ₂	"
	Decreases from 96 at 475° to 65 at 525°		475-525	CH ₄ +2O ₂	"

*From various works of Walsh, A. D., reported by Shtern (64).

activation energy for ignition delay determined by such a relationship is close to that determined by considering either product depletion or the rate of molar increase as the dependent variable in selecting a rate equation.

The Effect of Surfaces and Catalysts

From the first experimental work in oxidation of methane, it has been known that the reaction is extremely surface sensitive. The exact nature of the surface effect has not been fully understood. Only through radical chain theory have mechanisms which appear to point in the proper direction been formulated, but a full understanding of the effect is still far from being a reality.

As recently as 1931, Newitt and Haffner (46) concluded that the oxidation reaction in a steel vessel, being heterogeneous, is enhanced by increasing the surface/volume ratio in the reactor. It may be that their conclusion was based on an increase in water and carbon oxides at high surface/volume ratios.

Pease and Chesebro (55) in 1928, however, found that rate of oxidation of methane at 500°C in an empty glass tube was many times greater than in a tube filled with broken glass. Fort and Hinshelwood (16) observed the same effect in a quartz reactor. Bone and co-workers (10,11) observed the same effect with methane, ethane, and ethylene oxidation. Fort and Hinshelwood (16) determined that reaction rate was proportional to the vessel diameter to a power of 3 or 4.

Norrish and Reagh (51) studied the effect of vessel diameter on the rate of reaction at low pressures. They found that after an increase in vessel diameter above 16 mm, no further change in reaction rate occurred; below 5 mm the reaction could not be initiated even after 24 hours.

An interesting program by Kovalskii, Cherkov and Sadovnikov (33) in 1931 showed somewhat contrary results. They found that hydrofluoric treatment of the surface of a quartz vessel promoted the oxidation of ethane under stoichiometric conditions with oxygen. Exposure of the treated vessel to temperatures near the fusion point of quartz re-established the original slower rate of reaction. It was concluded that HF etching increased surface area tremendously and the added surface enhanced the reaction.

Shtern (66) pointed out that the retarding action of a surface can be due to chain breaking and termination steps, while accelerating action can be caused by initiation and branching steps. He cited the known initiating role of surfaces in a number of chain processes such as addition of hydrogen and chlorine, chlorination of ethylene and decomposition of several chlorine derivatives of hydrocarbons.

Kovalskii, Cherkov and Sadovnikov (33) made another discovery in the course of conducting oxidation of ethane in a quartz vessel. They found that the reaction rate increased with each successive test and attributed the result

to an increase in surface activity. Assuming that some material was continuously deposited or adsorbed, they subjected their reactor to evacuation at 1100°C before several experiments. They found the surface still active. The authors then assumed that successive reactions remove substances detrimental to reaction.

von Elbe, Lewis and Roth (74) determined that the opposite effect occurs in the oxidation of carbon monoxide at the second pressure limit. They found that evacuation of their quartz vessel to 10^{-6} mm and heating to 800°-900°C prior to a test enabled reproducible results; omission of the "bake-out" procedure resulted in erratic data. The general trend was observed that higher temperatures were necessary for explosion if the reactor was not conditioned.

They assumed that, since carbon monoxide was the only product, some dioxide must be adsorbed, and in some manner this process increased chain-breaking efficiency of the wall. They tested the theory by admitting a small amount of carbon dioxide to a "baked-out" vessel and then pumping out the carbon dioxide at room temperature. The results were equivalent to those obtained with an unbaked vessel.

Hoare and Walsh (28) established that activation energies and orders of reaction depend on the nature and the surface state of a vessel. They used four quartz vessels subjected to different treatments and compared the results. Figure 10 shows their observations in the form of pressure

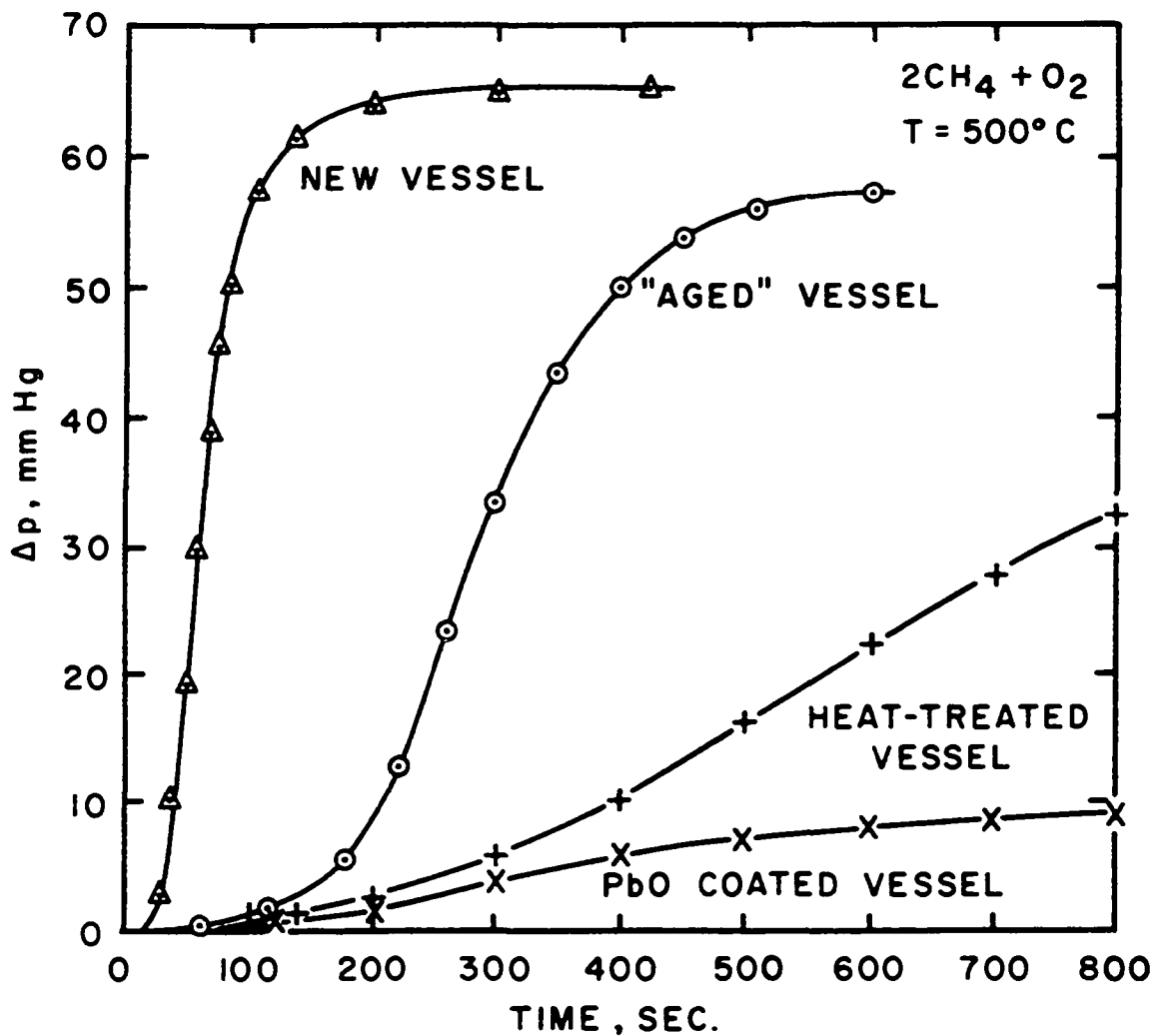


Figure 10. A Comparison of the Reaction Rates of Methane Oxidation in Vessels with Differently Treated Surfaces. (Initial Pressure: 450-500 mm Hg) (28).

rise as a function of time. They considered the "old" vessel as one which, through repeated tests, experienced devitrification of the quartz surface. The heat treatment involved a "bake-out" procedure similar to that of von Elbe et al. (28), mentioned above. The orders of reaction and the calculated activation energies are given in Table 4.

The orders presented in the table refer to a rate equation of the form:

$$w_{\max} = \alpha [\text{CH}_4]^m [\text{O}_2]^x [\text{N}_2]^t e^{-E/RT} \quad (40)$$

A sharp change in activation energy between "old" and acid treated vessels is shown. Table 5 shows similar observations over a higher temperature range. Both sets of data were obtained at low pressures. Because the authors found that activation energy was a function of both temperature and composition, a rate equation of the above form was not considered to be adequate. Searching for a mechanism to explain the results, Hoare and Walsh determined that carbon monoxide oxidation is strongly influenced by HF treatment.

Homogeneous catalysis has been studied by several authors. The accelerating effect of substances such as nitrogen dioxide, chlorine, bromine, hydrogen chloride, etc. has been well documented. Substances which could change the reaction through other chemical routes were, until recently, purely hypothetical. Rust and co-workers (60) discovered a change in chemical nature of oxidation

TABLE 4

THE REACTION ORDERS AT 500°C AND ACTIVATION ENERGIES
IN THE RANGE 462.5-525°C (27).

Reaction orders: m with respect to $[\text{CH}_4]$, x with respect to $[\text{O}_2]$, n with respect to $[\text{CH}_4+\text{O}_2]$, t with respect to $[\text{N}_2]$, E is the activation energy

	Vessel			
	Treated with HF	"Old"	Heated	Coated with PbO
n for $2\text{CH}_4+\text{O}_2$	3.3	4.8	4.8	4.9
m for	CH_4+2O_2 up to $2\text{CH}_4+\text{O}_2$	CH_4+5O_2 up to $5\text{CH}_4+\text{O}_2$	CH_4+2O_2 up to $5\text{CH}_4+2\text{O}_2$	CH_4+3O_2 up to $5\text{CH}_4+2\text{O}_2$
	1.6	2.3 to 1.9	2.4	2.0 to 2.4
x for	CH_4+2O_2 up to $2\text{CH}_4+\text{O}_2$	CH_4+3O_2 up to $7\text{CH}_4+\text{O}_2$	CH_4+6O_2 up to $2\text{CH}_4+\text{O}_2$	$2\text{CH}_4+5\text{O}_2$ up to $4\text{CH}_4+\text{O}_2$
	1.2	1.0 to 2.0	1.0 to 1.6	1.55
t for $2\text{CH}_4+\text{O}_2$	0.5	0.85	0.9	0.9
E for $2\text{CH}_4+\text{O}_2$ at	(300 mm) 475-525°	(450 mm) 475-525°	(700 mm) 462.5-500°	(700 mm) 462.5-525°
kcal/mole	Decreases from 40 at 475° to 25 between 500 & 525°	Decreases from 65 at 475° to 50 at 525°		
E for CH_4+2O_2 at	500-525° (150 mm)	475-525° (500 mm)		
kcal/mole	Decreases from 32 at 500° to 25 at 525°	Decreases from 96 at 475° to 65 at 525°		

TABLE 5

REACTION ORDERS AT 650° AND ACTIVATION ENERGIES
IN THE RANGE 575-675° DURING METHANE OXIDATION
(27)

Reaction orders: m with respect to $[\text{CH}_4]$; x with respect to $[\text{O}_2]$; n with respect to $[\text{CH}_4+\text{O}_2]$; t with respect to $[\text{N}_2]$, E is the activation energy.

	Vessel		
	Treated with HF	Heated	Coated with PbO
n for $2\text{CH}_4 + 3\text{O}_2$	--	3.4	3.7
n for $2\text{CH}_4 + \text{O}_2$	--	3.6	--
m for	$\text{CH}_4 + 2\text{O}_2$ up to $4\text{CH}_4 + \text{O}_2$ -1.0 to +0.4	$\text{CH}_4 + 2\text{O}_2$ up to $2\text{CH}_4 + \text{O}_2$ 0 to 0.7	$\text{CH}_4 + 2\text{O}_2$ up to $3\text{CH}_4 + \text{O}_2$ 0.2 to 1.0
x for	$\text{CH}_4 + 2\text{O}_2$ up to $2\text{CH}_4 + \text{O}_2$ 2.7 to 2.7	$\text{CH}_4 + 2\text{O}_2$ up to $2\text{CH}_4 + \text{O}_2$ 2.7 to 2.3	$\text{CH}_4 + 2\text{O}_2$ up to $6\text{CH}_4 + \text{O}_2$ 3.0 to 2.0
t for $2\text{CH}_4 + 3\text{O}_2$	Negative	0.4	0.3
t for $2\text{CH}_4 + \text{O}_2$	--	0.6	--
E kcal/mole for	$\text{CH}_4 + \text{O}_2$, 50 mm and 625-675° 43	$2\text{CH}_4 + 3\text{O}_2$, 100 mm and 600-675° 76	$2\text{CH}_4 + 3\text{O}_2$, 300 mm and 575-602.5° 57 to 48
E kcal/mole for		$2\text{CH}_4 + \text{O}_2$, 150 mm and 600-675° 57	$2\text{CH}_4 + 3\text{O}_2$, 200 mm and 600-662.5° 70 to 55

of propane by addition of hydrogen bromide. Maizus and Emanuel (37) performed a series of tests to investigate the preliminary results of Rust. Similar tests with nitrogen dioxide as a homogeneous additive were performed by Kane and Townend (30) after preliminary observations by Bone and Gardner (11), Bone and Allum (9), and Norrish and Wallace (52).

Shtern (66) presents convincing arguments to show that formation of some desirable, oxygen-containing products in increased amount due to catalysis is impossible. As far as alcohols, acids, ketones, and esters are concerned, the problem of increasing yields reduces to the problem of increasing the proportion of hydrocarbon that undergoes reaction. This increase may in some way be accomplished by shifting the termination reaction so that cessation of oxidation is accomplished, by adding extra oxygen after initial reaction, or by increasing the chain length. With aldehydes, however, which are intermediates and not end-products, the cessation of oxidation is not considered by Shtern to be feasible. He and Yenikolopyan (81) cited experimental evidence that catalysis cannot change the yield of formaldehyde. Shtern also stated that addition of substances capable of initiating free radicals more readily than the reactants, addition of an inert gas, variation in vessel size, and treatment of walls cannot increase aldehyde output. The argument is based on the following:

Consider the chain formation of an intermediate B and its subsequent reaction to end-product C by the scheme:



The rate of accumulation of B is given by:

$$\frac{d[B]}{dt} = \sum_{ij} A_{ij} N_i - \sum_{kl} B_{kl} N_l \quad (41)$$

which is a condensed version of the overall equation describing formation and destruction of B. Appendix B describes the formulation of the necessary equations for a chain sequence. The coefficients A_{ij} and B_{kl} are the kinetic coefficients equal to the product of a constant (reaction rate constant) and the concentration of the corresponding initial reactant or intermediate. The variables N_i and N_l are concentrations of active centers. Thus, in the above equation, the first term on the right is the sum of all elementary processes leading to formation of B, while the second term is the sum of all elementary processes leading to consumption of B. When $d[B]/dt$ is equal to zero, the concentration $[B]$ is at a maximum. The problem becomes that of showing that any change in N_i must be accompanied by a corresponding change in N_l and the maximum concentration of B is unchanged. Yenokolopyan considered two cases.

In the first case, a slowly reactive center N_1 is spontaneously initiated, the breaking of which determines the chain length. The concentration of active centers with time is described by a set of equations:

$$\frac{dN_1}{dt} = w_0 + \sum_i A_{ij} N_j - gN_1 \quad (42)$$

$$\frac{dN_j}{dt} = \sum_i A_{ij} N_j \quad (j \neq 1) \quad (43)$$

where A_{ij} are kinetic coefficients of the propagation reactions and g is the reaction constant for the chain breaking step. The destruction of the other rapidly reactive centers is neglected. The formation and consumption steps are included in the A_{ij} (the B_{ij} , as in equation 41, are included in the A_{ij} and are given opposite signs). Defining:

$$d_i = \frac{dN_i}{dt} \quad (i \neq 1) \quad (44)$$

and

$$d_1 = \frac{dN_1}{dt} + gN_1 - w_0 \quad (45)$$

The set of equations (45) reduces to a single matrix equation:

$$\vec{d}_i = [A_{ij}] \vec{N}_i \quad (46)$$

If all d_i can be assumed zero, the solution is:

$$N_i = \alpha_{ij} N_j \quad (47)$$

where the α_{ij} are constants. That is, all concentrations of active centers remain in proportion.

A second case, considered by Yenikolopyan, is one in which a rapidly reactive center is initiated spontaneously. The system of equations is of the form:

$$\frac{dN_1}{dt} = w_0 + \sum_j A_{1j} N_j = 0 \quad (48)$$

$$\frac{dN_2}{dt} = \sum_j A_{2j} N_j - g N_2 = 0$$

$$\frac{dN_i}{dt} = \sum_j A_{ij} N_j \quad (i \neq 1, 2) \quad (50)$$

In this set, it is assumed that termination is determined by destruction of some radical other than that generated in an initiation step. The matrix equation (46) applies with the definitions:

$$d_i = 0 \quad (i \neq 1, 2)$$

$$d_1 = -w_0$$

$$d_2 = gN_2$$

Again by assuming, instead, that all d_i are zero, the system of equations is solved as before:

$$N_i = \alpha_{ij} N_j \quad (49)$$

Substituting this expression into equation 41 where, as mentioned, the B_{kl} assume values of A_{ij} (negative values due to depletion steps) and letting the derivative go to

zero, the equation assumes the general form:

$$[B]_{\max} = f(A_{ij}) \quad (51)$$

Since a kinetic coefficient is defined as the product of a specific reaction rate constant (k_{ij}) and the concentration of the initial reactant, equation 51 is of the form:

$$[B]_{\max} = f(k_{ij} A_0) \quad (52)$$

where A_0 is the initial concentration of reactant A.

This result means any action leading to a change in concentration of initial active centers cannot lead to a change in the maximum concentration of the stable intermediate. Shtern points out that the development is valid only with very long chains. Further, the vector \vec{d}_i is not identically zero unless all termination and initiation steps are negligible.

To verify the result, Yenikolopyan studied oxidation of methane at 494°C under various conditions. Addition of inert gases, variation in vessel diameter, treatment of vessel, packing the reactor, and addition of homogeneous catalysts were the variables under study. Table 6 shows the results of the investigation as summarized by Shtern (66). It is seen that the maximum concentration of formaldehyde remained essentially constant, while the various system alterations changed the maximum rate of reaction. In view of the results

TABLE 6

THE VARIATION OF w_{\max} AND $[\text{HCHO}]_{\max}$ WITH TREATMENT
OF THE REACTION VESSEL

Mixture: $\text{CH}_4 + 2\text{O}_2$; $T = 494^\circ$

Treatment of vessel, catalyst	$[\text{HCHO}]_{\max}$ mm Hg	w_{\max} mm/Hg min
$\text{K}_2\text{B}_4\text{O}_7$ with packing, 0.1% NO_2	0.27	0.184
$\text{K}_2\text{B}_4\text{O}_7$ with packing, 0.5% NO_2	0.26	0.29
HF with packing, 0.5% NO_2	0.26	0.65
HF without packing, 0.1% NO_2 d = 33 mm	0.27	0.75
KCl without packing, 0.5% NO_2 d = 57 mm	0.26	1.5
H_2O without packing, 0.5% NO_2 ; d = 57 mm	0.25	1.72
H_2O without packing, without NO_2 ; d = 57 mm	0.21-0.24	

(Table reproduced from Ref. 66)

of Norrish and Reagh (page 87), the variation in rate was undoubtedly more dependent on catalyst addition than on the vessel diameter changes. Yenikolopyan concluded that any change in concentration of active centers cannot have as a result a change in the maximum concentration of intermediate products. He pointed out, however, that the result applies only to intermediates formed and consumed by chain means. If it is possible to obtain any method of consumption of intermediate by molecular or physical means, the concentration can be varied. Molecular depletion would then correspond exactly to the situation in matrix equation 46 when all d_i are not zero.

Yenikolopyan's analysis is valid only at conditions when $[B]$ is at a maximum. Variation in $[B]$ can be possible through changes in w_0 (again, all d_i are not zero). For instance, Yenikolopyan did not report whether the reaction could be made to occur at a lower temperature through catalysis. By causing the reaction to proceed at lower temperatures, the A_{ij} coefficient might be altered due to influence of activation energy terms, and the entire matrix equation could then be altered.

Medley and Cooley (40) presented a summary of state-of-the-art in theoretical and commercial liquid-phase oxidations. They showed selectivity of product distribution in the use of catalysts and strong variations in distribution from catalyst to catalyst. Tables 7 and 8 show the selectivity possible in the use of catalysis. The liquid phase work

TABLE 7

THE COMPOSITION OF THE PRODUCTS AT THE END OF THE
OXIDATION REACTION OF BUTANE - NO CATALYST

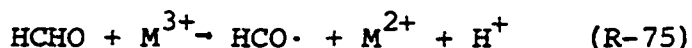
Mixture: $n\text{-C}_4\text{H}_{10} + \text{O}_2$; $P_{\text{init.}} = 500 \text{ mm Hg}$; $T = 270^\circ$.

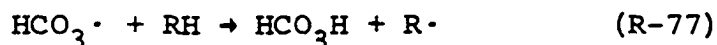
Product	Pressure, mm Hg	Product	Pressure, mm Hg
n-Butane	180	CO	68
Formic Acid	11	CO ₂	65
Acetic Acid	20	Acetone	8
Methyl Alcohol	38	Water	140
Methane	13	Formaldehyde	20

From Shtern (Ref. 66).

was done under very fuel-rich conditions, possible accounting for the wider distribution of products. Also, the pressure effect undoubtedly accounted for the increase in liquid products. It can be seen, however, that oxidation is not driven to completion and that even variation in catalyst can change the product distribution.

Because the density in a dense fluid system at extreme pressure approaches that of liquids, it is very likely that catalyzed high pressure oxidation of methane can undergo processes similar to liquid phase reactions. For instance, in the catalyzed oxidation of butane most of the formaldehyde goes to performic acid (40):





where M^{3+} is a metal catalyst in a trivalent state, while M^{2+} is the metal in a divalent oxidation state. Performic acid then goes to formic acid by:

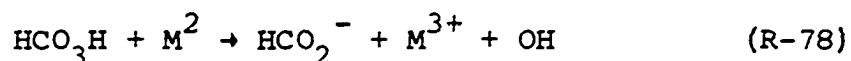


TABLE 8

LIQUID PHASE OXIDATION OF BUTANE IN A SOLVENT

(Pressure, 55 atm; temperature, 171-178°C) (39)

	Cobalt Catalyst	Manganese Catalyst
Liquid Product Distribution, wt. %		
Acetic acid	76	62
Formic acid	6	23
Acetaldehyde	1	1
Acetone	1	2
Methyl ethyl ketone	1	2
Ethyl alcohol	6	7
Methyl alcohol	4	3
2-Butanol	2	1
Propionic acid	Trace	Trace
Butyric acid	Trace	Trace
γ -Butyrolactone	Trace	Trace
Gaseous Product Distribution, wt. %		
Carbon dioxide	70	66
Carbon monoxide	21	25
Methane	4	3
Ethane	5	6

Little work has been performed, other than the low pressure studies of Yenikolopyan (81), Rust (60), Maizus and Emanuel (37), Kane and Townend (30, Bone and Allum (10)

and Hoare and Walsh (28) on the catalyzed oxidation of methane. The only data available on surface and catalytic effects in high pressure oxidation have been generated incidentally to the main objectives of early programs. That is, some authors observed the effect of reactor "aging" and the influence of the nature of the surface of internal heaters (26).

Some experimental work has been done on the catalytic oxidation of hydrocarbons at low or moderate pressures. Considerable recent work has involved very low hydrocarbon concentrations in air as the reacting mixture. This work has been performed with anti-pollution of exhaust streams as a major objective. Accomazzo and Nobe (1) studied the oxidation of methane and other hydrocarbons in concentrations less than 1450 ppm over the temperature range 140-510°C. They determined, in their flow reactor, an activation energy of 23,000 cal/mole.

Mezaki and Watson (42) concluded, from their study of oxidation of methane on palladium catalyst, that the rate determining step is the gaseous reaction of methane with absorbed oxygen.

CHAPTER IV

EXPERIMENTAL EQUIPMENT

The major portion of the experimental equipment has been described in detail elsewhere (26, 35), but sufficient modifications have been made to warrant a brief description of the apparatus. Following the convention employed in previous, more detailed descriptions (see above references), the overall system has been divided into the following basic units: feed section, compression section, reaction section and product collection section. A flow diagram of the feed and compression sections is shown in Figure 11. Figure 12 shows a flow diagram of the reaction and product collection sections.

Feed Section

Because of the explosion hazard involved in mixing methane and pure oxygen, feed preparation was conducted at low pressures. Actual mixing processes were all performed at pressures no greater than 7.5 atm. A secondary purpose for selection of this lower mixing pressure was that it enabled more complete depletion of the standard 1-A methane feed cylinders.

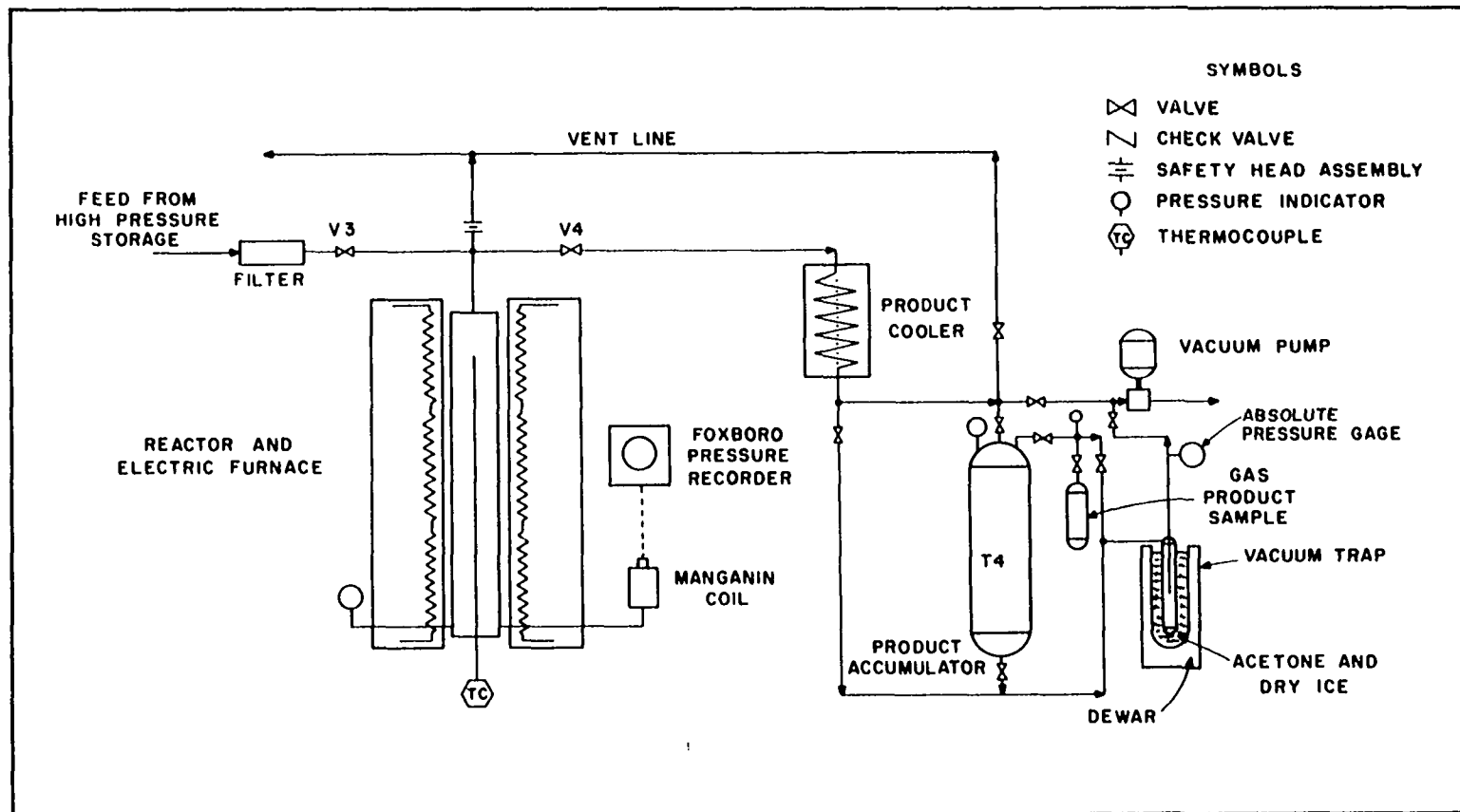


Figure 12. Process Flow Diagram of Reaction and Product Collection Systems. (From Lott (35) reproduced by permission.)

Methane and oxygen were fed alternately to the mixing tank (T1) through temporary lengths of copper tubing. This vessel was a conventional, breathing-air, supply bottle of 27 atm working pressure and had a volume of 300 liters. The vessel was equipped with a 34-atm working-pressure sight-gage.

Because the resultant pressure of the mixture was too low for practical utilization, the mixture was brought to about 20 atm by pumping water into the mixing tank. A Sprague air-operated piston pump, Model S-16C-100, performed this operation. This pump was capable of operation to 600 atm with an air supply of 6.8 atm. A 60 liter carboy was used to store the feed water. A filter in the feed line was incorporated. A fresh water feed line to the carboy was used to replenish the supply.

The mixture was transferred to a storage tank (T2) constructed of 4340 steel by Autoclave Engineers, Inc. This vessel was 20-cm diameter x 132-cm internal length with a working pressure of 1000 atm. The vessel was equipped with a safety head, in which a 1360-atm burst-disc was installed.

The transfer operation was conducted using a twin-cylinder displacement unit (P2), built at the University of Oklahoma. The gas mixture was admitted to one of the two cylinders, each approximately 18 liters in capacity; the cylinder was closed off, and hydraulic oil was pumped into the cylinder until the gas ullage was brought to about 400

atm. A Simplex, Model 20LA-H radial pump (P1), rated at 2.3 liters/min at 680 atm, was used to transfer the oil. After the pumping operation, a needle valve (V1), between the displacement unit and the storage tank, was opened to allow flow of the gas mixture to the storage tank until the pressures were equalized. The second cylinder was then filled with gas mixture and the operation was repeated. As this second cylinder was being filled with oil, the first cylinder was drained back to the oil supply reservoir. International Harvester Hi-Tran fluid was used as the hydraulic oil. All transfer lines to the storage tank were 6.35-mm x 3.2-mm stainless steel tubing with "Ermeto" fittings, with the exception of the inlet ports of the storage tank, which were Autoclave Engineers, Inc. "AE-cone" fittings. Additional pressurization of the gas mixture in the storage tank was accomplished by pumping water into the vessel, using the Sprague air pump. This gas accumulator (T2) thus became the primary storage vessel. The pressure level in this vessel was generally held at about 400 atm.

Because the gas mixture in the storage tank was pumped with and stored over water, a drier was installed immediately downstream of the vessel. The drier was a two-unit series train made from two Kuentzel pressure bombs. These stainless steel vessels, manufactured by Autoclave Engineers, Inc., were 2.54 cm i.d. x 20 cm internal length. Drierite was used as the drying agent. To avoid carryover

of particulate matter, the drier train was followed by a sintered metal filter cell, also manufactured by Autoclave Engineers, Inc.

All connections, fittings, and vessels between the primary storage tank and the compression section of the system were rated at 680 atm.

Compression Section

The dried, filtered gases leaving the primary storage tank at 400 atm (nominal) were further compressed before storage in the run feed tank (T3). A small batch compressor (C1), capable of pressurization to 1700 atm, was used to pressurize the feed gases.

The compressor was made from a cylindrical vessel, 3.34 cm i.d. x 7.62 cm o.d. x 40.7 cm internal length, lapped for internal uniformity. The single closure, sealed with an O-ring, had a tee-arrangement for two 14.3-mm AE cone connections. The other end of the compressor had a single 14.3-mm AE cone connection machined into the closed end.

Gases were compressed by pumping with oil, which was separated from the gas phase by a floating piston constructed of T6061 aluminum. The piston had a single O-ring seal.

The tee end of the compressor was placed downward with one lead, adapted to 6.35-mm "AE-cone" fittings, connected to a high pressure, air-operated oil pump (P3). The other branch of the tee was also reduced to 6.35-mm tubing

and became the oil return port.

The other end connection served the dual function of feed port and outlet. Autoclave Engineers 2000-atm valves were used to seal the compressor during operation. A check valve was placed immediately downstream of the compressor outlet to prevent return of high pressure gas from the run feed tank.

The oil pump was an S-C Corporation, Model 10-600, air-operated hydraulic pump. The intensifying air-oil piston had a 300 multiplication factor with a maximum operating pressure of 2000 atm. All high pressure sections were stainless steel, including inlet and outlet check valves, with the exception of the brass high pressure cylinder liner. Hydraulic fluid was Rohm and Haas Plexol 201. The hydraulic inlet line was filtered. A transparent acrylic plastic reservoir, calibrated in fractions of full piston travel of the gas compressor (C1), was used to monitor the quantity of oil fed to the gas compressor.

The effluent gases, once the back pressure against the outlet check valve (V2) was exceeded, were forced into the run feed tank. This vessel was a surplus 75-mm cannon barrel with end plugs welded in both ends. Two 6.35-mm "AE-cone" female connections were machined into one end plug. One of the ports was attached to a dip leg in the vessel. Maximum working pressure was 1700 atm. All process lines in the section between the compressor feed valve and

the outlet valves of the run feed tank were of 6.35-mm, o.d. x 2.11-mm i.d. stainless steel tubing. Fittings were of the "AE-cone" type.

Reactor

The experimental tests were performed in a small cylindrical reactor obtained from the University of Michigan. The reactor was constructed of 19-9 W-Mo stainless steel. This steel is a high chromium-nickel steel of the following composition:

C	=	0.12	percent
Mn	=	0.57	"
Si	=	0.64	"
S	=	0.01	"
P	=	0.024	"
Cr	=	19.32	"
W	=	1.38	"
Ni	=	9.32	"
Mo	=	0.33	"
Ti	=	0.42	"
Cb	=	0.51	"

This type of stainless steel was originally intended for use in turbines at temperatures of about 550°C. The reactor was originally designed for service at 680 atm and temperatures up to 650°C. Internal diameter of the reactor was 1.9 cm. Internal length was 79 cm. All process lines entered the thermowell end. The opposite end of the reactor was plugged. This method of piping was selected so that, by merely loosening the high pressure flanges at the thermowell end, the reactor could be swivelled about 45 degrees from the horizontal to facilitate filling and dumping of catalytic materials.

The thermowell passed through an annulus in the end flange and extended the entire length of the reactor, resting at the opposite end in a centering port. The thermowell was constructed of 18-8 stainless steel, 6.35-mm. o.d. x 2.38-mm i.d. Figure 13 is a set of views of the thermowell and closure assembly.

The two outlets of the thermowell closure were fitted with flanges. A 60° female countersink in each outlet was mated to a 59° male taper made of 19-9-W-Mo steel. A matching flange was used to complete the fitting closure. The taper adaptor was welded to short sections of high pressure tubing, which terminated in suitable "AE-cone" fittings.

The plug-end closure is shown schematically in Figure 14. A tapered plug, made of 19-9 W-Mo steel was used to seal the port.

All plumbing used in the sections of the overall reaction system between the feed valve of the compressor (C1) and the dump valve (V4) of the reactor (see Figure 12) was 6.35-mm o.d. x 2.11-mm i.d. stainless steel tubing assembled with "AE-cone" fittings with operating capability to 2000 atm. All threaded parts of the flange fittings used rather coarse, loose-fitting threads for ease of assembly after high-temperature operating periods. No galling of the threads has been experienced with these types of closures and threads in several programs in which this reactor has been used.*

*This reactor has had a history of service of over 20 years at the Universities of Michigan and Oklahoma.

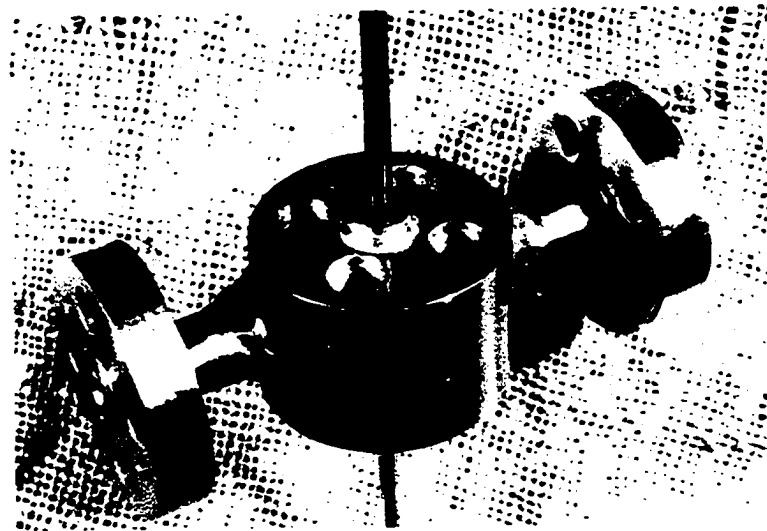
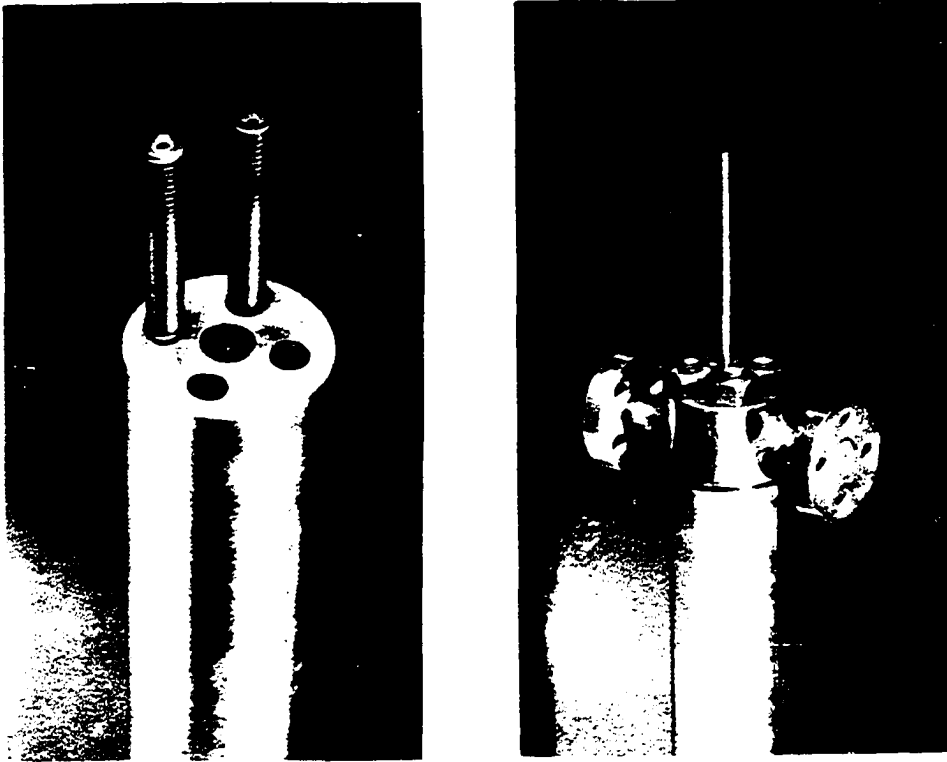


Figure 13. Thermowell and Head Closure Assembly.
(From Slipevich (69) reproduced by permission.)

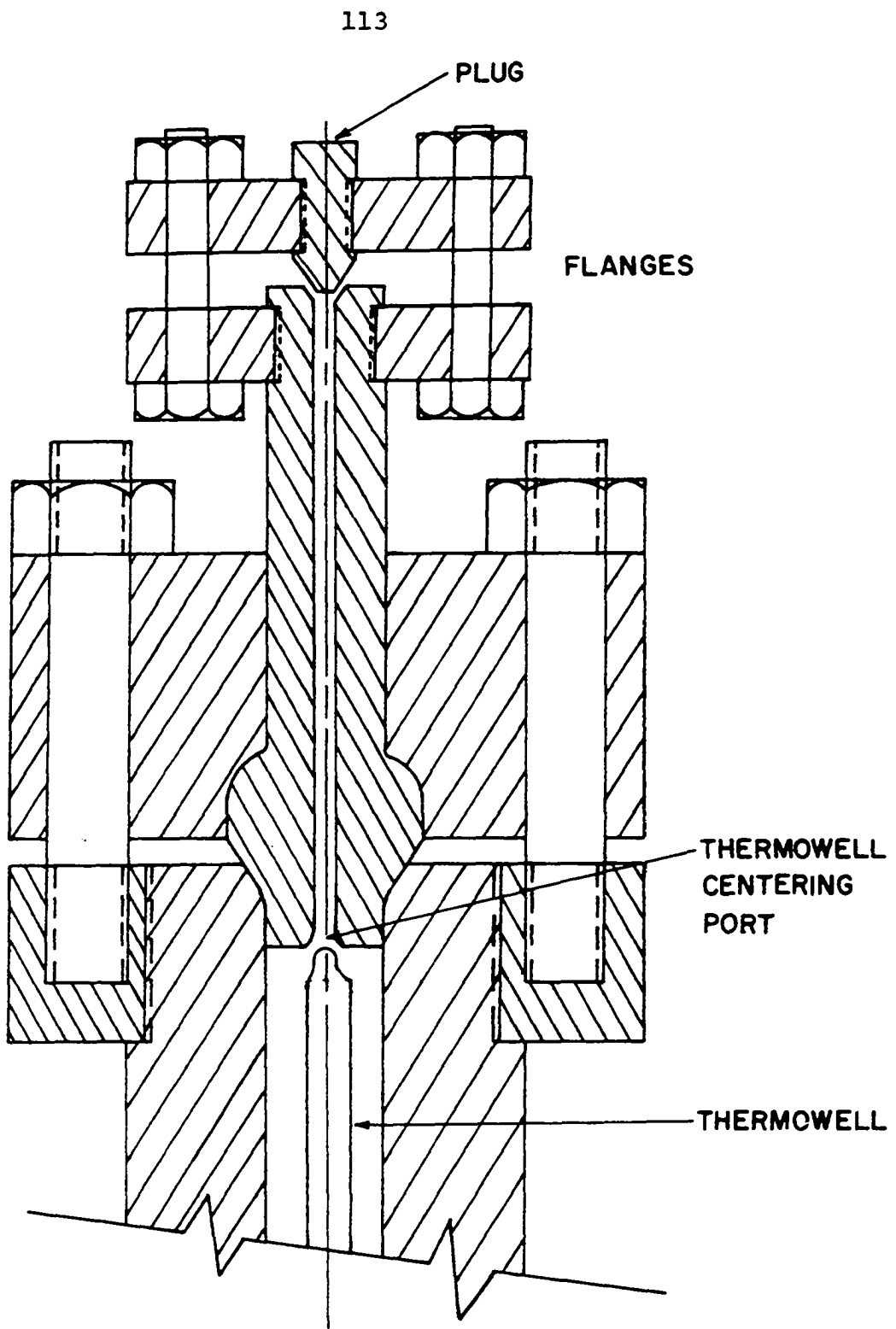


Figure 14. Plug-end Closure.

Assembly was facilitated through the use of feeler gages. Obviating the necessity for relying on torque wrenches for alignment of the flanges, the feeler-gage technique almost invariably gave leak-free assembly of the tapered connections. Torque-wrench assembly could have resulted in uneven tension in the bolts due to non-uniformity of finish of the threads and the buildup of scale after extended operation at elevated temperatures.

Figure 15 is a schematic drawing showing the heater wiring diagram, the placement of insulation, and the thermocouple wiring setup used. Three heater sections, each consisting of 25.9 meters of 20-gauge Nichrome A wire wrapped around a 3.18-mm layer of moldable asbestos sheet, were used to heat the reactor. Ten centimeters of Johns-Manville "Snap-Lok" insulation covered the heater wiring. The heaters were individually operated from a 240 V.A.C., 60 Hz source, with voltage control by three Variac auto-transformers. Ammeters in each circuit were used to set the current in each heater. Each circuit was fused for 7 ampere service.

Temperature measurement was provided by six iron-constantan thermocouples. Three thermocouples were placed in the reactor thermowell at spacings of 0.25, 0.50 and 0.75 of the internal length of the reactor, respectively. At the same spacing distances, three thermocouples were placed under the inner asbestos insulation beneath the three heaters.

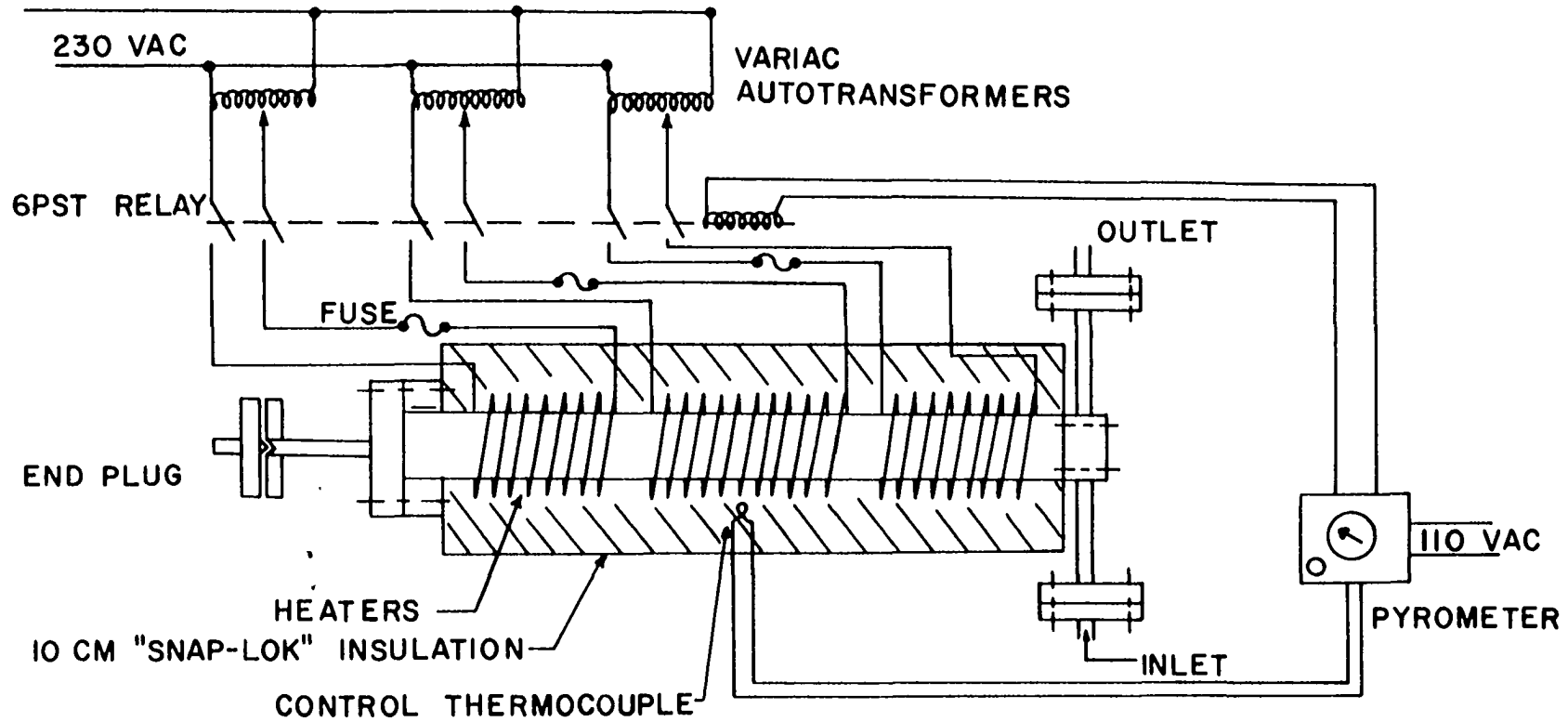


Figure 15. Reactor Heater Wiring Schematic.

End losses in the reactor resulted in currents of 2 amperes in the outer heaters and about 0.5 amperes in the center heater after adjustment for lengthwise temperature uniformity. Using a single traveling thermocouple (rather than the three used in conducting an experimental test), traverse of the reactor length showed a variation of only $\pm 1.0^{\circ}\text{C}$ from about the 5 to 95 percent distance points in the thermowell. At the extreme positions about 5°C dropoff was measured.

After a portion of the experimental program had been completed, an Assembly Products, Inc. "Simplytrol" meter-relay controller was added to the heater circuit. This device used the middle, outer thermocouple as a sensing element and switched the bank of three heaters as a unit through a 6PST relay, rated at 25 amperes. Addition of the controller enabled more rapid changes in reactor temperature between tests. Originally, changes in conditions demanded adjustment of the three auto-transformers and subsequent "zeroing-in" on the desired operating temperature. With the Simplytrol, the Variacs were adjusted so that continuous operation would give a uniform temperature of 500°C ; the controller was then allowed to cycle on and off at the desired temperature. No readjustment of the Variacs was then necessary.

After installation of the Simplytrol unit, the outer, middle thermocouple could not be used for measurement

purposes. However, uniformity in internal conditions could be ascertained because the voltages of the three thermowell thermocouples were unchanged.

The millivolt signals were recorded on a Bristol millivolt recorder model PH560. The recorder was originally scaled at 0-1.0 millivolt, but range spools were installed to give a pyrometric range equivalent to 0-500°C. A self-compensating cold junction was also installed. All thermocouples were terminated at a Leeds and Northrup multi-position, rotary switch, Model 8240. A single compensating pair of leads was connected between the switch and the recorder. Manipulation of the switch enabled selection of any of the five thermocouples.

A jack was installed in the recorder input line so that thermocouple output could be diverted to a Leeds and Northrup Model 8657-C potentiometer. This device enabled periodic, precise measurement of the reactor temperature for comparison with the recorder indication. One set of points of the rotary switch were shorted and one set left in an open position so that the potentiometer, in addition to temperature measurement, could be used to feed a known signal to the recorder for calibration purposes, or the recorder input terminals could be shorted for "zeroing."

Pressure was measured with a Manganin resistance coil wired to a Foxboro Dynalog recorder, Model 9420P, which gave a continuous circular recording with a 1-hour

revolution. The Manganin cell was a Harwood Engineering unit, Model E-1608, equipped with a superpressure jacket for pressures to 13,600 atm. Nominal resistances of the measurement coil and the reference coil were 120 ohms. Figure 16 shows the pressure measurement circuit in simplified form. The manganin cell was calibrated over the pressure range of interest by comparison with a Heise 0-3400 atm gage which was also incorporated in the system.

The reactor system was equipped with an Aminco Superpressure safety head in the feed line. The safety head was fitted with a rupture disc of laminated stainless steel designed for a rupture pressure of 1600 atm.

Product Collection System

The product receiver, consisting of two vessels connected in parallel, was connected to the reaction section through a water-immersed cooling coil. The two vessels depicted in Figure 12 as a single tank (T4), were provided with individual valves so that the reaction mixture could be diverted to either or both receivers, depending on the desired final pressure. One vessel, originally installed in the system, was a 61-cm section of 10-cm Schedule 40 pipe. Initial tests in a previous program showed that the vessel volume was inadequate to handle the products of runs at extreme pressures; the second receiver, a 8200-ml breathing-air bottle, was then installed in parallel.

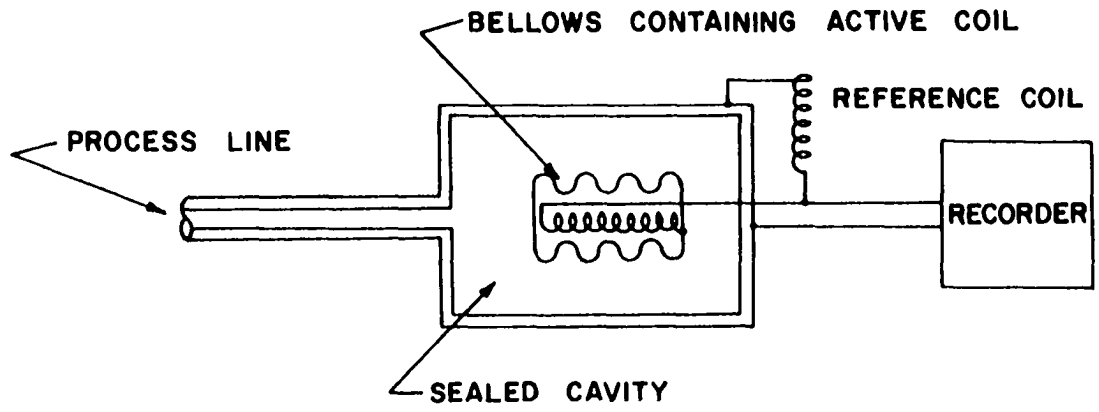


Figure 16. Pressure Measurement Circuit.

Three outlets to the receivers were provided: a vent leading to the common vent manifold located in the test cell, a vacuum connection at the top, and a vacuum connection at the bottom. The bottom tap was connected to two cold traps arranged in series. The traps, immersed in a dry ice/acetone mixture, provided collection of condensable products. An absolute pressure gage (0.5-1.0 atm abs) was installed in the trap line to help maintain a safe pressure level in the glass traps.

Photocatalytic Equipment Modification

A quartz mercury-vapor lamp was designed and built in cooperation with Ultra-violet Products, Inc. The lamp was 6-mm o.d. x 2-mm i.d. x 12.7-cm in length. The o.d./i.d. ratio of 3 was selected after preliminary calculations showed the collapsing pressure of fused quartz tubing to be about 5000 atm for such a ratio. Because the capability of handling at least 300 volts for striking purposes was necessary, and because the low-voltage lamp cost was prohibitive (as compared to a lamp operating at about 200 volts with a striking voltage of 800 volts), a high-voltage system was selected. The Ultra-violet Products lamp was designed to operate at room temperature at 200 volts with a striking voltage of 800 volts and a steady current of 18 milliamps. A ballast transformer with a high voltage initiation surge was used to provide the necessary power.

Figure 17 is a schematic drawing of the lamp. The lamp was installed in the reactor by modifying the end plug to accommodate an electrical lead-through. A Conax teflon/lava electrode, 0.238-mm dia, was used as the lead-through. One side of the 200-vac lead was attached to the electrode and the other lead was grounded to the reactor body. The two lamp leads (bare molybdenum wire) were attached to the electrode and a ground screw attached to the interior of the end plug. Figure 18 shows the lead-through assembly. The lamp was placed at the end of the reactor so that shorting of the "hot" molybdenum lead was avoided. The lamp was not centered in the reactor but rested on the lower surface of the bore.

High Pressure Test Cell

All equipment except the rotary oil pump and the Sprague air pump was located in a special test cell. The facility was a small room, 2.1-m x 2.7-m x 2.5-m high, constructed of 5-cm tongue and groove wood. Three of the cell walls were covered with 6.35-mm steel plates, butt welded together. The single external wall was provided with a large blow-out panel. A heavy rope blast mat was suspended outdoors, approximately a meter from the blow-out panel for shrapnel protection external to the building. The roof of the cell was covered with steel plate and rope blast mats. All valves which had to be operated with significant pressure in the lines were extended through the cell walls by "T" handles.

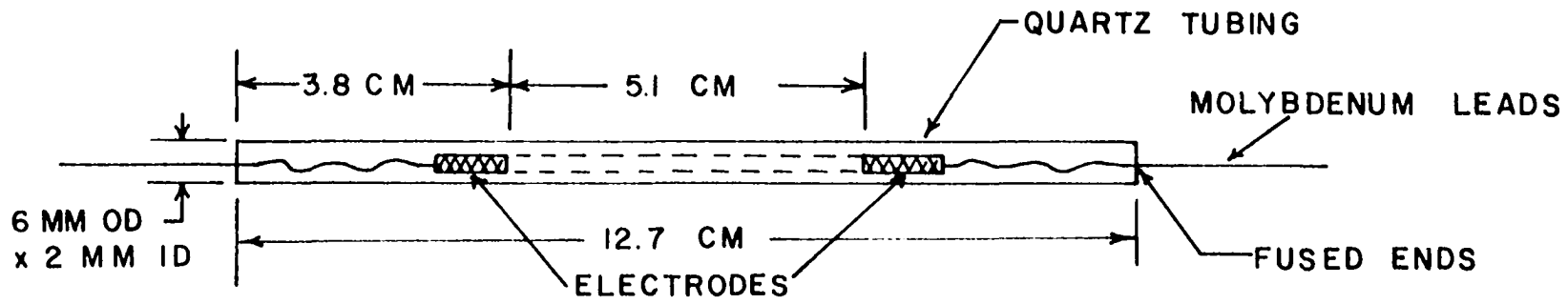


Figure 17. Mercury-Quartz Lamp Design.

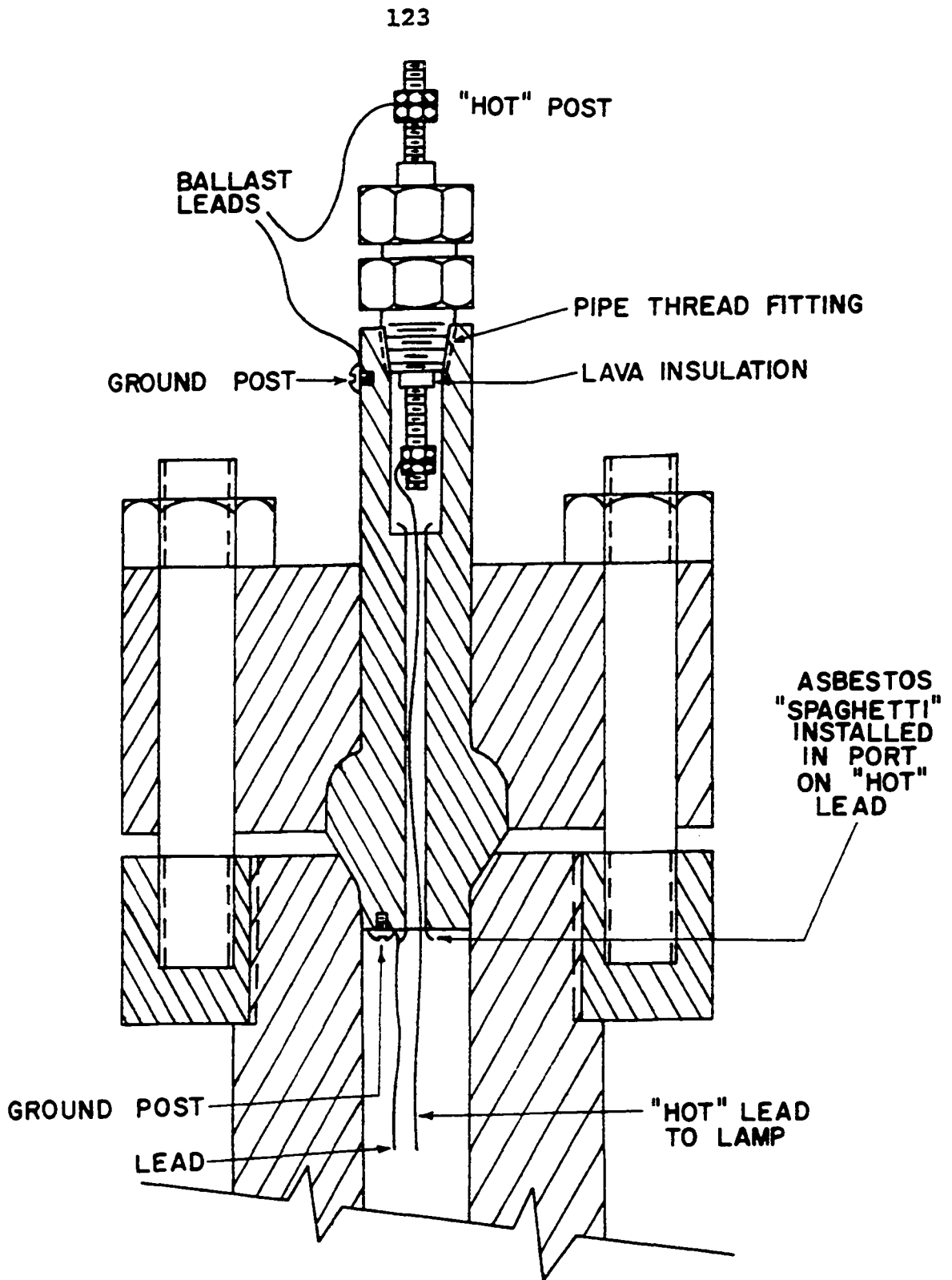


Figure 18. High-Voltage Lead-Through Assembly.

A high capacity vent fan was installed in the external wall and was left on continuously after initiation of the program. Adequate fire safety equipment was located near the cell.

Auxiliary plumbing within the cell included tap water, a common manifold vent line, a high pressure blowout vent line, a 10-atm air supply, and a vacuum manifold. Electrical outlets and adequate lighting also were installed.

CHAPTER V

EXPERIMENTAL PROCEDURE

Much of the procedure relating to feed stock preparation and compression has been previously reported (26, 35), and has been changed only slightly in the present work. However, for the sake of continuity, the entire operation will be described briefly. The nomenclature describing pieces of equipment refers to Figures 11 and 12.

Feed Stock Formulation

Methane was admitted to the mixing tank (T1) (previously evacuated or containing residual feed) directly from a 1-A cylinder. To obtain a final mixture ratio of about 10:1 methane to oxygen, about 6.1 atm of methane was admitted and sufficient oxygen added until a final pressure of about 7 atm was reached. The explosive limits of methane/oxygen at high pressures dictated the nominal mixture ratio used in this study. Introduction of oxygen last gave the smallest likelihood of creating an oxygen-rich zone in the system.

The Sprague air pump, (P1) was used to transfer water to the mixing tank (T1) until the pressure reached 20 atm. The pump then remained in operation to maintain

this pressure level as the feed mixture was transferred to the primary storage tank (T2).

The oil pumping system (P2) was used to perform the transfer. A cylinder of the displacement system was filled with gas, was isolated, and was pumped with oil until the pressure reached about 400 atm. The pump was shut down and the gas was discharged to the storage tank. The second cylinder was filled with gas and the process was repeated. During the second pumping operation the oil in the first cylinder was drained back to the oil reservoir. The incoming low-pressure gas from the mixing tank was used to help force the oil back. The recycle operation generally was faster than the pumping operation; therefore, the pump was in almost continuous operation, being shut down only long enough to expel the pressurized gases into the storage tank.

Depending on the state of pressurization of the storage tank, between 50 and 100 oil-pump cycles were necessary to deplete completely the gas in the mixing tank. After depletion of the gas, the mixing process was repeated to provide additional gas supply. Four charges in the mixing tank were necessary to attain a final pressure of 150 atm in the primary storage tank (T2). Each recycle demanded drainage of the mixing tank (T1) and subsequent filling and repressurization to 20 atm. This recycle step was the most time-consuming of the operation, taking about 6 hours per cycle.

Tank (T2) was brought to 300 atm by pumping water into the vessel through a water pump (P1). This vessel was then closed off, and the gas mixture was allowed to stand for several hours prior to operation. A complete fill of the storage accumulator provided feed stock for up to 45 tests. Periodic addition of water to the storage tank was made to maintain the pressure above 270 atm; the added water was volumetrically measured so that the exact ullage in the tank was known at all times.

Intermediate Compression

The gas in the primary storage tank (T2) was pumped into the run feed tank (T3) via the small intermediate compressor (C1). This unit was operated in much the same manner as the oil displacement system (P2). A charge of gas was admitted to the cylinder, the feed valve was shut, and oil was pumped below the floating piston by using the air-operated pump (P3). The gases were expelled into the run feed tank. When the piston reached the end of the cylinder, the outlet oil pressure of the oil pump (P3) rose sharply. The oil return valve (V5) and the intermediate compressor feed valve (V6) were then opened, draining oil back to the reservoir. A check valve (V2) between the compressor and run feed tank prevented back-flow from the tank. The operation was repeated until the desired pressure was reached. The pressure level was usually kept between 600 and 1000 atm.

Reactor Operation

Prior to each experimental test, the temperature of the reactor was brought to the desired level by adjusting the thermo-regulator control. The storage tank (T3) was brought to a pressure level sufficiently above the intended pressure of the reactor to enable proper filling.

The reactor was evacuated at the desired operating temperature for at least two hours prior to each test. The gas product receivers were evacuated at room temperature for at least the same amount of time. Liquid product traps were evacuated at room temperature for at least four hours before each experimental test.

The reactor dump valve was closed and reaction gas was admitted slowly to the reactor at the start of each test. The product receivers were maintained at vacuum during initial stages of each test, and isolation of the receivers was not accomplished until immediately prior to quenching of the reaction. When the reactor reached the desired pressure, the feed valve was closed, and an event marker was manually indicated on the temperature recorder. This point became time "zero" in the experimental chronology.

The reaction was allowed to proceed until a predetermined point was reached. Depending upon the objective of the test, one of the following three criteria was used to terminate the tests: (1) the reaction temperature reached a maximum, (2) the reaction pressure reached a maximum,

or (3) a pre-selected reaction time had been reached. At the point of desired cessation of each test, the receivers were isolated from the vacuum line, and the dump valve was opened, allowing reaction mixture to flow rapidly to the product receivers. The temperature and pressure of the receivers were recorded.

In each test series in which a heterogeneous additive was employed, a known quantity of additive was placed in the reactor and the reactor was sealed. After the series of tests, the material was carefully removed and weighed. The reactor was purged with compressed air to remove fines before the next additive was introduced.

Photochemical Reaction Studies

Operation of the reactor during photochemical studies was identical to the procedure outlined for the thermal studies with the exception of initiator addition and lamp operation steps.

A vessel containing the desired additive was attached through a high-pressure needle valve to a tee in the feed line to the reactor. The reactor and feed line were evacuated and isolated from the product receivers. The valve from the additive supply vessel was then opened, and the additive was allowed to enter the reactor in the vapor state. Transfer of the additive was completed when the additive ceased to boil or when the pressure equalized between the supply vessel and the reactor.

With acetone or formaldehyde (present as formalin, 37% formaldehyde in water) a glass feed vessel was used. A steel vessel was used when acetaldehyde was the additive.

After completion of initiator transfer, admittance of the methane/oxygen mixture proceeded in the usual manner. After a predetermined time the lamp was struck and operated continuously. After operation for several minutes the mixture was quenched and collected as before.

CHAPTER VI

ANALYTICAL EQUIPMENT AND PROCEDURE

Reaction products were collected in two phases: those condensable at -78°C (the atmospheric sublimation point of carbon dioxide) and the fixed gases. The former included water, methanol, formaldehyde, ethanol, methyl formate, acetic acid, and formic acid. The fixed gases included oxygen, nitrogen, methane, carbon monoxide, carbon dioxide, and ethane. Quantitative analyses of all products were accomplished by vapor phase chromatography.

Chromatographic Equipment Used

A Hewlett-Packard, F. and M. Scientific Division, Model 700 chromatograph was used exclusively in this program for quantitative analyses. The equipment is shown in Figure 19. The basic unit consisted of an oven, a temperature controller, a detector assembly, and a recorder. The proportional temperature controller was capable of regulating the oven temperature within 1°C from room temperature to 400°C . The detector assembly was a basic kathorometer with four WX tungsten filaments. Accessory equipment included a proportional temperature controller for the detector

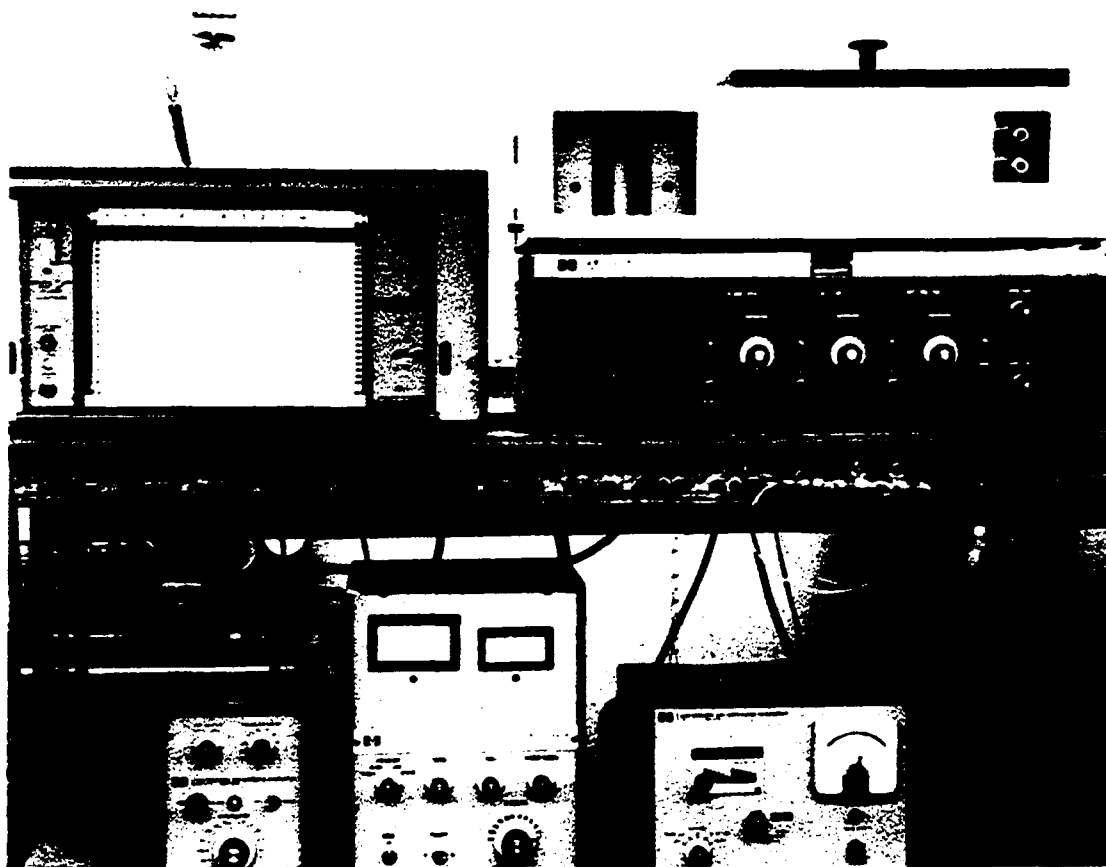


Figure 19. Chromatographic Equipment Used for Analyses.

assembly, a gas sampling valve and a temperature programmer, F. and M. Scientific Model 240.

The chromatograph was a dual column type which used parallel columns of identical packing characteristics. Sample injection was possible into either column with the unused column thus becoming the reference leg of the katharometer bridge. The employment of dual columns enabled drift-free operation with packing materials that "bleed" during high-temperature programming.

The carrier gas used in all cases was instrument grade helium. Pressure regulation was accomplished by a standard dual-stage regulator at the gas supply bottle. Flow regulation for the dual columns was maintained through two diaphragm regulators. Flow rates were set and monitored using calibrated rotameters. Occasional absolute flow measurements were made for verification purposes using a soap-bubble flow meter.

The output of the katharometer bridge was recorded on a Moseley, Model 7127A, potentiometric recorder. Full span was 1 mv DC. The recorder assembly was equipped with two auxiliary devices. Built into the recorder itself was a Disc integrator, which transposed peak areas into linear pen travel and recorded the output on a special, calibrated portion of the strip-chart. Areas were then determined directly by merely measuring total distance of travel of the secondary pen.

Although the basic chromatograph was equipped with a variable attenuation selector which consisted merely of a tapped rheostat, a second automatic attenuator was also employed in the katharometer output. This device, a Hewlett Packard Model 50B, automatically doubled the attenuation when any peak approached 95 percent of full pen travel and automatically halved the attenuation as the peak approached 32 percent from above. This unit enabled operation at extremely high sensitivity in the case of "trace" species and automatically prevented overshoot at the predominant peaks. Simultaneous operation of the attenuator and the integrator was not possible.

Each column was equipped with an injection port sealed with a rubber septum. The injection ports were thermally maintained several degrees higher than the column oven through the use of variable autotransformers. The septum ports enabled injection of liquid samples with a syringe.

Gas injection was accomplished with a sliding sample valve. This device alternately traps a small quantity of gas flowing in a loop made of 3.2-mm copper tubing and then diverts the carrier stream through the loop, thus picking up the sample. Highly reproducible sample size was thus possible through the use of this device. Only one column was equipped with a gas sample valve.

The gas analyses were made using two 0.9-meter columns of 6.35-mm stainless tubing packed with Molecular Sieves, Type 5A (60/80 mesh). In general, determination of carbon dioxide is not usually performed with molecular sieves, because, at the temperature necessary for good separation of oxygen, nitrogen, methane, and carbon monoxide, carbon dioxide is irreversibly absorbed. Carbon dioxide can, however, be driven from molecular sieves at about 225°C. Use of the temperature programmer, with a planned linear temperature increase (20°C/min) from 35°C to about 250°C, enabled adequate separation of all gaseous constituents at the lower temperatures and the desorption of carbon dioxide at about 225°C. Good reproducibility was obtained through the use of this technique.

Liquid analyses were made on a matched pair of 2.44-meter columns, consisting of 3.2-mm diameter stainless steel tubing, packed with Porapak T. This packing is basically porous polymer beads, marketed by Waters Associates, Inc. The material is relatively new and features the absence of "bleeding," no absorption of polar compounds, constant retention times, large surface area and rapid overload recovery. Until this material was introduced, formaldehyde analyses were generally conducted iodimetrically (26, 35, 70).

Some success has been reported with 8-8' thiodipropionitrile on Haloport F for chromatographic formaldehyde determination (2). This material was initially used in this program, but analysis of the organic acids was not possible with this packing. Porapak T, however, gave adequate indication of formic and acetic acids. Porapak T gave the capability of measurement of 0.01 percent formaldehyde in water, rivaling the Romijn iodimetric method (70).

The only problem in the use of Porapak T was that poor separation between water and methanol occurred at the temperatures necessary to provide adequate peak heights for formaldehyde. In fact, the uniqueness of the Porapak was demonstrated in that, contrary to the general trend with absorption packings, higher temperatures were required for formaldehyde, which comes off prior to water, than those immediately following water. This phenomenon required operation at two different temperatures to separate all components adequately. Operation of the programmer was impossible because a reverse program would have been required.

Peak height ratios were used for calibration purposes for all components except methanol. The methanol-water ratio was measured, again through proper calibration, using peak area measurements.

Analytical Procedure

The gas analyses were performed using the following operating conditions:

Columns 0.9 meters Molecular Sieves
5A

Helium Flow Rate . . . 60 ml/min

Oven Temperature . . . 35°C--Programmed to 250°C
@ 20°C/min--1 min after
start

Injection Port Tem-
perature 260°C

Detector Temperature. . 260°C

Regulator Pressure. . . 7.8 atm

Automatic attenuator. . On

Analyses of formaldehyde, water, methyl formate, ethanol, acetone, formic acid, and acetic acid were performed using the following conditions:

Columns 2.44 m Porapak T

Helium Flow Rate . . . 125 ml/min

Oven Temperature . . . 140°C stepped to 165°C four
minutes after water efflux

Injection Port Tem-
perature 260°C

Detector Temperature. . 260°C

Regulator Pressure. . . 7.8 atm

Automatic attenuator. . On

The water-methanol analyses were performed using the following conditions:

Columns 2.44 m. Porapak T
 Helium Flow Rate 125 ml/min
 Oven Temperature 85°C
 Injection Port Temperature 260°C
 Detector Temperature . . 260°C
 Regular Pressure 7.8 atm
 Automatic attenuator . . Off (integrator used)
 Retention times for the various components are given

below:

Gas Analysis

<u>Component</u>	<u>Retention Time</u>
Oxygen	2.8 min
Nitrogen	3.5 "
Methane	3.6 "
Carbon Monoxide	6.4 "
Ethane	10.0 "
Carbon Dioxide	15.0 "

Liquid Analysis (140/165°C)

<u>Component</u>	<u>Retention Time</u>
Formaldehyde	0.8 min
Water/Methanol	1.2 "
Methyl Formate	2.2 "
Ethanol	4.0 "
Formic Acid	13.0 "
Acetic Acid	16.0 "

Liquid Analysis (85°)

<u>Component</u>	<u>Retention Time</u>
Water	8.0 min
Methanol	12.0 "

Generally, the detector in a unit such as that described above is maintained about 10 degrees above the maximum column temperature. Because the columns and conditions were varied with frequent regularity (parallel research programs also used the analytical equipment), the detector was allowed to regulate permanently at a condition corresponding to the gas analysis; it may have been unnecessarily high for the liquid runs.

Gas analyses were performed by flowing, slightly above atmospheric pressure, the test gas from a sample bomb through the sampling valve and into a water-filled flask. The flow rate was adjusted until only a slow bubbling of the gas occurred in the flask. The inlet to the sample loop was closed and the bubbling was allowed to diminish until atmospheric pressure was indicated. The outlet of the sample loop was then closed, thus trapping about one ml of gas at atmospheric pressure in the loop. The sample valve was then pulled and rotated to the lock position; in this position the carrier gas detours through the sample loop, picks up the sample, and carries it into one of the columns.

The programmer was set for 20°C rise per minute; it was turned on at exactly one minute after the start of the run. This delay in initiation of the program enabled more complete separation of the basic air constituents prior to the methane efflux.

Liquid introduction was accomplished hypodermically in 1 μ l samples by injection through the rubber septum. In the case of the methanol/water separation, no program was employed. The integrator was aligned prior to each test to enable exact reading. With the other liquids, the integrator trace was ignored, but the automatic attenuator was turned on. In these latter tests, initiated at 140°C, the column temperature was adjusted rapidly to 165°C four minutes after the water peak. This switching operation was selected after several initial trials; it proved more effective in separation than a linear program.

The chromatograph was calibrated for gas analysis by mixing gas samples of various composition in 8.2 liter stainless steel cylinders. The gas components used to make the standards were all of 99 percent minimum purity. The mixtures were made manometrically and the final pressure in each bottle was about 2.7 atm abs. The results of the calibrations are given in Appendix E (Figs. E-1 through E-3). During actual analyses, triplicate tests were performed. The measured peak height ratios were transformed to mole percentages through the use of these calibration curves.

Liquid calibration standards were made both volumetrically and gravimetrically. In general, each component was mixed with water individually for calibration purposes. Other standards prepared with all components present showed no interference between constituents. Figures E-4 through E-9 in Appendix E are the calibration curves for the various liquid components.

Chemicals Used

The chemicals used for feed stock preparation and chromatograph calibration formulations were:

Oxygen - Air Reduction Company. 0.02% nitrogen

Methane - Phillips Petroleum Co. A typical vendor analysis is as follows:

Methane	99.05 mole percent
Ethane	0.12 " "
Carbon Dioxide	0.20 " "
Nitrogen	0.60 " "
Propane	0.03 " "

Carbon Dioxide - Matheson Co., Coleman grade, 99.99 percent purity

Carbon Monoxide - Matheson Co., CP Grade, 99.5 percent purity

Methanol - Baker and Adamson, 99.0 percent purity

Formaldehyde - Baker Chemical Co., 36.2 percent formalin solution, 12.0 percent methanol, remainder water

Formic Acid - Mallinkrodt Chemical Works, 88 per-
cent, remainder water

Methyl Formate - Matheson Coleman and Bell,
practical

Acetone - Baker and Adamson, 99.5 percent minimum
purity

Acetic Acid - Fisher Scientific Co., 80.82 per-
cent solution.

CHAPTER VII

RESULTS AND DISCUSSION

In this discussion, the following conventions and definitions apply. Ignition delay was considered to be the time interval between the end of the filling operation and the point of maximum temperature. The term, residence time, applies to those tests in which the reaction was terminated at any point other than at the temperature maximum. A reaction was arbitrarily considered to become explosive when the temperature rise exceeded 20°C. All pressures are given in gauge values unless specified to be absolute units.

The experimental program was divided into four areas of study.

(1) Ignition delay was determined for a mixture with a 10/1 (nominal value) molar ratio of methane and oxygen at various conditions of surface-to-volume ratio (S/V). The ratio was varied from 3.5 to 5.5 (10)⁵cm⁻¹ by packing the reactor with stainless steel balls and two grades of alumina pellets.

(2) The effect of catalytic materials on ignition delay was determined. These catalysts were Kao-spheres,

cobalt molybdate, silica-magnesia, silica-alumina, and nickel oxide.

(3) Time-temperature-species histories were determined with each of the reactor preparations listed above.

Pressure in these three phases of study was varied from 100 to 750 atmospheres. Temperature was varied from 262 to 363°C.

(4) A brief feasibility study was made of photocatalytic ignition of the methane-oxygen mixture.

Table 9 presents the test conditions used in all experiments up to run 251. Runs 252 through 261, the photocatalytic portion of the program, are described in a separate section. Table 10 includes the feed stock preparations used in all tests. Five separate formulations were required.

Table A-1 in Appendix A presents all data taken in the first three phases of study. Included are actual test temperatures, pressures, ignition delays, residence times, and outlet product composition. Table A-2, also in Appendix A, presents species production as percentages of the depleted reactants.

Reaction pressure was taken as the average value measured during a run. Variation in pressure was generally less than two percent.

Heating of the reaction mixture due to compression during the filling operation occurred in all tests. In a number of tests, temperature rose to a maximum and then

TABLE 9

TEST CONDITIONS

Reaction Run No.	Reactor Preparation	Feed Stock Code
1 - 24	No Additives, S/V = 3.5 cm ⁻¹	FS-1
25 - 53	No Additives, S/V = 3.5 cm ⁻¹	FS-2
54 - 65	Stainless Beads, S/V = 13.4 cm ⁻¹	FS-2
66 - 79	Stainless Beads, S/V = 7.3 cm ⁻¹	FS-2
80 - 92	Stainless Beads, S/V = 7.3 cm ⁻¹	FS-3
93 - 103	No Additives, S/B = 3.5 cm ⁻¹	FS-3
104 - 113	Tabular Alumina, S/V = 545 cm ⁻¹	FS-3
114 - 125	Activated Alumina, S/B = 5.5(10) ⁵ cm ⁻¹	FS-3
126 - 148	Kao-Spheres*	FS-3
149 - 170	Cobalt-Molybdate*	FS-4
171 - 188	Silica-Alumina*	FS-4
189 - 204	Silica-Magnesia*	FS-4
205 - 228	Nickel Oxide*	FS-5
229 - 238	Cobalt-Molybdate*	FS-5
239 - 251	Activated Alumina, S/V = 5.5(10) ⁵ cm ⁻¹	FS-5

*All catalysts had S/V in excess of 5(10)⁵ cm⁻¹.

TABLE 10

FEED-STOCK COMPOSITIONS

Feed Stock Number	Molar Ratios					Runs Used In
	CH ₄ /CH ₄	O ₂ /CH ₄	N ₂ /CH ₄	C ₂ H ₆ /CH ₄	CO ₂ /CH ₄	
FS-1	1.0	0.10631	0.0023	0.0016	0.0	1- 24
FS-2	1.0	0.0938	0.0042	0.0011	0.0020	25- 79
FS-3	1.0	0.1232	0.0041	0.00267	0.00178	80-148
FS-4	1.0	0.0956	0.00371	0.00127	0.00163	149-204
FS-5	1.0	0.0954	0.0036	0.0015	0.0020	205-261

decreased to the initial set-point value as the rate of heat dissipation exceeded the rate of heat generation. In other tests, addition of cold feed gas after reaching the point of temperature maximum resulted in a decrease in temperature to slightly below the set-point. Finally, some tests resulted in a temperature rise due to filling, but temperature did not return to the set-point. In these latter tests, reaction was initiated during the filling operation and auto-acceleration occurred immediately. Temperature rise at the instant of ignition was invariably in excess of the 20°C criterion for explosion in these latter tests. In all non-explosive tests, in which temperature fell to or near the set-point, the minimum temperature attained was taken as the initial reaction temperature and was reported as such in Table A-1 in Appendix A. In those tests which resulted in immediate ignition, initial temperature was considered to be the initial reactor temperature.

Using the above definition of ignition delay, initial tests in the present program showed strong agreement with the data of Lott (35). An arithmetic plot of ignition delay (called residence time by Lott) versus time has already been presented (Figure 6, page 69). The shape of this curve suggested the possibility of a correlation between the logarithm of ignition delay and reciprocal temperature. Melvin also observed the mentioned relationship in his series of tests at pressures to 110 atmospheres (41).

Figure 20 includes all data taken with the 19-9DL reactor in tests which did not involve high-surface additives or catalysts; the data of several other authors are included. Comparison of similar plots involving only the data of Lott and the data of the present work initially showed that this superposition of data was possible. Although the reactor used by Lott did not have the same surface-to-volume ratio as that used in this study (1.8 cm^{-1} in Lott's reactor compared to 3.5 cm^{-1} for the present case) the variation due to this effect was within the spread of either set of data. Both sets of data, thus, were presented in the single plot.

Also included in the plot are data of Hardwicke (26) and Newitt and Haffner (46). Hardwicke's reactor was estimated to have a surface-to-volume ratio of about 3.9 cm^{-1} , slightly higher than that of the present program. Newitt and Haffner used a reactor with an S/V of about 1.3 cm^{-1} .

The data taken at each nominal pressure were represented as straight lines, as suggested by Semenov (63) for short induction times in chain reactions with branching and for longer ignition delays in thermal explosions and chain reactions without braching (see page 33).

It was observed that points which fell beyond a reasonable spread of data at a given pressure always were accountable in terms of non-attainment of the desired operating pressure. For instance, if the desired pressure

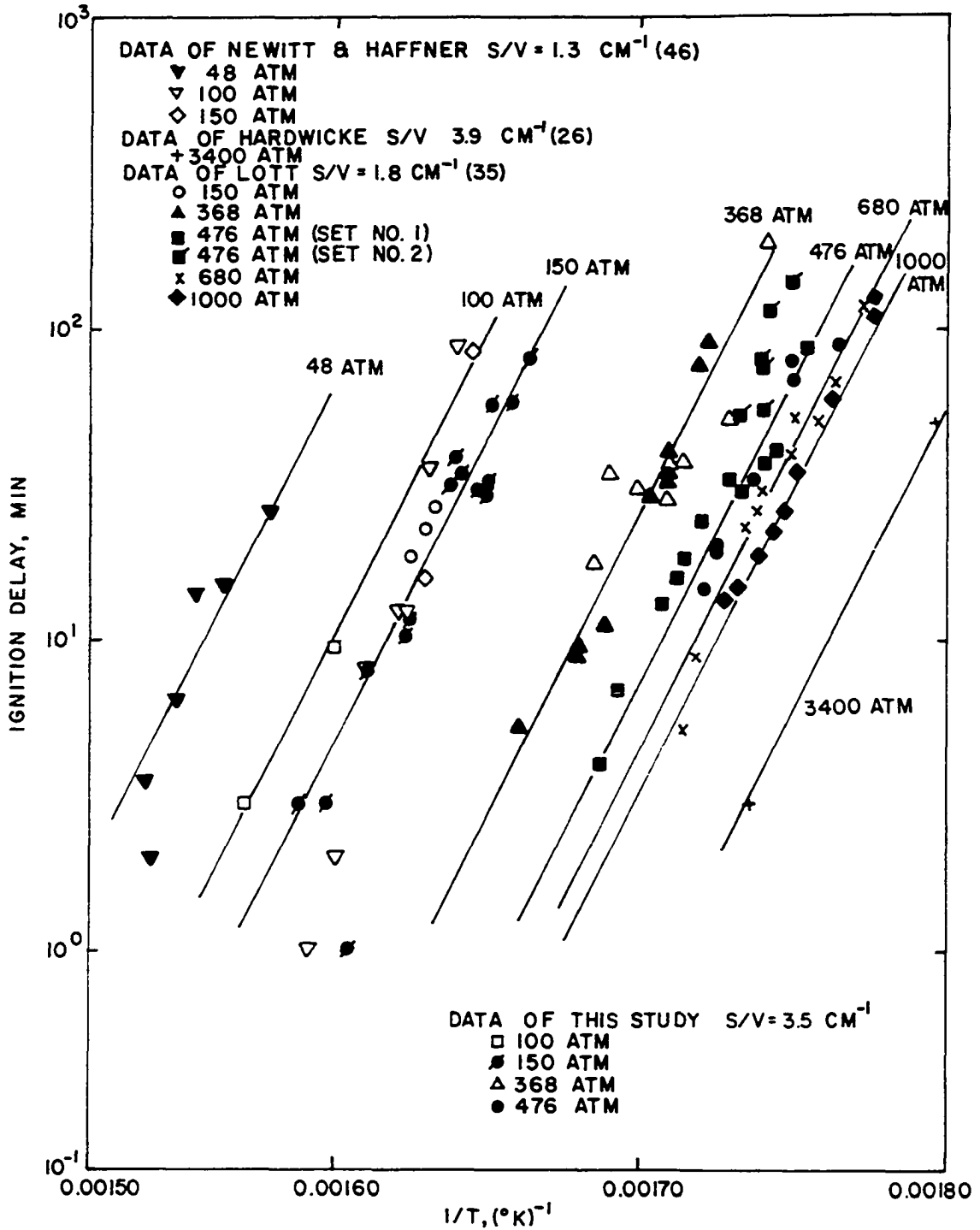


Figure 20. Ignition Delay as Function of Temperature at Various Pressures.

was 680 atm, attainment of only 600 atm would always result in ignition delays greater than the true 680 atm line.

At very short ignition delays, the points for some curves were well below the lines representing the majority of points. This feature is attributed to the inability to measure delays accurately at short times and to the onset of rapid auto-acceleration prior to completion of filling.

Melvin (41) determined the "order" of ignition delay with respect to pressure by least square regression between the logarithm of ignition delay and the logarithm of pressure. Such an attempt in the present instance did not give a reasonable correlation between ignition delay and pressure over the entire pressure range; that is, an order change somewhere in the pressure range covered was indicated.

A graphical relationship between ignition delay and pressure was constructed in the following manner: The straight line of Figure 20 for 680 atm was selected arbitrarily as a reference. A factor was then determined for each additional set of data such that multiplication of each point, determined at a pressure different from 680 atm, by that factor would put the point within the 680 atm correlation. By successive iteration between determination of a factor for each nominal pressure level and reassignment of the location of the best line through each set of data, the correlation shown in Figure 21 was assembled. The pressure factor, ψ , can be described mathematically.

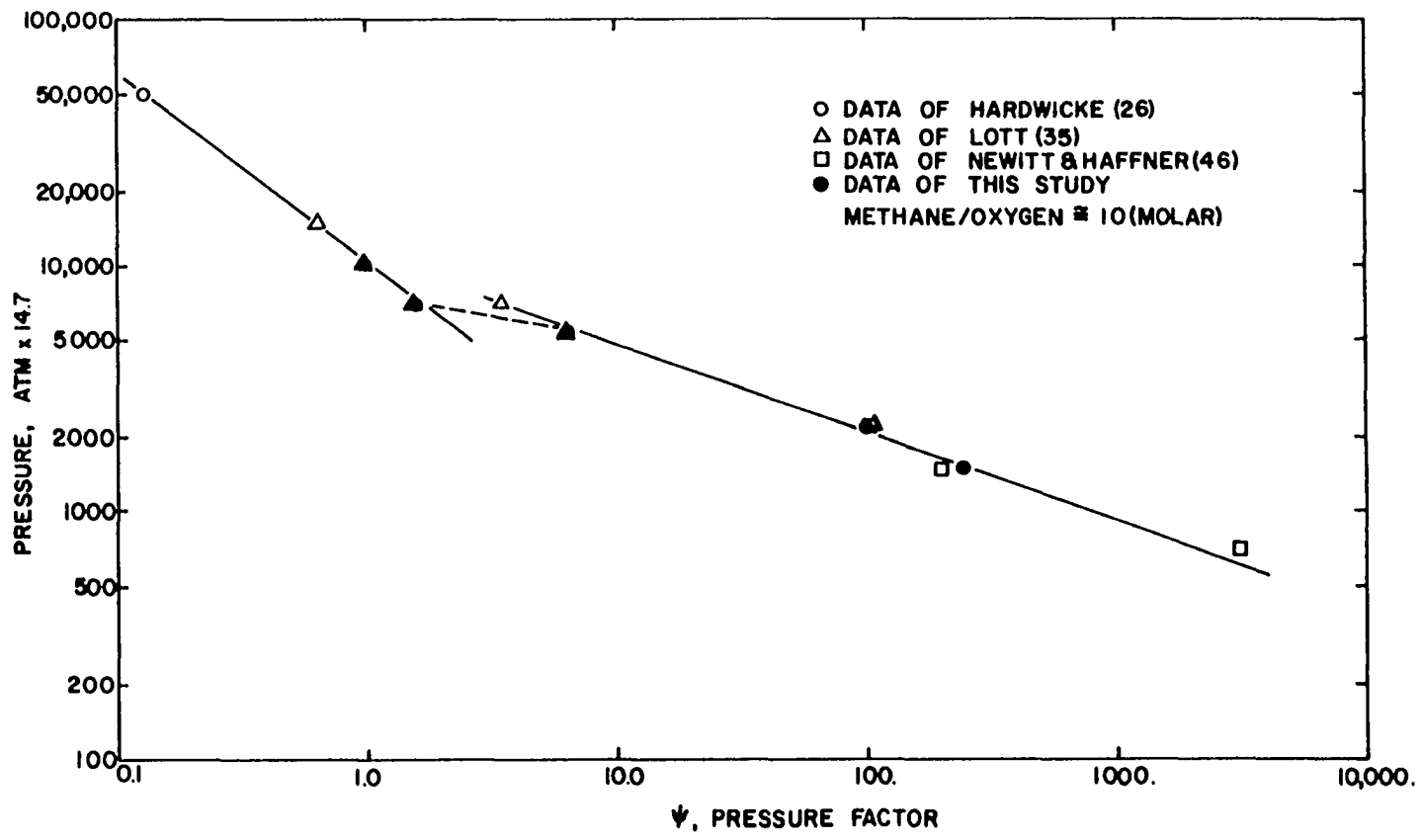


Figure 21. Pressure Correction Factor for Ignition Delay.

Assume a logarithmic relationship between ignition delay and reciprocal temperature at 680 atm, and between the same variables at some pressure, P:

$$\ln t_r = \ln A_r + B/T \quad (53)$$

$$\ln t_p = \ln A_p + B/T \quad (54)$$

where t_r is the ignition delay at 680 atm, t_p is the ignition delay at pressure, P, $\ln A_p$ is the intercept at pressure P, $\ln A_r$ is the intercept at 680 atm, B is a constant, and T in the absolute temperature.

In order that the data can be made to fall on the same line, only the intercept need be changed. Define the factor, ψ , by:

$$t_p/t_r = \psi \quad (55)$$

Substituting t_p/ψ for t_r in equation 53, one obtains

$$\ln\left(\frac{t_p}{\psi}\right) = \ln A_r + B/T \quad (56)$$

or in exponential form:

$$t_p = \psi A_r e^{B/T} \quad (57)$$

Since the slopes are unchanged, all intercepts are determined from A_r by

$$A_p = \psi A_r \quad (58)$$

Included in Figure 21 are data of Lott (35), Newitt and Haffner (46), and Hardwicke (26). It is apparent that two distinct straight lines result, and an order change at about 476 atm is indicated. Lott reported an apparent order change at 475 atm by accumulating two distinct sets of data for ignition delay at that pressure. Curiously, there was no apparent spread of data between the two sets; all points belonged decisively to one set or the other. Lott showed these sets as Curve 1 and Curve 2 (see Figure 6).

The two straight lines of Figure 21 each are of the form:

$$\psi = k P^n$$

where ψ is defined as the pressure correction factor and k and n are constants. The constant, n , is defined as the "order" for ignition delay with respect to pressure. The determined orders were -1.3 for the high pressure regime and -2.8 for the low pressure regime. Neumann and Egerov (45) determined a value of -1.8 for ignition at much higher temperatures and at low pressures. Because atmospheric tests were not conducted in this program, a second change in order at lower pressures was not verified.

Figure 22 shows the relationship between t/ψ , the pressure-corrected ignition delay, and $1/T$. The data of Newitt and Haffner (46) show the largest deviation, probably due to unresolved surface effects.

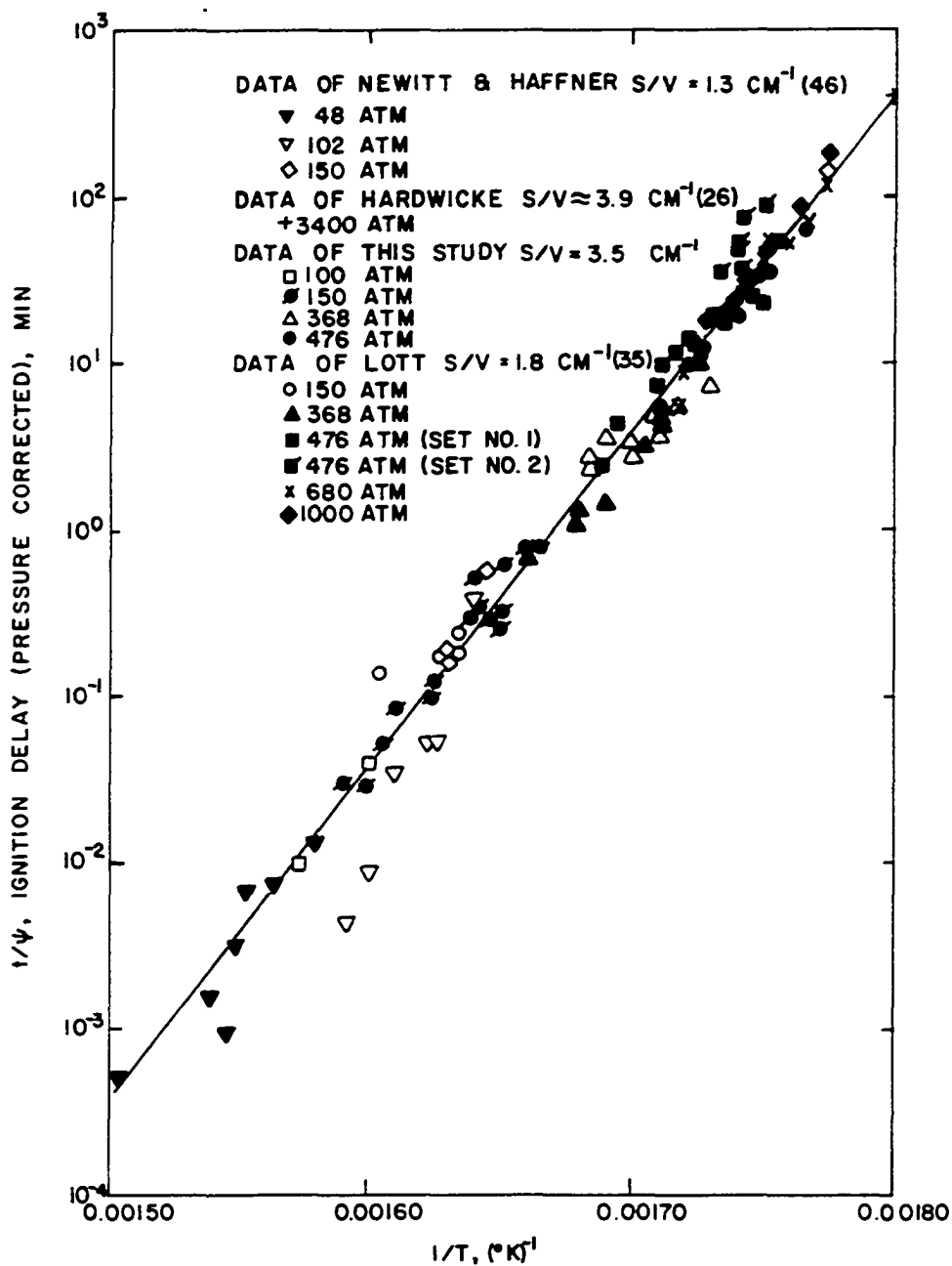


Figure 22. Pressure-Corrected Ignition Delay as a Function of Temperature.

The set of points designated as Curve 2 by Lott in his presentation is seen to be somewhat removed from the correlation of Figure 22. The values of ψ used for these points were taken from the high pressure region of Figure 21. By assuming that the set of data designated Curve 2 by Lott was applicable to the low pressure regime of Figure 21, it was found that these points correlate well. This modification will be shown later.

Because later tests involving heterogeneous additives had surface-volume ratios far removed from that of the empty reactor, the influence of the surface/volume ratio on ignition delay was determined.

Surface-to-volume (S/V) ratio was altered in several tests by adding stainless steel ball bearings, 4.77 mm in diameter. Two S/V ratios were covered, but the resultant S/V ratios were still far below that expected for many of the catalysts.

Hardwicke (26) reported no surface effect due to alumina in high pressure oxidation; thus, two grades of alumina were obtained from the Aluminum Corporation of America (ALCOA) for use as additives for increasing the surface/volume ratio still further. These materials were T-162 tabular alumina, a dense, slightly porous material in 3.2-mm balls and F-110 activated alumina, a highly porous material with large surface/mass ratio, also in 3.2-mm balls.

Pertinent properties are given in Table 11.

TABLE 11
PROPERTIES OF ALUMINA ADDITIVES

	T-162	F-100
Porosity	3.0%	0.44 cc/gm
Bulk Density	2.18 gm/cu-cm	0.98 gm/cu-cm
Surface Area	0.05 m ² /gm	165 m ² /gm

The values of the surface/volume ratio of the various reactors used in this and previous studies are summarized in Table 12.

TABLE 12
SURFACE/VOLUME RATIO OF VARIOUS
REACTOR SYSTEMS

Reactor of:	S/V (cm ² /cm ³)
Newitt & Haffner (46)	1.3*
Lott (35)	1.8
This work (no additives)	3.5
" " (stainless beads)	13.4
" " " "	7.3
" " (T-162 alumina)	545.
" " (F-110 act. alumina)	5.5(10) ⁶
Hardwicke (26)	3.9*

*Estimated values.

It was found that, in general, high surface conditions lengthened ignition delay considerably. Therefore, a relationship between ignition delay and S/V seemed necessary.

By plotting (t/ψ) for each of the additives in turn on a graph on which the straight line of Figure 22 was superimposed, values of a surface/volume correction factor were determined. These values, β , are defined as:

$$\beta = \frac{(t/\psi)_i}{(t/\psi)_{\text{ref.}}} \quad (59)$$

where $(t/\psi)_{\text{ref.}}$ is the pressure-corrected ignition delay to which all other values were referred, and $(t/\psi)_i$ refers to the pressure-corrected ignition delay under any other S/V conditions. For convenience, the pressure-corrected ignition delay for the empty reactor ($S/V = 3.5 \text{ cm}^{-1}$) of the present study was used as a reference. A typical construction is shown in Figure 23.

A plot of $\log \beta$ versus $\log (S/V)$ is presented in Figure 24. The data of Newitt and Haffner resulted in the point at lowest S/V. These data were included because of the obvious deviation from the earlier correlation of t/ψ versus $1/T$, (Figure 22). It can be seen that little variation in β occurs for S/V ratios above about 10^4 cm^{-1} . This observation is invaluable in that all catalysts used in later tests fell into the region of S/V values such that β was approximately constant at 5.5.

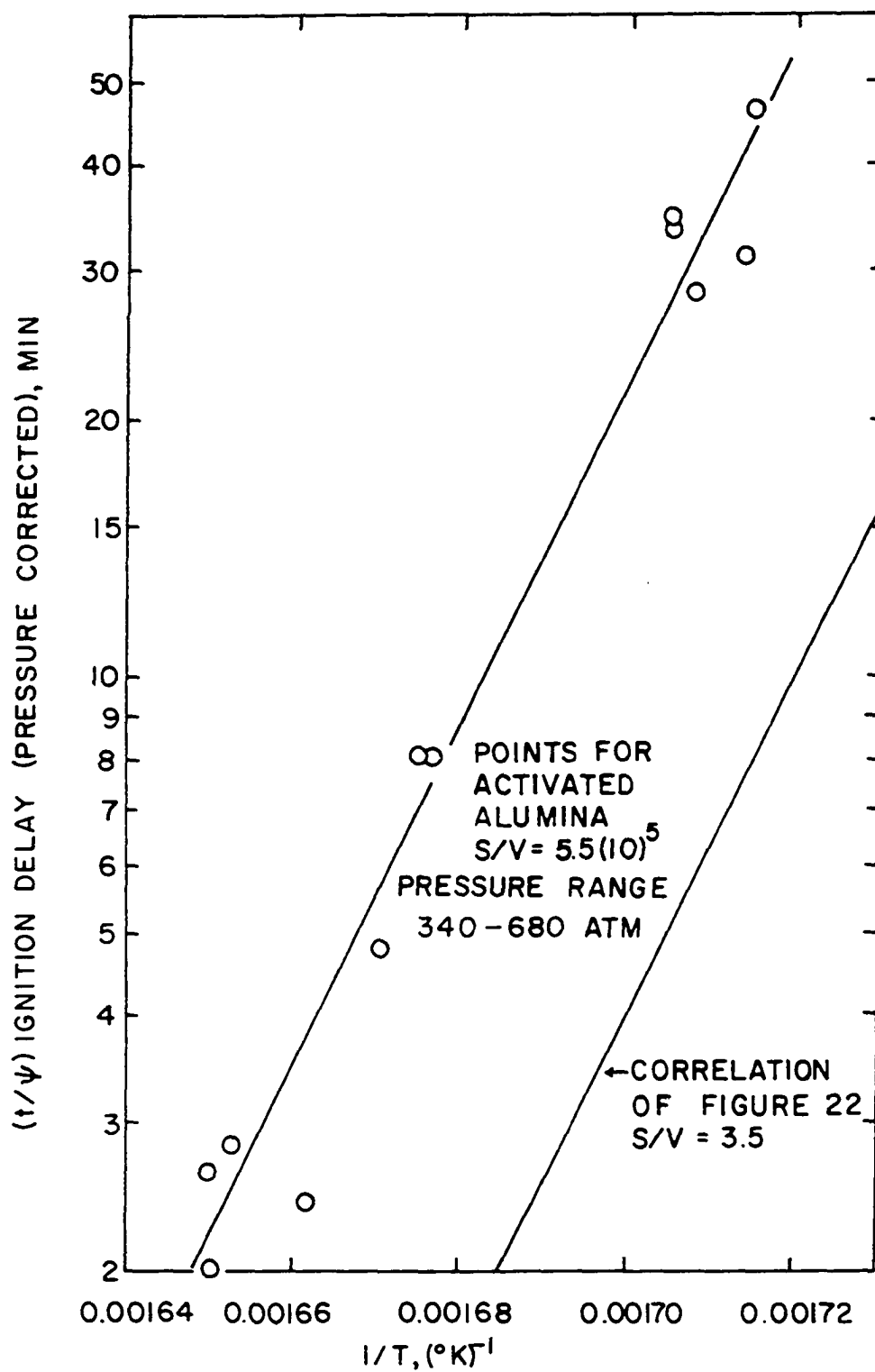


Figure 23. Graphical Determination of Surface Factor.

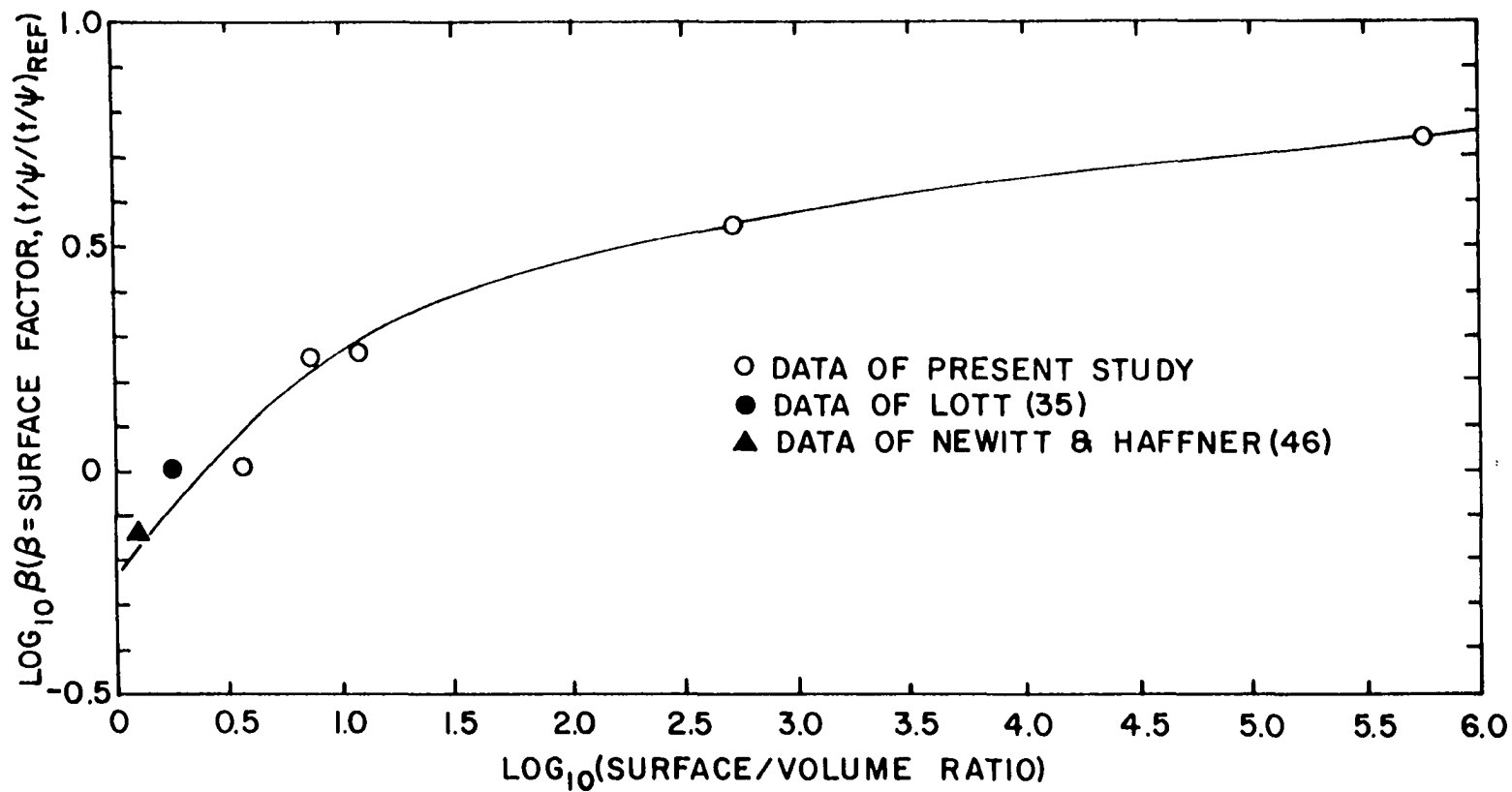


Figure 24. Surface Factor for Correction of Ignition Delays.

In three-body reactions in which the presence of a third molecule, reactor packing, or reactor wall is necessary for absorption of excess bond energy, the reaction rate becomes independent of the concentration of the third body at high concentrations of the third body (see Appendix B). This result is reflected in the asymptotic approach of β toward a constant value at S/V ratios in excess of about 10^4 . At low values of S/V, the slope of $\log \beta$ versus $\log (S/V)$ is approximately unity, a condition also expected in three-body reactions at low concentrations of the third body (see Appendix A).

Ignition delay, corrected for both pressure and surface/volume ratio, is presented in Figure 25, as a function of reciprocal temperature. This curve became the basis for evaluation of catalytic activity in later tests. It was found that data taken at a high surface/volume ratio and at about 476 atm correlated better if the low pressure curve for ψ was used. This observation implies that the two regimes are relatable to surface effects in some manner. It is possible that the reaction shifts from a heterogeneous reaction, which is dependent on diffusional effects, to a homogenous system.

The data of Lott at 476 atm in the range designated by him as Curve 2 were now assumed to be applicable to the low pressures region in determination of ψ . These points were seen to fall well within the correlation.

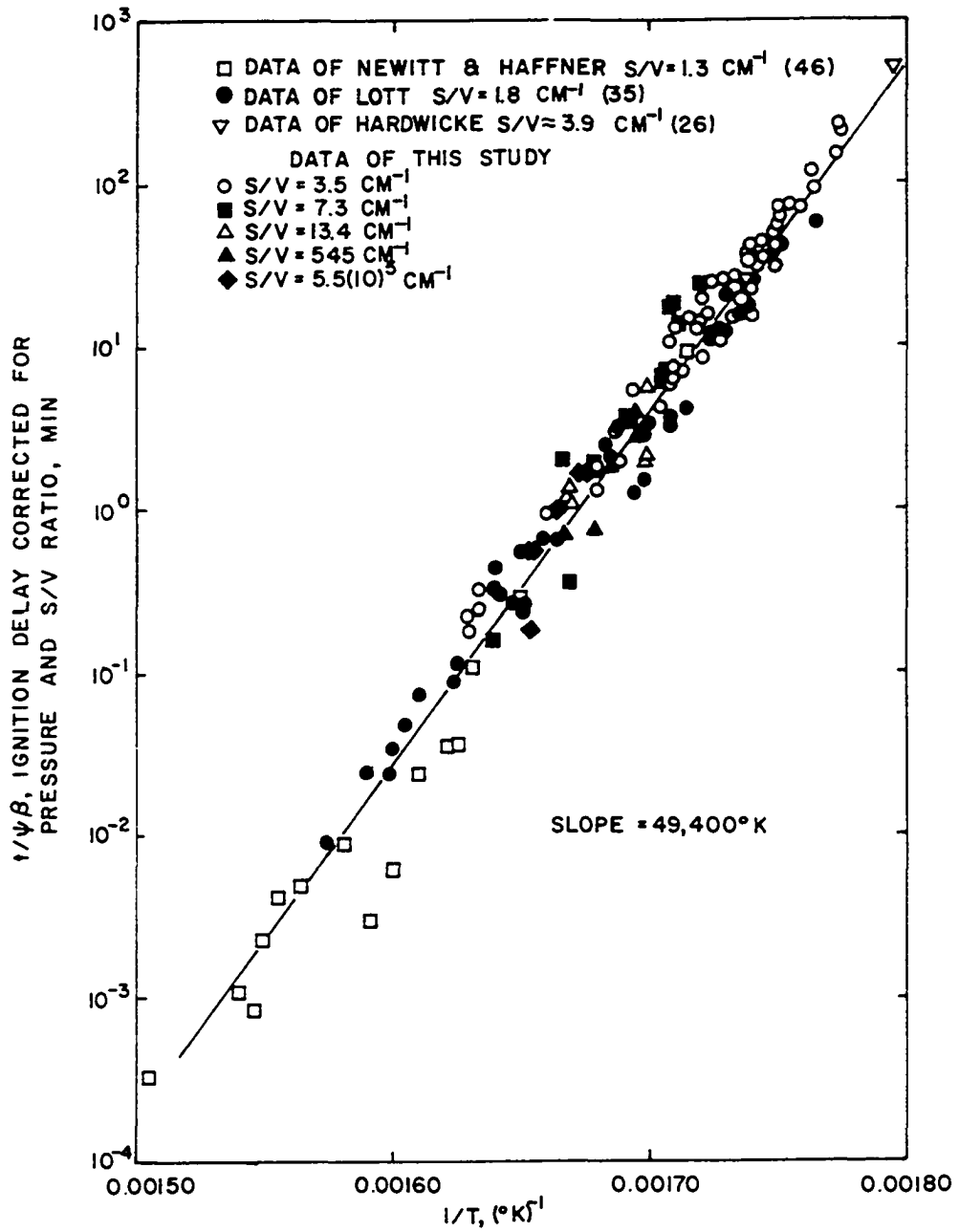


Figure 25. Ignition Delay Corrected for Pressure and Surface Effects as Function of Temperature.

Activation Energy from Ignition Delay

The correlation of Figure 25 is represented by the following equation:

$$\frac{t}{\psi^B} = Ae^{B/T} \quad (60)$$

where A and B are constants. Semenov (63) showed that ignition delay can be represented by a function of the form:

$$t = k P^n e^{E/RT} \quad (61)$$

where E is activation energy for ignition delay and n is the "order" with respect to pressure. It has already been shown that ψ is proportional to pressure to a power. The constant B in the exponential of equation 60 is thus equal to activation energy divided by R, the gas constant.

The slope of the corrected ignition delay curve of Figure 25 was determined to be 49,400 Deg. K. This result leads to determination of an activation energy of 98 kcal/mole.

Melvin (41) reported a value of about 42 kcal/mole for activation energy determined from equation delay over a temperature range of 352 to 496°C and at 100 atm. Neumann and Egerov (45), however, reported a value of 81 kcal/mole, which is more in agreement with the present determination. Their work was done at low pressure. Several others, working at low pressures have determined activation energy. Vanpee (71) over the temperature range 377-422°C determined E to be 93 kcal/mole; and Fort and Hinshel (16) determined E to be 62 kcal/mole over the range, 447°-487°C.

Other published results were summarized earlier in Table 3, page 85. The table infers that activation energy increases with decreasing temperature. The result of Melvin (41), however, which was determined at pressures within the range of the present study appear to contradict the above inference. Melvin defined ignition delay as the time from end of fill to the point at which temperature departed from a slow linear rise to auto-acceleration.

It was felt possible that the definition of ignition delay as time to maximum temperature, rather than to point of onset of auto-acceleration, could have caused the high activation energy obtained in the present study. To find if the method of correlation of Melvin would result in a lower activation energy with the data of the present study, the data were inspected to determine the point of onset of auto-acceleration in each test. The logarithms of times to these points were plotted versus $1/T$ as before. Using this method, an activation energy of 95 kcal/mole was again obtained. The closeness of this value to that obtained earlier implies that the time from start of auto-acceleration to the maximum temperature is proportional to the total ignition delay.

It should be recalled that the data of Melvin applied to pre-explosive conditions, a condition attained only in a small portion of the non-catalytic tests in this series. The data of Lott, however, contained results of

many tests in which explosion occurred (according to the definition used here). Using the data of Lott, a plot of time interval up to auto-acceleration versus $1/T$ was made. Again, an activation energy of about 95-98 kcal/mole was obtained.

Activation energy measured by Melvin was reasonably constant at about 43 kcal/mole over a wide range of mixture ratios. Because the data of Lott and that of the present study fell within the range of mixture ratios measured by Melvin, the discrepancy could not be attributed to a variation in mixture ratio.

Melvin also determined activation energies during the explosive reaction itself to be about 23 kcal/mole, a value far removed from the values obtained for the slow reaction or the moderately fast reaction leading to auto-acceleration. With this apparent discrepancy in mind, ignition delays of only the non-explosive reactions of the present reciprocal study were correlated with inverse maximum temperature rather than with inverse initial temperature (Figure 26). Again, an activation energy of 92.5 kcal/mole was obtained. This slope may be due, in part, to temperature rises being generally less than 10% of the initial temperature. The same pressure dependence occurred as before.

However, when ignition delays of explosive reactions were correlated with $1/T_{\max}$, an activation energy of 27,700

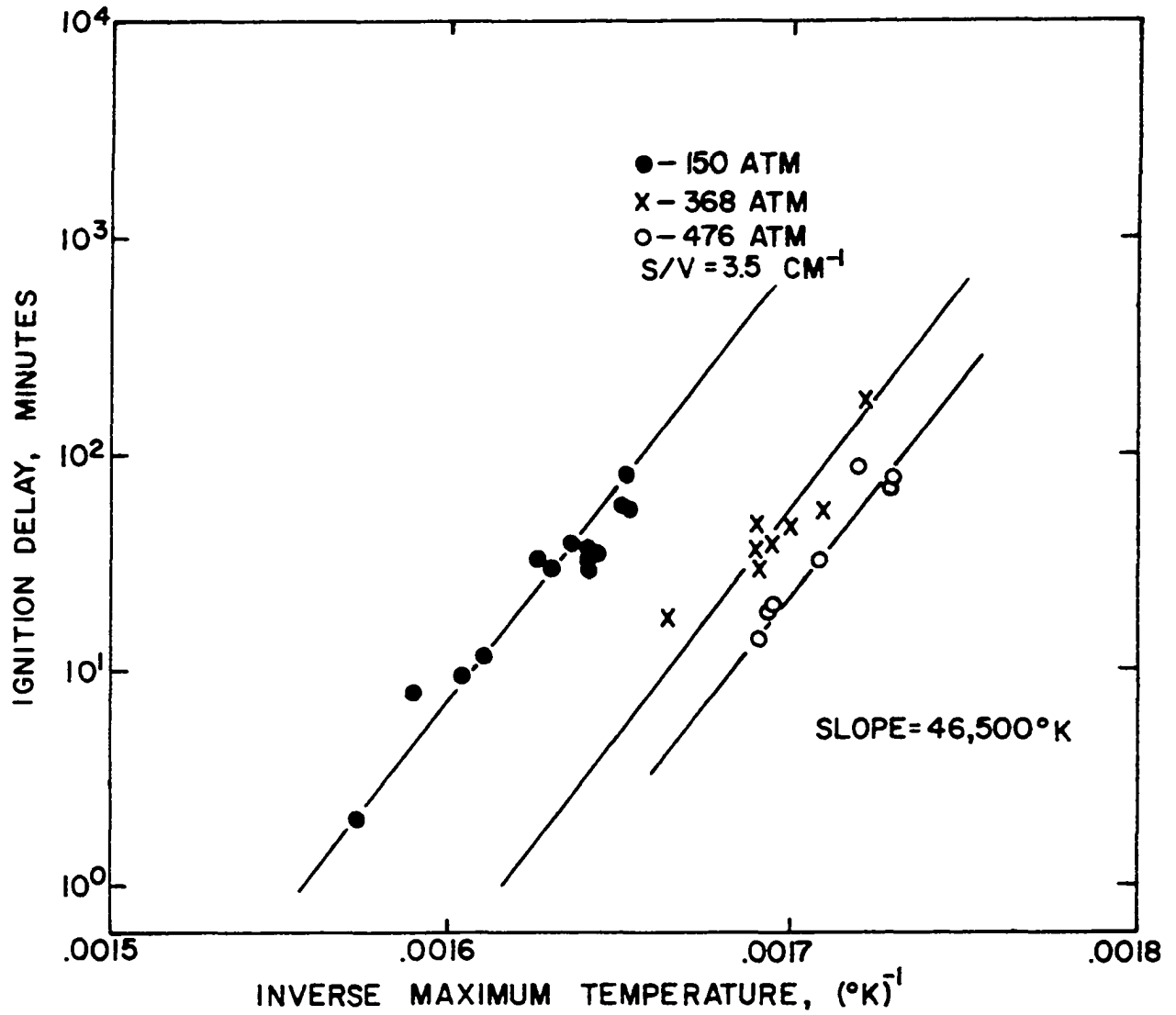


Figure 26. Ignition Delay as a Function of Maximum Temperature for Non-Explosive Tests.

kcal/mole was obtained (Figure 27). In this case, however, no pressure dependence was observed. This observation implies that, for a given ignition delay at two different pressures, the maximum attained temperatures are equal regardless of initial temperature. Consistent with the above, Melvin (41) found that little effect of pressure on explosive reaction rate is observed above 70 atm.

The fact that T_{\max} should be a result of, rather than a cause of, variation in ignition delay makes the implications of the correlations of Figures 26 and 27 uncertain. However, it is apparent that, due to the variation in activation energies, two different mechanisms are involved in explosive and non-explosive reactions.

Effect of Catalysts on Ignition Delay

The influence of metallic surfaces and inactive porous material on ignition delay has been shown. Activation energy was not seen to be a function of surface/volume ratio. Therefore, any observed changes in ignition delay due to presence of catalysts were felt to be due to catalysis only. All catalysts used had very high S/V ratios and fell in the region of constant correction factor ($\beta \approx 5.5$)

Several Catalytic materials were chosen for screening in this program. Selection was made from the following general categories:

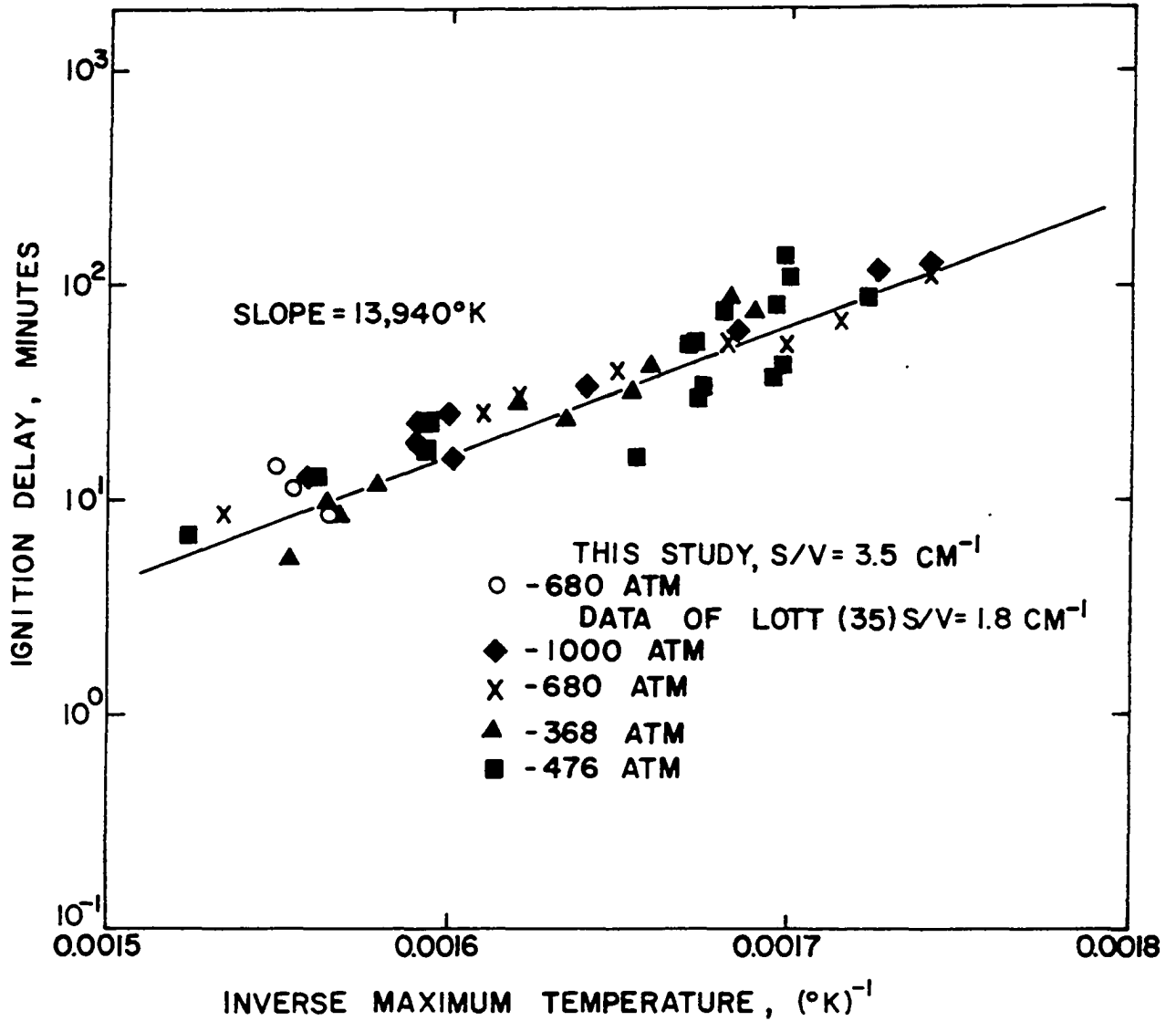


Figure 27. Ignition Delay as a Function of Maximum Temperature for Explosive Tests.

- (1) Hydrogenation Catalyst
- (2) Oxidation Catalyst

The following specific materials were selected:

(1) Kaolin, obtained from Houdry Process and Chemical Co., as mineral-processed Kao-Spheres, 3.2-mm diameter balls.

(2) Cobalt Molybdate, obtained from Houdry Process and Chemical Co., as 3.2-mm extrudes, approximately 9.5-mm long.

(3) Nickel Catalyst, obtained from the Harshaw Chemical Company, as 3.2-mm diameter extrudes, 3.2-mm long in the form of 15% nickel oxide on alumina.

(4) Silica-Alumina, obtained from W. R. Grace and Co., as 3.2-mm balls.

(5) Silica-Magnesia, obtained from W. R. Grace and Co., as 3.2-mm balls.

Each catalyst was used in a series of tests over the temperature and pressure ranges of the previous portion of study.

Figures 28 through 31 show the effect of temperature on ignition delay, corrected for surface-volume ratio and for pressure. In each case a straight line reasonably represented the data. The solid line with the parallel dotted lines on either side represent the non-catalytic reference correlation and the band within which all reference data fell. Nickel catalyst was not included in this method of

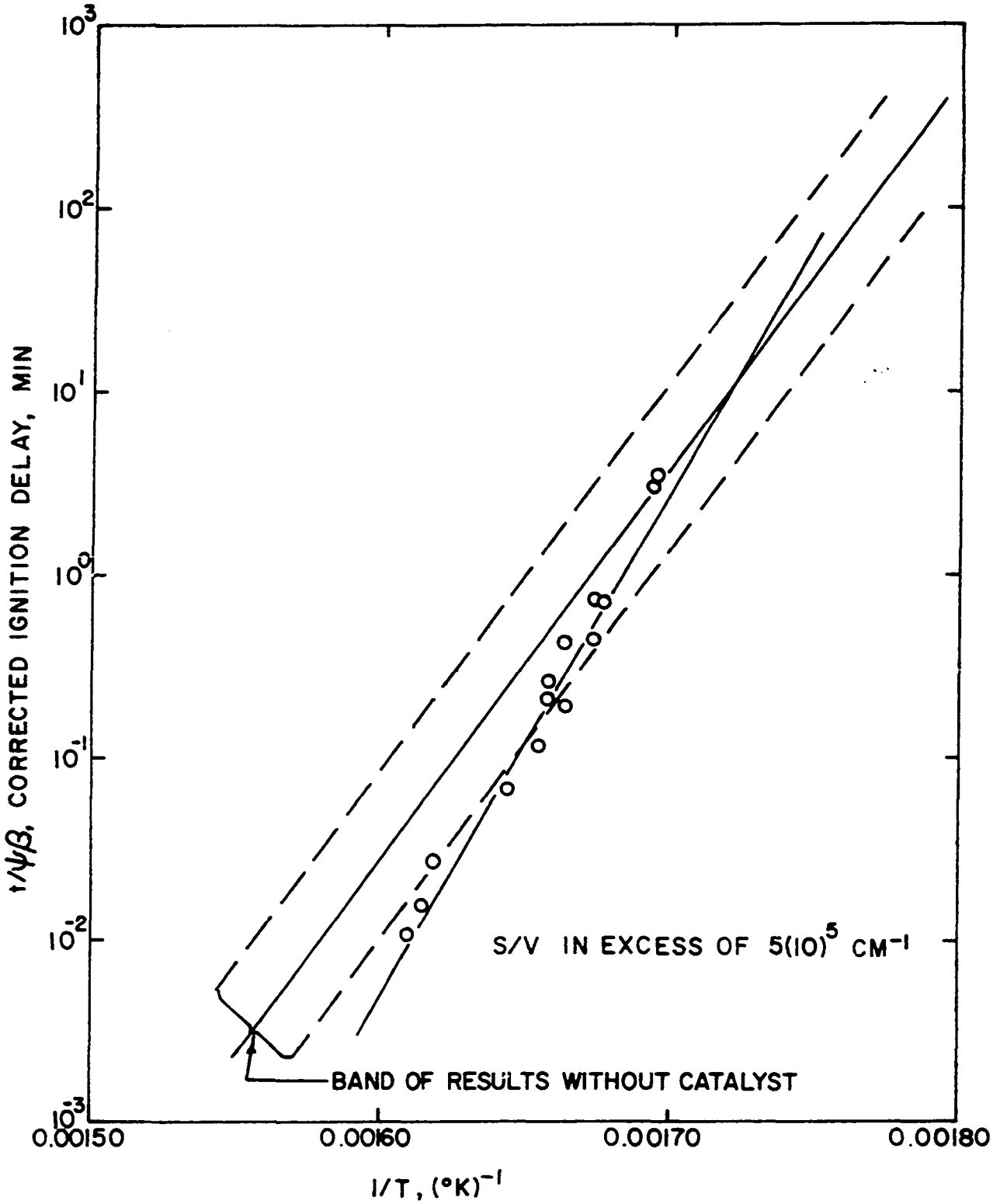


Figure 28. Ignition Delay using Kao-Spheres Catalyst.

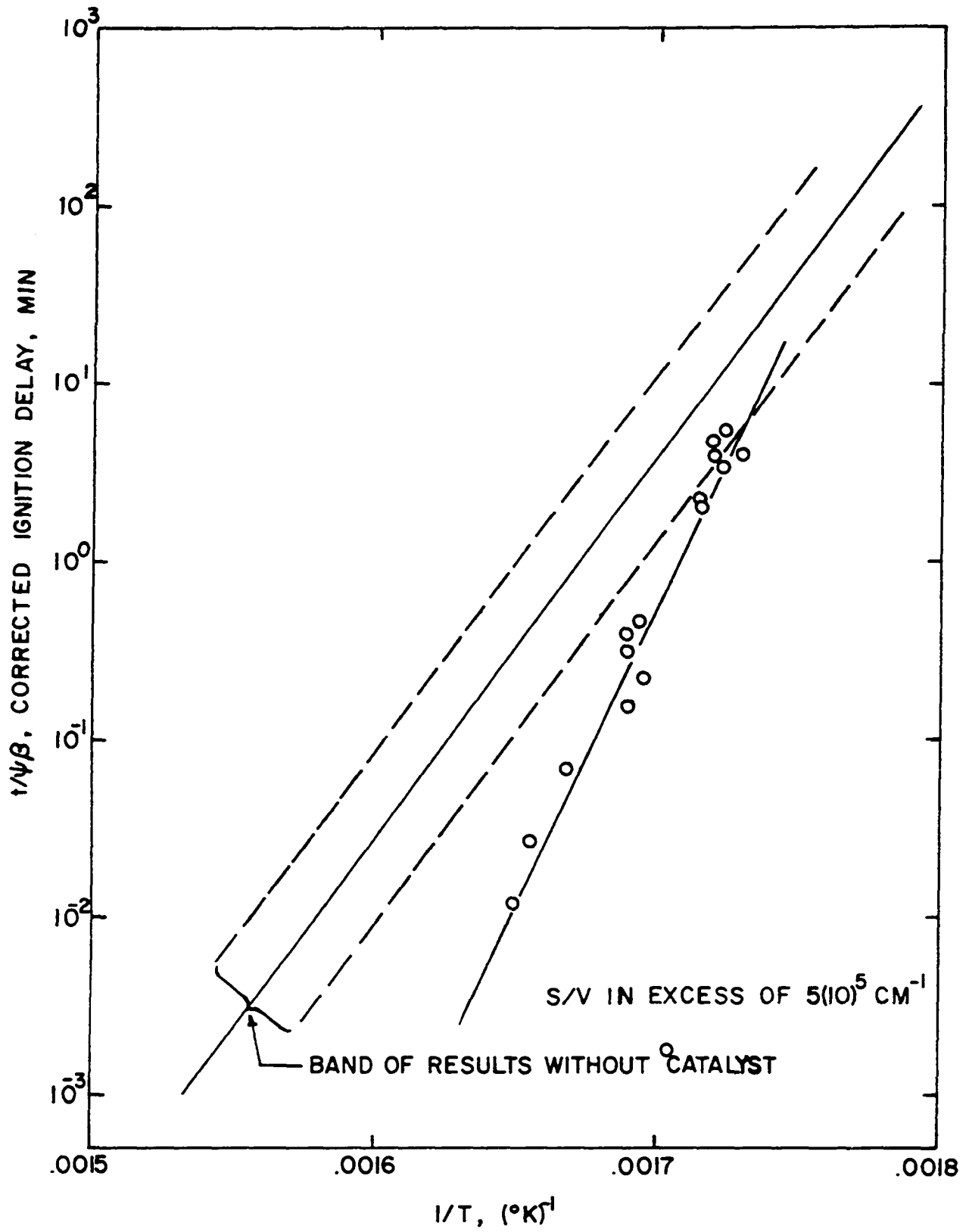


Figure 29. Ignition Delay Using Cobalt Molybdate Catalyst.

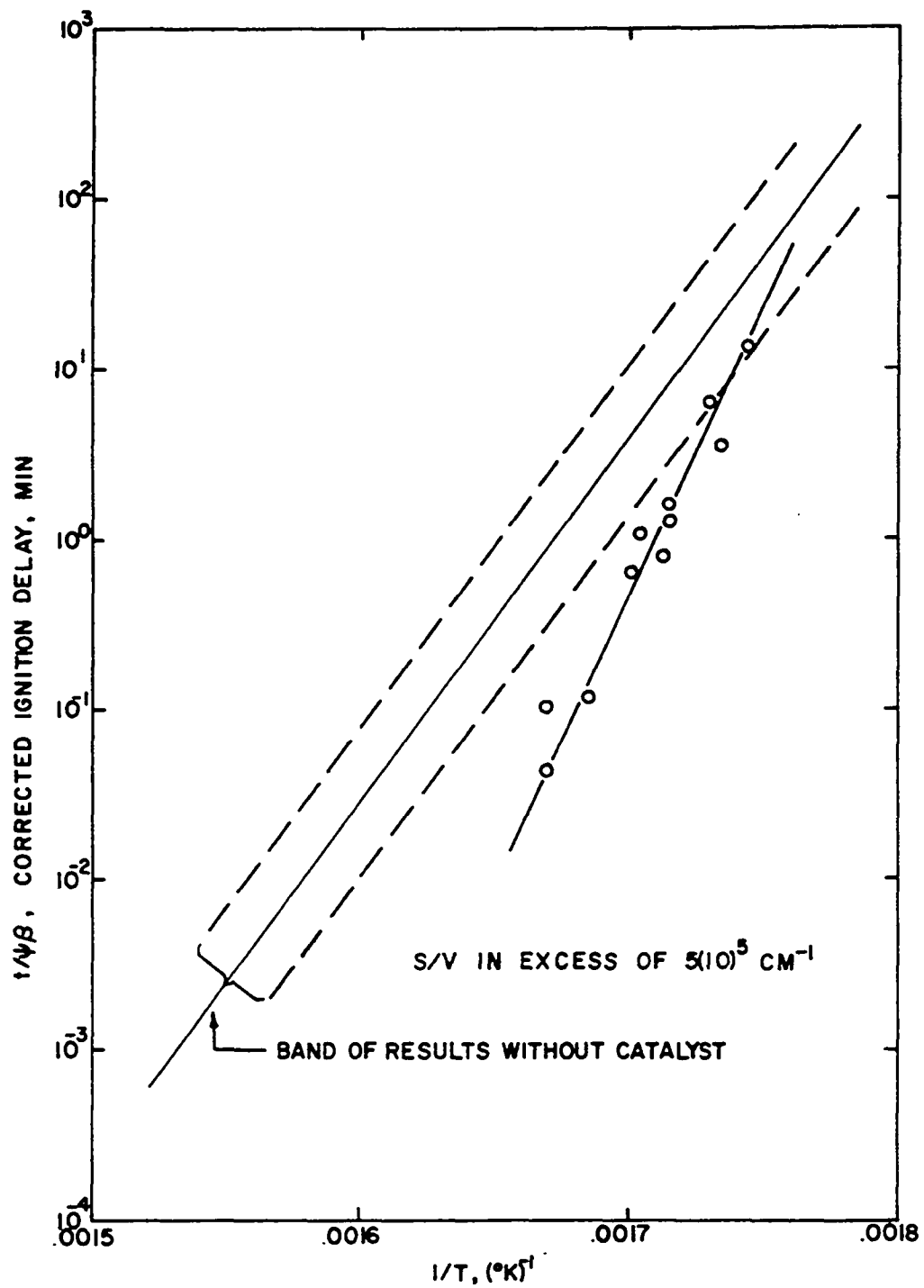


Figure 30. Ignition Delay Using Silica-Alumina Catalyst.

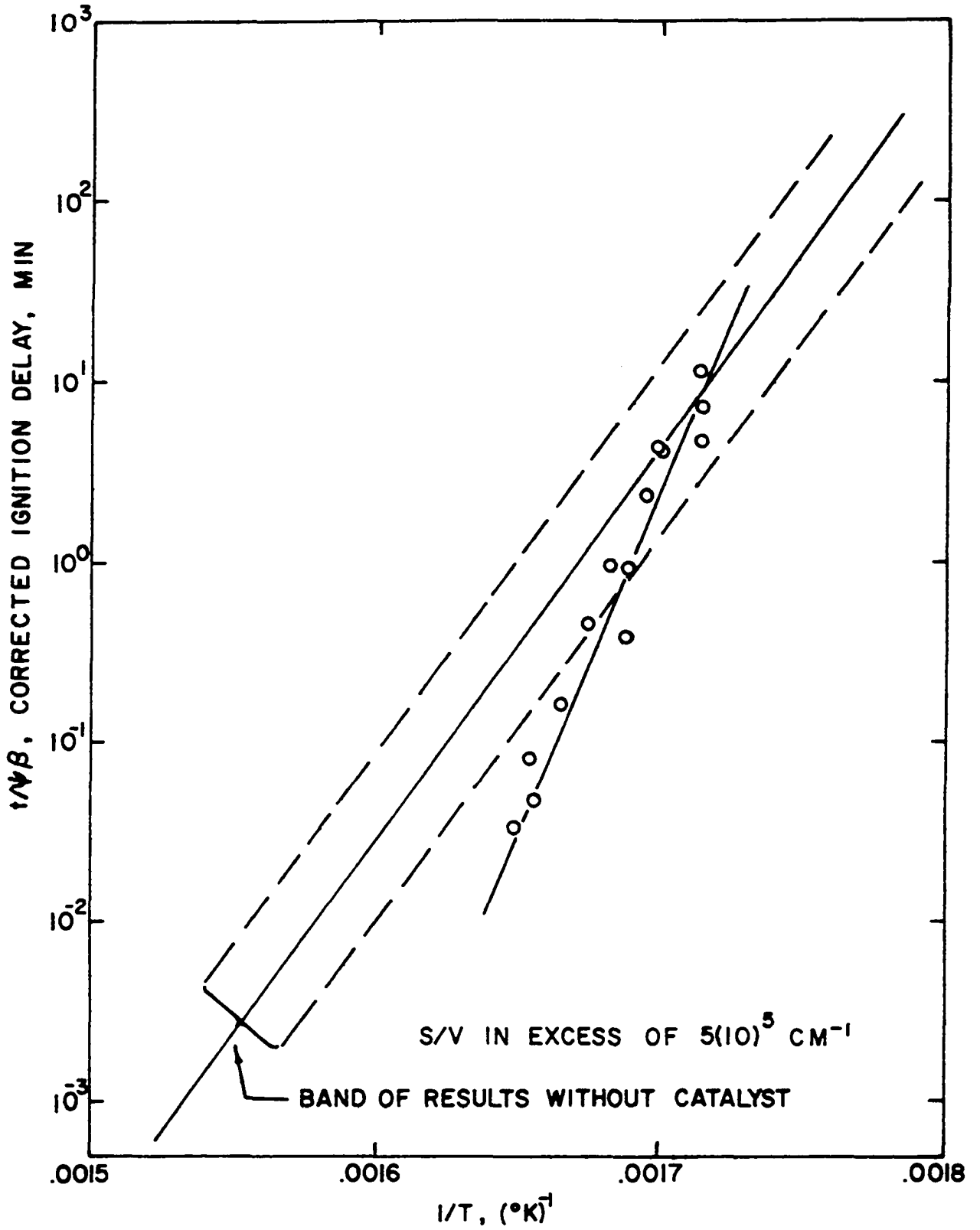


Figure 31. Ignition Delay Using Silica-Magnesia Catalyst.

analysis; extreme differences in mechanism, as will be shown later, prevented such a correlation. In the case of Kao-Spheres (Figure 28) the line through the data may not be the best representation; most of the data fall approximately within the band of non-catalytic data.

Activation energies were calculated from each plot; these values are summarized below:

<u>Catalyst</u>	<u>Activation Energy for Ignition Delay</u> kcal/mole
Kao-Spheres	126
Cobalt-Molybdate	154
Silica Alumina	158
Silica Magnesia	174

In each case, the activation energy was higher than in the non-catalyzed reaction, indicating a much stronger influence of temperature on the reaction. Although activation energies were higher in the catalyzed tests, the trend was toward shorter delays at high temperatures, possibly due to pre-exponential terms being markedly lower than in the reference tests.

The reduction in ignition delay implies that each catalyst increased the overall rate of reaction. It is unlikely that this increase was due to a decrease in chain termination. Each of the catalysts used should have presented a much more active surface for destruction of peroxides. It is felt, rather, that the decrease in ignition

delay was due to an increase in the rate of the initiation step. This premise gives strong support to the generally-accepted theory that slow oxidation is both surface-initiated and surface-quenched.

Product Distribution of Non-Catalyzed Tests

Table A-1 in Appendix A presents product analyses determined in this phase of the program. In general, each test resulted in the following gases: unreacted methane and oxygen, ethane, carbon dioxide, and carbon monoxide.

Liquid products contained water, methanol and formaldehyde in the general case, with some tests resulting in formation of formic acid, methyl formate, acetic acid, and ethanol. The acids and the ester were formed only at the higher pressures.

Because a sampling technique, which would enable removal of reactants and products during a test without upsetting the source of reaction, was not devised, a large number of tests of varying residence time were necessary. Fortunately, ignition delay was highly reproducible, enabling termination of tests at any time and the collection of time-temperature-concentration data points.

Overall mole fractions were determined from the chromatographic analyses, the known reactor volume, and the measured pressures and temperatures. Values of compressibility were necessary to determine the exact amount

of reactants and to combine the liquid and gas analyses.

The Benedict-Webb-Rubin (BWR) equation of state for methane (8) was used to determine compressibilities and reactant and product densities. An IBM 360, Model 40 computer was programmed to perform the calculations. The program determined in order: reactant and product compressibilities, densities, overall concentrations, material balances, and distributions of products formed as percentages of depleted reactants. Compressibilities were based on constants for the BWR equation for pure methane (8). The variation due to presence of other materials was not considered because of the low concentrations of these materials; furthermore, necessary adjustments to the material balance calculations (described later) minimized the error due to omission of the effect of these materials.

The effect of neglecting the influence of oxygen in calculating the compressibilities was tested by using the BWR equation in a form which treated binary mixtures. The available constants for oxygen (65) were not adequate at elevated pressures. These constants were modified for high pressure applicability.

By using the binary form of the equation with these new constants the compressibilities were slightly different from those determined for pure methane. The iterative steps in the material balance calculations,

however, reduced the error due to neglecting oxygen in calculation of compressibilities to well within that due to error in measurement of pressure. Thus, in order to conserve computation time, the form of the BWR equation based on pure methane was used throughout this study.

The BWR constants for methane were modified also for increased applicability at high pressures. The modification of these values becomes significant only above about 1000 atm., which was beyond the range of this study. The revised numbers are presented in Table C-1 in Appendix C, with the recommendation given that at pressures above 1000 atm they be used instead of the former published values.

The program for the calculation of product distributions and the material balances was written with the following steps in mind: First, carbon dioxide entering as a feed impurity was considered to remain inert and was deducted from that amount in the product. Second, the amounts of ethanol and acetic acid were considered to be formed first from the depleted ethane, and only the amount over that possibly formed from ethane, originally present as an impurity in the feed, was considered to be due to methane oxidation. Third, because the compressibilities at the dump pressures were felt to be more certain than those at the elevated feed pressures, the calculated feed amount based on compressibility for the higher pressure was

adjusted to give a close balance on carbon and hydrogen. Finally, because of the uncertainty in trapping all condensibles, the liquid product weight was adjusted so that all depleted oxygen unaccounted for was distributed among liquid products in the measured proportions.

These adjustments in almost all cases varied the initial material balances only slightly. The overall compositions before and after adjustment were not changed.

The material balance calculations were based on the ratio of inlet mass to outlet mass. These values are also presented in Table A-1 in Appendix A. The material balances were all in the range, 0.92-1.03 gm in/gm out. As stated, the computer program also determined product distribution, expressed as functions of reacted oxygen and reacted methane. These data are presented in Table A-2 in Appendix A.

Using the calculated overall mole fractions and the time-temperature data, reaction chronologies were constructed and are shown in Figures 32 through 46. The figures represent non-catalyzed reactions at various pressures and at surface/volume ratios between 3.5 and $5.5(10)^5 \text{ cm}^{-1}$.

All the gases mentioned earlier (except ethane) are shown in the figures. Liquid products shown, however, include only water, formaldehyde and methanol. The other liquid products were omitted from the graphs; they are listed, as they occurred, in Table A-1. The acids and methyl formate were formed, as mentioned, only at the higher

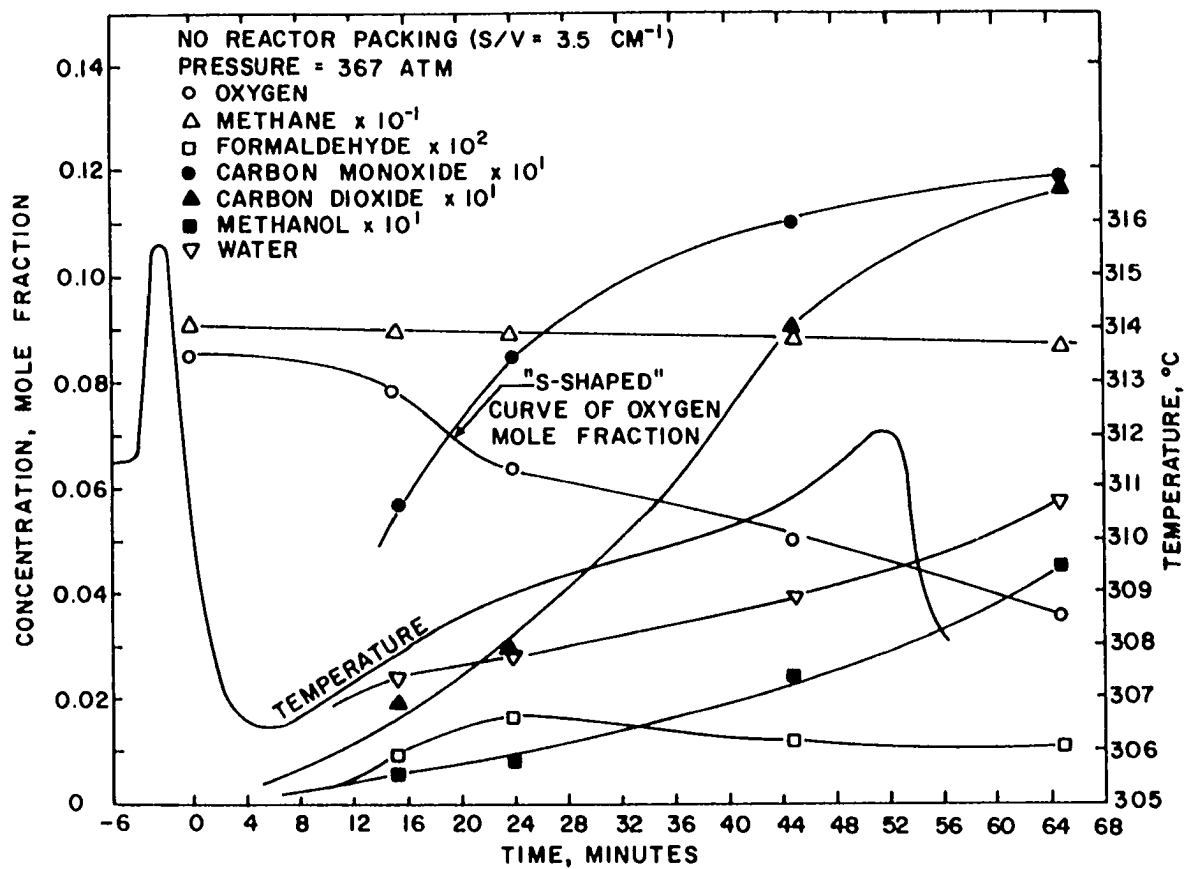


Figure 32. Reaction History at 367 atm, 306.5°C, and S/V of 3.5 cm⁻¹.

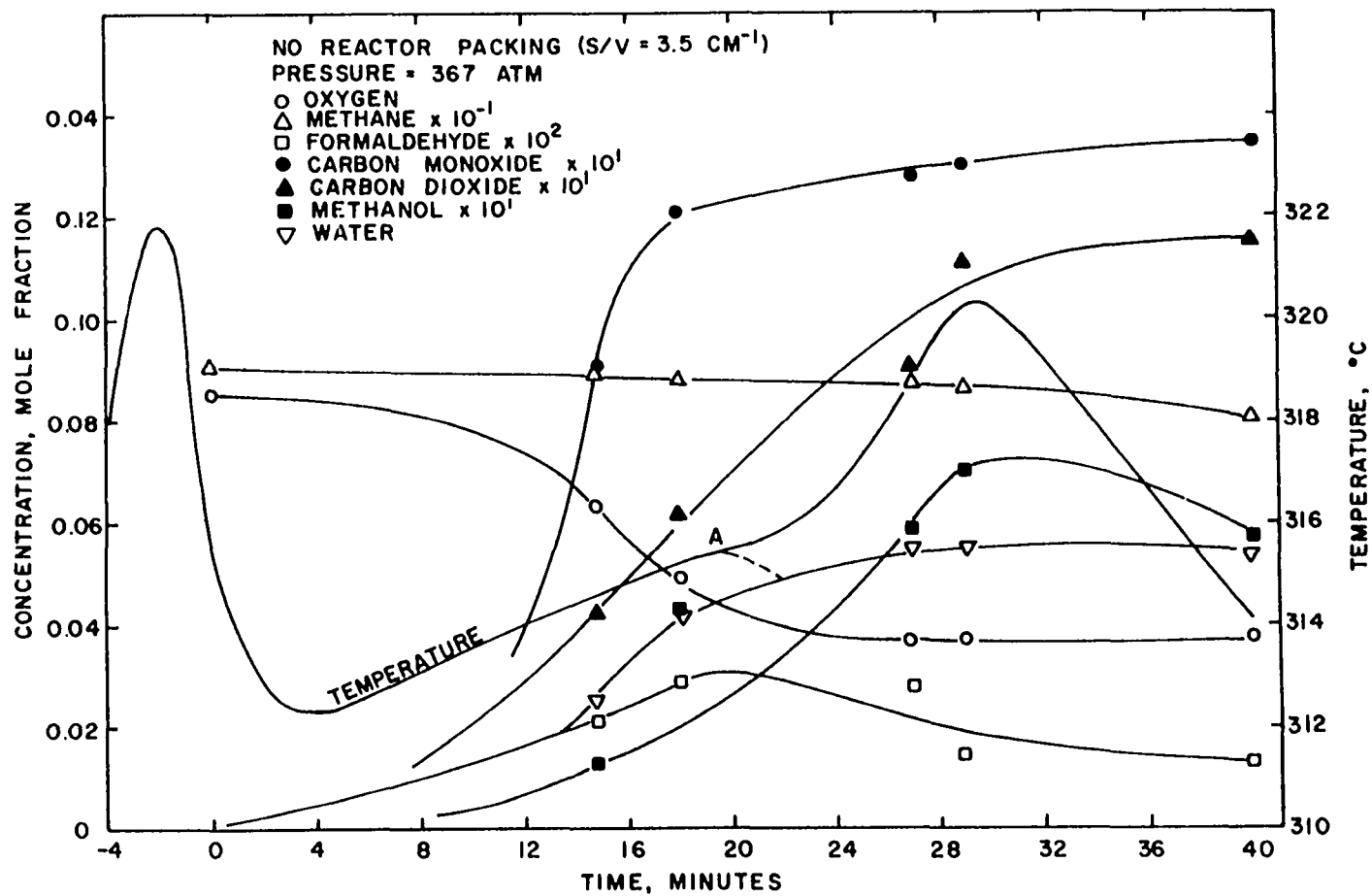


Figure 33. Reaction History at 367 atm, 312.3°C, and S/V of 3.5 cm⁻¹.

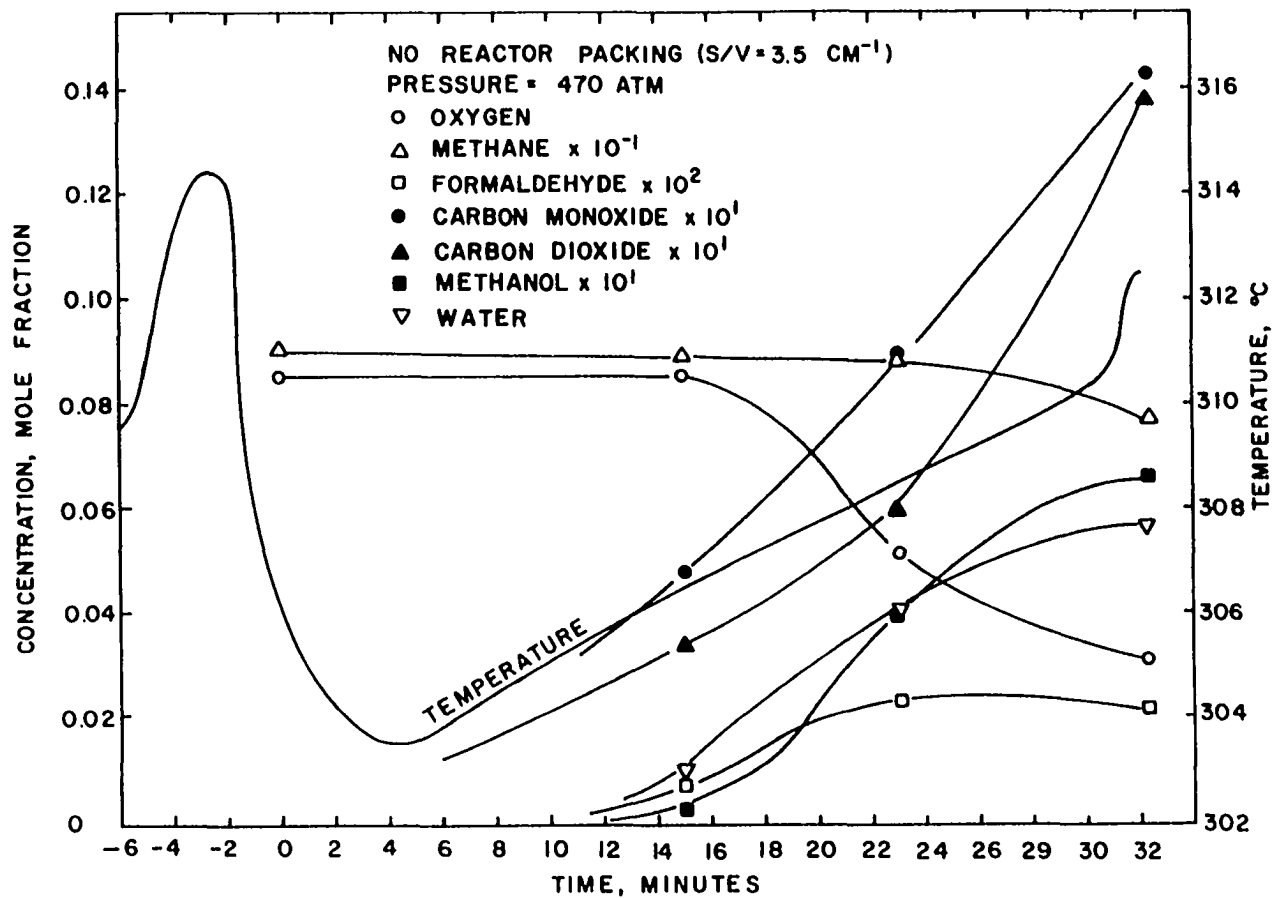


Figure 34. Reaction History at 470 atm, 303.5°C, and S/V of 3.5 cm⁻¹.

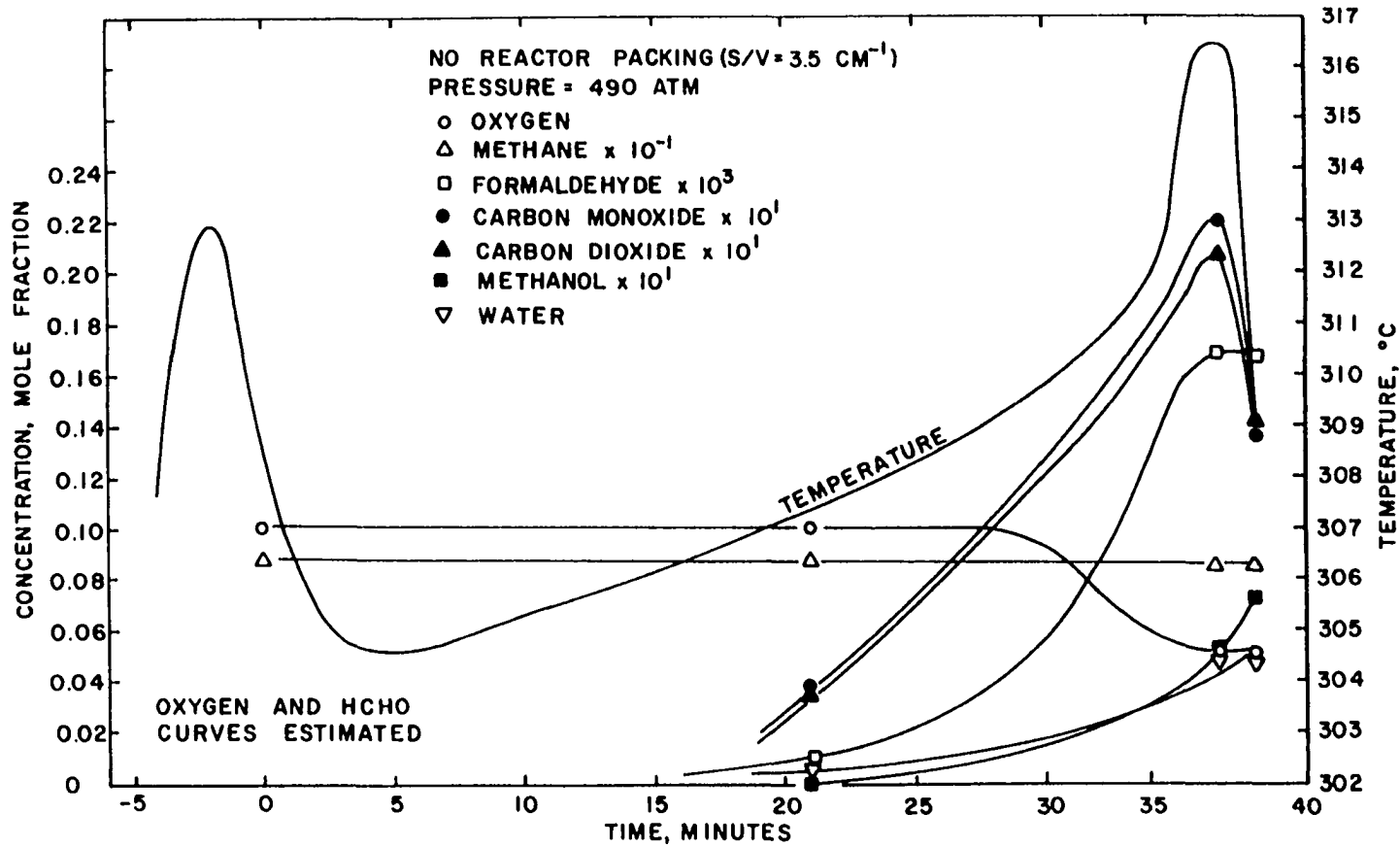


Figure 35. Reaction History at 490 atm, 304.6°C, and S/V of 3.5 cm⁻¹.

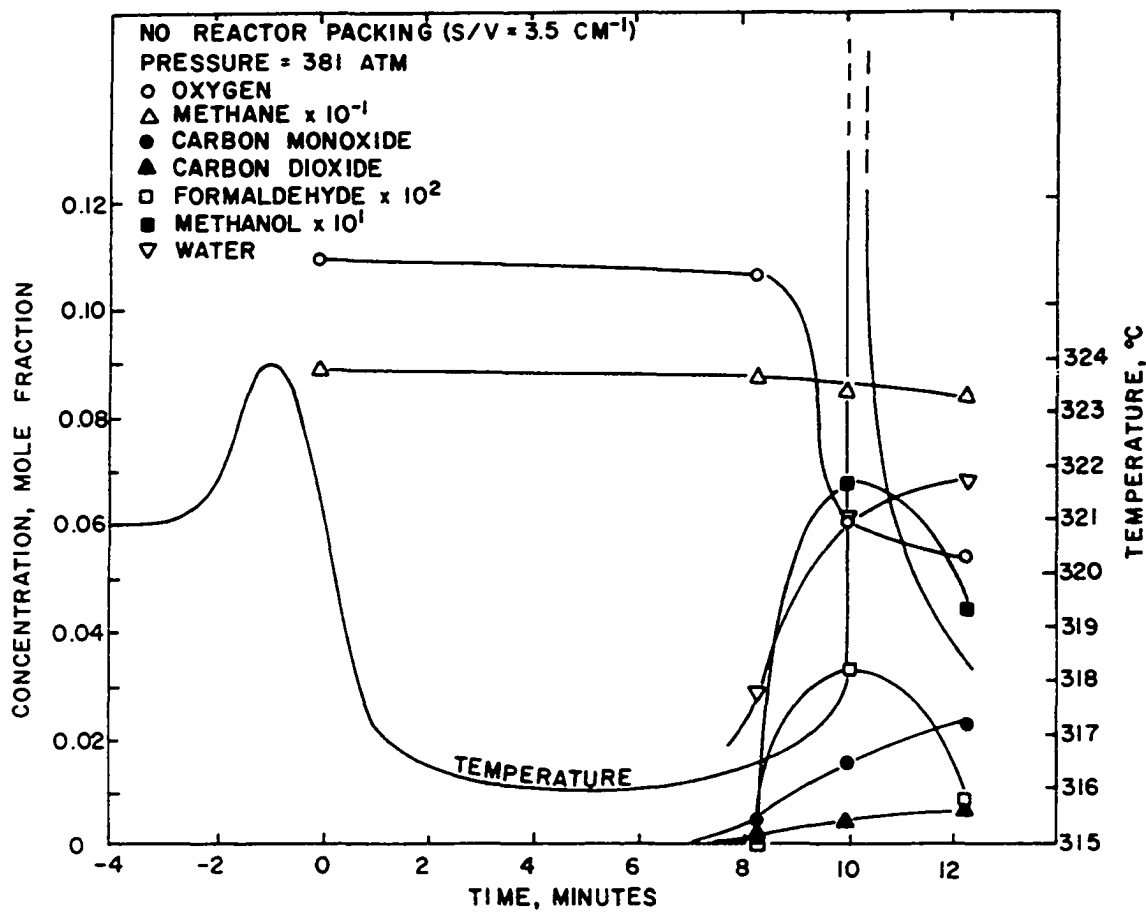


Figure 36. Reaction History at 381 atm, 316°C, and S/V of 3.5 cm⁻¹.

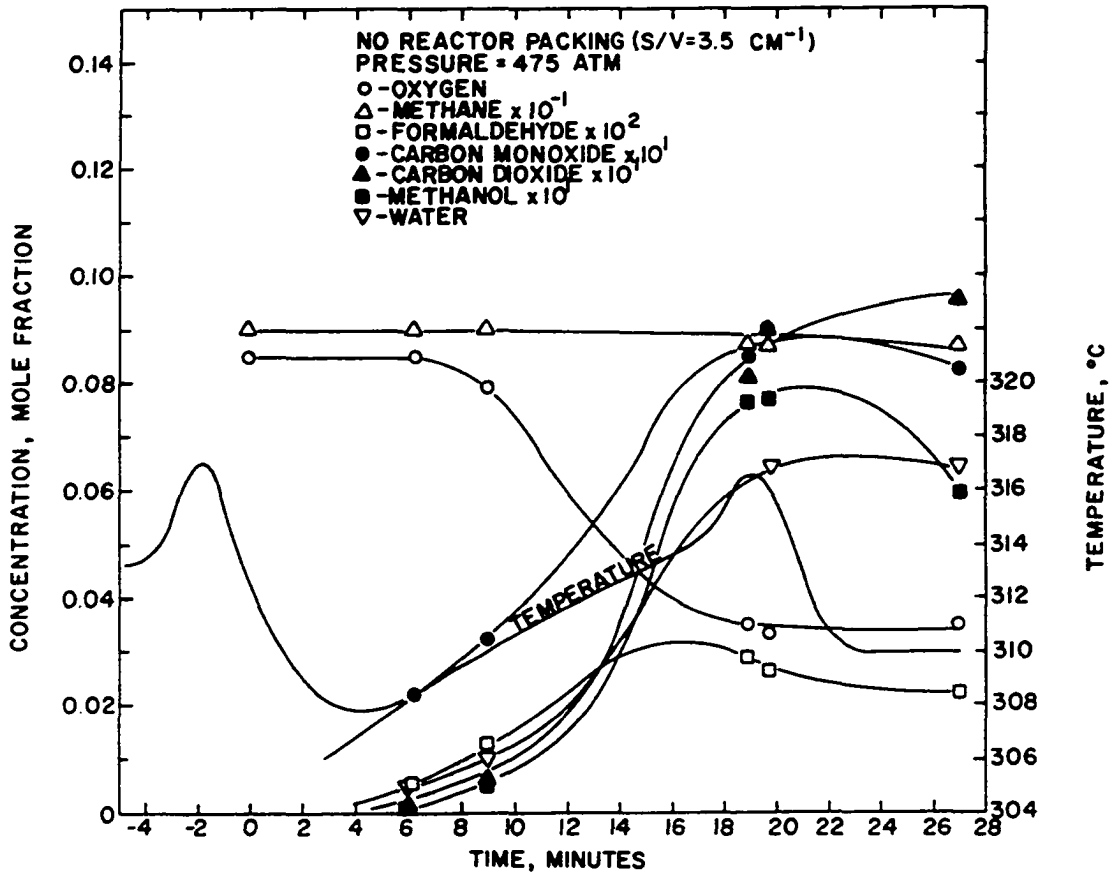


Figure 37. Reaction History at 475 atm, 307.9°C, and S/V of 3.5 cm^{-1} .

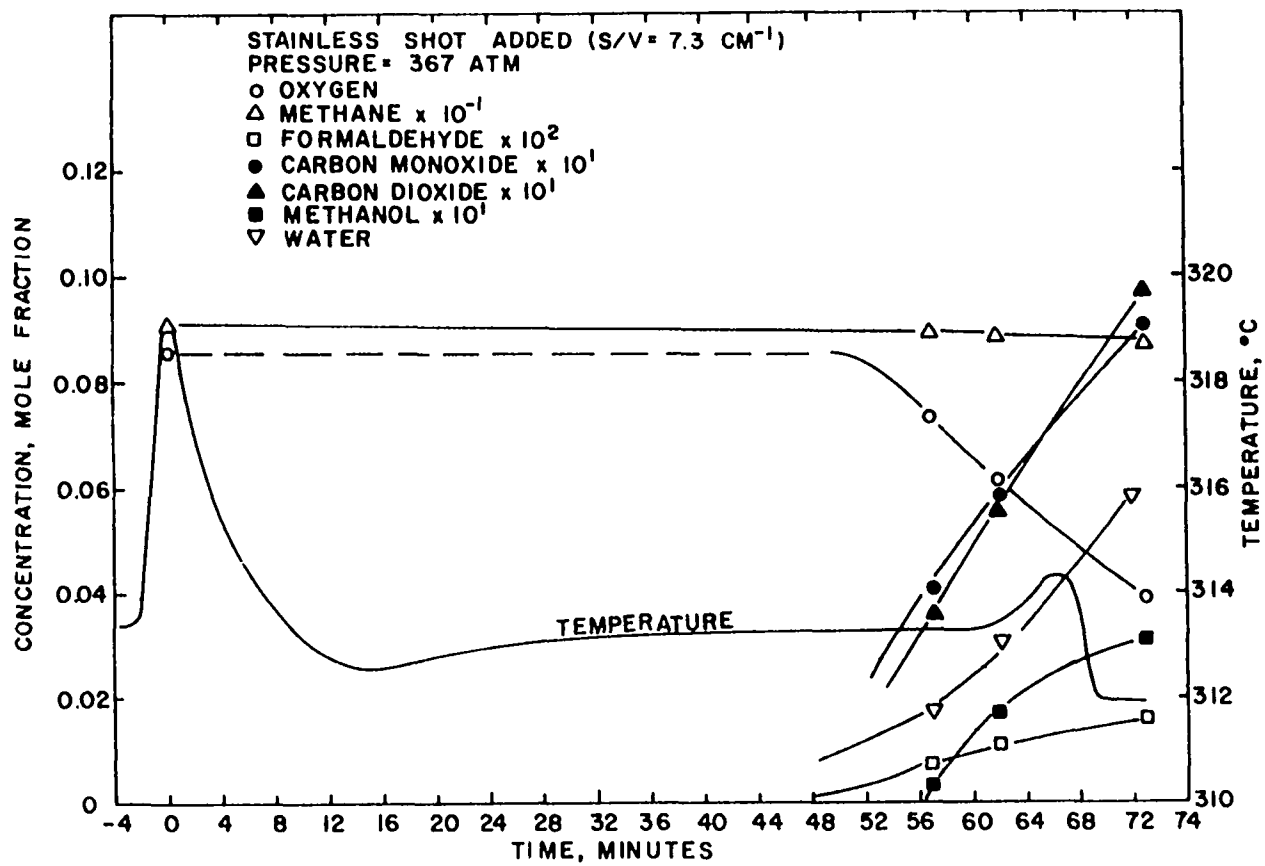


Figure 38. Reaction History at 367 atm, 312.6°C, and S/V of 7.3 cm⁻¹.

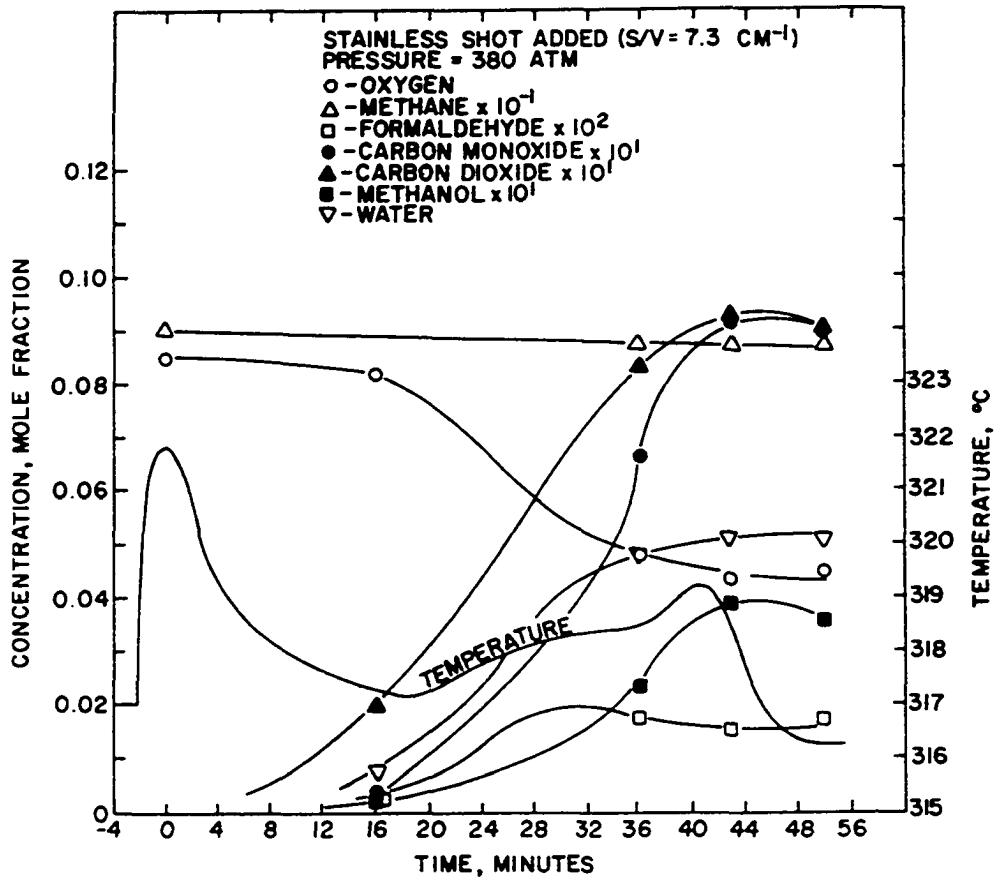


Figure 39. Reaction History at 380 atm, 317.2°C, and S/V of 7.3 cm^{-1} .

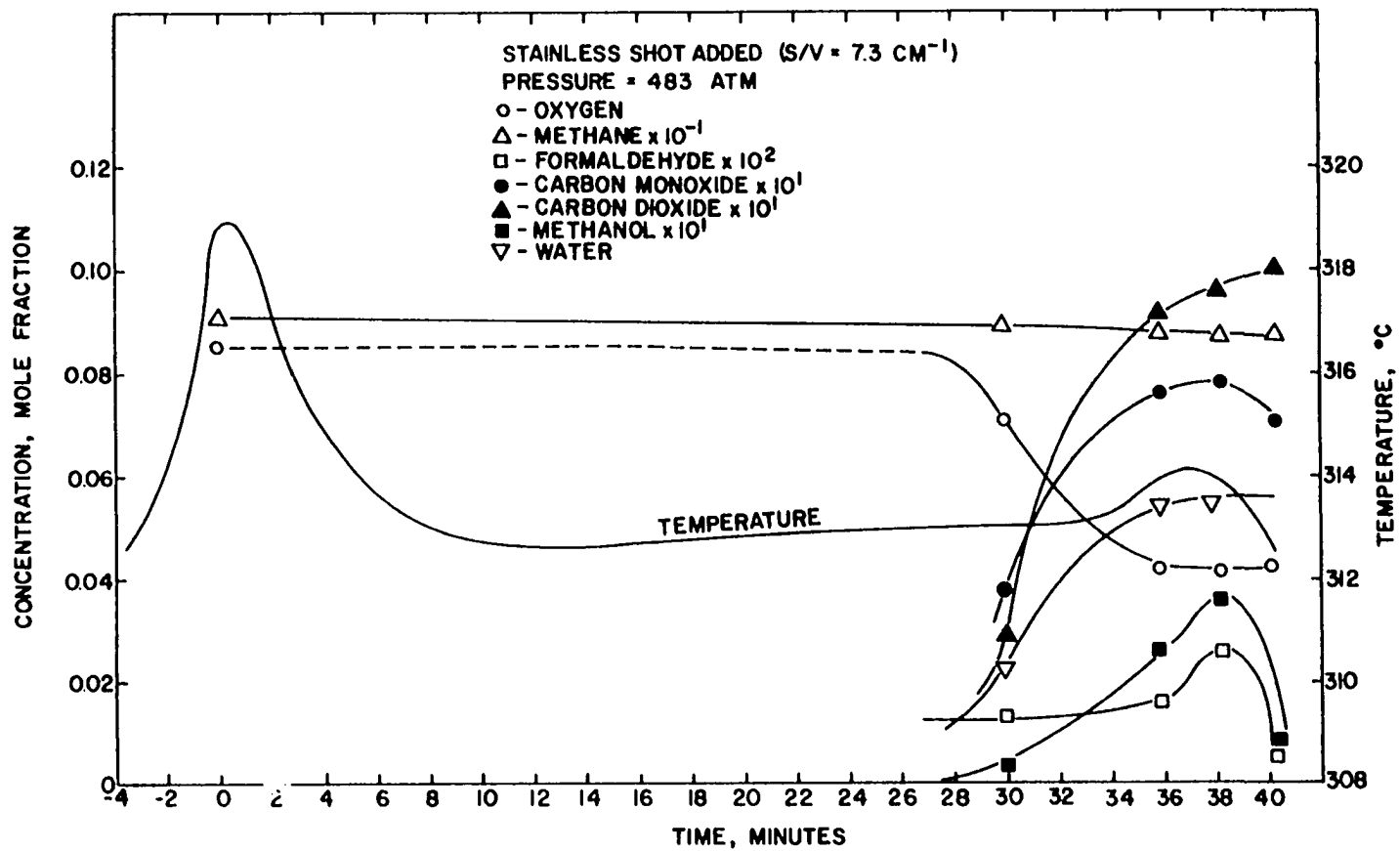


Figure 40. Reaction History at 433 atm, 312.6°C, and S/V of 7.3 cm⁻¹.

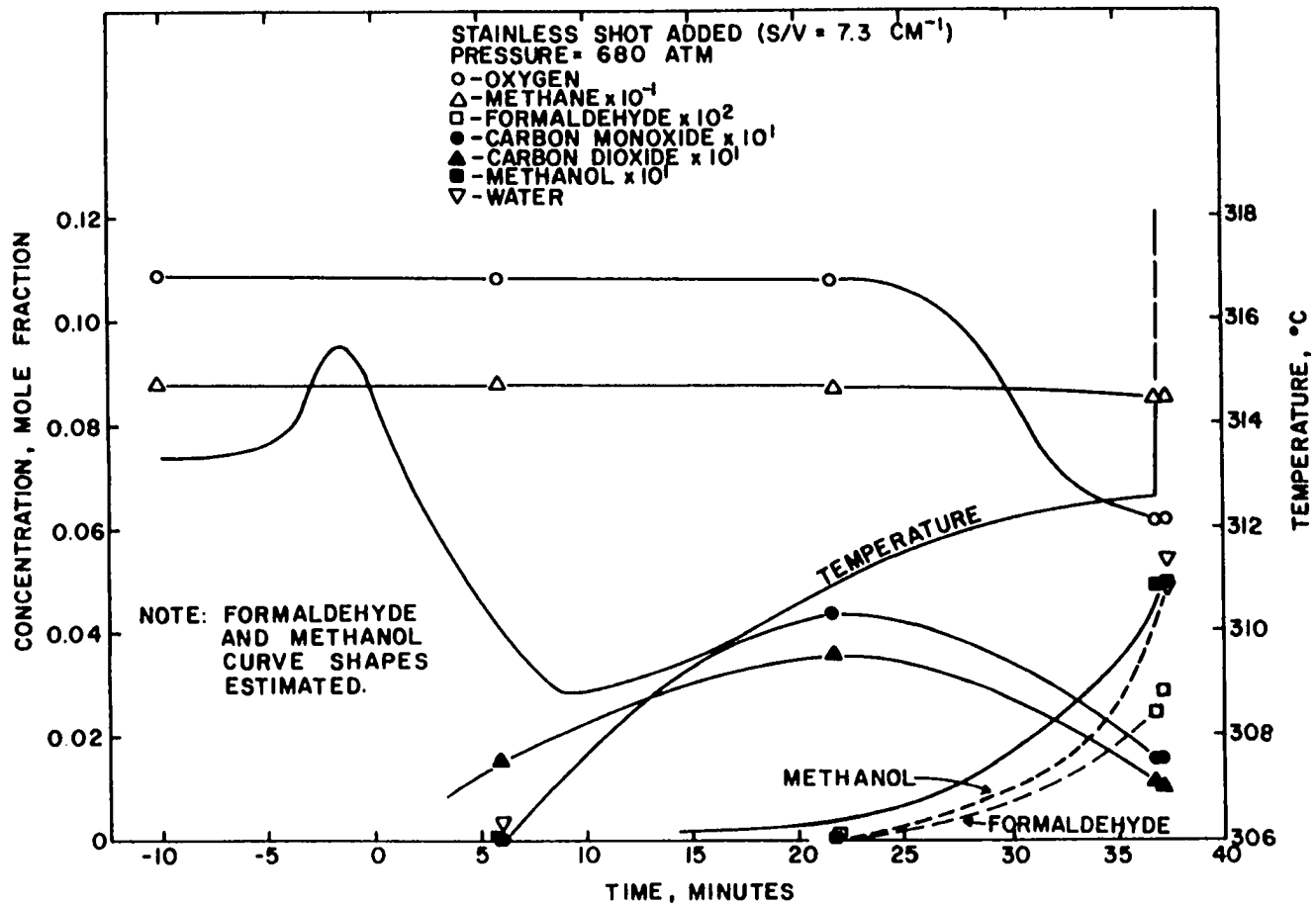


Figure 41. Reaction History at 680 atm, 308.8°C, and S/V of 7.3 cm⁻¹.

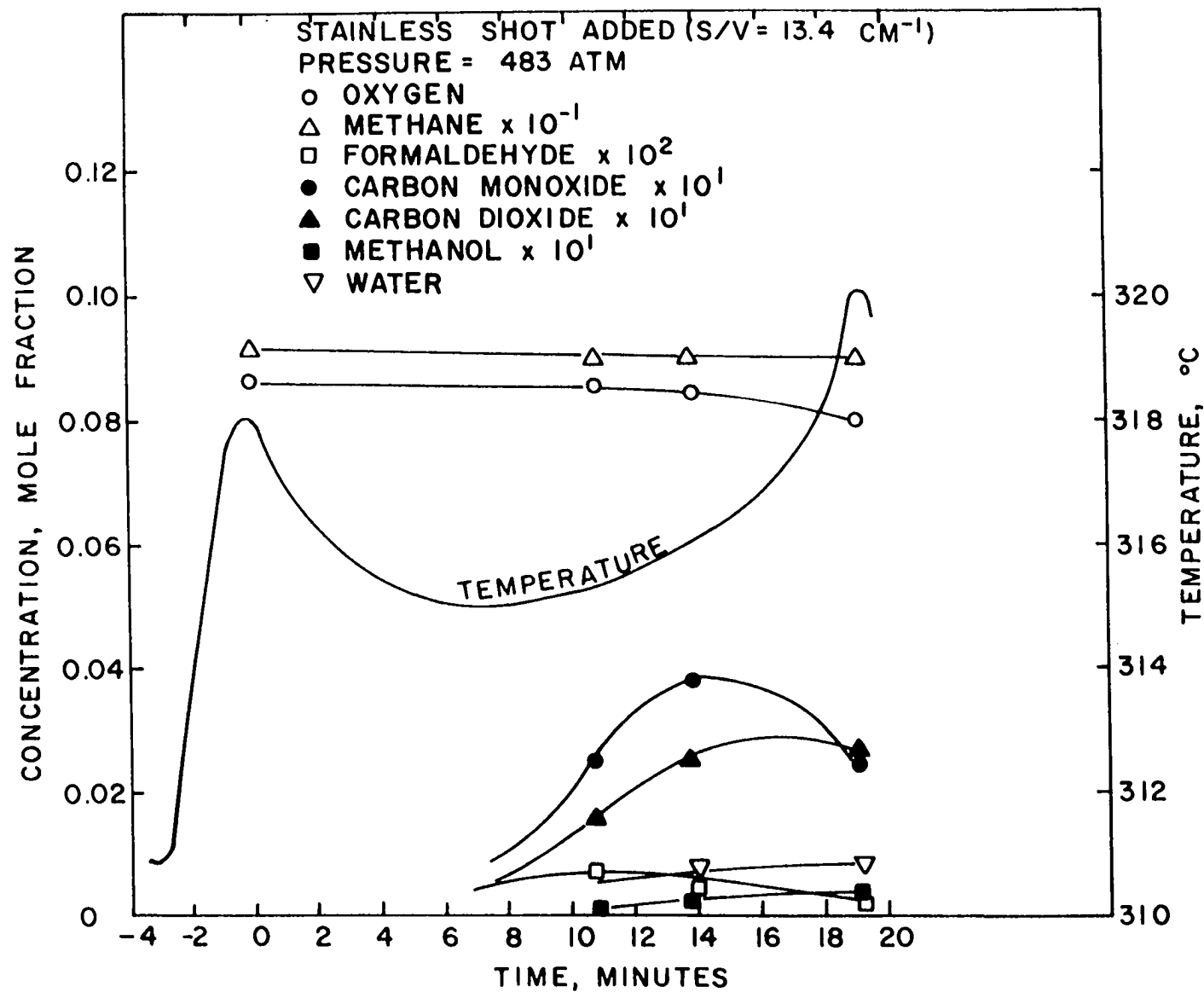


Figure 42. Reaction History at 483 atm., 315°C, and S/V of 13.4 cm^{-1} .

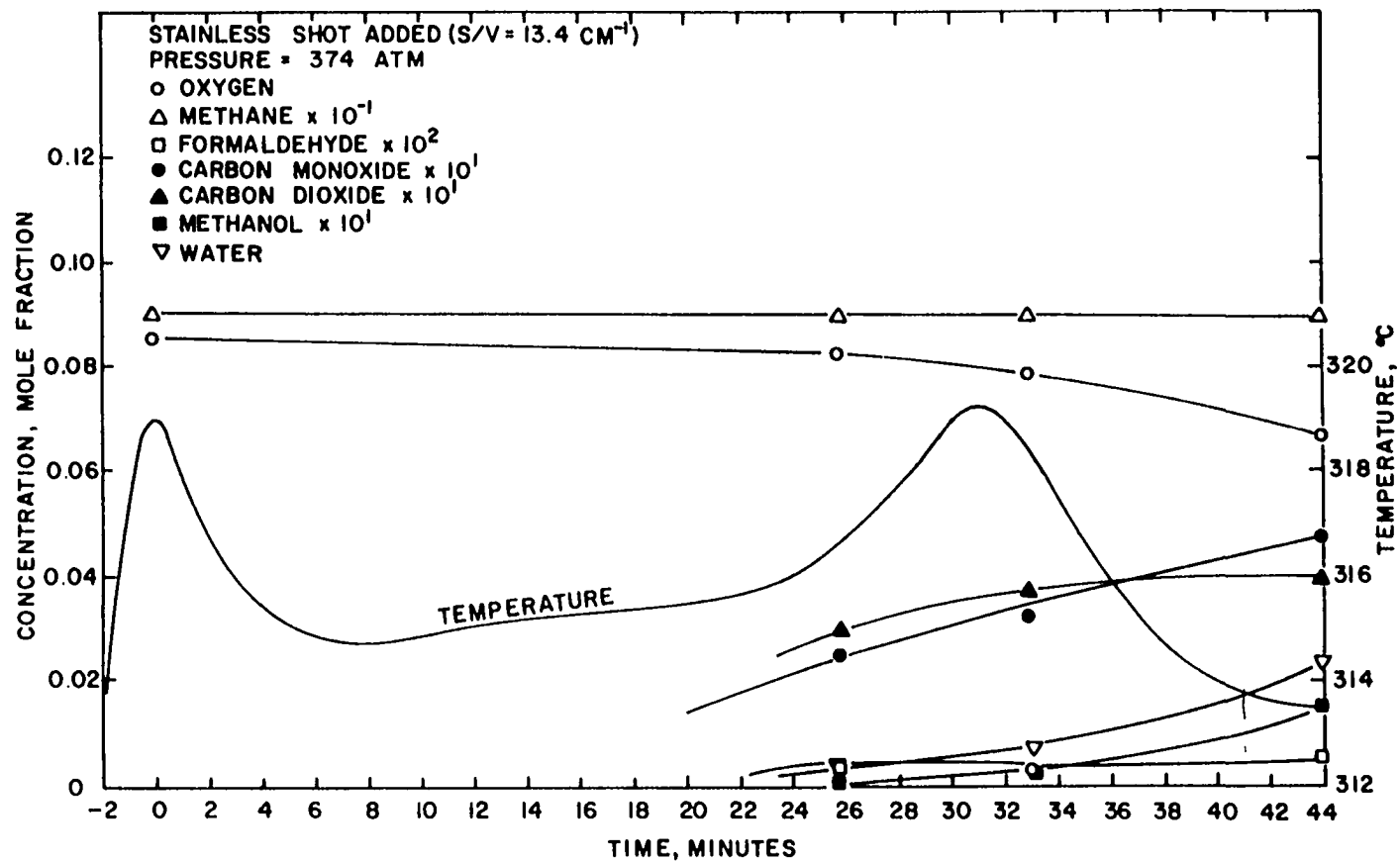


Figure 43. Reaction History at 374 atm, 314.7°C, and S/V of 13.4 cm⁻¹.

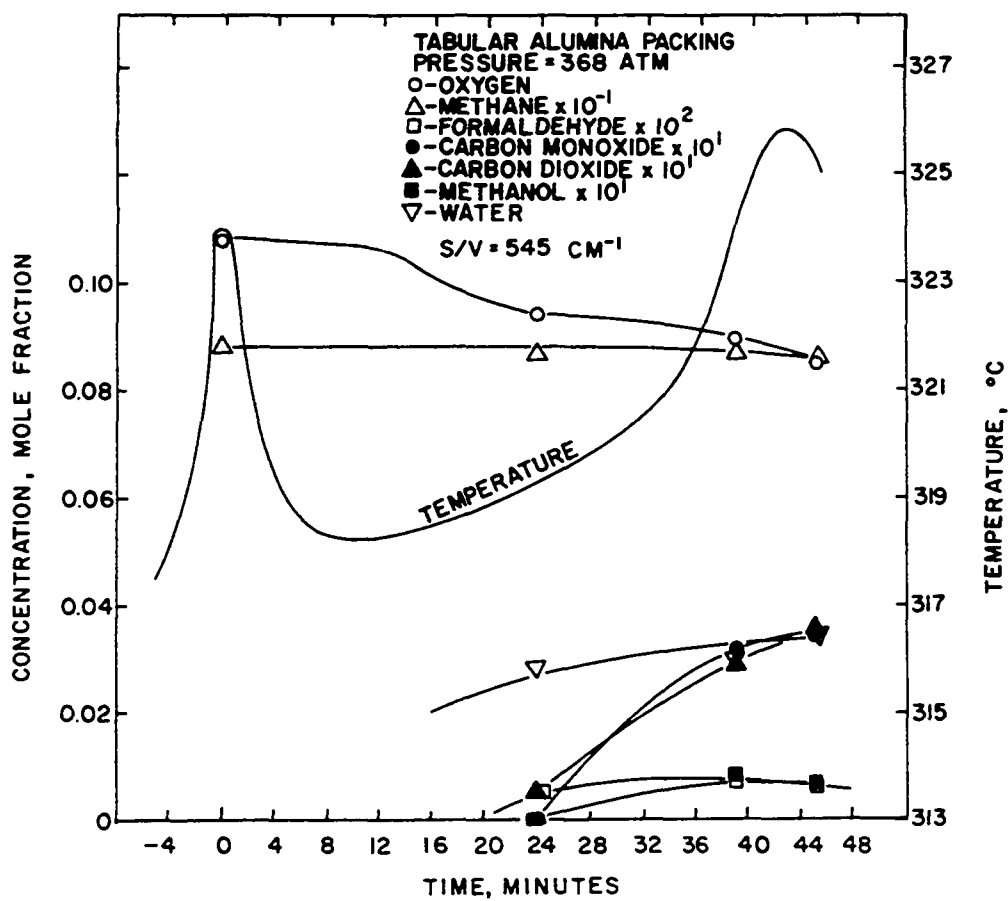


Figure 44. Reaction History at 368 atm, 318.2°C, and S/V 545 cm⁻¹.

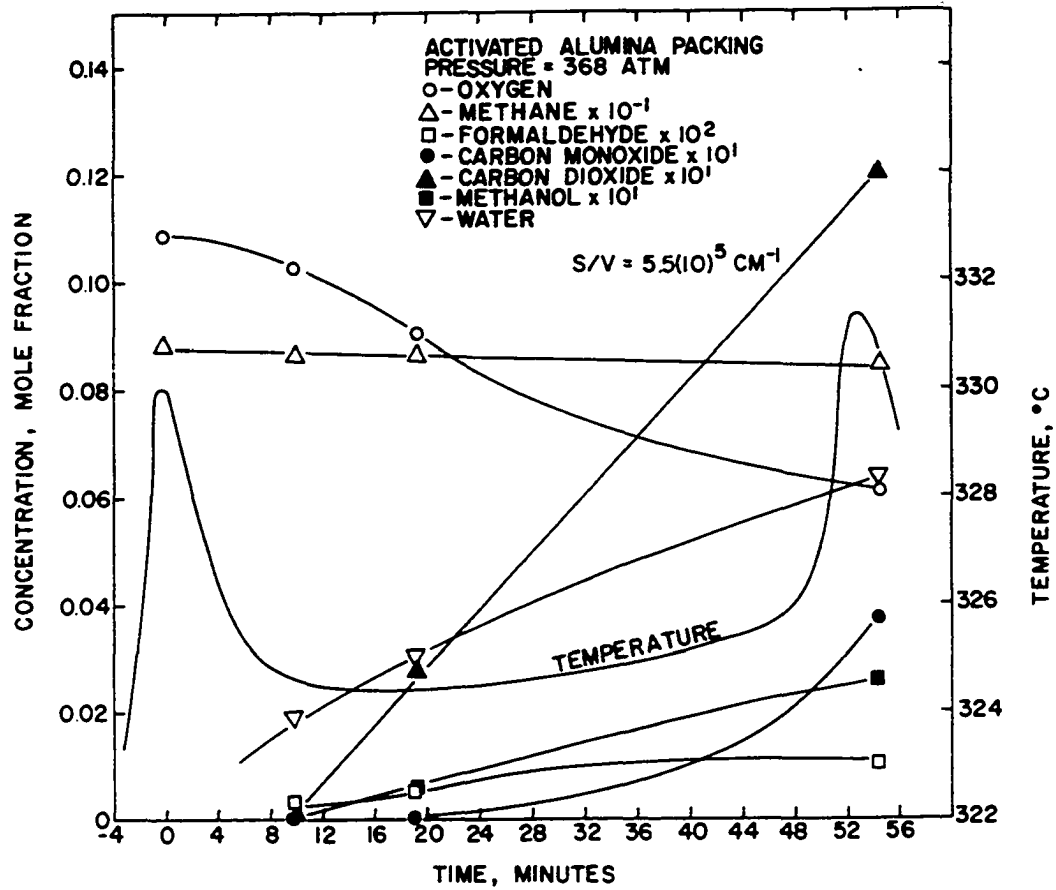


Figure 45. Reaction History at 368 atm, 324.6°C, and S/V of $5.5(10)^5 \text{ cm}^{-1}$.

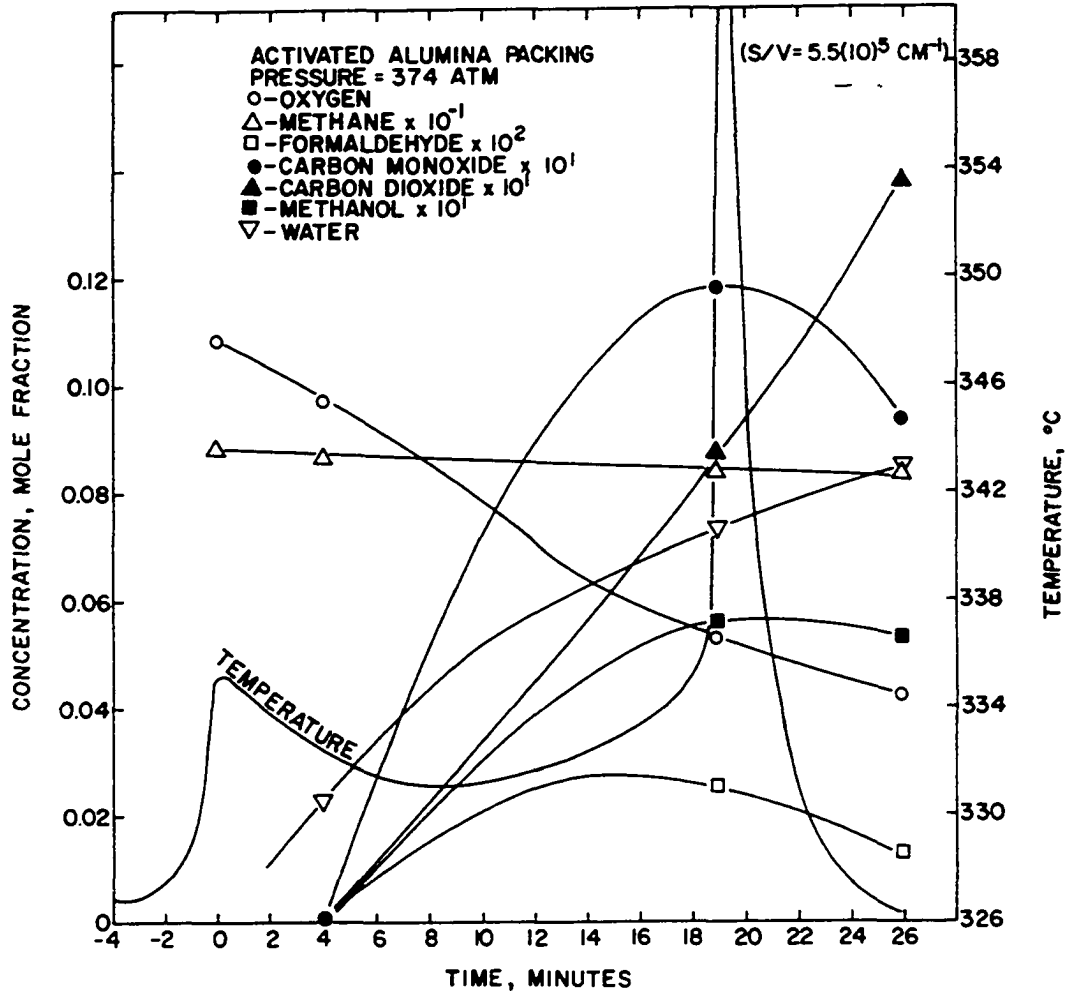


Figure 46. Reaction History at 374 atm, 331°C, and S/V of $5.5(10)^5 \text{ cm}^{-1}$.

pressures covered. A brief discussion on the formation of ethanol is desirable before proceeding to a detailed discussion of the major product distributions shown in Figures 32 through 46.

Although the formation of ethanol was observed over a wide pressure range, it seemed to be more favorable at the lower pressures. As much as 0.24 percent ethanol was observed in some tests at 150 atm. This value represents a concentration in excess of that which could have been formed from the ethane impurity initially present in the feed. The fact that ethanol appeared to be suppressed at high pressures suggests the pair of schemes: (1) ethanol is formed in a mole-increasing step (e.g., two molecules react to form three) or (2) lower diffusion rates at high pressures retard ethanol production, suggesting a termination reaction at the surface of the reactor.

It is well known that elevated pressure favors production of methanol. The termination reaction for methanol (mechanism of Hardwicke et al. (27)):



shows molar reduction. The formation of ethanol, however, is suppressed at elevated pressures. In some cases, ethane was recovered in the collector in quantities exceeding the amount of ethane in the initial charge, which implies the existence of a termination reaction involving two $\text{CH}_3\cdot$ radicals.

If ethane is formed mainly in a $\text{CH}_3\cdot\text{-CH}_3\cdot$ termination reaction, the retardation of ethanol production at elevated pressures might be explained in that the cross-termination of HLS-14 should be predominant, depleting the $\text{CH}_3\cdot$ supply. Retardation of ethane formation as a termination step necessarily halts formation of oxygenated products having two carbon atoms. Thus, it appears that ethanol and acetic acid are formed from ethane through a mechanism similar to the steps suggested for oxidation of methane.

Hydrogen was not detected in any test in the current series. Melvin (41) reported as much as 3% hydrogen production at 357°C and 100 atm in the explosive reaction of methane with 40% air. At richer mixtures, hydrogen production was considerably less. In non-explosive reactions with mixture ratios comparable to those of the present study, Melvin reported only minute quantities of hydrogen. The formation of hydrogen at higher oxygen concentrations suggests, because of higher explosion temperatures, the oxygen-catalyzed pyrolysis of methane as a source of hydrogen.

Returning to the reaction chronologies depicted in Figures 32 to 46, and considering now only the major products formed, the history of the non-explosive reaction can be described in detail. Occasionally, reference will be made to the overall mechanism of Hardwicke, Lott, and Sliepcevich (27), which was presented on page 77. This

mechanism was selected as a reference because no results in this and later sections refuted its applicability to high pressure oxidation of methane.

In Figure 32, as an example of a typical non-explosive reaction, the filling operation is shown as a four-minute period prior to the acquisition of target pressure. Point of attainment of the target pressure (367 atm) was taken as "time zero." A 4°C rise in temperature was observed during filling. After cessation of filling, a minimum temperature of 306.5° occurred after about 5 minutes. Little oxygen depletion occurred during this period. Temperature began to rise due to electrical heating and reaction thermal effects. A somewhat faster thermal acceleration occurred after about 36 minutes. Temperature reached a maximum of 312° at 52 minutes, followed by a very rapid temperature drop.

Oxygen consumption reached a maximum rate at about 19 minutes after an induction period of about 8 minutes. Oxygen consumption again decreased at about 24 minutes and remained nearly linear throughout the remainder of the test. The overall appearance of the oxygen concentration curve is referred to as "S-shaped." This shape of concentration curve is indicative of an inductive reaction involving degenerate branching.

Newitt and Haffner (46) showed the existence of temperature maxima somewhat after the occurrence of maximum

oxygen consumption rate, but they did not comment on this observation. This thermal lag cannot be wholly attributed to mass effects in the temperature measurement system. Two observations refute this possibility. First, in tests in which pressure exhibited a sharp rise due to explosion, the occurrence of thermal and pressure maxima were almost coincident (temperature lagged pressure by only about 0.1 minute, a reasonable value for conduction effects). Second, in tests in which auto-acceleration did not occur (temperature rose nearly linearly to a maximum), the sharp dropoff in temperature always occurred very quickly, indicating again that the response of the thermocouples could not account for lags of up to 30 minutes between maximum oxygen consumption rates and temperature maxima.

In all cases, formaldehyde was seen to reach a maximum concentration shortly after the point of maximum oxygen reaction rate. It would first seem that the explanation for the thermal lag would be that oxygen consumption accelerates after the induction period, giving formaldehyde and carbon oxides. Formaldehyde, in turn, would then reach a critical concentration near the point of maximum rate of oxygen consumption and would then react rapidly, causing heating. However, the thermal maximum was observed, at times, to lag also the formaldehyde maximum by several minutes.

In low pressure oxidation studies, methanol is not produced in significant quantity. It is formed, however, at

high pressures. The maximum in methanol concentration was almost coincident with the thermal peak in both explosive and non-explosive tests. It appears, then, that there must be a distinct connection between thermal lag and the formation of methanol.

At atmospheric pressure, maxima in temperature, oxygen depletion rate, and appearance of formaldehyde are all coincident. Ignition occurs if, as stated by Shtern (66), the balance between heat production and heat dissipation is upset at the time of these maxima. In other words, because exothermic reactions reach a peak in occurrence at this point, if ignition is to occur it will occur at the time of maximum oxygen depletion or not at all. If ignition does not occur, the reaction settles back to a condition which maintains a proper balance in thermal effects.

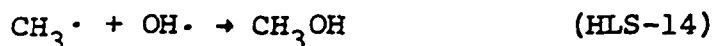
By considering the appearance of typical time-temperature-species plots, the following observations were made for high pressure oxidation. If ignition did not occur, temperature passed through a maximum some time after oxygen depletion had experienced its maximum rate (Figure 33). The peak in methanol concentration was approximately coincident with the temperature maximum. Formaldehyde concentration was at its highest level soon after the maximum in oxygen usage.

If ignition does occur, it can take place at (a) the instant of maximum formaldehyde concentration, or (b) at some

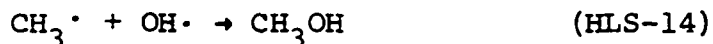
time long after the maxima in formaldehyde concentration and oxygen usage rate (Figures 36 and 46).

Thus it appears that, unlike low pressure ignition in which a thermal balance must be verified at a single critical condition, high pressure ignition can occur over a wide range of conditions. Shtern pointed out that, with degenerate branching, isothermal chain ignition does not occur, but explosions are due to occurrence of a thermal "avalanche."

This consideration implies that, in view of the above results, some exothermic reaction must occur well after the formaldehyde maximum at high pressures. This reaction must be relatively sensitive to temperature changes so that it can be driven to a very high rate with only a slight increase in temperature. This critical step is considered to be the termination of OH· and CH₃· radicals:

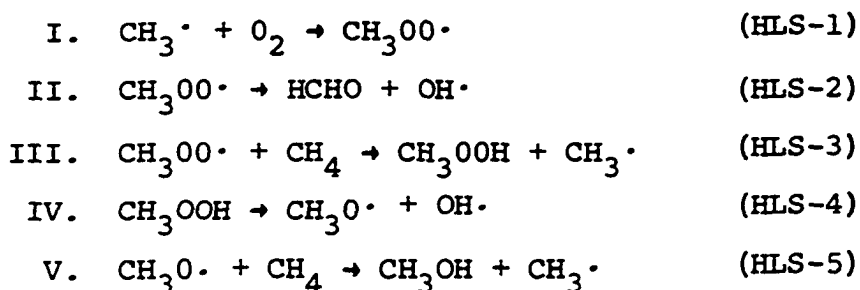


Vedeneyev et al. (72) listed energies of formation of CH₃· and OH· radicals of 33 and 9.3 kcal/mole, respectively. Using a value for the heat of formation of -48.1 kcal/mole for methanol (24), the reaction:



is seen to be exothermic by 90.4 kcal/mole. Because the reaction involves only radicals, the activation energy for HLS-14 must be quite small.

The alternative scheme for production of methanol is (see mechanism of Hardwicke et al., p 77):



The heats of formation of $\text{CH}_3\text{OO}\cdot$ radicals and CH_3OOH molecules were estimated using the following equation:

$$\Delta H_r \approx D[\text{CH}_3\text{O}-\text{OH}] = \Delta H_f(\text{CH}_3\text{O}\cdot) + \Delta H_f(\text{OH}\cdot) - \Delta H_f(\text{CH}_3\text{OOH})$$

That is, the heat of a dissociation reaction (ΔH_r) is approximately equal to the bond energy involved (denoted by D), which is equal to the difference between the sum of the heats of formation of the products and the heats of formation of the reactants. Vedeneyev et al. (69) listed the bond strength of $\text{CH}_3\text{O}-\text{OH}$ as about 39 kcal/mole. Also listed were heats of formation for $\text{OH}\cdot$ and CH_3O radicals of 9.3 and -0.5 kcal/mole, respectively. Using these data, the heat of formation of CH_3OOH is calculated to be

$$\Delta H_f(\text{CH}_3\text{OOH}) = 0.5 + 9.3 - 39 = -30 \text{ kcal/mole}$$

Vedeneyev also listed the bond energy $D[\text{CH}_3\text{OO}-\text{H}]$ as 90 kcal/mole. Since the heat of formation of $\text{H}\cdot$ is 52.1 kcal/mole (23), a similar sequence leads to $\Delta H_f(\text{CH}_3\text{OO}\cdot) = 7.9$ kcal/mole. Thus, the heats of reaction for the above five chain steps are:

$$\begin{array}{lll}
 \Delta H_r & \text{(I)} & = -25.1 \text{ kcal/mole} \\
 \Delta H_r & \text{(II)} & = -26.3 \quad "
 \end{array}$$

ΔH_r	(III)	=	13.0 kcal/mole
ΔH_r	(IV)	=	38.8 "
ΔH_r	(V)	=	3.3 "

The observation that temperature maxima do not always occur at the point of maximum rate of consumption of oxygen, but occasionally at a point during rapid formation of methanol presents the likelihood that high methanol formation is the cause of, and not the effect of, thermal lag in non-explosive tests and in some explosive tests. The chain formation of methanol by the scheme of Hardwicke et al. (27) involves two exothermic steps (HLS-1 and HLS-2). Both of these steps should release heat near the formaldehyde maximum. The actual formation of methanol (HLS-5) is endothermic by 3.3 kcal/mole at the reference conditions. However, the termination step (HLS-14) is highly exothermic. Further, the above authors showed that all methanol cannot be made by the methylperoxy radical chain scheme under non-isothermal conditions.

The possibility is thus raised that, in the absence of methanol production, temperature would indeed reach a maximum at the maximum rate of consumption of oxygen. However, with the exothermic termination reaction, heat generation continues beyond this point. A maximum in temperature occurs, finally, at the point of maximum usage of $\text{CH}_3\cdot$ and $\text{OH}\cdot$ radicals.

Competition for $\text{OH}\cdot$ and $\text{CH}_3\cdot$ radicals is between the cross-termination step giving methanol and steps HLS-1, -8, -14, -15, -18, and -20 in the mechanism on page 77. Reactions HLS-18 and HLS-20, of course, may be redundant.

After sufficient oxygen has been removed from the system, reaction HLS-1 becomes less important. This depletion occurs at the time formaldehyde reaches a maximum. Reaction HLS-8, though less energetic than HLS-14, must be assumed to be relatively fast near the formaldehyde maximum point. However, if $\text{CH}_3\cdot$ is present in appreciable quantity, reaction HLS-14 should be competitive. Reaction HLS-15, the reaction of $\text{HCO}\cdot$ with $\text{OH}\cdot$, must be controlled by the rate of destruction of formaldehyde. Since formaldehyde was not observed to decrease completely to zero concentration, the action of $\text{OH}\cdot$ on formaldehyde must slow down some time after the maximum in formaldehyde concentration has been passed. Thus, the exothermic reaction of $\text{OH}\cdot$ with $\text{CH}_3\cdot$ must be included as a very important step in the high pressure process.

In tests in which the reaction was studied at times well beyond the point of maximum temperature, methanol concentration was observed to level off or even to decrease with time. The decrease may have been due to the molecular reactions of oxidation to formic acid or gaseous oxides or to the esterification reaction. The fact that the rate of methanol production was observed to decrease indicates that $\text{CH}_3\cdot$ and $\text{OH}\cdot$ radicals had been exhausted. The termination

removed the source of energy (reaction HLS-14) and temperature then passed through a maximum. Figure 33, one of the graphs showing actual test results, schematically presents this premise. In the absence of methanol production, temperature would normally have peaked at point A.

In those tests in which explosion occurred near the point of maximum formaldehyde concentration, it is felt that the initial temperature was sufficiently high for reactions HLS-1 and HLS-2 to take place to such an extent that auto-acceleration can occur due to the exothermicity of these steps alone. Then, because of the formation of methyl peroxy radicals ($\text{CH}_3\text{OO}\cdot$) in acceleration of reaction HLS-2, production of methanol occurs also due to the effects of branching reaction HLS-4.

The question arises: Why is not methanol produced at low pressures if $\text{CH}_3\cdot$ and $\text{OH}\cdot$ radicals are present under these conditions? The answer seems to be that the production of $\text{CH}_3\cdot$ via reactions HLS-3 and HLS-5 must be at a rate much higher than that of the initiation step (HLS-0). In addition, the suggestion that $\text{OH}\cdot$, rather than $\text{HO}_2\cdot$, is the primary reactant with formaldehyde (reaction HLS-8) as postulated by Medley and Cooley seems to be substantiated. It can be reasoned that if $\text{HO}_2\cdot$ were the primary reactant with formaldehyde, sufficient $\text{OH}\cdot$ would remain at low pressures to form methanol with $\text{CH}_3\cdot$. Without the additional chain production of $\text{OH}\cdot$ through the peroxide

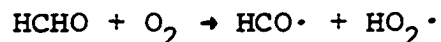
intermediate at low pressures, insufficient $\text{CH}_3\cdot$ and $\text{OH}\cdot$ are produced to form sizable amounts of methanol by termination. In addition, and perhaps more simply, the termination formation of methanol is a mole-reducing step favored by elevated pressures.

Cessation of methanol production was observed in a striking manner in some tests. Temperature was seen to increase nearly linearly throughout the test, but auto-acceleration did not occur. A sudden drop in temperature then occurred. This sudden drop indicated that a source of heat had been removed or that an endothermic reaction had suddenly occurred. It is unlikely that an endothermic reaction would appear with such suddenness. However, the existence of a continuing endothermic reaction or simple heat carry-off occurring simultaneously with methanol production due to termination (an exothermic reaction) is conceivable. Exhaustion of $\text{CH}_3\cdot$ and $\text{OH}\cdot$ radicals due to termination would have allowed the endothermic reaction or high heat loss to predominate, and possibly, in a very rapid manner.

Several of the figures show carbon dioxide production at the same time as carbon monoxide formation. Melvin (41) explained the appearance of carbon dioxide (CO_2) by supposing that carbon monoxide (CO) is immediately oxidized to carbon dioxide during the ignition delay. Hardwicke et al. (27) suggested, instead, the molecular oxidation of formaldehyde (reaction HLS-8) as

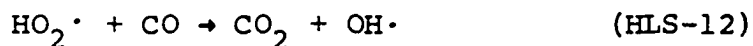
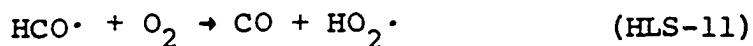
being the producing step. Bone and Gardner (11) reported little production of carbon dioxide in oxidation of formaldehyde, which possibly reduces the likelihood of carbon dioxide formed by reaction HLS-10. Reaction HLS-12, however, utilizes the idea of Melvin, but it suggests oxidation of carbon monoxide by chain carrier means ($\text{HO}_2\cdot$) rather than by molecular oxygen.

McConkey and Wilkinson (38) suggested attack on formaldehyde by oxygen to be:



Reaction of $\text{HCO}\cdot$ with oxygen gives carbon monoxide and $\text{HO}_2\cdot$ radicals. The further oxidation of carbon monoxide can proceed via reaction HLS-12 of Hardwicke et al. The hydrogen abstraction above seems more probable than full oxidation in one step to water and carbon dioxide.

Two chain propagation steps in the mechanism of Hardwicke et al. were:



Stationary-state analysis, based on only these two reactions, for $\text{HO}_2\cdot$ gives:

$$\frac{k_{12}}{k_{11}} = \frac{[\text{HCO}\cdot][\text{O}_2]}{[\text{CO}][\text{HO}_2\cdot]} \quad (62)$$

In early stages of reaction when only oxygen, of the four

species mentioned, is present in appreciable quantity, $k_{12} > k_{11}$, suggesting that the two steps can be combined to give:



Other steps, of course, are involved in the generation of $\text{HCO}\cdot$ and $\text{HO}_2\cdot$, and in the depletion of both species. However, until an appreciable quantity of radicals is accumulated, the ratio of reaction constants will be much in excess of unity. As radicals accumulate, along with formaldehyde, which is the source of $\text{HCO}\cdot$, the ratio tends toward and less than unity. This consideration in itself can explain adequately the occurrence of carbon dioxide in early stages of reaction, and the molecular oxidation step (HLS-10) may be superfluous. It will be shown later that the early appearance of carbon dioxide at extreme pressures as reported by Hardwicke (26) can be due in fact to the unavoidable progression of oxidation well beyond the initial slow rate.

At the highest level of surface/volume ratio (use of activated alumina) achieved for non-catalytic studies, the typical "s-shaped" curve for oxygen concentration was retained. However, non-explosive tests resulted in oxygen depletion of only about half that of the tests conducted with the empty reactor. All oxygenated products were produced in correspondingly low amounts. These observations emphasize the tendency of surfaces to quench the reaction by destroying radicals.

In explosive tests, however, methanol production was comparable to that of a low-surface test. A homogeneous termination of $\text{CH}_3\cdot$ and $\text{OH}\cdot$ radicals is thus suggested.

The apparent discrepancy between activation energy for ignition delay, as measured in this study, with that measured by Melvin (41) (see page 161) can now be reconsidered.

Melvin reported a value of activation energy of 42 kcal/mole for ignition delay at about 100 atm. over a temperature range of 352° to 496°C. The present study resulted in a value of 98 kcal/mole. It is likely, in view of the very short ignition delays experienced by Melvin (200 seconds or less), that thermal ignition occurred in his tests near the point of maximum usage of oxygen due to reactions HLS-1 and HLS-2. Thermal maxima in most of the present study were due to the termination step, HLS-14, resulting in much longer ignition delays.

As temperature is increased, the time to the thermal maximum due to HLS-14 decreases consistent with a temperature dependence based on an activation energy 98 kcal/mole. The time to the point of rapid usage of oxygen also decreases, but in this case, according to an activation energy of only 42 kcal/mole. Thus at some temperature, the two time periods are identical. The discrepancy, then, is not due to differences in experimental technique, but it is the result of differences in the reaction causing ignition.

It is recalled that the data of Lott (35) for explosive tests correlated with an activation energy of 98 kcal/mole. This result indicates that explosion in his series of tests was primarily observed at the second of the two possible instances for ignition (i.e., at the point of influence of the termination reaction HLS-14 and not at the point of greatest influence of HLS-1 and HLS-2).

Because only long residence times were desired in the present study, very short ignition delays (of the order of one minute) were not intentionally induced. Furthermore, when such short delays occurred, no further attempt was made to investigate the history of that reaction up to that ignition delay by measurement of still shorter residence times. Thus, insufficient data were taken to determine fully the activation energy based on the ignition being forced to occur at the point of rapid usage of oxygen.

Order of Reaction

Because methane was present only in very high concentration, determination of an order with respect to methane was not felt to be possible. The order with respect to oxygen only was determined for several non-catalytic tests from 368 to 489 atm and from 306.4° to 317.2°C.

The method of reference curves (see Appendix D) was used to estimate the order with respect to oxygen for a rate equation of the form:

$$\frac{-dy_o}{dt} = k y_o^n \quad (63)$$

where y_o is oxygen mole fraction, t is time, k is the reaction rate constant, and n is the order of reaction.

Temperature was assumed to remain constant in each determination; further, total moles were not observed to vary significantly in any test. Thus, the necessary factors for conversion of y_o to concentration are included in k .

Particular portions of curves of y_o versus t that were subjected to analysis were the initial slow reaction and the region of rapid depletion of oxygen. Figure 47 shows a typical construction for the rapid consumption of oxygen in the series of tests at 367 atm and initial temperature of 312.4°C (Figure 33). It can be seen that an apparent order of about 3.7 results in a concentration curve very close to that measured.

Table 13 summarizes the obtained results. Order with respect to oxygen in the region of rapid usage of oxygen is from 3.4 to 4 for the non-explosive tests analyzed. Under explosive conditions, the order jumps sharply, being in excess of 10 at 381 atm and 316.1°C. The initial, slow reaction was characteristic of zero order, however, since the oxygen mole fraction was linear with time.

Melvin determined order during the slow reaction to be 0.6 when considering the influence of oxygen on

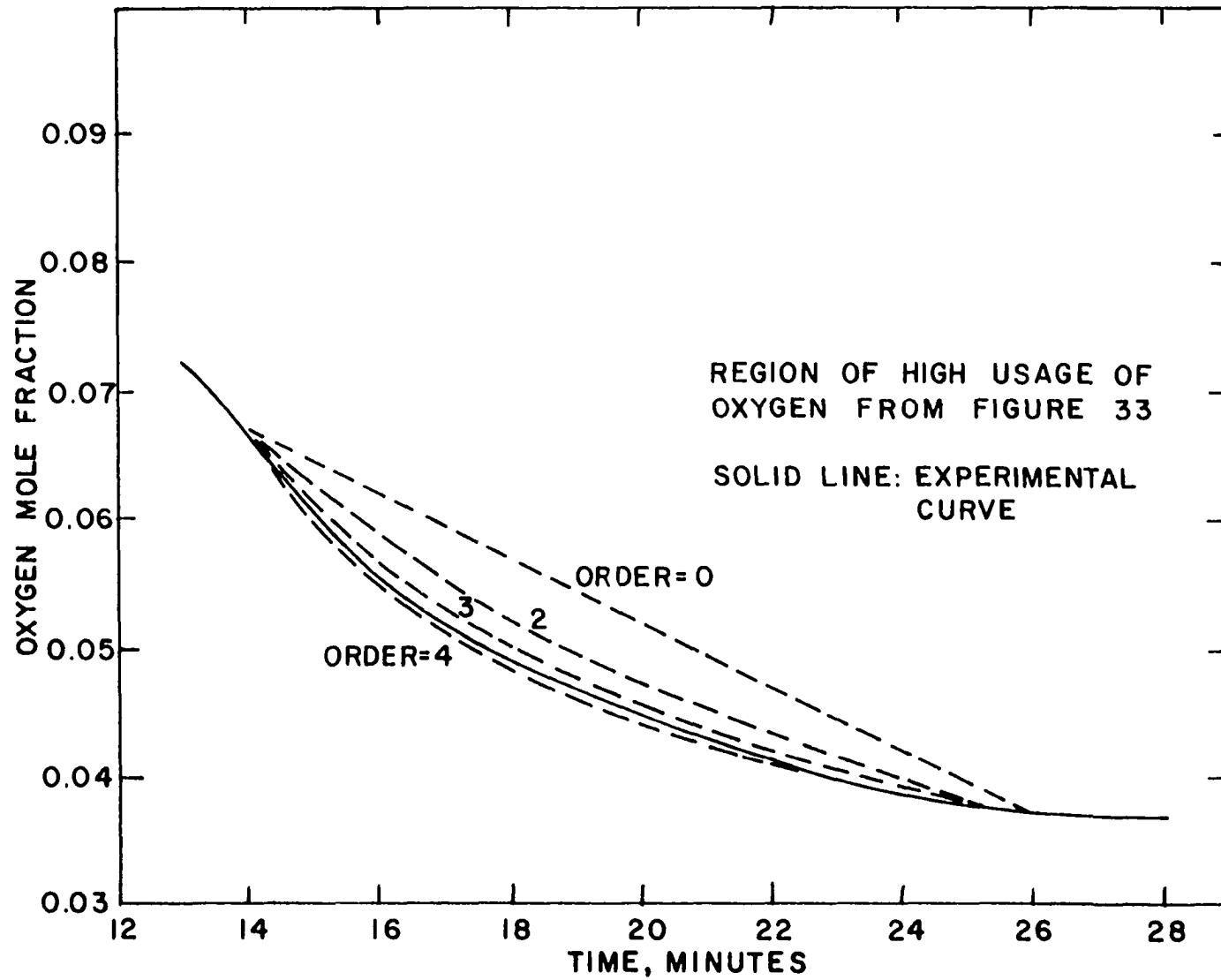


Figure 47. Determination of Order by Method of Reference Curves.

TABLE 13
 APPARENT ORDER OF NON-EXPLOSIVE TESTS DURING
 PERIOD OF RAPID USAGE OF OXYGEN

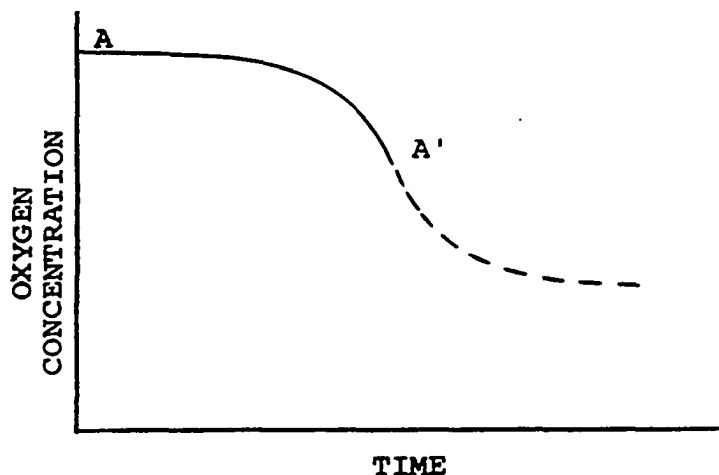
Pressure atm	Initial Temperature °C	Surface/Volume Ratio cm ² /cm ³	Apparent Order w/r to Oxygen
367	312.4	3.5	3.7
367	306.4	3.5	4
381	316.1	3.5	10*
490	303.5	3.5	3.5
374	317.2	7.3	4
483	312.6	7.3	3.4
476	307.8	3.5	4

*Explosion occurred.

ignition delay, rather than on rate of oxygen consumption. This result will give an order for oxygen of -0.6 in the rate equation.

Shtern (64) reported a trend toward zero order for the slow reaction as temperature is lowered (see Table 2). He showed that orders of 3 have been determined for mixtures at fuel/oxygen ratios of about 6. At a ratio of 3, however, the order fell to 2. Reactor preparation was not reported to influence the order.

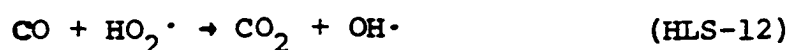
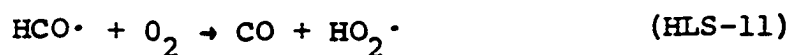
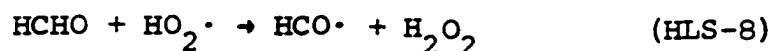
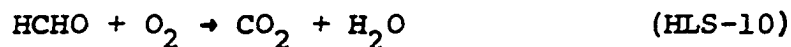
Hardwicke, Lott, and Sliepcevich (27) reported that an order of -2 for oxygen concentration gave a reasonable correlation of reaction constant and reciprocal temperature. A negative order, at first inspection, implies an inhibiting effect due to oxygen. However, it is possible that the correlation, based on values of the reaction rate constant calculated from initial and final oxygen concentrations, could result in negative orders if data points included values in both the zero-order and high-order regimes. That is, the upper portion of the "s-shaped" oxygen concentration curve (down to the maximum rate), taken by itself, does have a negative contour because it includes the transition region. It is quite possible, then, that Hardwicke et al. had data which were in both regimes of oxidation; i.e., in the zero order and higher order regimes. The accompanying sketch shows the region in a typical oxygen concentration curve, which if studied alone, could imply a negative order (region A-A').



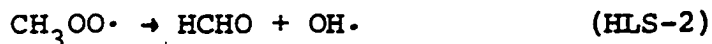
Formaldehyde and Methanol Production

Table A-1 in Appendix A shows calculated values of the ratio of the sum of formaldehyde, carbon monoxide and carbon dioxide produced in each run to the amount of methanol produced. This ratio was suggested by Hardwicke et al. (27) as a convenient criterion for showing a mechanistic change as the reaction proceeded to non-isothermal conditions.

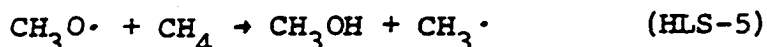
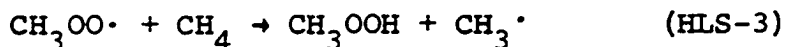
Selection of the ratio was based on the assumption that all carbon monoxide and carbon dioxide are formed from formaldehyde by the following steps (numbered in the convention of Hardwicke et al.):



It was proposed that formaldehyde was made from methyl peroxy radical:



The methyl peroxy radical also leads to production of methanol:



The ratio, $\text{HCHO} + \text{CO} + \text{CO}_2/\text{CH}_3\text{OH}$, for several tests is shown in Figure 48. The abscissa is a dimensionless time defined as the ratio of actual residence time to the ignition delay for that set of operating conditions. The ratio decreases abruptly at a reduced time of about 0.4, approaching a value of about 4 at reduced times of about one or larger.

The dotted line of Figure 48 shows values of the ratio for high conditions of S/V. It appears that increased S/V leads to a reduction in the amount of methanol. This result is understandable because high surface would be expected to be detrimental to production and/or stability of peroxides, which are essential for methanol production. In addition, surface destruction of $\text{CH}_3\cdot$ and $\text{OH}\cdot$ would be expected.

The influence of methanol production on the above ratio takes place in the latter stages of the region of linear usage of oxygen (reduced time of about 0.4 or 0.5)

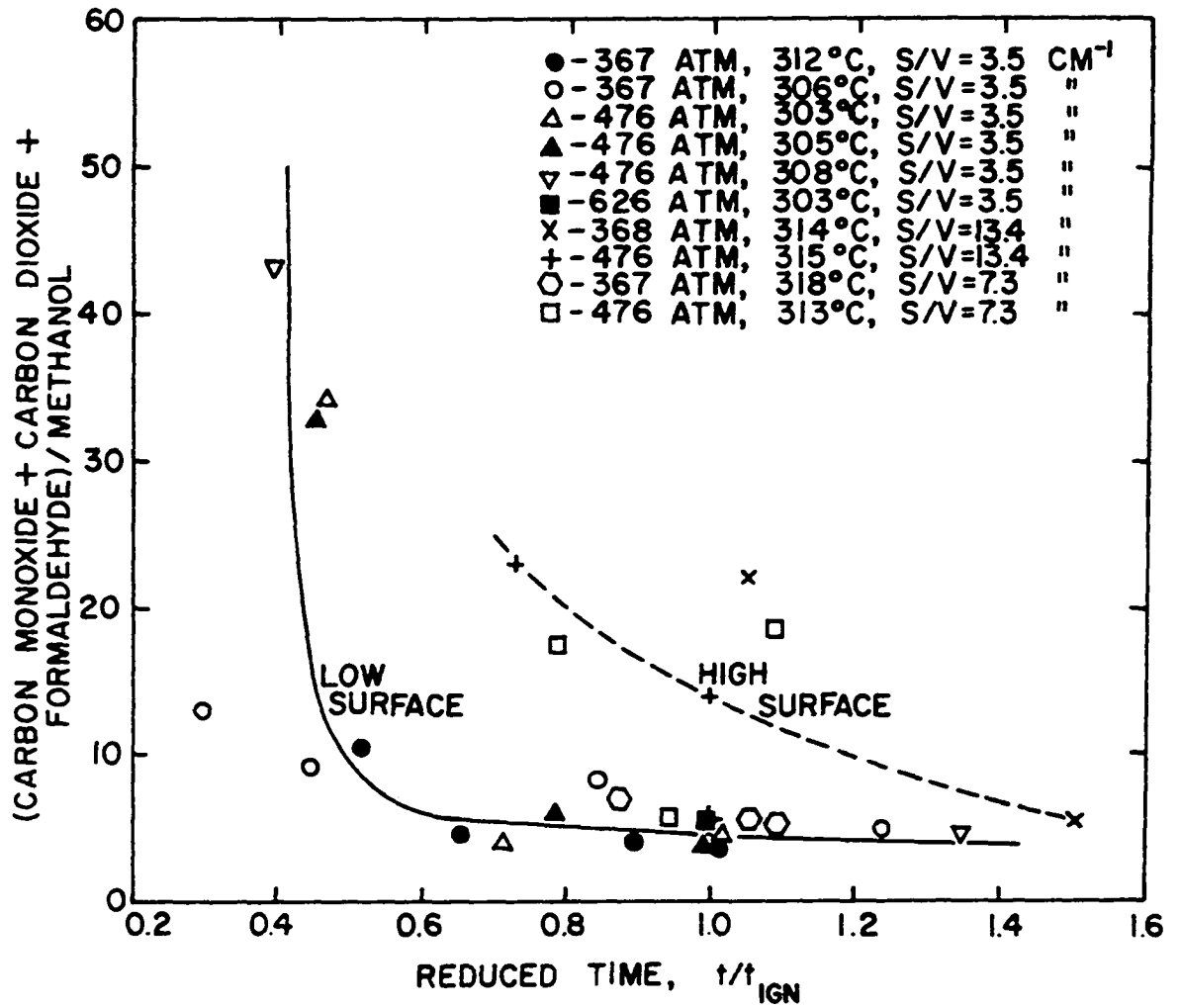


Figure 48. Influence of Residence Time on Ratio: $(\text{CO} + \text{CO}_2 + \text{HCHO}) / \text{CH}_3\text{OH}$.

and not at reduced times greater than 0.5. The rather abrupt reduction in the ratio indicates that methylhydroperoxide formation and/or dissociation occurs relatively suddenly.

Furthermore, the rapid drop in ratio seems to indicate that usage of oxygen in this region is relateable to production of methanol and/or depletion of formaldehyde. Because a decrease in CO/CO_2 occurs in about this same region (see Figure 50), molecular oxidation of carbon monoxide cannot be discounted in considering the usage of oxygen. Further, the ratio of Figure 48 would not be effected to a large degree because total moles of carbon oxides do not change as rapidly as oxygen concentration in this region.

Hardwicke and co-workers showed (by making some approximations of the magnitudes of activation energies and pre-exponential terms) that the ratio of the rates of reactions HLS-3 and HLS-2 is 0.63. They state that the concentration of methyl hydroperoxide is 0.63 times that of formaldehyde. This assertion is not strictly true. It will be correct only if all reactions leading to destruction of formaldehyde proceed at a rate equivalent to that of reaction HLS-4. Or, alternatively, all reactions leading to depletion of both intermediates must be extremely slow compared to reactions HLS-2 and HLS-3.

To make an accurate statement about the relative concentrations of formaldehyde and methylhydroperoxide, one must consider all depletion reactions. Thus, the statement of Hardwicke, et al., applies only to the very early stages of oxidation, at which time the $\text{OH}\cdot$ and $\text{HO}_2\cdot$ radicals are in extremely short supply. Nevertheless, the purpose of the development of Hardwicke et al. is valuable in that a convenient criterion for indicating the progression of methanol formation from a propagation reaction to a termination reaction is given.

Qualitatively, one can consider the formation of alcohol in the following manner. For every methylperoxy radical ($\text{CH}_3\text{OO}\cdot$) formed, a molecule of $\text{OH}\cdot$ is produced. Reaction of $\text{CH}_3\text{OO}\cdot$ with methane leads to a $\text{CH}_3\cdot$ radical. Dissociation of methylhydroperoxide leads to an additional $\text{OH}\cdot$ radical and a $\text{CH}_3\text{O}\cdot$ radical. Reaction of this latter radical with methane produces methanol and an additional $\text{CH}_3\cdot$ radical. Thus, the normal chain sequence leading toward production of methanol and formaldehyde also produces in great quantity those radicals necessary for production of additional methanol in a termination reaction. Of course, $\text{CH}_3\cdot$ and $\text{OH}\cdot$ radicals enter into all the normal reactions attributed to them in greater quantity than before as well as the termination reaction.

This same sequence is possible at low pressures, but it is generally accepted that reaction HLS-2 is so much

faster than reaction HLS-1 that production of methylhydroperoxide is minimized. The principle of Le Chatalier suggests that dissociation of $\text{CH}_3\text{OO}\cdot$ leading toward formaldehyde production is hindered at high pressure, releasing more of these radicals for reaction with CH_4 to form CH_3OOH . In this context, the production of methanol is quasi-autocatalytic; that is, the more methanol that is produced by chain reaction the more is produced in a termination reaction involving radical side-products of the chain reaction.

If reaction HLS-4 is significantly faster than reaction HLS-3, buildup of CH_3OOH must occur. Because reaction HLS-4 is not favored by pressure, it is quite likely that such buildup occurs until the peroxide reaches such a concentration that homogeneous dissociation occurs with suddenness. This rapid dissociation may well be the process occurring at high pressure and causing the thermal lag which has been observed.

Detection of CH_3OOH was not made; however, there was an indication that the peroxide may have indeed been formed. In conducting the chromatographic analyses for the liquid products, it was observed that, in addition to a normal air (or oxygen/nitrogen separation) peak, a peak occurred in some runs at a residence time characteristic of methane. It is very likely that dissociation of the peroxide with evolution of methane and oxygen occurs in the chromatographic column.

This idea was tested with hydrogen peroxide. No peaks occurred other than water, the preservative (acetophenetidin), and the oxygen-nitrogen pair. The oxygen peak was many times larger than that attributable to air leakage alone (based on size of the nitrogen peak). The methane peaks observed earlier were thus attributed to presence of methylhydroperoxide, but positive identification of methylhydroperoxide, as such, was not made.

McConkey and Wilkinson (38) showed a second order dependence of formaldehyde partial pressure on methane and oxygen. That is, partial pressure of formaldehyde was a linear function of the product of methane and oxygen partial pressures.

Because the relative concentrations of methane and oxygen were unchanged in the present program, such a relationship could not be shown. The results of McConkey and Wilkinson also suggested a second order due to pressure, although a considerable quantity of nitrogen was present.

Since considerable variation in temperature, pressure, and surface-volume ratio was made in this program, insufficient data were available at one given set of operating conditions to investigate the effect of single variables on the formaldehyde concentration. Further, since formaldehyde concentration was shown to be a function of time (McConkey and Wilkinson investigated steady-state phenomena in a fluidized bed, flow reactor), this additional variable was necessarily introduced.

However, the effect of several variables was determined using maximum formaldehyde concentration only as the dependent variable.

Test points used to determine the effect of these variables included only those runs with S/V values less than 13.4 cm^{-1} . At higher S/V values, increased curvature of $\log \beta$ (the S/V correction factor) versus $\log S/V$ (Figure 24) suggested that a single, constant value for the S/V exponent could not be determined.

A linear regression technique, using the logarithmic version of the following equation was employed:

$$y_f = AP^n (S/V)^m e^{-E/RT} \quad (64)$$

where y_f is the maximum formaldehyde concentration, A is a constant, n and m are orders with respect to pressure (P) and surface/volume ratio (S/V), respectively, E is activation energy, R is the gas constant and T is absolute temperature.

The following constants were determined:

$$A = -60$$

$$n = 2.6$$

$$m = -1.8$$

$$E = 61,000 \text{ cal/mole}$$

Figure 49 shows actual vs. calculated values of formaldehyde concentration. Maximum deviation between actual and calculated values was about 30%.

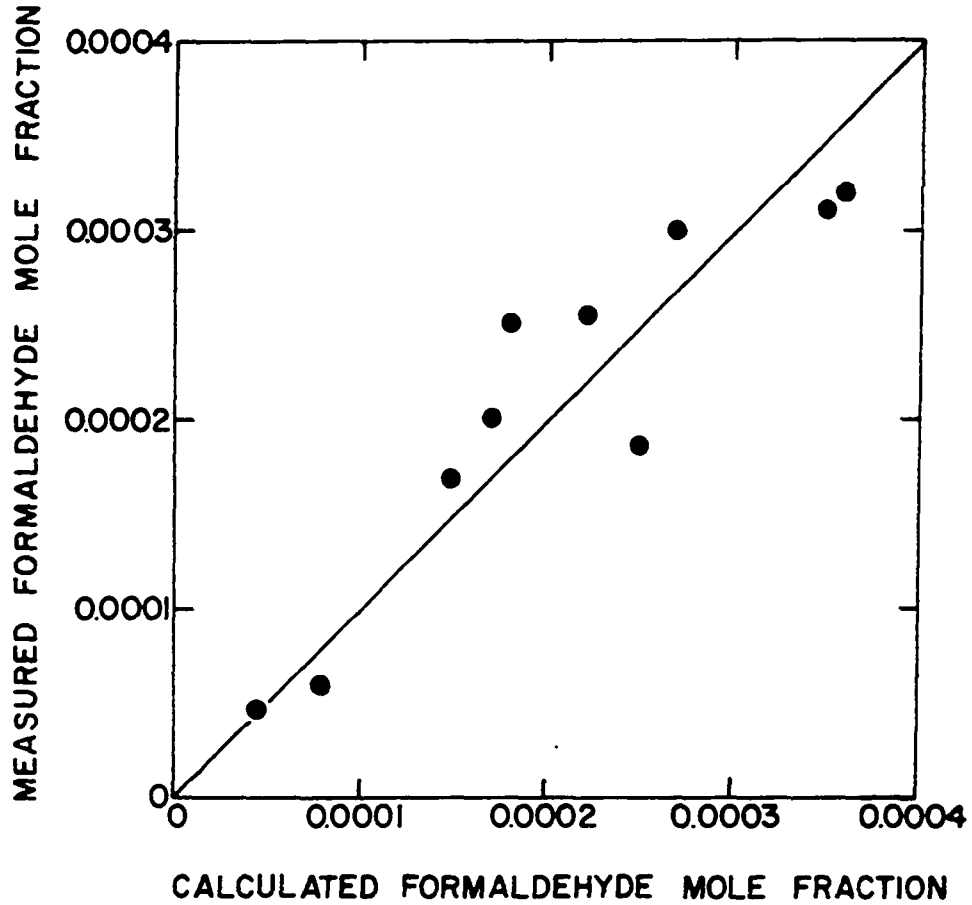


Figure 49. Actual and Calculated Values of Maximum Formaldehyde Mole Fraction at Non-Explosive Conditions.

Shtern (66) reported an activation energy for maximum formaldehyde production of 10,000 cal/mole. In the reported work, tests were conducted at low pressures under explosive conditions.

The pressure exponent is very close to that measured for the low pressure regime of ignition delay (page 152). Surface/volume exponent is close to the value determined by drawing the best straight line through the data up to $S/V = 13.4 \text{ cm}^{-1}$ in Figure 24, the plot of surface/volume factor for ignition delay versus S/V .

Data of explosive tests were not included in the regression. Attempts at incorporating these points resulted in much greater deviation between actual and calculated values. It is felt that the regression holds only up to certain temperature levels for each set of pressure and S/V conditions. At these critical conditions, no additional net HCHO can be formed due to increased rates of reaction of formaldehyde with oxygen and radicals. This assertion is in accord with the findings of many workers who showed that addition of formaldehyde over a certain critical amount drives the reaction toward explosion.

Carbon Monoxide-Carbon Dioxide Ratio

Included in Table A-1 in Appendix A are measured values of the ratio of carbon monoxide to carbon dioxide for each test. It was found that the ratio depends strongly on surface conditions and residence time, and somewhat, on pressure and temperature.

Figure 50 includes data from several tests including some involving alumina additives. Only those data which were used in assembling complete reaction histories appear in this figure. The abscissa is in dimensionless time defined as the ratio of residence time to the normal ignition delay for that set of operating conditions. It can be seen that the CO/CO_2 ratio is about unity at ignition in the general case. The ratio approaches unity from above at times up to ignition and approaches some value below unity asymptotically after the temperature maximum has been passed.

In short tests, the ratio appears to be very high, dropping rapidly at about a reduced time of 0.4. In most tests, this point coincides with the latter stages of the isothermal region.

Lott (35) reported a linear variation between about 0.1 and 2.2 for the CO/CO_2 ratio as a function of temperature at each pressure level. It was found that superposition of all these data presented a reasonable linear correspondence between ratio and temperature with no apparent pressure dependence. The points which deviated sharply (in a manner which would give very large ratios), were those which corresponded to explosive tests. It should be recalled that Lott's work involved only tests which were allowed to progress to a maximum temperature and were quenched rapidly at that point. This point corresponds to a reduced time of 1.0 in each test.

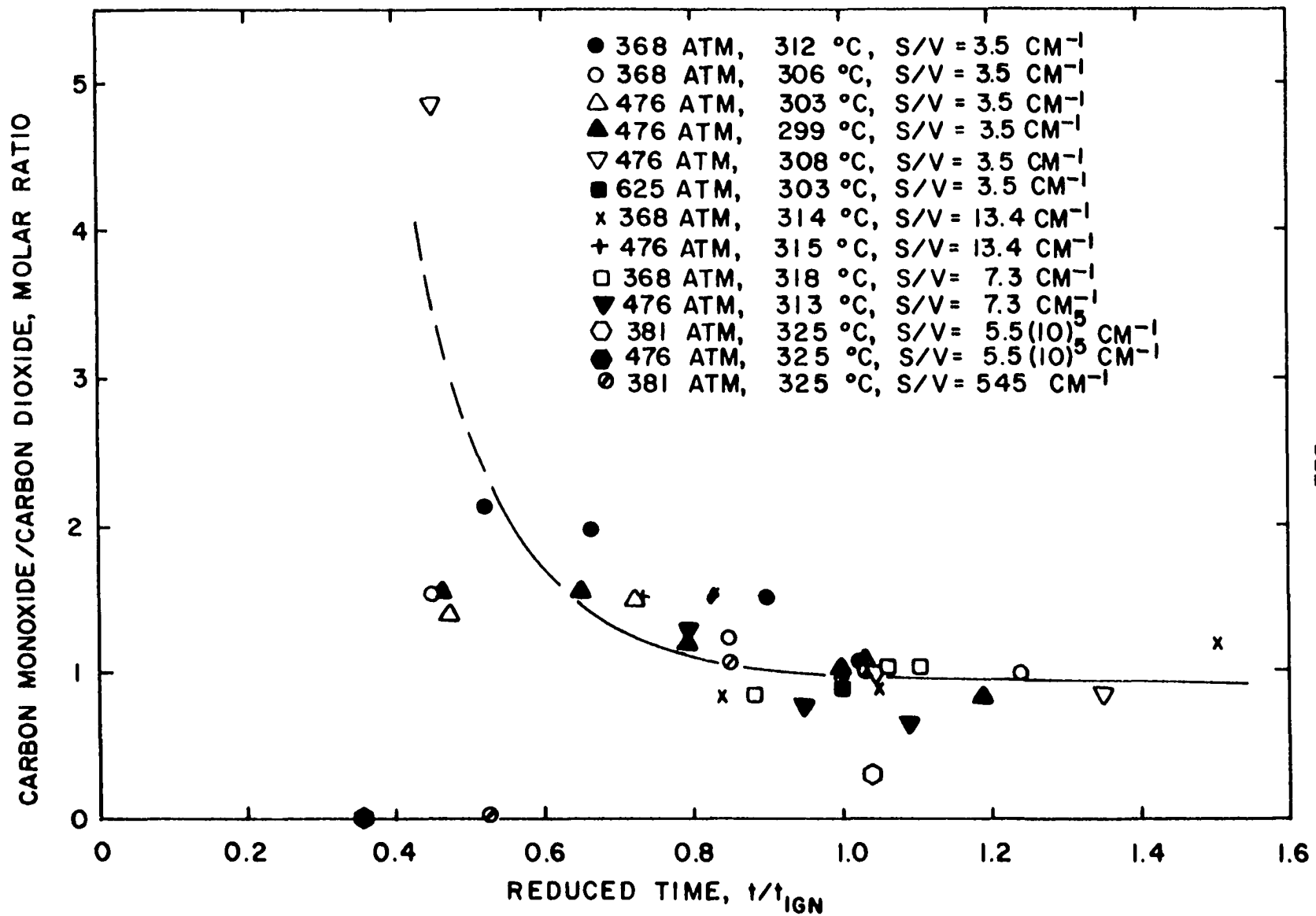


Figure 50. Carbon Monoxide/Carbon Dioxide Ratio as Function of Residence Time.

In the present instance, there are insufficient data to warrant attempts at determining a temperature-ratio relationship at each time value. However, the general influence of time on the CO/CO_2 is clearly shown.

It is interesting that several of the tests with alumina (high S/V) resulted in points well below the general trend. This observation undoubtedly indicates that oxidation of carbon monoxide to carbon dioxide is occurring at high surface/volume conditions. Even though the steel-packed and alumina-packed reactors showed no catalytic effect on ignition delay, the effect on carbon monoxide and carbon dioxide production is apparent.

In isolated tests with ignition delays below about 5 minutes, the CO/CO_2 ratio was markedly higher (even though t/t_{ign} was at or near unity), as Lott observed. This observation can be shown by noting, in Table A-1, Appendix A, the ratios measured for nearly instantaneous ignition conditions in Runs 3, 5, 11, 70, 78, 82, and 86. In each case, CO/CO_2 is higher than unity at reduced times at, or slightly above, unity. This observation further emphasizes the probability that carbon monoxide is oxidized to carbon dioxide at surfaces. Under near-explosive conditions, insufficient time is available for significant diffusion of carbon monoxide to the surfaces for oxidation to continue. Some of the oxidation of carbon monoxide, after a temperature maximum has passed, must be due to molecular oxygen. This

conclusion is based on the assumption that radicals are exhausted after temperature maxima and the fact that the CO/CO₂ ratios are decreased only slightly with time after maxima have occurred.

Hardwicke (26) reported CO/CO₂ ratios less than unity and the early production of carbon dioxide during his experimental tests. It appears very likely that "time zero" in his test was already in the region of rapid depletion of oxygen. This observation has already been suggested in connection with determination of order (page 210).

Periodicity in Oxidation

In one test (No. 84) a cyclic behavior was observed which could not be explained on the basis of heater operation. The test showed a 2°C temperature cycle having a period of 28 minutes. The heater cycle was about 5 minutes and caused an observable temperature fluctuation of only about ± 0.2°C. Thus, the phenomenon observed could not be attributed to normal electrical heat input and end losses.

The initial temperature was 308.1°C with an initial pressure of 653 atm. Surface-to-volume ratio was 19.9 cm⁻¹. The actual test duration was 59.6 minutes to the temperature maximum. A leak was observed during the test. At the time of the temperature maximum, pressure had fallen to 571 atm.

It is likely that the oscillation was caused by occurrence of an exothermic reaction which occurred at a certain concentration of intermediates or active centers.

Initial temperature was too low to enable normal acceleration; thus, temperature fell back to the set-point due to heat losses. Figure 48 showed that the measured ratio for $(\text{HCHO} + \text{CO} + \text{CO}_2)/\text{CH}_3\text{OH}$ of 7.3 should have placed the test in the region of rapid depletion of oxygen. Figure 25, the ignition delay correlation, however, predicts an ignition delay of about 25 minutes for the test conditions.

Many observers report the appearance of cyclic oxidation (for higher hydrocarbons) during filling operations of a batch reactor. The occurrence has been attributed to quenching action by incoming, unburned reactants on the accumulated active centers.

The gradually falling pressure, signifying loss of reactants due to leakage, may have produced a similar effect. It is possible that a first order dissociation of accumulated methylhydroperoxide occurs at a specified concentration. Momentary attainment of this concentration, followed by a decrease in concentration due to total charge loss, could have accounted for the drop in temperature. The loss in material then prevented normal auto-acceleration. The reaction finally attained ignition because the driving force for leakage decreased, and the rate of loss of material was reduced.

Catalyzed Tests

Time-temperature-species histories of the oxidation reaction under the influence of several catalytic materials

were determined. Operating conditions again involved the pressure range, 150 to 680 atm, and the temperature range, 303° to 335°C.

Because of the higher slope of ignition delay versus $1/T$, as shown earlier, slow reaction occurred over a much narrower range of temperatures than in the uncatalyzed systems. Most tests that were allowed to progress to a temperature maximum resulted in maximum temperatures in excess of those measured in non-catalyzed tests. Most of the temperature maxima were consistent with explosive rates of reaction.

Kao-Spheres

In tests which were allowed to progress to temperature maxima, non-explosive conditions were difficult to maintain, that is, reaction occurred only with violence. Tests quenched short of the point of auto-acceleration not apply in the above statement.

The general shapes of the species concentration curves, Figure 51 through 53, are, at times, significantly different from those observed in non-catalytic tests. At a reaction temperature of about 327°C and a pressure of 374 atm, the oxygen concentration curve appears to have two regions of rapid usage, (a "double-S" shape: Figure 51, Path A). Oxygen consumption reached a high rate at about 5 minutes, accompanied by the familiar formaldehyde maximum. Methanol production began to increase. At about

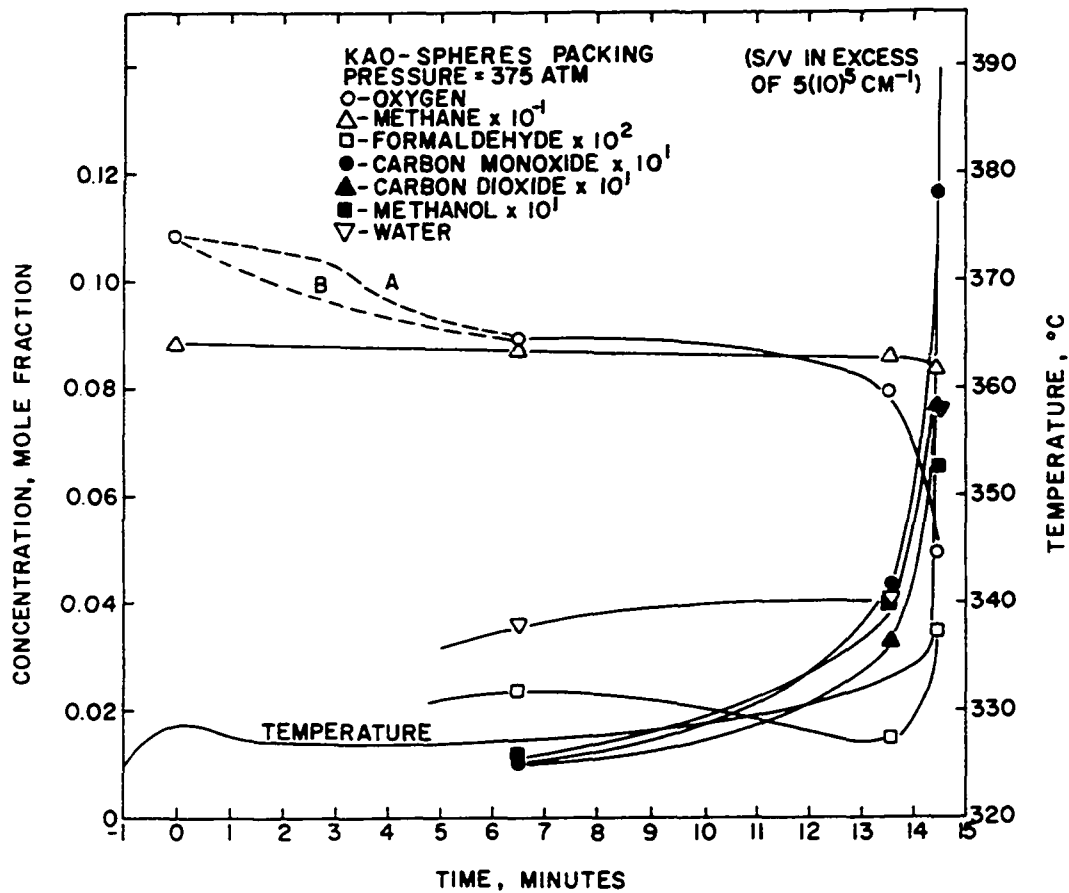


Figure 51. Reaction History at 375 atm, 327°C, and S/V in Excess of $5(10)^5 \text{ cm}^{-1}$ with Kao-Spheres Catalyst.

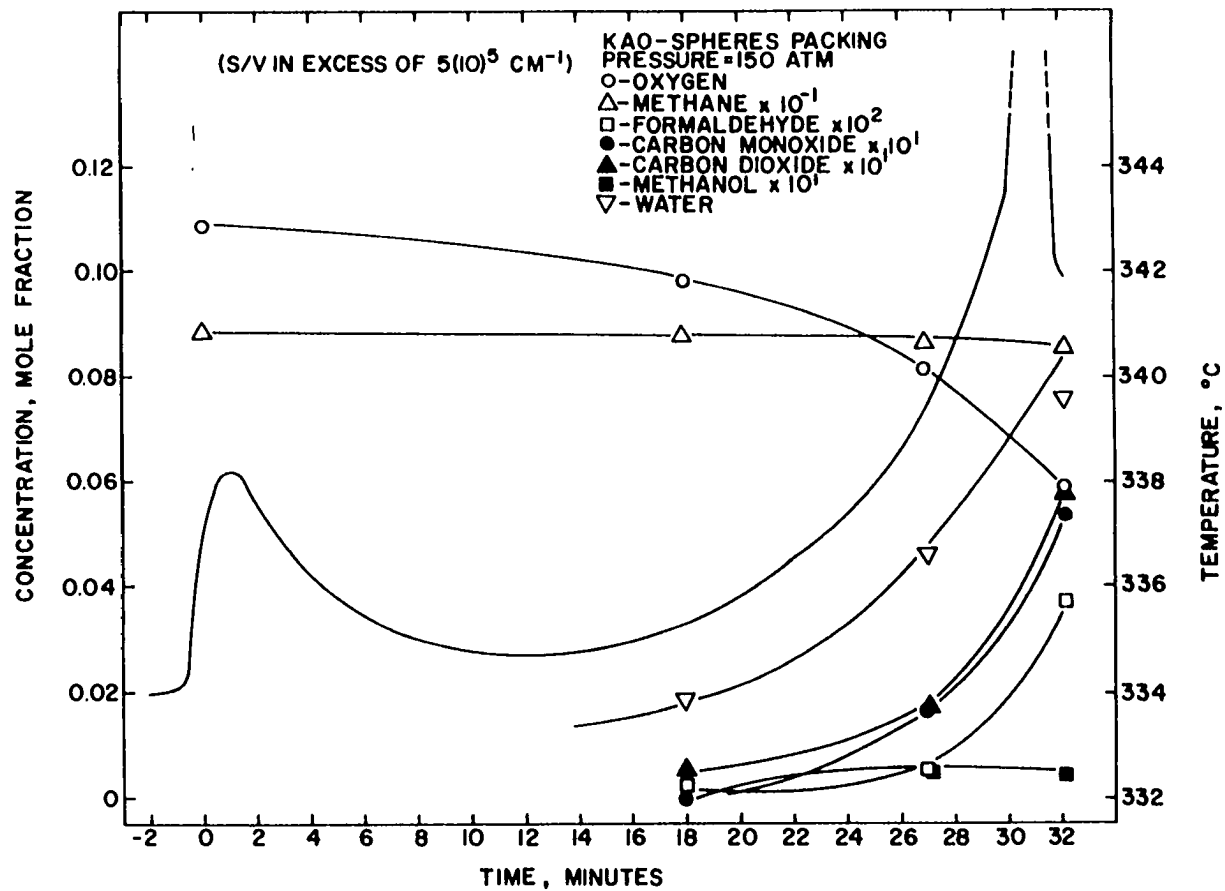


Figure 52. Reaction History at 150 atm, 337°C, and S/V in Excess of $5(10)^5 \text{ cm}^{-1}$ with Kao-Spheres Catalyst.

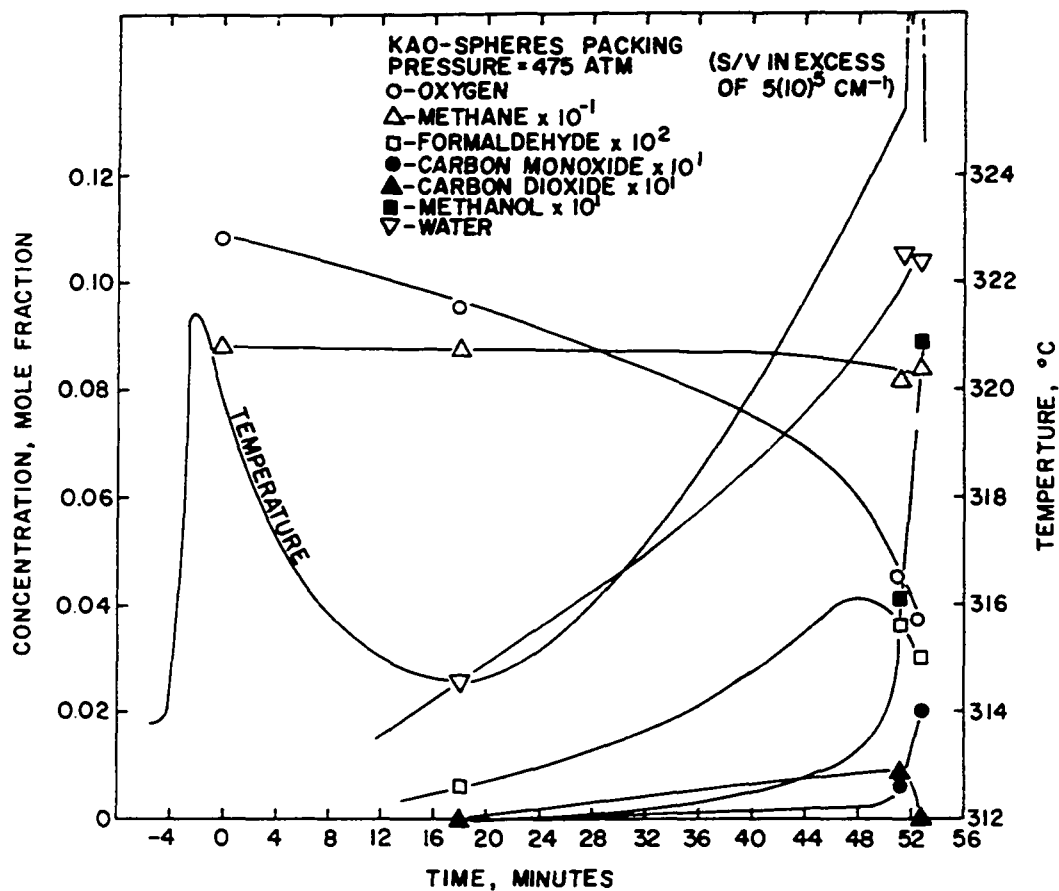


Figure 53. Reaction History at 476 atm, 314.5°C, and S/V in Excess of $5(10)^5 \text{ cm}^{-1}$ with Kao-Spheres Catalyst.

12 minutes, oxygen consumption again accelerated. Methanol production then increased sharply. Explosion occurred at 14 minutes. Formaldehyde concentration increased again, at a very sharp rate, at the point of explosion.

It should be pointed out that the "double-S" shape of oxygen concentration was arbitrary. Oxygen depletion may have begun immediately at an order in excess of zero and may have then leveled off before proceeding to the second maximum rate. This alternative path is shown as path B. However, earlier tests, which showed a formaldehyde maximum very shortly after the rapid decrease in oxygen content, can make path A a likelihood. In either case, it can be postulated that the initiation step is catalyzed, producing a supply of radicals leading toward production of formaldehyde. It is possible that dissociation of methylhydroperoxide occurs heterogeneously, leading toward inert products rather than those radicals necessary for production of methanol and subsequent auto-acceleration.

The reaction stabilizes at a normal zero-order rate, producing a second quantity of intermediates which leads this time toward auto-acceleration. These observations suggest that homogeneous dissociation of CH_3OOH is necessary for rapid production of methanol.

At 150 atm, also under explosive conditions, formaldehyde was observed to increase sharply at explosion, but the initial acceleration of oxygen consumption was not evident.

At 447 atm, however, formaldehyde concentration showed a normal maximum near the point of highest oxygen consumption.

Silica-Alumina Catalyst

Explosive conditions similar to these observed for Kao-Spheres were also common in this series. Formaldehyde concentration was seen to coincide with temperature rise, rather than to precede it as in non-catalyzed tests. Methanol production was very high. Both carbon oxides increased rapidly, with carbon monoxide assuming prominence during the isothermal portion of the tests. Oxygen consumption occurred immediately after filling, with little, if any, induction lag. Typical results are shown in Figure 54.

Silica-Magnesia Catalyst

The "double-S" curve for oxygen concentration was again observed with silica-magnesia. This result is shown in Figure 55. The tests at 368 atm and 320.5°C, however, were not explosive, as was the case with Kao-Spheres at 374 atm and 327°C. Again, formaldehyde appeared to undergo two periods of buildup, each lagging acceleration of oxygen usage by a small amount. Carbon dioxide production exceeded carbon monoxide production throughout the period and rapidly increased at the temperature maximum.

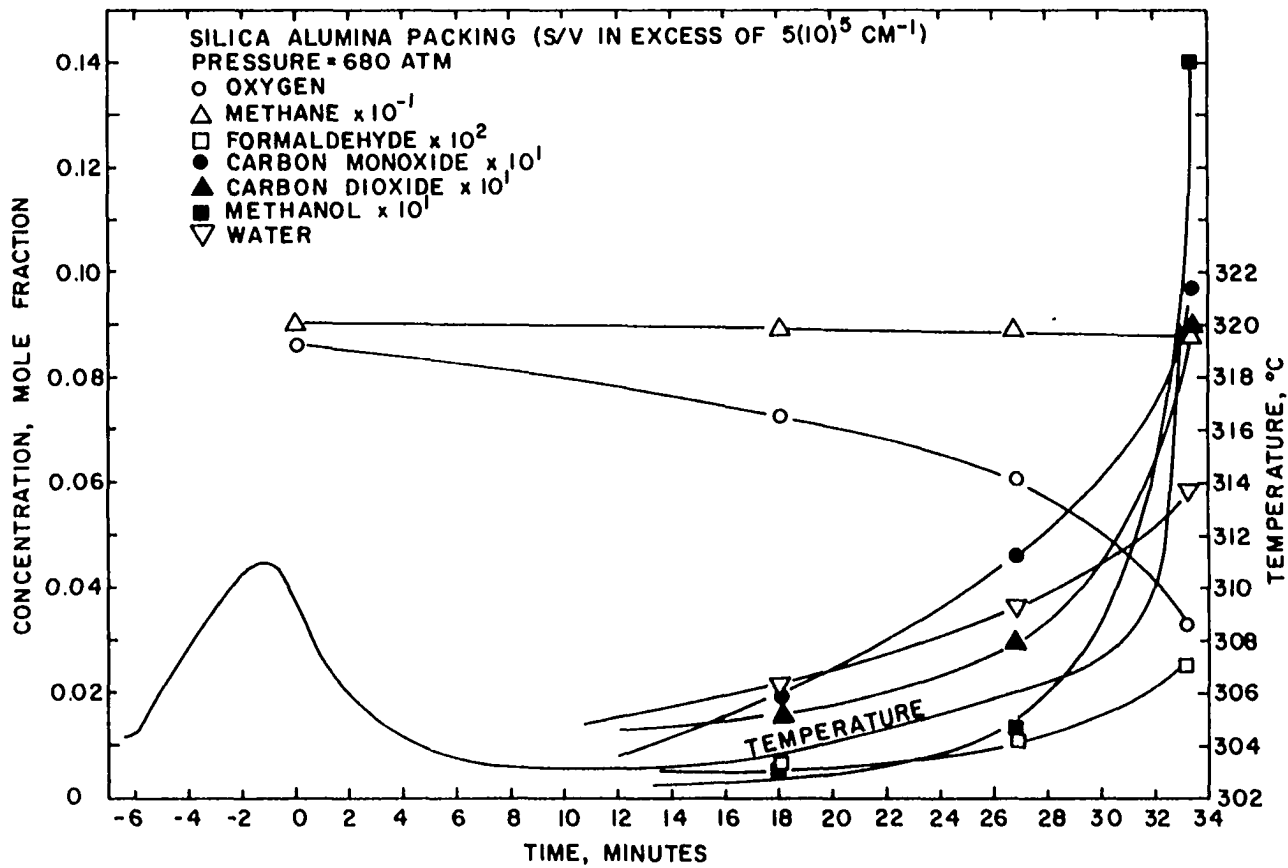


Figure 54. Reaction History at 680 atm, 303.1°C, and S/V in Excess of $5(10)^5 \text{ cm}^{-1}$ with Silica-Alumina Catalyst.

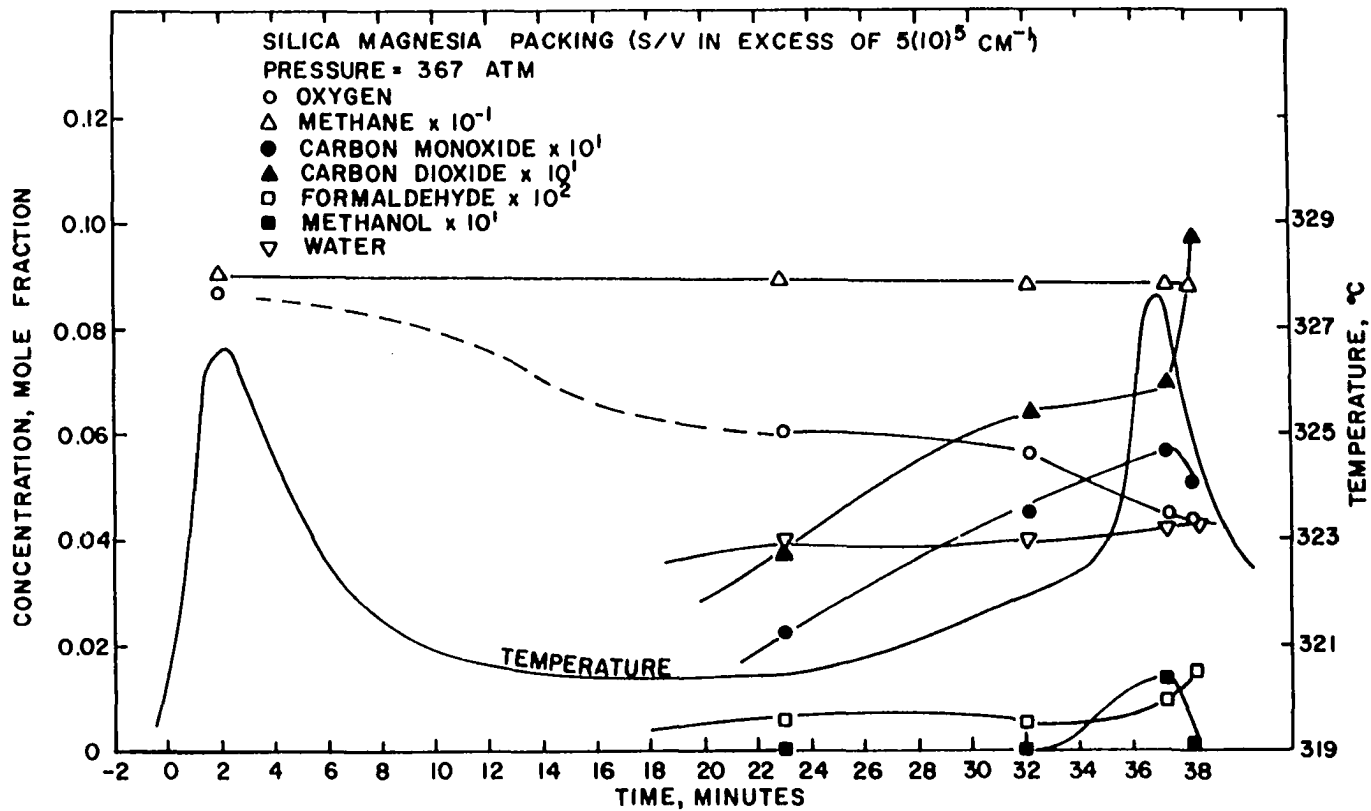


Figure 55. Reaction History at 367 atm, 320.3°C, and S/V in Excess of $5(10)^5 \text{ cm}^{-1}$ with Silica-Magnesia Catalyst.

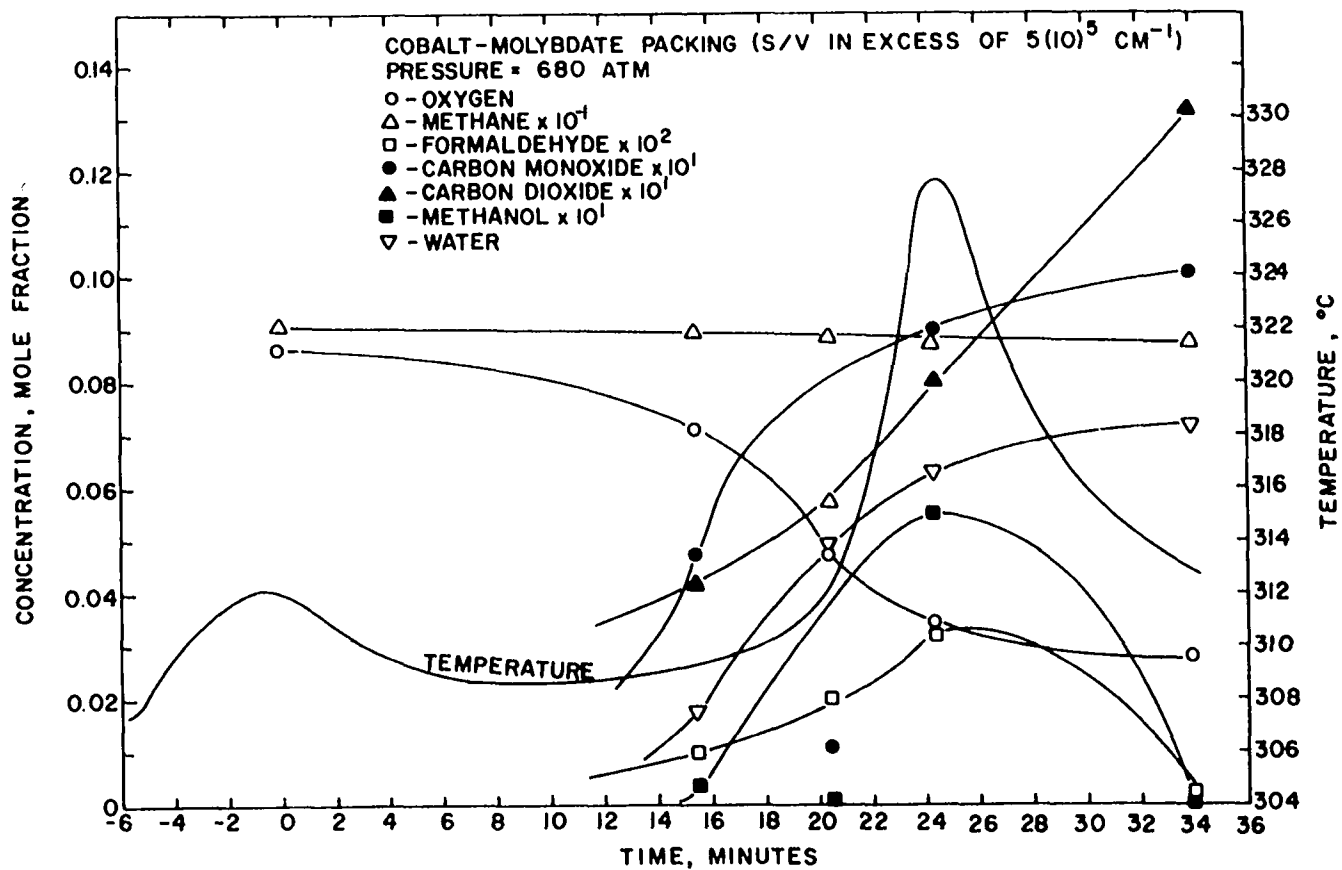


Figure 56. Reaction History at 680 atm, 308.6°C, and S/V in Excess of $5(10)^5$ with Cobalt Molybdate Catalyst.

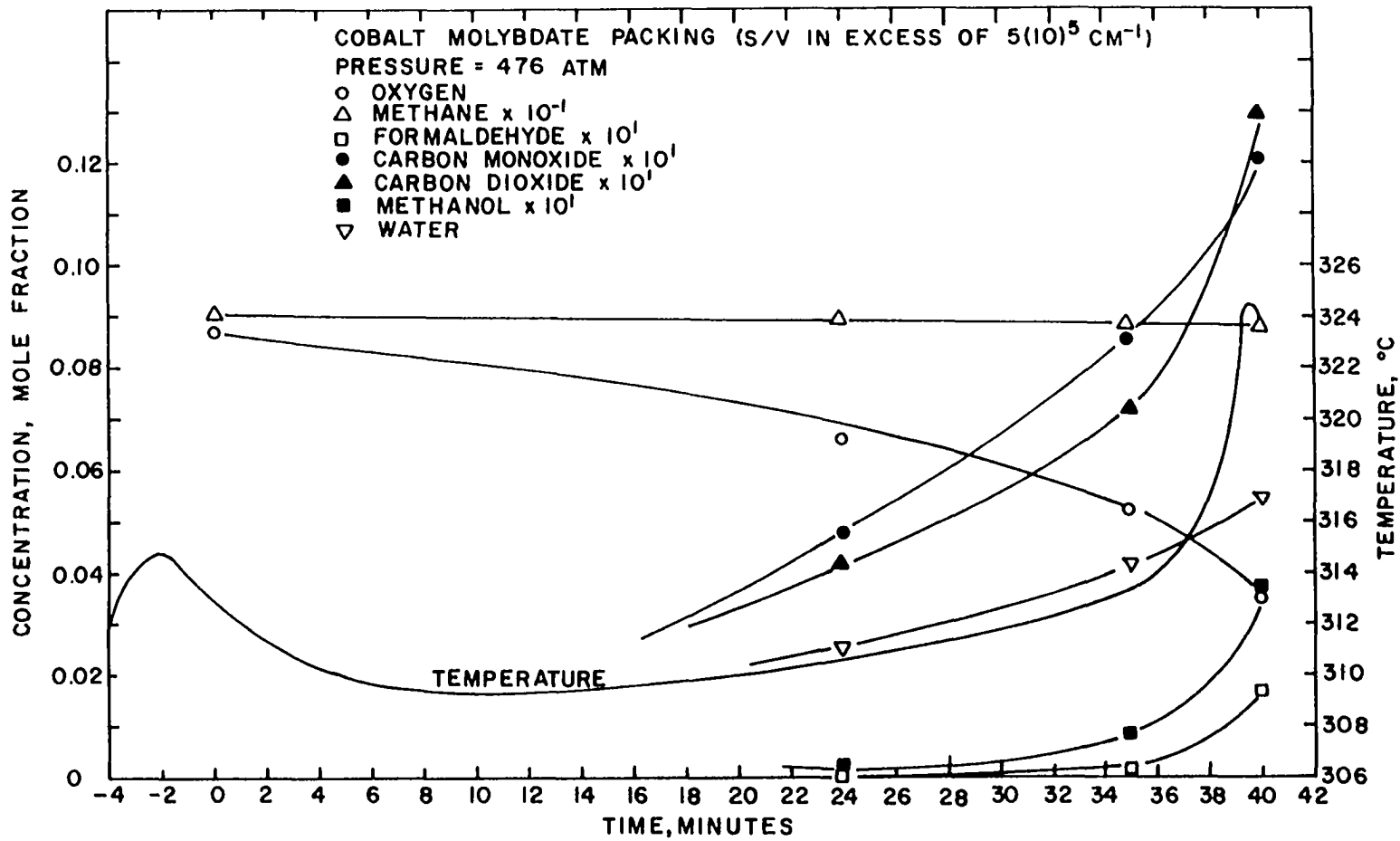


Figure 57. Reaction History at 476 atm, 309.2°C, and S/V in Excess of $5(10)^5 \text{ cm}^{-1}$ with Cobalt Molybdate Catalyst.

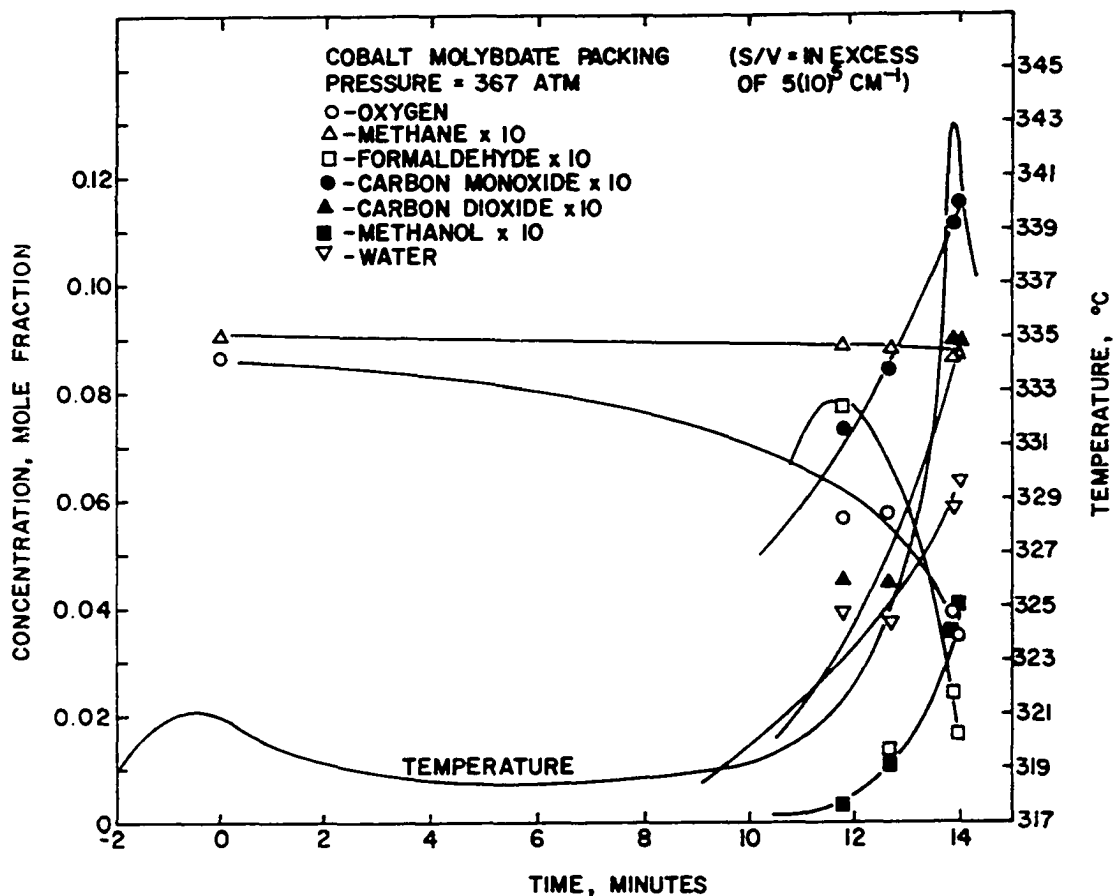


Figure 58. Reaction History at 367 atm, 318.4°C, and S/V in Excess of $5(10)^5 \text{ cm}^{-1}$ with Cobalt Molybdate Catalyst.

Cobalt-Molybdate Catalyst

Typical reaction histories for the catalyst are shown in Figure 56 through 58.

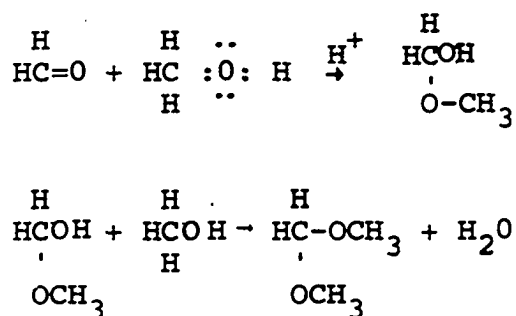
Extensive investigation of the cobalt-molybdate (C-M) catalyzed reaction was made after initial tests showed sharp differences from all other tests conducted to that point. Little or no induction time was observed; depletion of oxygen began immediately with the rapid production of carbon oxides, formaldehyde and water.

The stated differences were not, in general, concerned with concentrations of the seven major components measured earlier. Formaldehyde production was, however, considerably higher than in most other tests involving high S/V conditions. At 477 atm and 309°C, formaldehyde reached one of the highest concentrations observed in all tests. At 477 atm and above formaldehyde production was coincident with temperature increase.

The sharpest difference was in the appearance of minor products not observed earlier. It was immediately apparent that the liquid product was dissimilar from that of earlier tests on the basis of odor alone. A very strong pungent odor was a characteristic of all C-M tests.

Chromatographic analysis also showed three peaks not observed in earlier tests. These peaks were tentatively identified as isopropanol, methylal and ethyl formate. None of these liquids in pure form had the odor characteristic of C-M test products. All were present only in trace amounts.

Production of ethyl formate presents no mechanistic problems; the compound arises undoubtedly through steps similar to production of methyl formate or through a simple esterification reaction between formic acid, water and ethanol. Methylal can be produced in a non-chain mechanism by the addition of an alcohol and the carbonyl group of formaldehyde in the presence of an acidic catalyst:



The hemiacetal formed in the first step is unstable and normally reverts to the original reactants. However, a small amount can react with additional alcohol to yield methylal.

Mass spectrometric analysis showed that considerable acetaldehyde was produced during C-M catalyzed tests. Similar analyses of representative tests with the other catalysts and in the unpacked reactor showed only minute quantities of acetaldehyde. With the Porapak chromatographic column, acetaldehyde is not well separated from methanol at the conditions used, accounting for the initial lack of detection. Acetaldehyde might be formed from $\text{CH}_3\cdot$ and $\text{HCO}\cdot$.

Increased formaldehyde production could supply these radicals.

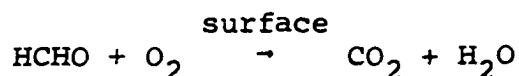
Mass spectrometric analysis showed no other significant peaks that could account for the odoriferous impurity. It was assumed that only the slightest trace amount of an unknown substance was responsible for the odor or that the combination of acetaldehyde, with the normally present constituents in the right proportion, caused it.

In some non-catalyzed tests, there was evidence that ethane was produced under certain conditions. Then, with ethane as a starting point, presence of all other two-carbon atom (and higher) compounds can be explained via a chain mechanism similar to that for methane.

High production of both formaldehyde and acetaldehyde leads to a conclusion that cobalt-molybdate catalyst would not improve aldehyde production directly unless formation of aldehydes or the generation of radicals leading to aldehyde production were heterogeneous processes. However, other observations indicate that increased aldehyde production is due to catalysis of other steps and not due to the catalyzed formation of aldehyde itself.

The immediate depletion of oxygen without evidence of an induction period indicates that the initiation step can be accelerated with C-M catalyst. In many uncatalyzed tests there was evidence that carbon dioxide was either produced during the initial stages of reaction by a chain mechanism or was the result of rapid oxidation of carbon

monoxide by $\text{HO}_2\cdot$ radicals. Predominance of carbon monoxide in early stages of C-M tests, however, indicates that the catalyst may be a strong destroyer of $\text{HO}_2\cdot$ radicals. Another possibility is that direct oxidation, and not the formation, of formaldehyde may be heterogeneous:



Cobalt-molybdate may selectively adsorb methane (higher initiation rate suggests this) preventing heterogeneous oxidation of formaldehyde. Hence, a higher formaldehyde concentration is possible, and production of carbon dioxide is retarded as was observed.

Nickel-Catalyzed Oxidations

Slow oxidation of methane was conducted in several tests using nickel catalyst. This catalyst, described earlier, was the only material evaluated which has been generally accepted to be a true oxidation-promoting catalyst. Table 14 summarizes the results of this portion of the program.

Under conditions in which the other catalysts resulted in the standard "S-shaped" curve for oxygen concentration, signifying existence of an induction period, reactions with nickel catalyst were characterized by complete absence of an induction period. That is, reaction commenced immediately, perhaps even during the filling operation.

TABLE 14

RESULTS OF NICKEL-CATALYZED REACTIONS

Pressure atm	Initial Temp °C	O ₂ ^a	CO ^a	Analysis CO ₂ ^a	HCHO ^b	MeOH ^b	Res Time Min	Ignition ?
150	262	0.0807	nil	0.0062	nil	nil	61.5	no
"	264	0.0872	nil	0.0028	nil	nil	6.3	no
"	280	0.0702	trace	0.010	nil	nil	57.0	no
"	280	0.0780	nil	0.0043	nil	nil	12.3	no
"	300	0.0655	nil	0.0146	0.0007	nil	16.3	no
"	311	0.0563	trace	0.0043	0.0011	nil	65.7	no
"	312	0.0730	nil	0.0092	nil	nil	12.0	no
"	311	0.0550	nil	0.0150	0.0007	nil	34.2	no
"	312	0.0566	nil	0.0158	0.0006	nil	33.2	no
"	323	0.0504	trace	0.0190	0.0003	nil	202.8	no
"	304	0.0603	nil	0.0123	nil	nil	8.0	no
"	322	0.0520	nil	0.0178	trace	nil	33.0	no
"	326	0.0711	nil	0.010	0.0005	nil	4.2	no
"	333	0.0620	nil	0.0154	-c-	-c-	6.2	no
"	337	0.0673	trace	0.0149	0.00175	0.0015	0.8	yes
"	340	-d-	-d-	-d-	0.0012	trace	0.8	yes
367	311	0.0495	nil	0.0186	0.0013	0.0940	60.0	no
"	311	0.0820	nil	0.0072	nil	0.0072	4.0	no
"	320	0.0570	0.0090	0.0120	0.0022	0.152	0.1	yes
442	311	0.0667	nil	0.0090	-c-	-c-	10.0	no
447	285	0.0840	nil	0.0040	nil	nil	6.0	no
"	286	0.00740	nil	0.0080	nil	nil	33.8	no
"	311	0.0441	0.0084	0.0160	0.0007	0.2240	0.1	yes

Initial O₂/CH₄ ratio = 0.0952 moles/mole

a - Gas analysis on basis of moles/mole CH₄

c - No liquid samples taken

b - Liquid analysis on basis of gm/gm H₂O

d - No gas samples taken

Oxygen concentration was observed to decrease immediately in a manner characteristic of reactions not dependent on a stable intermediate. Figure 59 shows this feature for tests made at 150 atm and temperatures varying from 262°C to 340°C.

In the course of conducting the tests at 150 atm, it was found that, in general, temperature remained constant at the initial value after an initial period of heating due to compression on filling. Above 337°C, however, temperature did not fall to the initial value, but it remained at the maximum for a short period and then rose explosively at ignition. Explosive reactions were also observed at higher pressures. At 367 atm explosion occurred at 320°C, and at 477 atm, explosion occurred at 311°C.

Of considerable importance was the complete absence of methanol production in the non-explosive tests. Some formaldehyde was produced, but in very low concentration. No carbon monoxide was produced in any of the non-explosive tests. Trace amounts of carbon monoxide were produced in the tests which underwent explosive reaction.

It is apparent that presence of nickel promotes the rapid oxidation of methane. The reaction proceeds rapidly to completion, resulting in formation of water and carbon dioxide.

The absence of methanol at pressures normally conducive to its formation implies that a surface reaction is

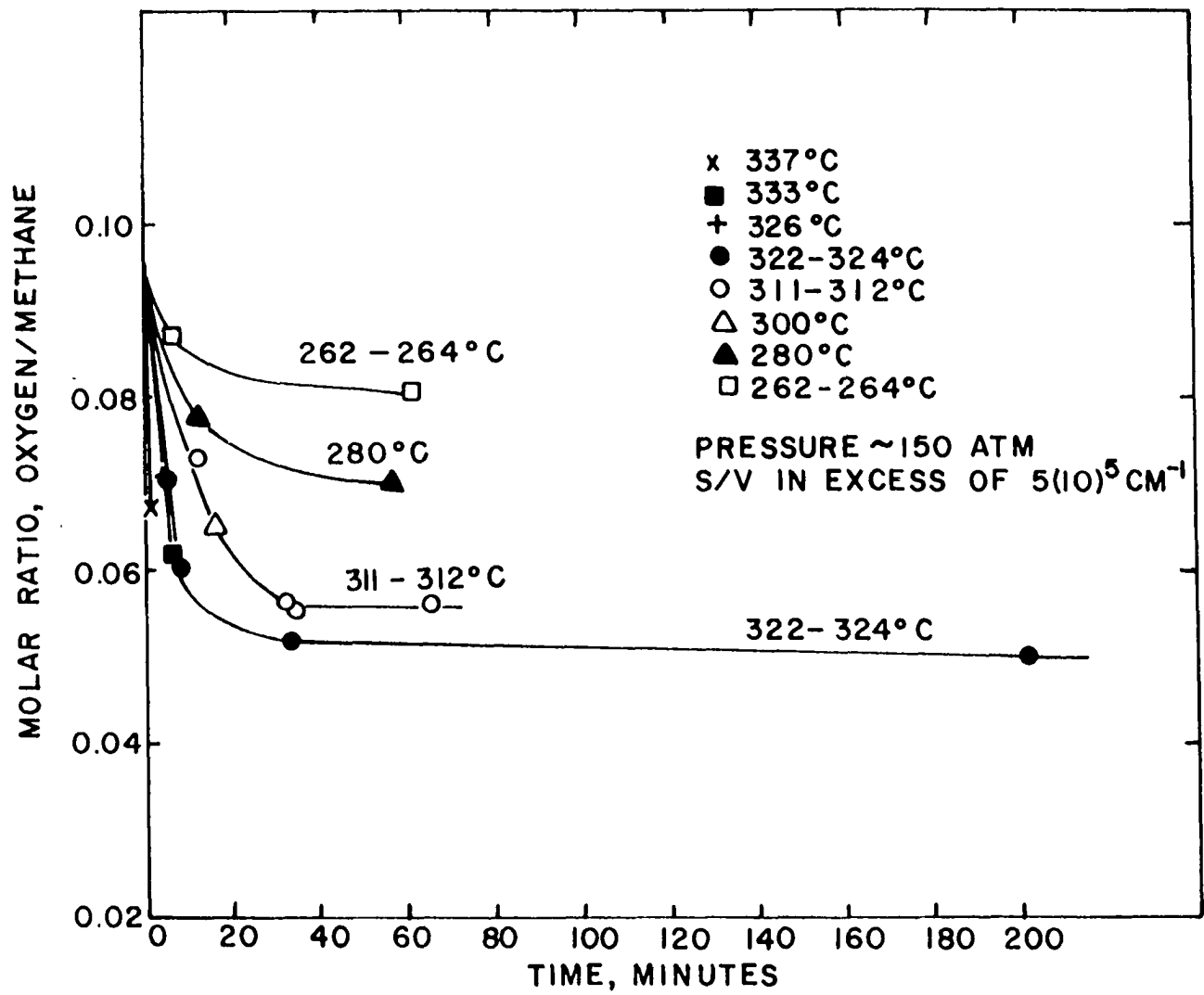


Figure 59. Oxygen Concentration as a Function of Time with Nickel Catalyst.

involved. Under non-catalytic conditions, termination of $\text{CH}_3\cdot$ and $\text{OH}\cdot$ radicals results in formation of methanol with evolution of heat. The fact that considerable methanol is formed at high temperatures even in the presence of nickel, as reactions tend toward explosive rates, seems to lend support to the premise that the $\text{CH}_3\cdot + \text{OH}\cdot$ termination step is homogeneous. At elevated temperatures reactions in the vapor phase are sufficiently rapid that diffusion to the wall is not allowed to occur before explosion occurs.

Figure 60 is a graph of initial rate of oxygen depletion as a function of temperature for the series of tests at 150 atm. It can be seen that the initial rate is approximately a linear function of temperature up to about 310°C . At this temperature, the reaction tends to become explosive.

A determination of activation energy was made by plotting initial rate as a function of reciprocal temperature, as in Figure 61. The data from non-explosive tests result in a slope of -9950 , indicating an activation energy of 19.8 kcal/mole. The sharp break in the curve indicates the transition to explosive rates even more clearly than is shown in Figure 60.

Photochemical Initiation

It was found that the mercury-quartz lamp was operable under only a limited range of temperatures. By using a voltmeter across the lamp leads, the information presented in Table 15 was assembled. Operation of the lamp

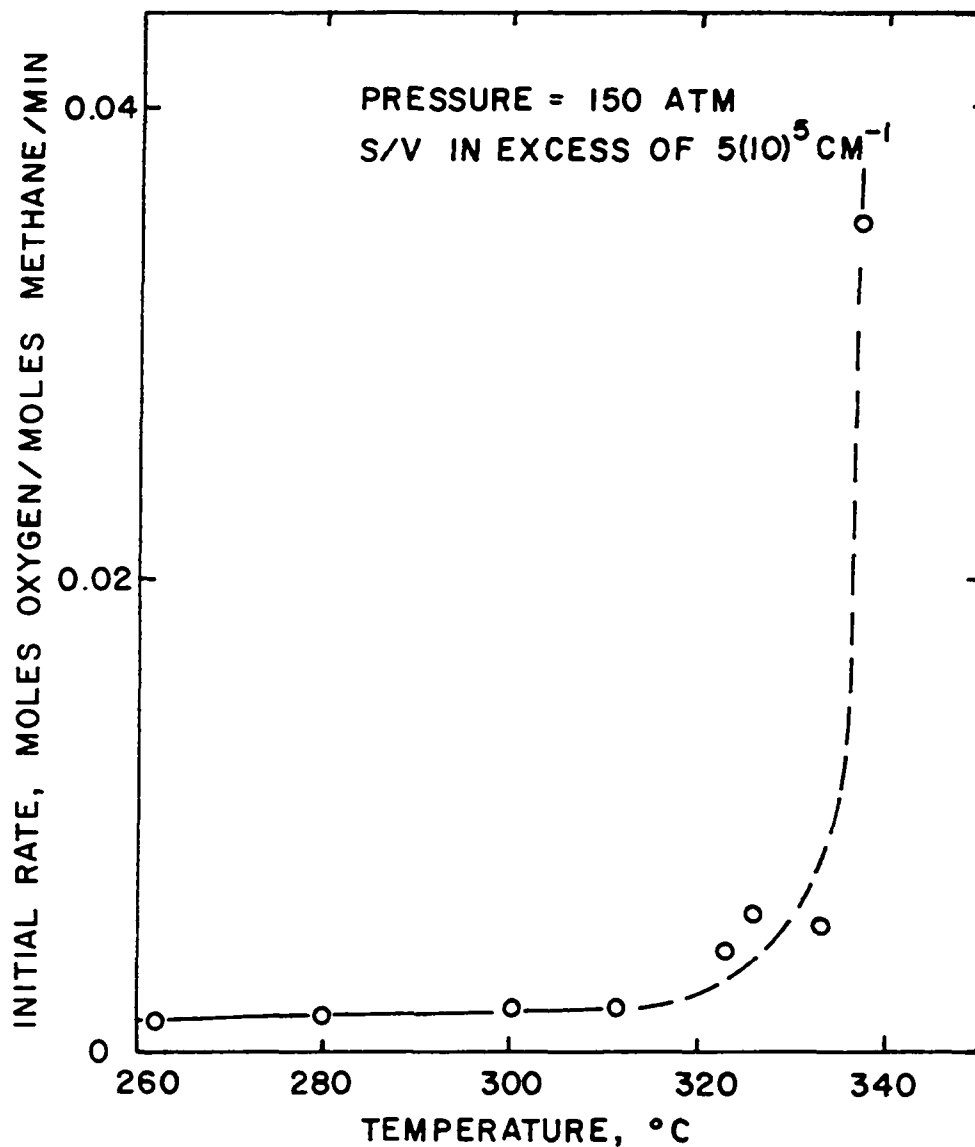


Figure 60. Initial Rate of Oxygen Depletion as a Function of Temperature for Nickel-Catalyzed Oxidation.

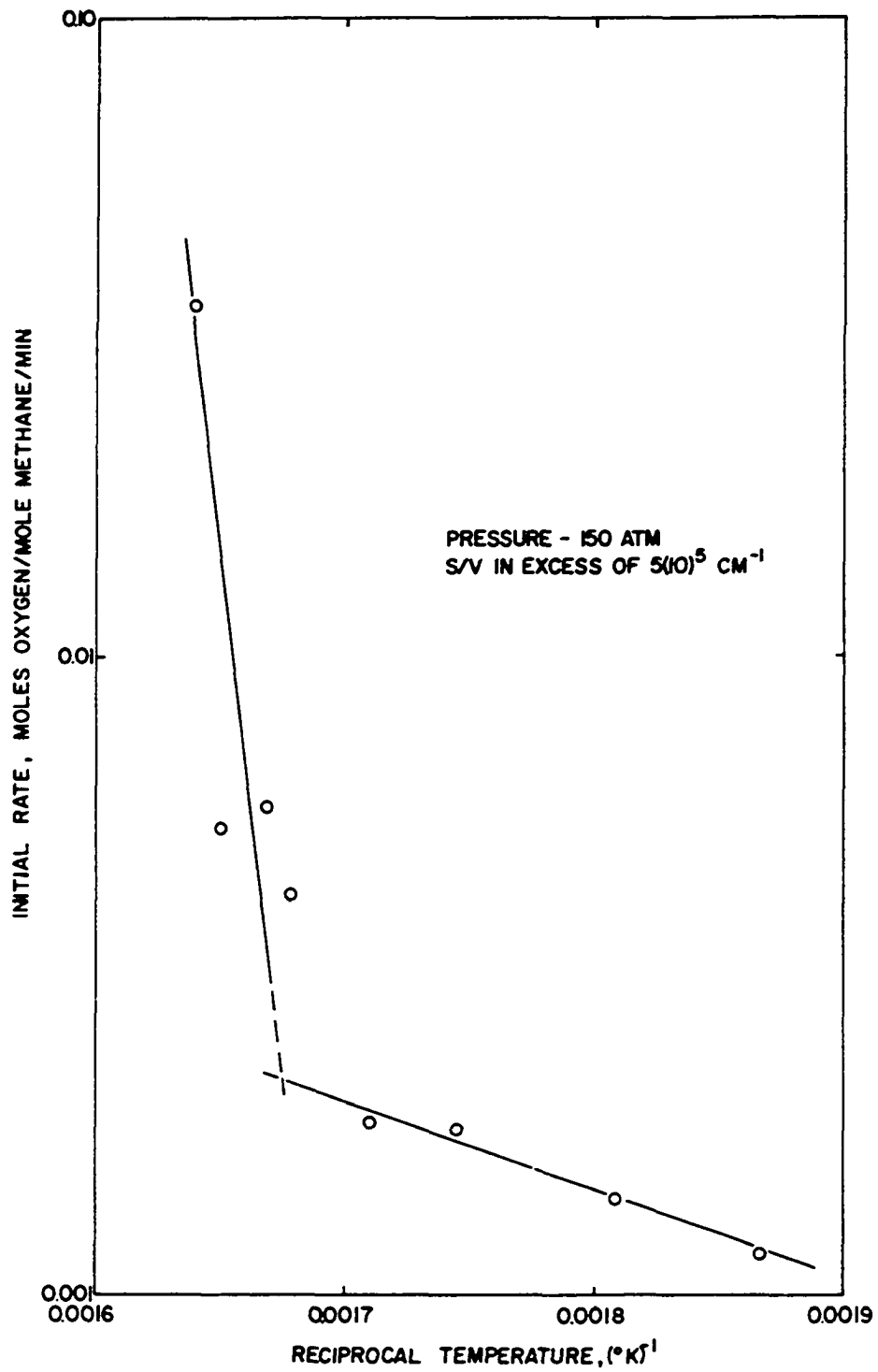


Figure 61. Initial Rate of Oxygen Depletion as a Function of Reciprocal Temperature for Nickel-Catalyzed Oxidation.

TABLE 15

OPERATING VOLTAGE OF Hg LAMP AS A FUNCTION
OF TEMPERATURE

Temperature °C	Voltage
25	210
150	212
204	250
215	300
238	540
250	650*
254	730*
264	730*
270	1300

*Oscillating voltage signifying unsteady operation.

was always indicated by a voltage drop of 200 to 730 volts. Under inoperative conditions, the voltage was about 1300 volts, while a direct short showed no voltage drop.

The lamp ceased steady operation at about 250 volts. It was not possible to illuminate reaction mixtures undergoing normal oxidation at the test conditions used in earlier phases of this study. However, it was hoped that proper selection of additives would enable initiation of oxidation at temperatures well below those necessary for thermal initiation.

Three initiators were used. Acetone, formaldehyde, and acetaldehyde were added to the reaction mixture in

separate tests, and the mixture was subjected to illumination at various times.

Table 16 summarizes the test conditions in the brief series of runs.

TABLE 16
PHOTOINITIATION FEASIBILITY TESTS

Test No.	Pressure atm	Temperature °C	Additive	Test Duration min	Light on at min
252	340	273	None	106	15
254	150	260	200 mm/Hg Acetone	90	10
255	122	147	6 ppm Formaldehyde	360	1.3
256	119	64	1 atm Acetaldehyde	164	5
257	143	120	1 atm Acetaldehyde	79	6
261	163	23	1 atm Acetaldehyde	64	10

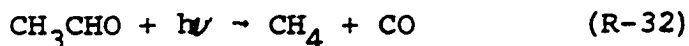
Table 17 summarizes the inlet and outlet conditions. These values were calculated from the chromatographic analysis. Usage of oxygen occurred in each test. The highest amount used was only about 12 percent in Run 257. This test incorporated the highest temperature used in which acetaldehyde was employed as an initiator. In two tests (256 and 257) methane content increased. Two initiation reactions for acetaldehyde were suggested earlier (Reactions R-32 and R-35) which could have directly or indirectly led to methane

TABLE 17
PHOTOCHEMICAL TEST REACTANTS AND PRODUCTS

Run No.	Weight of Species, gm									
	252		254		256		257		261	
	Inlet	Outlet	Inlet	Outlet	Inlet	Outlet	Inlet	Outlet	Inlet	Outlet
CH ₄	35.71	35.60	19.25	19.30	12.52	12.85	20.80	21.60	28.00	27.80
O ₂	6.12	5.89	3.67	3.32	2.38	2.08	3.96	3.50	5.35	5.25
N ₂	0.28	0.22	0.12	0.23	0.07	0.11	0.13	0.19	0.18	0.11
CO	0.0	0.0	0.0	0.0	0.0	0.0	0.0	0.12	0.0	0.0
C ₂ H _b	0.06	0.06	0.0	0.0	0.04	0.0	0.06	0.0	0.08	0.0
CO ₂	0.19	0.19	0.06	0.06	0.07	0.09	0.12	0.06	0.17	0.13
HCHO		0.21	0.0	0.0008	--	0.002	--	0.002	--	0.004
H ₂ O		0.13	0.0	0.39	--	0.145	--	0.079	--	0.338
CH ₃ CHO	--	--	--	--	0.36	0.011	0.40	0.008	0.40	0.034
HCOOH	--	--	--	--	--	0.004	--	0.0	--	0.012
CH ₃ COOH	--	--	--	--	--	0.159	--	0.0927	--	0.350
Acetone	--	--	0.018	0.0	--	--	--	--	--	--
CH ₃ OH	--	--	--	--	--	--	--	--	0.0003	0.003

Note: Run 255 was not included. Insufficient liquid was produced for analysis.

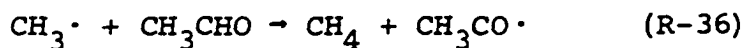
production:



Both these initiation steps would produce carbon monoxide, which was not formed. Formation of methane through R-32 or by recombination of H· and CH₃· from R-35 is thus unlikely. Another initiation reaction might have been:



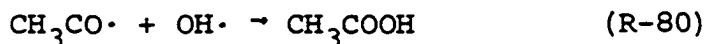
Reaction of CH₃· radicals with acetaldehyde can give methane:



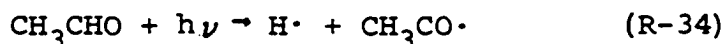
The acetyl radical (CH₃CO·) normally decomposes at low pressures to carbon monoxide, which, as stated, was not observed:



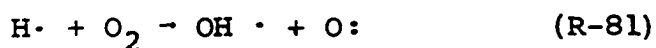
If however, the acetyl radical does not decompose, but reacts instead with hydroxyl radicals (OH·) acetic acid is formed, which was observed in runs 256 and 261:



The OH· radicals could come from a secondary initiation step:



with oxidation of the hydrogen atom due to



The OH· radical could then react directly with the acetyl radical producing acetic acid in termination. Some formaldehyde was formed also which suggests the initiation step producing CHO· (R-33) also occurs.

Slight production of methane with acetone was also indicated (Run 254). However, the high nitrogen content in the products indicates some leakage occurred during pump-down. The indicated methane increase is probably experimental error. Curiously, however, there was a reasonable mass balance between oxygen usage and formation of products.

With no initiator, only formaldehyde and water were formed. This result is entirely plausible in view of the mechanism of Hardwick, et al., page 77. Because the temperature of Run 252 was well below that which results in an appreciable rate in the thermal reaction, it is felt that the small amount of formaldehyde which may have been formed thermally was photolyzed by:



No hydrogen was detected, however.

None of the tests resulted in auto-acceleration of the reaction to the extent that appreciable quantities of methane were oxidized. All oxygen appeared to be used in

conversion of acetaldehyde to acetic acid and/or formation of water. Lack of production of carbon oxides may indicate that if a suitable initiator type and concentration were found, the very low temperatures employed can suppress unwanted carbon oxides. It would seem desirable that appreciable quantities of OH· radicals must be formed to draw methane into the overall reaction. With this suggestion in mind, a suitable initiator might be methylhydroperoxide which would lead to production of both formaldehyde and methanol.

Considerable insight might be gained in the normal, thermal mechanism if a suitable light source were devised which would be operable at the elevated temperatures usually used. In this manner, the batch reaction could be illuminated at or slightly below the formaldehyde maximum. Formation of H· and HCO· radicals could lead to production of acids and aldehydes with suppression of the oxidation of formaldehyde.

The High-Pressure Mechanism

All results in this study were related adequately to the overall mechanism of Hardwick, Lott, and Sliepcevich (27). No refutation of this overall mechanism or its individual steps was found. This mechanism was presented on page 77.

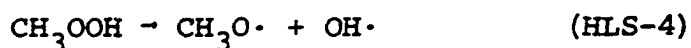
Of extreme importance in the scheme are the steps describing the formation of the methyl peroxy radical:



the production of methylhydroperoxide:



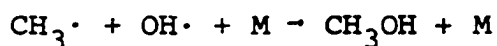
the destruction of the peroxide:



and the formation of methanol by a termination reaction:

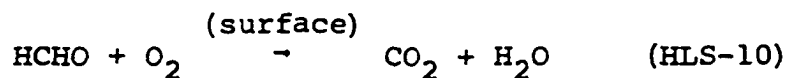


These steps are necessary to explain high pressure oxidation of methane. The termination step (HLS-14) has been shown to be homogeneous. Because radical-radical reactions generally need a third body to dissipate the exothermic energy, a three-body reaction may be more correct:



The assertion of homogeneity indicates that the species M must be a third gaseous molecule and not the reactor wall.

Some of the work described in the section dealing with catalysis indicated that the branching step, HLS-10, can be a heterogeneous reaction and should be indicated in the mechanism:



CHAPTER VIII

Conclusions

The mechanism of Hardwicke, Lott, and Sliepcevich, (27) can be used to describe the oxidation of methane under conditions of high surface/volume ratio and catalysis. Furthermore, the mechanism provides an adequate description of the process occurring during both slow, inductive reaction and explosion.

As is well known, explosion occurs in a non-isothermal batch reaction of methane and oxygen if the balance between heat generation at heat dissipation is upset. At low pressures the balance must be maintained, to prevent explosion, at the instant of highest usage of oxygen. At the point the highest total rate of exothermic reactions, ignition occurs.

As pressure is increased, methanol production occurs due to a termination reaction of hydroxyl ($\text{OH}\cdot$) and methyl ($\text{CH}_3\cdot$) radicals. Methanol production by this reaction occurs with evolution of energy and can reach a maximum rate several minutes after the point of highest rate of usage of oxygen. If the reaction proceeds beyond

the point of maximum rate of oxygen usage, temperature can continue to rise to a maximum several minutes later, coincident with the methanol maximum. The energy balance can then be upset, producing explosions at any time between the point of maximum usage of oxygen and the methanol maximum.

Defining ignition delay as the time interval between introduction of reactants into a batch reactor and the point of maximum temperature, ignition delay can be correlated with pressure, surface-to-volume ratio, and reciprocal temperature. Over the pressure range 48 to 3400 atm., the temperature range 255 to 360°C and the range of surface/volume ratios (S/V) of 1.3 cm^{-1} to $5.5(10)^5 \text{ cm}^{-1}$, ignition delay is represented by an equation of the form:

$$t \sim \beta P^n e^{E/RT}$$

where t is ignition delay, P is pressure, T is absolute temperature, R is the gas constant, E is an activation energy, n is the order with respect to pressure, and β is a function dependent on surface/volume ratio. The activation energy, E , is 98 kcal/mole. The order with respect to pressure, n , is -1.3 above 476 atm. and -2.8 below this pressure. The function, β , is proportional to S/V (surface/volume) to the first order at low values

of S/V and approaches a constant value of about 6 (zero order dependence on S/V) at values of S/V above about 10^4 cm^{-1} .

Formation of methanol occurs in chain steps resulting from the formation of an intermediate, methylhydroperoxide, which is stable at high pressures. The chain sequence also generates the radicals ($\text{OH}\cdot$ and $\text{CH}_3\cdot$) necessary for methanol production in a termination step. In explosions, the termination step produces considerably more methanol than the chain step.

Ignition delay and product distribution in the oxidation of methane at a 10/1 molar ratio. (methane/oxygen) can be altered with heterogeneous catalysts. Use of silica-alumina, silica-magnesia, kaolin or cobalt molybdate increases the effect of temperature on ignition delay by altering the activation energy. Nickel catalyst, however, causes the reaction to proceed rapidly without an induction period.

In addition to its effect on ignition delay, cobalt molybdate causes increased production of aldehydes. The initiation steps of the reaction are also accelerated by this catalyst.

Higher production of methanol under explosive conditions, in either catalyzed or non-catalyzed systems, than that formed in non-explosive tests indicates that the termination production of methanol is homogeneous.

Carbon monoxide is produced before carbon dioxide in tests at low surface/volume ratio. In non-explosive

reactions the ratio of concentrations of carbon monoxide to carbon dioxide decreases to below unity as the temperature maximum is passed. If the temperature maximum reaches explosive rates, the ratio becomes much greater than unity. High S/V conditions lead to oxidation of carbon monoxide to carbon dioxide.

Use of acetaldehyde or acetone as an initiator in the photochemical oxidation of methane, up to 260°C and at moderate pressure (ca. 150 atm.) does not lead to appreciable consumption of methane. All oxygen usage can be accounted for in reactions with radicals formed from the initiator. Using acetaldehyde, production of methane can, in fact, occur.

It is suggested that future work with this reactant combination be involved in the accurate determination of order at high pressure through variation of mole fraction as well as pressure. The early, nearly isothermal region of the reaction is of interest. A means of peroxide detection would be an extremely valuable tool. It is suggested that a micro-sampling technique be devised for continuous analysis during the reaction.

Although methane could not be drawn into an oxidation reaction by photochemical dissociation of aldehydes under the limited range of conditions used, it is felt that continued investigation in this field might be fruitful. Other initiators and a light source which is operable during a normal inductive reaction, should be sought.

NOMENCLATURE

- A = Matrix of Kinetic Coefficients
= Pre-exponential Factor in Arrhenius Equation
- a = Kinetic Coefficient of Chain Propagation
- D = Bond Energy of Molecule
- d = Rate of Change of Concentration of Active Centers (vector or individual values)
- E = Activation Energy
- f = Kinetic Coefficient of Chain Branching
= Subscript Denoting either Final Value or Formation Value
- g = Kinetic Coefficient of Chain Termination
- H = Enthalpy
- h = Planck Constant
- k = Specific Reaction Rate Constant
- M = Molecular Weight
- N, n = Concentration of Active Centers
- N_o, n_o = Number of Final or Intermediate Products Produced Per Second Per Unit Time
- P = Pressure
= Steric Factor

R	= Gas Constant
S	= Surface Area
T	= Temperature
t	= Time
V	= Volume
x	= Amount of Reactant Depleted
w	= Rate of Reaction
w_{CR}	= Critical Reaction Rate
w_O	= Rate of Initiation Step
y	= Mole Fraction
y_f	= Final Mole Fraction
y_i	= Initial Mole Fraction
y_O	= Mole Fraction of Oxygen

Greek Symbols

α	= Coefficient of Proportionality
β	= Surface/Volume Correction Factor
Δ	= Operator Designating Difference
ν	= Frequency
ρ	= Density
ψ	= Pressure Correction Factor

Mechanism Identification Codes

H	= Mechanism of Hardwicke
HLS	= Mechanism of Hardwicke, Lott, and Sliepcevich
L	= Mechanism of Lott
S	= Mechanism of Semenov

V = Mechanism of Lewis and von Elbe

Y = Mechanism of Yenikolopyan

LITERATURE

1. Accomazzo, M. A., and Nobe, K., I.&E.C. Proc. Des. and Dev., Vol. 4, 425, Oct. (1965).
2. Albright, L. F. and Winter, W. M., I.&E.C. Product Res. and Dev., Vol. 5, No. 3, Sept. (1966).
3. Alyea, N. H. and Frost, A. A., J. Amer. Chem. Soc., 55, 3227 (1933).
4. Amagat, E. H., Comptes Rendus, 100, 633 (1885) and 107, 522 (1888).
5. Bardwell, J. and Hinshelwood, C. N., Proc. Roy. Soc., A205, 375 (1951).
6. Bell, E. R., Raley, J. H., Rust, F. F., Seubold, F. H., and Vaughan, W. E., Discussions Faraday Soc., 10, 242 (1951).
7. Bell, K. M. and Tipper, C. F. H., Proc. Roy. Soc. A238, 258 (1956).
8. Benedict, M., Webb, G. B., and Ruben, L. C., Chem. Eng. Prog., 47, 419 (1951).
9. Blondell, R. V., Cook, W. G. A., Hoare, D. E., and Milne, G. S., Tenth Symposium (Int.) on Combustion, Combustion Institute, Pittsburgh (1965).
10. Bone, W. A. and Allum, R. E., Proc. Roy. Soc. A134, 578 (1932).
11. Bone, W. A., and Gardner, J. B., Proc. Roy. Soc. (London), A154, 297 (1936).
12. Cassano, A. E., Silveston, P. L., and Smith, J. M., I.&E.C., Vol. 59, No. 1, Jan. (1967).
13. Chamberlain, G. H. N., Hoare, D. E., and Walsh, A. D., Discussions Faraday Society, 14, 97 (1966).

14. Deffet, L. and Ficks, F., The Physics and Chemistry of High Pressure, Papers from Symposium June 1962, Soc. of Chem. Industry, London (1963).
15. Egerton, A. C., Minkoff, G. J., and Salooja, K. C., Combustion and Flame, 1, 25 (1957).
16. Fort, R. and Hinshelwood, D. N., Proc. Roy. Soc. A129, 284 (1930).
17. Frank-Kamenetskii, D. A., Diffusion and Heat Exchange in Chemical Kinetics, Trans. by N. Thon, Princeton U. Press, Princeton (1955).
18. Frank-Kamenetskii, D. A., and Salnikov, L. C. R., Zhur. Fiz. Khim., 17, 79 (1943).
19. Furman, M. S., Khimicheskaya Promyshlennost, No's. 1-2, 24 (1946).
20. Furman, M. S., Shestakova, A. D., and Radle-Desyatnik, I. Sh., Trudy GIAP, No. 1, 100 (1953)
21. Furman, M. S. and Tsiklis, D. S., Doklady Akademii Nauk SSSR, 91, 597 (1953).
22. Gaydon, A. G., Moore, N. P. W., and Simonson, J. R., Proc. Roy. Soc., A230, 1 (1955).
23. Gilchrist, A., The Physics and Chemistry of High Pressures, Papers from Symposium June 1962, Soc. of Chem. Industry, London (1962).
24. Handbook of Chemistry and Physics, Weast, R. D., Editor, 45th Ed., Chemical Rubber Co. Publication, Cleveland (1965).
25. Harding, A. J. and Norrish, R. G. W., Proc. Roy. Soc., A212, 291 (1962).
26. Hardwicke, N. L., Ph.D. Dissertation, University of Oklahoma (1965).
27. Hardwicke, N. L., Lott, J. L., and Slipevich, C. M., Mechanism for the High Pressure Oxidation of Methane, in publication.
28. Hoare, D. E. and Walsh, A. D., Fifth Symposium (Int.) on Combustion, Reinhold, New York, 467 (1955).
29. Ingold, K. U., Bryce, W. A., J. Chem. Phys., 24, 360 (1956).

30. Kane, G. P. and Townend, D. T. A., Proc. Roy. Soc., A160, 174 (1937).
31. Karmilova, L. V., Yenikolopyan, N. S. and Nalbandyan, A. B., J. Phys. Chem. (Moscow), 34, 261 (1960).
32. Knox, J. H. and Norrish, R. G. W., Proc. Roy. Soc. (London), A221, 151 (1954).
33. Kovalskii, A. A., Sadovnikov, P. Ya. and Chirkov, N. M., Zh. fiz. khim., 4, 50 (1933).
34. Lewis, B. and von Elbe, G., Combustion Flames and Explosions of Gases, Academic Press, New York (1951).
35. Lott, J. L., Ph.D. Dissertation, University of Oklahoma (1965).
36. Lott, J. L. and Slipevich, C. M., I.&E.C. Proc. Des. and Dev., 6, 67 (1967).
37. Maizus, Z. K. and Emanuel, N. M., Dokl. Akad. Nauk. SSSR, 87, 241, 437, 801 (1952 and 89, 1049 (1953)).
38. McConkey, B. H. and Wilkinson, P. R., I.&E.C. Proc. Des. and Dev., Vol. 6, No. 4, 437 (1967).
39. McEwan, A. C., and Tipper, C. F. H., Proc. Roy. Soc., A220, 266 (1953).
40. Medley, H. D., and Cooley, S. D., Adv. in Petroleum Refining, Vol. 3, 309 (1960).
41. Melvin, A., Combustion and Flame, Vol. 10, No. 2 (1966).
42. Mezaki, R. and Watson, C. C., I.&E.C., Prod. Des. and Dev., Vol. 5, No. 1, 62 Jan. (1966).
43. Minkoff, G. J. and Tipper, C. F. H., Chemistry of Combustion Reactions, Butterworth, London. (1962).
44. Nalbandyan, A. B., Acta. phys. chim. U.R.S.S. 19, (1944) and 20, 31 (1945).
45. Neumann, M. B. and Egerov, L. N., Phys. Z. Soujet, 1, 700, (1932).
46. Newitt, D. M. and Haffner, A. E., Proc. Roy. Soc. (London), A134, 591 (1932).

47. Newitt, D. M. and Szego, P., Proc. Roy. Soc. (London), A147, 555, (1934).
48. Newitt, D. M. and Thornes, L. S., J. Chem. Soc., 1957 (1937).
49. Norrish, R. G. W., Discussions Faraday Soc., 10, 269 (1951).
50. Norrish, R. G. W. and Foord, S. G., Proc. Roy. Soc. (London), A157, 503, (1936).
51. Norrish, R. G. W. and Reagh, J. D., Proc. Roy. Soc., A176, 496 (1940).
52. Norrish, R. G. W. and Wallace, J., Proc. Roy. Soc., A145, 307 (1934).
53. Noyes, W. A., Leighton, P. A., The Photochemistry of Gases, Reinhold, New York (1941).
54. Pease, R. N., J. Am. Chem. Soc., 51, 1839 (1929).
55. Pease, R. N. and Cheesebro, P. R., Proc. Nat. Acad. Sci., 14, 472 (1928).
56. Pryor, W. A., Free Radicals, McGraw Hill, New York (1966).
57. Ridge, M. J., Rev. Pure and Appl. Chem. (Australia), 6, 121 (1956).
58. Robertson, N. C., "The Partial Oxidation of the Simple Paraffinic Hydrocarbons," The Chemistry of Petroleum Hydrocarbons, Vol. 11, 365, Reinhold, New York, New York (1955).
59. Russell, G. A., J. Am. Chem. Soc., 79, 3871. (1957).
60. Rust, F. and others, Ind. Eng. Chem., 41, 2595, 2597, 2604, 2609, 2612 (1949).
61. Salnikov, L. C. R., Acad. Sci. U.R.S.S., 60, 405.
62. Satterfield, C. N. and Reid, R. C., J. Phys. Chem., 59, 283 (1955).
63. Semenov, N. N., Some Problems of Chemical Kinetics and Reactivity, Princeton Univ. Press, London, Translated by M. Boudart (1959).

64. Semenov, N. N., Zh. fiz. khim., 4, 4 (1933).
65. Seshadri, D. N., Viswanath, D. S. and Kuloor, N. R., J. Chem. and Eng. Data, 12, No. 1, 3 (1967).
66. Shtern, V. Ya., The Gas-Phase Oxidation of Hydrocarbons, Pergamon, New York, (1964).
67. Sleppy, W. C. and Calvert, J. G., J. Am. Chem. Soc., 81, 769 (1959).
68. Small, N. J. H. and Ubbelohde, A. R., J. Appl. Chem., 3, 193 (1953).
69. Slipecevich, C. M., Ph.D. Dissertation, University of Michigan (1947).
70. Sutton, F., A Systematic Handbook of Volumetric Analysis, Churchill, London (1935).
71. Vanpee, M., Ann. Min. Belg., 48, 44 (1948).
72. Vedenegev, V. I., et al., Bond Energies, Ionization Potentials and Electron Affinities, St. Martin's Press, New York (1966).
73. von Elbe, G., "Chemical Kinetics of Hydrocarbon Combustion," in Fifth Symposium (Int.) on Combustion, Reinhold, New York (1955).
74. von Elbe, G., Lewis B., and Roth, W., Fifth Symposium (Int.) on Combustion, 610, Reinhold, New York (1955).
75. Walling, C., Free Radicals in Solution, Wiley, New York (1957).
76. Warren, D. R., Proc. Roy. Soc., A211, 22, 245 (1952).
77. Waters, W. A., The Chemistry of Free Radicals, Clarendon Press, Oxford, (1946).
78. Yashikawa, K., Bull. Inst. Phys. Chem. Res. Japan, 10(4), 305, (1931).
79. Yenikolopyan, N. S., Seventh Symposium (Int.) on Combustion, p. 157, Butterworth & Co., London (1959).

80. Yenikolopyan, N. S., Zh. fiz. khim. 33, 642 (1959).
81. Yenikolopyan, N. S., Korolev, G. V., and Savushkina, G. P., Zh. fiz. khim., 31, 865 (1957).

APPENDIX A

EXPERIMENTAL RESULTS

On the following pages, a summary of experimental data is presented. Table A-1 presents test conditions, as well as measured product concentrations. Table A-2 presents product distributions as percentages of reacted methane and oxygen, respectively.

Experimental Test Parameters
and Outlet Product
Compositions

TEST PARAMETERS										OVERALL OUTLET COMPOSITION, MOLE PERCENT													
SUB NO.	PRESSURE AIR, ABS.	TEMP. DEG. C	IGNITION DELAY MIP.	HOLD TIME MIP. (1)	RES. TIME MIP. (2)	LIQUID FUELED GR.	MATERIAL BALANCE GR./GR. (3)	CO/CO2 MOLAR RATIO	HC/CO+CO2 CO2/HC/CO MOLAR RATIO	SUB NO.	C#	O2	N2	CO	C2H6	CO2	H2O	HCOH	H2ON	HTON	HF (1)	FAC (2)	ACAC (3)
4	375.1	Jul.0	188.8	1.5	0.0	2.88	0.92	1.01	3.28	2	84.72	1.08	0.53	1.61	0.05	1.58	9.41	0.03	0.98	0.0	0.0	0.0	0.0
5	463.5	JJJ.0	0.1	1.3	0.0	3.22	0.92	3.22	6.13	3	88.09	1.30	0.48	2.06	0.32	0.82	9.71	0.03	0.57	0.01	0.0	0.0	0.0
6	531.6	298.0	88.8	1.0	0.0	4.09	0.95	1.00	2.50	4	84.62	1.48	0.57	1.35	0.07	1.35	9.17	0.04	1.09	0.0	0.0	0.26	0.0
7	469.1	368.0	1.0	1.6	0.0	3.09	0.93	2.39	1.27	5	83.96	1.10	0.50	2.01	0.13	0.88	8.96	0.03	2.26	0.04	0.0	0.17	0.0
8	381.1	318.0	32.0	1.0	0.0	2.81	0.92	1.12	1.73	6	85.04	1.64	0.50	1.31	0.0	1.17	8.88	0.03	1.88	0.0	0.01	0.0	0.0
9	381.1	318.0	11.0	0.0	0.0	2.59	0.95	1.35	2.89	7	84.58	1.56	0.48	2.54	0.17	1.88	7.24	0.01	1.53	0.01	0.0	0.0	0.0
10	150.6	337.0	3.0	0.3	0.0	1.54	0.95	2.22	1.44	9	85.99	3.30	0.61	1.38	0.0	0.60	7.27	0.04	1.37	0.02	0.0	0.0	0.0
11	150.6	337.0	10.5	0.1	0.0	1.35	0.93	1.95	1.49	10	85.77	3.43	0.62	1.37	0.08	0.70	6.56	0.03	1.41	0.02	0.0	0.0	0.0
12	150.6	337.0	1.0	2.0	0.0	1.48	0.94	2.44	1.25	11	85.48	3.72	0.62	1.36	0.32	0.56	6.32	0.03	1.56	0.02	0.0	0.0	0.0
13	150.6	337.0	32.0	1.2	0.0	1.35	0.97	1.50	3.11	12	85.38	3.05	0.51	1.40	0.0	0.94	8.11	0.04	0.77	0.04	0.0	0.0	0.0
14	168.2	323.0	0.0	0.0	900.0	1.35	0.97	0.82	12.39	14	85.50	3.04	0.40	1.12	0.0	1.38	7.95	0.01	9.20	0.24	0.0	0.0	0.0
15	173.0	337.0	39.0	2.0	0.0	1.44	0.93	1.25	2.43	15	85.96	3.24	0.43	1.15	0.0	0.92	7.03	0.02	0.87	0.21	0.0	0.0	0.0
16	150.6	337.0	57.0	1.0	0.0	0.28	1.01	1.38	128.99	16	87.40	5.46	0.51	2.82	0.08	2.04	1.62	0.0	0.04	0.03	0.0	0.0	0.0
17	137.0	330.0	58.0	8.0	0.0	1.18	0.92	1.49	2.30	17	86.18	3.03	0.43	1.32	0.0	0.80	7.11	0.02	0.94	0.11	0.0	0.0	0.0
18	150.6	337.0	80.0	16.0	0.0	1.32	0.94	1.51	2.87	18	85.57	3.00	0.48	1.29	0.0	0.85	7.78	0.01	0.75	0.12	0.0	0.0	0.0
19	150.6	337.0	38.5	0.0	0.0	1.41	0.97	1.71	8.87	19	85.32	3.29	0.68	1.43	0.0	0.84	8.20	0.02	0.26	0.01	0.0	0.0	0.0
20	150.6	337.5	33.0	2.0	0.0	1.44	0.94	1.59	2.02	20	85.95	3.24	0.62	1.23	0.0	0.77	7.37	0.02	1.00	0.04	0.0	0.0	0.0
21	150.6	337.0	29.0	0.2	0.0	1.45	0.94	1.70	2.08	21	82.35	3.00	3.38	1.30	0.0	0.77	8.18	0.03	1.01	0.04	0.0	0.0	0.0
22	150.6	337.0	11.8	0.2	0.0	1.38	0.94	1.83	1.91	22	85.70	3.01	0.46	1.29	0.0	0.71	7.76	0.04	1.06	0.02	0.0	0.0	0.01
23	137.0	337.0	4.0	0.1	0.0	1.33	0.94	2.00	1.24	23	85.58	2.85	0.53	1.46	0.0	0.73	6.85	0.01	1.77	0.04	0.0	0.24	0.0
24	150.6	337.0	3.0	0.1	0.0	1.21	0.92	1.74	2.51	24	86.89	2.91	0.47	1.81	0.0	0.80	7.50	0.0	0.88	0.01	0.0	0.0	0.0
25	307.1	337.0	57.0	1.0	0.0	1.49	0.98	1.12	5.62	25	87.33	3.17	0.43	1.74	0.0	1.54	5.12	0.01	0.59	0.01	0.0	0.0	0.0
26	415.9	321.0	7.0	0.1	0.0	2.70	0.98	1.37	2.36	26	87.22	3.59	0.43	1.43	0.0	1.85	5.21	0.01	1.04	0.01	0.0	0.01	0.0
27	381.1	320.0	18.0	0.2	0.0	2.58	0.98	1.93	2.40	27	86.94	3.72	0.23	1.29	0.42	0.47	5.49	0.02	0.83	0.0	0.0	0.0	0.0
28	381.1	312.5	36.0	6.0	0.0	2.11	0.99	1.16	4.35	28	87.35	3.77	0.47	1.34	0.0	1.14	5.35	0.01	0.58	0.0	0.0	0.0	0.0
29	375.1	312.5	28.5	0.3	0.0	2.44	0.99	1.09	3.35	29	86.92	3.70	0.44	1.21	0.0	1.11	5.51	0.01	0.70	0.0	0.0	0.0	0.0
30	371.7	310.0	38.0	0.5	0.0	2.45	0.98	1.04	2.33	30	87.27	3.63	0.55	1.31	0.0	1.24	4.89	0.01	1.10	0.0	0.0	0.0	0.0
31	361.3	306.0	53.0	12.0	0.0	2.38	0.98	1.01	5.21	31	87.11	3.59	0.70	1.19	0.0	1.18	5.80	0.01	0.46	0.0	0.0	0.0	0.0
32	371.7	306.0	0.0	0.0	45.0	1.55	0.99	1.23	8.23	32	86.20	5.06	0.61	1.11	0.0	0.90	3.90	0.01	0.25	0.0	0.0	0.0	0.0
33	368.3	306.0	0.0	0.0	38.0	0.99	1.01	3.19	50.37	33	85.54	7.01	0.81	1.48	0.0	0.46	1.06	0.0	0.04	0.0	0.0	0.0	0.0
34	381.1	307.0	0.0	0.0	24.0	1.13	0.98	1.54	8.88	34	85.82	6.42	0.48	0.45	0.0	0.29	2.86	0.02	0.09	0.0	0.0	0.0	0.0
35	381.1	306.0	0.0	0.0	15.4	0.92	0.98	3.01	12.43	35	85.83	6.74	0.40	0.57	0.0	0.43	2.57	0.02	0.13	0.0	0.0	0.0	0.0
36	381.1	312.5	0.0	0.0	18.8	1.00	0.99	2.12	10.41	36	85.21	6.32	0.44	0.90	0.0	0.40	2.40	0.01	0.06	0.0	0.0	0.0	0.0
37	381.1	312.5	0.0	0.0	18.0	1.03	0.99	1.97	4.37	37	84.09	4.92	0.48	1.21	0.0	0.41	2.21	0.02	0.13	0.0	0.0	0.0	0.0
38	381.1	312.0	0.0	0.0	27.0	2.32	0.98	1.52	3.94	38	87.30	3.71	0.54	1.38	0.0	0.91	5.57	0.03	0.59	0.0	0.0	0.0	0.0
39	514.6	302.5	32.0	0.3	0.0	3.09	0.98	1.44	4.32	39	87.32	3.15	0.39	1.44	8.0	1.38	5.63	0.02	0.66	0.0	0.0	0.01	0.01
40	507.8	303.4	0.0	0.0	23.0	2.21	0.99	1.49	3.82	40	86.38	5.19	0.45	0.90	0.0	0.40	4.06	0.02	0.40	0.0	0.0	0.01	0.01
41	489.0	303.4	0.0	0.0	15.0	0.82	1.00	1.38	34.23	41	89.24	4.56	0.45	0.48	0.0	0.35	0.88	0.01	0.02	0.0	0.0	0.01	0.0
42	477.1	299.0	69.5	0.3	0.0	3.75	0.96	1.03	3.47	42	86.74	2.35	0.43	1.24	0.0	1.21	7.26	0.03	0.71	0.0	0.0	0.01	0.02

TABLE A-1 (Continued)

TEST PARAMETERS										OVERALL OUTLET COMPOSITION, MOLE PERCENT													
EXP NO.	WELL NO.	TEMP. DEG. C	IGNITION DELAY MIN.	HOLD TIME MIN. (1)	RES. TIME MIN. (2)	LIQUID TURNED ON.	MATERIAL BALANCE GR./GR. (3)	CO/CO2 MOLAR RATIO	HCOR+CO2/HCOR MOLAR RATIO	EXP NO.	CH4	O2	H2	CO	C2H6	CO2	H2O	HCOR	HCOR	HTOR	HF(1)	FA(2)	ACAC(3)
84	658.0	308.1	59.6	1.2	0.0	3.50	0.98	0.50	7.29	84	84.46	4.04	0.34	0.95	0.0	1.91	7.97	0.02	0.39	0.0	0.0	0.0	0.0
85	671.0	312.0	0.0	0.0	4.0	0.15	1.01	0.0	29.88	85	88.07	10.85	0.34	0.0	0.24	0.16	0.32	0.0	0.01	0.0	0.0	0.0	0.0
86	704.8	315.3	1.6	0.0	0.0	3.42	0.98	10.25	9.81	86	84.19	5.55	0.42	2.46	0.0	0.09	6.66	0.01	0.28	0.0	0.0	0.0	0.0
87	645.5	307.5	0.0	0.0	63.0	0.87	1.02	0.88	149.72	87	87.47	9.79	0.29	0.20	0.0	0.30	2.00	0.0	0.0	0.0	0.0	0.0	0.0
88	644.2	310.0	0.0	0.0	49.5	0.34	1.02	1.03	116.67	88	87.42	9.54	0.44	0.98	0.0	0.95	0.72	0.0	0.02	0.0	0.0	0.0	0.0
89	681.2	311.1	24.0	0.0	0.0	4.06	0.98	0.19	2.04	89	84.78	5.66	0.74	0.20	0.0	1.02	7.02	0.02	0.60	0.01	0.0	0.0	0.0
90	666.8	312.0	36.3	0.0	0.0	2.72	0.98	1.39	5.44	90	84.94	6.12	0.76	1.59	0.0	1.15	4.97	0.02	0.49	0.01	0.0	0.0	0.0
91	667.6	311.5	37.3	0.0	0.0	2.91	1.00	1.48	5.00	91	84.94	6.19	0.51	1.48	0.0	1.00	5.42	0.02	0.50	0.01	0.0	0.0	0.0
92	684.4	310.4	0.0	0.0	21.4	0.08	1.03	1.23	370.97	92	87.41	10.78	0.92	0.44	0.0	0.35	0.16	0.0	0.0	0.0	0.0	0.0	0.0
93	688.7	315.0	8.9	1.4	0.0	2.85	0.98	3.65	6.58	93	83.93	5.37	0.70	2.25	0.0	0.43	6.73	0.02	0.44	0.0	0.0	0.0	0.0
94	666.7	314.4	11.0	0.0	0.0	2.79	0.98	3.28	3.38	94	84.23	5.99	1.02	1.61	0.0	0.49	6.08	0.03	0.44	0.0	0.0	0.0	0.0
95	681.9	315.4	0.0	0.0	8.3	0.12	1.02	1.72	57.87	95	87.46	10.60	0.57	0.46	0.0	0.27	0.28	0.0	0.01	0.0	0.0	0.0	0.0
96	687.0	305.0	77.4	1.3	0.0	3.02	0.98	0.97	6.52	96	84.58	4.88	0.35	1.34	0.0	1.40	7.08	0.02	0.43	0.0	0.0	0.0	0.0
97	504.4	301.0	36.4	1.5	0.0	3.37	0.97	0.93	3.83	97	84.50	5.19	0.87	1.34	0.0	1.43	5.96	0.02	0.73	0.0	0.0	0.0	0.0
98	494.2	305.0	0.0	0.0	36.7	2.59	0.98	1.07	8.09	98	85.00	5.10	0.43	2.20	0.0	2.04	4.71	0.02	0.53	0.0	0.0	0.0	0.0
99	490.8	305.0	0.0	0.0	21.0	0.26	1.02	1.11	IMP.	99	87.51	10.46	0.77	0.38	0.0	0.34	0.60	0.0	0.0	0.0	0.0	0.0	0.0
100	613.2	294.0	0.0	0.0	51.0	0.30	1.00	1.42	74.02	100	88.34	10.07	0.25	0.57	0.0	0.40	0.61	0.0	0.01	0.0	0.0	0.0	0.0
101	626.4	303.0	35.0	0.8	0.0	3.46	0.98	0.89	5.68	101	84.78	5.01	0.42	1.39	0.0	1.55	6.38	0.02	0.52	0.0	0.0	0.0	0.0
102	718.4	305.0	15.5	0.0	0.0	3.88	0.97	2.04	4.15	102	83.73	4.78	0.84	2.40	0.10	1.17	4.08	0.02	0.67	0.0	0.0	0.0	0.0
103	752.7	307.5	11.3	2.7	0.0	4.55	0.94	2.00	3.33	103	83.97	4.09	0.43	2.44	0.05	1.22	6.73	0.02	1.04	0.0	0.0	0.0	0.0
105	648.7	314.2	67.0	7.0	0.0	1.48	1.01	0.69	7.86	105	85.59	4.04	1.00	0.31	0.0	0.46	3.54	0.01	0.10	0.0	0.0	0.0	0.0
106	443.1	315.4	60.5	0.5	0.0	1.09	1.00	0.94	17.41	106	85.95	4.49	1.15	0.44	0.0	0.35	3.47	0.01	0.07	0.0	0.0	0.0	0.0
107	641.9	320.0	45.8	1.4	0.0	1.11	0.99	1.01	9.48	107	84.34	4.54	1.14	0.35	0.0	0.35	3.47	0.01	0.07	0.0	0.0	0.0	0.0
108	454.7	321.5	27.6	0.2	0.0	1.61	0.99	1.14	20.47	108	84.21	7.80	0.48	0.50	0.0	0.44	4.59	0.01	0.05	0.0	0.0	0.0	0.0
109	385.3	320.0	0.0	0.0	39.0	0.97	1.00	1.08	7.32	109	84.82	4.97	0.57	0.32	0.0	0.29	3.00	0.01	0.08	0.0	0.0	0.0	0.0
110	392.1	320.0	0.0	0.0	24.0	0.94	1.00	0.0	IMP.	110	84.82	4.94	0.82	0.0	0.0	0.46	2.83	0.01	0.0	0.0	0.0	0.0	0.0
111	474.5	322.5	0.0	0.0	18.0	1.08	1.00	1.00	IMP.	111	87.29	4.73	0.18	0.40	0.0	0.39	3.07	0.0	0.0	0.0	0.0	0.0	0.0
112	370.0	350.3	14.3	0.3	0.0	1.29	0.99	1.34	24.44	112	85.72	4.06	1.18	0.50	0.0	0.37	4.20	0.01	0.04	0.0	0.0	0.0	0.0
113	484.0	324.0	4.4	0.2	0.0	2.93	0.98	1.94	3.83	113	85.22	5.67	0.02	1.20	0.0	0.61	4.44	0.03	0.48	0.0	0.0	0.0	0.0
114	347.9	313.0	0.0	0.0	152.0	0.88	1.00	0.0	10.75	114	86.04	4.92	1.29	0.0	0.0	0.44	3.30	0.0	0.04	0.0	0.0	0.0	0.0
115	341.1	321.5	0.0	0.0	114.6	0.92	0.99	0.0	IMP.	115	84.04	4.69	1.44	0.0	0.0	0.55	3.31	0.0	0.0	0.0	0.0	0.0	0.0
116	395.5	330.0	5.5	0.0	0.0	3.36	0.97	2.09	7.28	116	83.75	5.24	1.26	1.44	0.0	0.79	7.02	0.01	0.34	0.01	0.0	0.0	0.0
117	385.3	325.0	52.5	1.8	0.0	2.44	0.99	0.31	6.09	117	84.47	4.07	1.30	0.38	0.0	1.20	6.34	0.01	0.24	0.0	0.0	0.0	0.0
118	381.9	325.0	0.0	0.0	19.4	1.11	0.99	0.0	4.90	118	84.38	4.83	1.22	0.0	0.0	0.0	1.61	0.0	0.0	0.0	0.0	0.0	0.0
119	392.1	325.0	0.0	0.0	10.0	0.57	1.00	IMP.	IMP.	119	84.66	10.26	1.55	0.0	0.0	0.0	1.61	0.0	0.0	0.0	0.0	0.0	0.0
120	385.3	330.0	0.0	0.0	4.0	0.80	0.99	IMP.	IMP.	120	84.79	4.74	1.35	0.0	0.0	0.0	1.61	0.0	0.0	0.0	0.0	0.0	0.0
121	447.4	325.0	27.6	0.5	0.0	3.81	0.97	0.89	4.42	121	83.56	4.34	1.12	1.19	0.0	1.33	7.94	0.01	0.57	0.0	0.0	0.0	0.0
122	488.0	325.2	0.0	0.0	24.0	1.44	1.00	0.29	10.07	122	85.84	7.95	1.18	0.37	0.0	1.24	3.20	0.01	0.16	0.0	0.0	0.0	0.0
123	432.9	332.5	9.6	0.0	0.0	3.20	0.96	1.78	3.97	123	83.94	5.30	1.16	1.27	0.0	0.72	7.11	0.02	0.51	0.0	0.0	0.0	0.0
124	381.9	331.5	19.0	7.0	0.0	3.33	0.97	0.68	4.41	124	83.46	4.23	1.08	0.94	0.0	1.39	6.43	0.01	0.53	0.0	0.0	0.0	0.0

TABLE A-2

Yield of Products as Percentages
of Reacted Methane and Oxygen

YIELD AS PERCENT OF REACTED METHANE										YIELD AS PERCENT OF REACTED OXYGEN									
SUM COMB. NO.	CH4 PERCENT	HCOH	MEOH	ETOH	HF(1)	FAC(2)	ACAC(3)	CO	CO2	SUM COMB. NO. PERCENT	H2O	HCOH	MEOH	ETOH	HF(1)	FAC(2)	ACAC(3)	CO	CO2
1	4.05	0.78	23.39	0.0	0.0	0.0	0.0	38.19	37.64	2	88.52	0.06	1.66	0.0	0.0	0.0	0.0	2.71	5.33
2	4.23	0.81	13.97	0.39	0.0	0.0	0.0	64.74	20.09	3	86.11	0.11	1.96	0.03	0.0	0.0	0.0	9.08	5.68
3	4.25	0.98	26.61	0.21	0.24	6.32	0.0	32.82	32.02	4	84.32	0.10	2.73	0.01	0.02	1.30	0.0	3.37	6.74
4	5.21	0.57	41.99	1.42	0.0	3.18	0.0	37.26	15.58	5	88.30	0.10	7.30	0.12	0.0	1.10	0.0	6.88	5.83
5	3.72	0.77	36.87	0.17	0.40	0.0	0.0	32.85	29.33	6	82.54	0.06	3.00	0.01	0.03	0.0	0.0	2.70	4.83
6	6.00	0.20	25.61	0.34	0.0	0.0	0.0	42.39	31.46	7	83.71	0.02	2.97	0.02	0.0	0.0	0.0	4.92	7.29
7	3.64	1.12	40.57	0.97	0.0	0.0	0.0	39.58	17.79	8	65.06	0.08	3.06	0.04	0.0	0.0	0.0	2.99	2.67
8	3.60	0.86	39.74	0.94	0.0	0.0	0.0	38.65	19.80	9	63.77	0.05	2.68	0.03	0.0	0.0	0.0	2.61	2.67
9	3.50	0.94	43.81	1.37	0.0	0.0	0.0	38.22	15.66	10	63.77	0.08	1.97	0.06	0.0	0.0	0.0	3.47	2.84
10	3.90	1.16	23.47	3.61	0.0	0.0	0.0	43.05	28.70	11	60.72	0.08	1.97	0.06	0.0	0.0	0.0	3.47	2.84
11	3.59	0.69	34.47	5.84	0.0	0.0	0.0	36.67	24.34	12	67.61	0.05	2.00	0.18	0.0	0.0	0.0	1.79	3.38
12	3.64	0.24	6.32	15.39	0.0	0.0	0.0	35.21	42.84	13	64.15	0.01	2.00	0.18	0.0	0.0	0.0	2.26	3.00
13	3.30	0.64	25.56	12.39	0.0	0.0	0.0	38.12	27.89	14	67.83	0.01	0.19	0.23	0.0	0.0	0.0	1.05	2.56
14	4.97	0.08	0.76	1.38	0.0	0.0	0.0	56.88	41.10	15	63.52	0.03	1.30	0.03	0.0	0.0	0.0	1.74	2.78
15	4.69	0.63	24.31	6.54	0.0	0.0	0.0	38.65	25.88	16	44.04	0.0	0.03	0.03	0.0	0.0	0.0	2.57	3.71
16	3.38	0.43	23.81	7.77	0.0	0.0	0.0	40.94	27.05	17	67.84	0.02	1.26	0.15	0.0	0.0	0.0	1.72	2.30
17	3.38	0.63	18.09	0.45	0.0	0.0	0.0	56.05	32.77	18	68.15	0.02	1.02	0.17	0.0	0.0	0.0	1.75	2.31
18	4.84	0.74	32.29	2.47	0.0	0.0	0.0	39.64	24.86	19	64.55	0.04	0.34	0.01	0.0	0.0	0.0	1.89	2.21
19	4.84	0.74	32.29	2.47	0.0	0.0	0.0	39.64	24.86	20	65.53	0.04	1.62	0.06	0.0	0.0	0.0	1.99	2.50
20	4.84	0.74	32.29	2.47	0.0	0.0	0.0	39.64	24.86	21	66.77	0.04	1.56	0.07	0.0	0.0	0.0	2.02	2.38
21	4.38	1.21	33.77	1.21	0.0	0.0	0.40	41.03	22.38	22	67.98	0.06	1.74	0.03	0.0	0.02	0.0	2.12	2.31
22	4.10	0.15	41.77	1.97	0.0	5.65	0.0	38.04	17.02	23	69.99	0.01	3.23	0.08	0.0	0.89	0.0	2.67	2.67
23	2.41	0.10	28.35	0.36	0.0	0.0	0.0	45.44	25.75	24	69.00	0.0	1.19	0.01	0.0	0.0	0.0	1.91	2.17
24	3.43	0.34	15.01	0.57	0.0	0.0	0.0	44.37	19.71	25	62.71	0.03	1.12	0.02	0.0	0.0	0.0	3.31	5.93
25	3.43	0.40	29.52	0.66	0.0	0.19	0.0	40.03	29.20	26	57.57	0.04	3.26	0.04	0.0	0.04	0.0	4.41	6.44
26	3.22	0.69	29.38	0.24	0.0	0.07	0.0	45.86	23.79	27	55.89	0.07	2.95	0.01	0.0	0.21	0.0	4.61	4.78
27	3.18	0.43	18.65	0.26	0.0	0.0	0.0	43.28	37.38	28	55.40	0.03	1.88	0.01	0.0	0.0	0.0	2.97	5.13
28	3.78	0.49	22.94	0.24	0.0	0.08	0.0	39.80	36.45	29	56.30	0.04	1.72	0.01	0.0	0.01	0.0	2.98	5.13
29	3.70	0.46	23.94	0.46	0.0	0.0	0.0	41.91	41.15	30	57.34	0.02	2.80	0.01	0.0	0.0	0.0	2.31	6.38
30	3.26	0.55	10.83	0.11	0.0	0.0	0.0	48.74	39.72	31	57.24	0.03	1.90	0.0	0.0	0.0	0.0	2.60	5.15
31	2.42	0.55	10.83	0.11	0.0	0.0	0.0	48.74	39.72	32	40.37	0.03	0.36	0.0	0.0	0.0	0.0	2.54	4.48
32	1.59	1.94	10.13	0.0	0.0	0.0	0.0	42.51	23.36	33	17.83	0.01	0.14	0.0	0.0	0.0	0.0	5.49	3.48
33	0.54	1.94	10.13	0.0	0.0	0.0	0.0	52.33	34.57	34	20.12	0.01	0.45	0.0	0.0	0.0	0.0	1.29	1.68
34	1.20	1.83	4.27	0.0	0.0	0.0	0.0	66.68	22.80	35	20.12	0.05	0.26	0.0	0.0	0.0	0.0	2.42	1.61
35	1.20	1.83	4.27	0.0	0.0	0.0	0.0	66.68	22.80	36	25.38	0.07	0.41	0.0	0.0	0.0	0.0	2.88	2.72
36	1.24	1.22	18.40	0.0	0.0	2.30	0.0	51.95	26.33	37	41.84	0.10	1.43	0.0	0.0	0.36	0.0	4.07	4.13
37	4.27	0.98	20.22	0.0	0.0	0.14	0.0	47.42	31.24	38	56.05	0.06	1.63	0.0	0.0	0.02	0.0	3.62	5.03
38	3.15	0.61	18.55	0.12	0.26	0.31	0.63	40.52	38.99	39	62.00	0.08	1.81	0.01	0.03	0.06	0.06	3.85	7.61
39	1.83	1.22	20.44	0.0	0.0	0.73	0.77	45.95	30.89	40	38.56	0.09	1.87	0.0	0.0	0.11	0.04	3.31	4.45
40	2.47	0.78	4.78	0.0	0.0	1.50	0.56	54.80	39.57	41	0.27	0.02	0.07	0.0	0.0	0.08	0.01	1.39	2.01
41	2.90	0.60	22.11	0.02	0.0	0.16	0.93	38.49	37.50	42	71.95	0.07	2.01	0.0	0.0	0.03	0.08	3.50	6.81

TABLE A-2 (Continued)

RUN NO.	CONV. PERCENT	YIELD AS PERCENT OF REACTED ETHANE										CONV. PERCENT	YIELD AS PERCENT OF REACTED OXYGEN									
		HCOH	MEOH	ETOH	MP(1)	PAC(1)	PAC(2)	ACAC(3)	CO	CO2	H2O		ACOH	MEOH	ETOH	MP(1)	PAC(1)	PAC(2)	ACAC(3)	CO	CO2	
44	1.03	0.74	3.69	0.0	0.0	0.0	0.0	0.39	57.46	37.73	44	10.33	96.16	0.02	0.10	0.0	0.0	0.0	0.0	0.0	1.60	2.10
45	1.28	0.80	2.91	0.0	0.0	0.0	0.0	0.36	58.11	37.22	45	12.67	95.13	0.02	0.10	0.0	0.0	0.0	0.0	0.0	2.05	2.33
46	1.57	1.52	14.53	0.0	0.0	0.0	0.0	0.0	46.60	37.15	46	58.70	97.22	0.10	0.32	0.0	0.0	0.0	0.0	0.0	2.98	4.18
47	0.10	4.69	15.12	0.0	0.0	0.0	0.0	2.82	48.38	28.68	47	19.14	97.16	0.10	0.32	0.0	0.0	0.0	0.0	0.0	1.07	1.09
48	1.52	0.61	22.72	0.12	0.0	0.0	0.19	0.75	38.38	41.20	48	59.45	90.57	0.08	1.52	0.0	0.0	0.02	0.05	0.08	2.20	5.16
49	2.18	1.01	29.07	0.16	0.0	0.0	0.35	0.99	34.08	38.08	49	59.51	89.34	0.08	2.50	0.01	0.0	0.02	0.08	0.08	2.70	5.46
50	2.11	0.92	24.27	0.21	0.0	0.0	0.19	1.26	33.86	38.19	50	57.59	91.35	0.06	1.31	0.01	0.0	0.02	0.08	0.08	4.07	4.07
51	0.14	2.00	10.83	0.0	0.0	0.0	0.19	1.11	11.68	18.08	51	6.88	95.73	0.09	2.12	0.0	0.0	0.24	0.03	0.09	2.10	5.40
52	2.14	1.12	25.30	0.0	0.0	0.0	0.25	0.93	32.41	32.41	52	56.36	88.40	0.09	2.12	0.0	0.0	0.99	0.09	0.09	2.82	5.43
53	2.10	1.40	4.53	0.0	0.0	0.0	0.23	0.57	55.08	38.20	53	0.0	98.37	0.02	0.05	0.0	0.0	0.01	0.01	0.01	0.65	0.90
54	0.0	0.45	0.0	0.0	0.0	0.0	0.0	0.0	0.0	99.55	54	1.66	98.83	0.0	0.0	0.0	0.0	0.0	0.0	0.0	0.0	0.17
55	1.33	1.37	21.16	0.52	0.0	0.0	0.21	0.79	49.16	26.39	55	28.01	98.78	0.06	0.89	0.01	0.0	0.02	0.03	0.03	2.06	2.20
56	0.0	0.54	5.85	1.10	0.0	0.0	0.0	0.0	49.20	42.42	56	5.38	99.04	0.0	0.04	0.0	0.01	0.0	0.0	0.0	0.33	0.58
57	1.18	0.56	8.90	0.22	0.0	0.0	0.0	0.0	47.81	42.51	57	7.31	98.78	0.0	0.08	0.0	0.0	0.0	0.0	0.0	0.41	0.73
58	1.46	0.10	0.75	0.0	0.0	0.0	0.0	0.0	35.15	64.00	58	6.44	98.61	0.0	0.01	0.0	0.0	0.0	0.0	0.0	0.25	0.93
59	1.37	0.0	0.03	0.0	0.0	0.0	0.0	0.0	51.57	48.39	59	0.66	98.94	0.0	0.0	0.0	0.0	0.0	0.0	0.0	0.37	0.68
60	1.08	0.47	6.70	0.19	0.0	0.0	0.73	43.83	48.08	33.25	60	6.31	98.57	0.01	0.06	0.0	0.0	0.0	0.01	0.01	0.42	0.93
61	1.30	0.62	4.49	0.0	0.0	0.0	0.61	56.26	36.02	61	7.35	97.88	0.01	0.07	0.0	0.0	0.0	0.0	0.01	0.01	0.82	1.11
62	0.56	1.56	11.18	1.57	0.0	0.0	1.21	51.28	33.25	62	8.82	98.43	0.02	0.13	0.01	0.0	0.0	0.0	0.01	0.01	0.61	0.79
63	1.14	0.46	4.28	0.0	0.0	0.0	0.49	48.19	50.59	63	8.82	98.43	0.0	0.05	0.0	0.0	0.0	0.0	0.01	0.01	0.61	0.79
64	1.17	0.63	1.73	0.0	0.0	0.0	0.22	48.67	52.75	64	3.52	98.80	0.0	0.01	0.0	0.0	0.0	0.0	0.01	0.01	0.35	1.08
65	1.06	0.94	14.92	0.18	0.0	0.0	0.0	0.0	45.97	38.80	65	21.98	98.80	0.01	0.28	0.0	0.0	0.0	0.0	0.0	0.87	1.08
66	2.01	0.71	13.98	1.62	0.0	0.0	0.76	40.12	42.82	66	33.82	97.78	0.03	0.52	0.04	0.0	0.0	0.0	0.03	0.03	0.87	1.08
67	1.87	1.02	13.04	0.21	0.0	0.0	1.29	41.20	41.20	67	27.43	93.78	0.02	0.36	0.0	0.0	0.0	0.0	0.03	0.03	1.77	3.77
68	2.68	1.20	17.16	0.0	0.0	0.0	0.0	0.0	36.74	48.90	68	50.19	93.14	0.04	0.79	0.0	0.0	0.0	0.0	0.0	1.19	2.35
69	3.68	1.03	19.59	0.56	0.0	0.0	0.87	67.79	17.07	69	43.70	87.14	0.02	0.34	0.0	0.0	0.0	0.0	0.0	0.0	1.69	4.13
70	2.90	1.05	27.21	0.58	0.0	0.0	0.0	47.80	22.25	70	43.88	89.20	0.09	2.41	0.04	0.0	0.0	0.0	0.10	0.10	6.23	3.76
71	2.73	0.69	17.20	0.23	0.0	0.0	1.10	40.58	41.25	71	48.35	93.72	0.03	0.77	0.01	0.0	0.0	0.0	0.0	0.0	4.23	3.94
72	2.12	0.80	16.22	0.43	0.0	0.0	0.64	41.00	41.11	72	46.32	93.72	0.03	0.67	0.01	0.0	0.0	0.03	0.03	1.80	3.67	
73	2.73	0.99	13.23	1.28	0.0	0.0	0.80	36.94	46.75	73	42.89	95.31	0.03	0.67	0.02	0.0	0.0	0.03	0.03	1.70	3.60	
74	1.78	0.93	4.25	0.0	0.0	0.0	0.67	49.64	46.50	74	33.77	97.60	0.01	0.46	0.0	0.0	0.0	0.01	0.01	0.74	1.34	
75	2.84	0.29	4.91	0.0	0.0	0.0	0.0	38.81	56.02	75	23.62	95.07	0.01	0.16	0.0	0.0	0.0	0.0	0.0	0.0	1.23	3.84
76	2.31	0.81	13.54	0.0	0.0	0.0	0.0	46.74	46.74	76	49.19	97.88	0.03	0.56	0.0	0.0	0.0	0.0	0.0	0.0	0.62	3.50
77	0.87	1.43	5.31	0.0	0.0	0.0	0.0	52.39	28.47	77	16.10	97.57	0.03	1.62	0.0	0.0	0.0	0.0	0.0	0.0	1.91	3.50
78	1.62	1.24	22.21	0.30	0.0	0.0	0.65	50.95	24.42	78	42.81	98.52	0.08	1.62	0.02	0.0	0.0	0.05	0.05	1.73	3.77	
79	1.19	0.75	12.33	0.0	0.0	0.0	0.0	42.78	48.19	79	42.81	98.52	0.03	0.03	0.0	0.0	0.0	0.0	0.0	0.0	1.52	3.77
80	0.36	0.65	2.56	0.0	0.0	0.0	0.0	48.11	52.68	80	18.72	98.02	0.01	0.05	0.0	0.0	0.0	0.0	0.0	0.0	4.80	2.16
81	2.12	0.85	2.88	1.18	0.0	0.0	1.18	53.73	32.61	81	47.82	88.48	0.03	0.46	0.05	0.0	0.0	0.0	0.11	0.11	8.00	2.66
82	0.22	11.92	18.79	0.0	0.0	0.0	0.0	37.17	79.79	82	52.10	97.79	0.02	0.0	0.0	0.0	0.0	0.0	0.0	0.0	4.80	2.66
83	0.46	0.71	18.79	0.0	0.0	0.0	0.0	39.13	48.43	83	28.86	95.79	0.02	0.83	0.0	0.0	0.0	0.0	0.0	0.0	1.16	2.59

TABLE A-2 (continued)

YIELD AS PERCENT OF REACTED METHANE													YIELD AS PERCENT OF REACTED OXYGEN												
SUB COMB. NO.	COMB. PERCENT	HCOH	HCHO	FTHO	HF(1)	FAC(2)	ACAC(3)	CO	CO2	H2O	HCOH	HCHO	FTHO	HF(1)	FAC(2)	ACAC(3)	CO	CO2							
																			CO	CO2					
84	2.611	0.51	12.07	0.0	0.0	0.0	0.0	29.03	58.39	91.00	0.03	0.69	0.0	0.0	0.0	0.0	1.65	6.64							
85	0.134	0.39	3.22	0.0	0.0	0.0	0.49	0.0	95.90	94.59	0.0	0.01	0.0	0.0	0.0	0.0	0.0	0.80							
86	4.61	0.34	9.25	0.0	0.0	0.0	0.0	87.51	2.89	47.81	0.19	5.23	0.0	0.0	0.0	0.0	49.49	3.27							
87	0.84	0.83	0.66	0.0	0.0	0.0	0.0	39.16	59.35	98.38	0.01	0.01	0.0	0.0	0.0	0.0	0.40	1.21							
88	1.35	0.09	0.85	0.0	0.0	0.0	0.0	50.28	48.78	13.00	0.0	0.04	0.0	0.0	0.0	0.0	2.32	4.50							
89	4.36	1.38	32.58	0.06	0.0	0.0	0.0	10.56	54.82	47.06	0.05	1.42	0.02	0.0	0.0	0.0	0.46	4.78							
90	4.19	0.75	14.99	0.39	0.0	0.0	0.0	48.74	35.12	90	0.0	1.56	0.02	0.0	0.0	0.0	5.00	6.20							
91	3.05	0.62	16.59	0.49	0.0	0.0	0.0	49.10	33.20	91	0.0	1.44	0.02	0.0	0.0	0.0	4.90	6.63							
92	1.51	0.05	13.17	0.14	0.0	0.0	0.0	55.04	44.63	92	0.0	0.01	0.0	0.0	0.0	0.0	1.23	1.99							
93	3.62	0.55	13.17	0.14	0.0	0.0	0.0	67.62	18.52	93	0.0	2.03	0.01	0.0	0.0	0.0	10.44	5.72							
94	3.54	0.11	11.70	0.01	0.0	0.0	0.0	57.95	17.69	94	0.0	0.04	0.0	0.0	0.0	0.0	8.95	1.50							
95	0.58	0.30	12.31	0.0	0.0	0.0	0.0	42.32	43.38	95	0.0	0.04	0.0	0.0	0.0	0.0	1.29	1.50							
96	2.91	0.48	20.70	0.0	0.0	0.0	0.0	38.44	40.39	96	0.0	0.93	0.0	0.0	0.0	0.0	2.97	6.14							
97	4.00	0.35	11.00	0.0	0.0	0.0	0.0	45.78	42.97	97	0.0	1.30	0.0	0.0	0.0	0.0	3.41	10.13							
98	1.32	0.18	1.33	0.0	0.0	0.0	0.0	52.50	47.36	98	0.0	0.0	0.0	0.0	0.0	0.0	5.41	1.70							
99	0.15	0.51	14.97	0.16	0.0	0.0	0.0	39.91	44.52	99	0.0	0.04	0.0	0.0	0.0	0.0	1.74	2.45							
100	4.03	0.56	19.37	0.16	0.0	0.0	0.0	53.66	26.25	100	0.0	1.33	0.0	0.0	0.0	0.0	0.94	7.93							
101	4.70	0.43	22.05	0.12	0.0	0.0	0.0	35.59	25.81	101	0.0	3.55	0.0	0.0	0.0	0.0	3.58	9.63							
102	1.44	1.24	11.29	0.0	0.0	0.0	0.0	35.60	51.87	102	0.02	4.43	0.01	0.0	0.0	0.0	10.36	10.36							
103	4.41	0.74	5.43	0.0	0.0	0.0	0.0	46.01	47.78	103	0.01	0.09	0.0	0.0	0.0	0.0	0.51	1.50							
104	1.22	1.41	9.54	0.0	0.0	0.0	0.0	44.94	44.69	104	0.0	0.14	0.0	0.0	0.0	0.0	0.74	1.58							
105	4.54	1.16	4.66	0.0	0.0	0.0	0.0	50.51	43.68	105	0.02	0.10	0.0	0.0	0.0	0.0	1.06	1.30							
106	0.54	0.89	1.00	12.02	0.0	0.0	0.0	45.25	90.30	106	0.01	0.17	0.0	0.0	0.0	0.0	0.64	1.44							
107	0.69	0.63	0.0	0.0	0.0	0.0	0.0	49.72	49.66	107	0.0	0.0	0.0	0.0	0.0	0.0	0.0	1.17							
108	0.60	0.42	0.0	0.0	0.0	0.0	0.0	58.88	28.44	108	0.0	0.0	0.0	0.0	0.0	0.0	0.0	1.51							
109	4.04	0.58	14.11	0.0	0.0	0.0	0.0	20.28	65.03	109	0.05	1.26	0.0	0.0	0.0	0.0	0.99	1.48							
110	4.04	0.58	14.11	0.0	0.0	0.0	0.0	81.55	0.0	110	0.02	0.38	0.0	0.0	0.0	0.0	0.55	3.53							
111	1.61	2.9	70.84	0.0	0.0	0.0	0.0	0.0	0.0	111	0.0	70.84	0.0	0.0	0.0	0.0	0.0	0.65	0.65						
112	1.33	0.0	0.0	0.0	0.0	0.0	0.0	0.0	0.0	112	0.0	0.0	0.0	0.0	0.0	0.0	0.0	0.0	0.0						
113	4.08	0.41	18.45	0.0	0.0	0.0	0.0	38.31	42.48	113	0.03	1.40	0.0	0.0	0.0	0.0	2.91	6.50							
114	2.99	0.41	18.45	0.0	0.0	0.0	0.0	20.37	28.08	114	0.08	1.24	0.0	0.0	0.0	0.0	0.57	3.91							
121	3.44	0.90	20.33	0.0	0.0	0.0	0.0	50.32	28.56	121	0.0	1.74	0.0	0.0	0.0	0.0	4.34	4.95							
122	3.58	0.44	14.50	0.0	0.0	0.0	0.0	32.70	48.36	122	0.02	0.99	0.0	0.0	0.0	0.0	1.76	5.20							

TABLE A-2 (Continued)

NUM CONV. NO.	CHN PERCENT	HCOH	HCHO	ETOH	ME(1)	FAC(2)	ACAC(3)	CO	CO2	NUM CONV. NO.	O2 PERCENT	H2O	HCOH	HCHO	H2O	ME(1)	FAC(2)	ACAC(3)	CO	CO2	YIELD AS PERCENT OF REACTED METHANE										YIELD AS PERCENT OF REACTED OXYGEN									
																					HCOH	HCHO	ETOH	ME(1)	FAC(2)	ACAC(3)	CO	CO2	HCOH	HCHO	H2O	ME(1)	FAC(2)	ACAC(3)	CO	CO2	HCOH	HCHO	H2O	ME(1)
125	4.30	0.95	21.14	0.0	0.0	0.0	0.0	48.78	33.13	125	50.65	90.50	0.07	1.51	0.0	0.0	0.0	0.0	4.0	3.19	4.73																			
126	3.49	0.62	30.56	0.0	0.0	0.0	0.0	63.83	4.79	126	53.58	57.46	0.33	12.41	0.0	0.0	0.0	0.0	0.0	25.91	3.89																			
127	3.51	1.32	25.11	0.0	0.0	0.0	0.0	44.40	29.17	127	53.27	89.28	0.11	2.09	0.0	0.0	0.0	0.0	0.0	3.70	8.86																			
128	1.58	1.29	34.19	0.0	0.0	0.0	0.0	36.67	27.84	128	26.17	94.68	0.05	1.43	0.0	0.0	0.0	0.0	0.0	1.58	2.33																			
129	0.0	37.51	62.49	0.0	0.0	0.0	0.0	0.0	0.0	129	16.66	0.0	37.51	62.49	0.0	0.0	0.0	0.0	0.0	0.0	0.0																			
130	1.55	0.70	16.40	0.0	0.0	0.0	0.0	71.74	11.16	130	59.65	76.11	0.15	3.52	0.0	0.0	0.0	0.0	0.0	0.0	0.0																			
131	1.41	1.10	18.80	0.0	0.0	0.0	0.0	33.20	46.90	131	61.76	91.68	0.05	0.81	0.0	0.0	0.0	0.0	0.0	15.42	4.80																			
132	0.92	1.46	49.08	0.0	0.0	0.0	0.0	49.45	0.0	132	62.45	0.0	0.0	49.08	0.0	0.0	0.0	0.0	0.0	4.43	4.04																			
133	0.28	1.86	21.24	0.0	0.0	0.0	0.0	32.01	44.88	133	56.13	92.13	0.09	1.01	0.0	0.0	0.0	0.0	0.0	4.52	0.0																			
134	0.0	99.99	0.0	0.0	0.0	0.0	0.0	0.0	0.0	134	10.89	0.0	99.99	0.0	0.0	0.0	0.0	0.0	0.0	0.0	0.0																			
135	0.0	1.36	12.12	0.0	0.0	0.0	0.0	26.82	58.11	135	31.42	98.24	0.02	0.15	0.0	0.0	0.0	0.0	0.0	0.0	0.0																			
136	4.47	0.91	18.54	0.0	0.0	0.0	0.0	61.09	19.47	136	61.19	82.20	0.18	2.76	0.0	0.0	0.0	0.0	0.0	9.30	1.30																			
137	1.27	1.59	28.29	0.0	0.0	0.0	0.0	37.37	32.75	137	55.91	90.97	0.11	1.92	0.0	0.0	0.0	0.0	0.0	2.58	4.46																			
138	0.55	4.78	44.63	0.0	0.0	0.0	0.0	38.30	34.28	138	34.14	96.14	0.08	0.71	0.0	0.0	0.0	0.0	0.0	1.10	1.97																			
139	0.0	0.89	32.65	0.0	0.0	0.0	0.0	58.46	0.0	139	18.35	0.0	8.49	32.65	0.0	0.0	0.0	0.0	0.0	58.46	0.0																			
140	1.55	1.62	40.07	0.0	0.0	0.0	0.0	49.36	28.95	140	54.05	90.59	0.12	1.46	0.0	0.0	0.0	0.0	0.0	3.60	4.23																			
141	1.04	3.13	3.81	0.0	0.0	0.0	0.0	44.78	48.29	141	44.57	98.37	0.03	0.08	0.0	0.0	0.0	0.0	0.0	0.49	1.06																			
142	0.45	1.36	12.72	0.0	0.0	0.0	0.0	42.00	43.92	142	23.38	99.43	0.01	0.05	0.0	0.0	0.0	0.0	0.0	0.17	0.35																			
143	0.0	2.88	0.0	0.0	0.0	0.0	0.0	0.0	97.12	143	8.67	99.94	0.0	0.0	0.0	0.0	0.0	0.0	0.0	0.17	0.06																			
144	1.43	1.51	33.74	0.0	0.0	0.0	0.0	42.76	22.00	144	43.03	95.51	0.06	1.24	0.0	0.0	0.0	0.0	0.0	1.37	1.62																			
145	1.18	1.69	34.59	0.0	0.0	0.0	0.0	41.08	22.68	145	43.05	95.78	0.06	1.19	0.0	0.0	0.0	0.0	0.0	1.41	1.56																			
146	4.74	0.57	30.74	0.0	0.0	0.0	0.0	52.08	36.61	146	43.32	94.90	0.02	0.40	0.0	0.0	0.0	0.0	0.0	1.94	2.73																			
147	1.33	1.01	21.62	0.0	0.0	0.0	0.0	38.75	20.62	147	53.94	96.06	0.01	0.61	0.0	0.0	0.0	0.0	0.0	1.10	1.88																			
148	2.77	0.48	5.51	0.0	0.0	0.0	0.0	42.01	37.51	148	32.71	97.19	0.03	0.10	0.0	0.0	0.0	0.0	0.0	0.82	1.88																			
149	4.47	1.01	14.75	0.0	0.0	0.0	0.0	46.50	30.19	149	54.45	92.16	0.06	0.84	0.0	0.0	0.0	0.0	0.0	2.66	4.28																			
150	1.09	0.96	12.76	0.0	0.0	0.0	0.0	59.74	31.54	150	32.85	94.58	0.08	0.32	0.0	0.0	0.0	0.0	0.0	2.66	2.60																			
151	1.58	0.83	12.57	0.0	0.0	0.0	0.0	41.88	42.92	151	59.18	92.68	0.03	0.62	0.0	0.0	0.0	0.0	0.0	2.06	4.41																			
152	4.44	5.49	12.16	0.0	0.0	0.0	0.0	39.64	42.42	152	54.54	94.43	0.02	0.93	0.0	0.0	0.0	0.0	0.0	2.06	4.41																			
153	0.51	0.46	1.49	0.0	0.0	0.0	0.0	52.22	45.83	153	24.45	96.69	0.01	0.23	0.0	0.0	0.0	0.0	0.0	1.19	2.08																			
154	1.34	0.64	5.03	0.0	0.0	0.0	0.0	37.79	43.07	154	38.75	93.96	0.03	0.03	0.0	0.0	0.0	0.0	0.0	2.16	3.68																			
155	4.31	0.79	19.85	0.0	0.0	0.0	0.0	37.79	41.47	155	59.66	90.87	0.06	1.48	0.0	0.0	0.0	0.0	0.0	2.81	6.18																			
156	1.68	1.44	8.32	0.0	0.0	0.0	0.0	45.82	44.27	156	59.67	90.87	0.08	0.83	0.0	0.0	0.0	0.0	0.0	2.90	5.61																			
157	1.56	7.34	7.15	0.0	0.0	0.0	0.0	48.71	37.00	157	39.64	91.82	0.10	0.43	0.0	0.0	0.0	0.0	0.0	2.90	5.61																			
158	4.79	0.59	28.53	0.0	0.0	0.0	0.0	47.34	22.98	158	64.71	80.03	0.03	0.43	0.0	0.0	0.0	0.0	0.0	7.46	7.46																			
159	4.76	0.56	42.38	0.0	0.0	0.0	0.0	37.57	15.95	159	57.91	78.15	0.11	0.47	0.0	0.0	0.0	0.0	0.0	7.51	7.63																			
160	1.79	0.09	0.0	0.0	0.0	0.0	0.0	43.60	56.95	160	47.23	88.04	0.01	0.0	0.0	0.0	0.0	0.0	0.0	2.40	6.17																			
161	2.55	1.20	22.22	0.0	0.0	0.0	0.0	40.11	36.20	161	59.20	88.04	0.11	1.95	0.0	0.0	0.0	0.0	0.0	3.53	6.17																			
162	0.51	2.80	4.35	0.0	0.0	0.0	0.0	35.23	80.62	162	17.60	95.86	0.03	0.02	0.0	0.0	0.0	0.0	0.0	1.49	2.00																			
163	0.54	1.05	3.94	0.0	0.0	0.0	0.0	50.88	44.52	163	18.43	95.86	0.03	0.11	0.0	0.0	0.0	0.0	0.0	0.86	2.58																			
164	2.44	1.06	5.82	0.0	0.0	0.0	0.0	41.41	51.90	164	44.24	92.11	0.06	0.30	0.0	0.0	0.0	0.0	0.0	2.16	5.39																			

TABLE A-2 (Continued)

MUN. CONC. FCNTR	MUN. CONC. FCNTR	HCOH	HBOH	EBOH	MP(1)	PAC(2)	ACAC(3)	CO	CO2	MUN. CONC. FCNTR	MUN. CONC. FCNTR	HCOH	HBOH	EBOH	MP(1)	PAC(2)	ACAC(3)	CO	CO2	YIELD AS PERCENT OF REACTED METHANE		YIELD AS PERCENT OF REACTED OXYGEN	
																				CO	CO2	CO	CO2
165	1.52	1.08	16.82	0.90	0.0	0.0	0.0	58.62	26.59	165	50.52	95.89	0.04	0.55	0.01	0.0	0.0	0.0	1.78	1.72			
166	2.47	2.08	1.80	0.0	0.0	0.0	0.0	55.76	40.76	166	56.68	97.18	0.04	0.03	0.0	0.0	0.0	0.0	0.0	1.12	1.03		
167	1.44	1.11	5.58	0.0	0.0	0.0	0.0	60.00	33.11	167	48.78	96.79	0.03	0.13	0.0	0.0	0.0	0.0	0.0	1.44	1.60		
168	1.47	0.49	3.83	0.0	0.0	0.0	0.0	50.11	45.17	168	56.00	97.02	0.02	0.04	0.0	0.0	0.0	0.0	0.0	1.03	1.86		
169	4.10	0.66	16.31	0.0	0.0	0.0	0.0	46.87	36.15	169	59.22	91.88	0.04	0.97	0.0	0.0	0.0	0.0	0.0	2.79	4.31		
170	6.60	5.97	2.46	0.0	0.0	0.0	0.0	58.76	34.88	170	34.11	98.42	0.19	0.08	0.0	0.0	0.0	0.0	0.0	1.64	2.27		
172	4.67	0.53	47.89	0.0	0.0	0.0	0.0	44.33	27.85	172	54.11	92.40	0.02	1.01	0.0	0.0	0.0	0.0	0.0	1.64	2.04		
173	1.23	1.02	12.88	0.0	0.0	0.0	0.0	56.19	30.11	173	39.41	97.73	0.02	0.22	0.0	0.0	0.0	0.0	0.98	1.05			
174	2.55	0.33	45.58	0.0	0.0	0.0	0.0	33.91	29.81	174	54.31	89.41	0.04	6.01	0.0	0.0	0.0	0.0	4.48	5.23			
175	4.56	0.83	31.95	0.0	0.0	0.0	0.0	59.55	29.85	175	59.55	89.49	0.07	0.56	0.0	0.0	0.0	0.0	2.65	4.88			
176	1.36	1.63	14.38	0.0	0.0	0.0	0.0	48.97	25.02	176	35.55	94.74	0.06	0.56	0.0	0.0	0.0	0.0	1.91	2.71			
177	4.77	1.06	33.16	0.0	0.0	0.0	0.0	39.97	25.62	177	58.01	94.01	0.12	3.70	0.0	0.0	0.0	0.0	4.46	5.71			
178	1.16	1.26	9.83	0.0	0.0	0.0	0.0	65.87	23.86	178	28.71	91.97	0.08	0.58	0.0	0.0	0.0	0.0	1.91	2.71			
179	0.33	1.10	9.83	0.0	0.0	0.0	0.0	28.00	21.42	179	28.50	91.04	0.02	0.21	0.0	0.0	0.0	0.0	1.08	1.66			
180	3.44	0.57	49.70	0.25	0.0	0.0	0.0	44.26	25.22	180	62.51	78.85	0.10	5.02	0.0	0.0	0.0	0.0	7.48	8.51			
181	4.55	0.80	42.45	0.0	0.0	0.0	0.0	29.35	27.05	181	62.52	81.65	0.12	6.14	0.0	0.0	0.0	0.0	4.27	3.09			
182	0.56	1.36	15.45	0.0	0.0	0.0	0.0	50.66	37.54	182	49.29	98.95	0.05	0.59	0.0	0.0	0.0	0.0	1.93	2.82			
183	4.41	1.76	18.20	0.0	0.0	0.0	0.0	35.55	38.06	183	16.13	87.07	0.09	2.07	0.0	0.0	0.0	0.0	3.48	6.29			
184	2.29	0.95	31.40	0.0	0.0	0.0	0.0	43.32	47.93	184	65.10	92.86	0.03	0.22	0.0	0.0	0.0	0.0	1.71	1.18			
185	1.63	1.00	13.75	0.0	0.0	0.0	0.0	30.33	25.03	185	61.65	89.50	0.07	1.02	0.0	0.0	0.0	0.0	3.48	6.29			
186	4.53	0.81	37.68	0.0	0.0	0.0	0.0	54.57	37.82	186	61.10	89.50	0.07	1.02	0.0	0.0	0.0	0.0	4.43	6.10			
187	1.53	1.56	3.88	0.0	0.0	0.0	0.0	52.07	27.82	187	29.49	92.68	0.10	4.81	0.0	0.0	0.0	0.0	2.91	3.99			
188	4.94	1.40	13.46	0.0	0.0	0.0	0.0	21.32	26.18	188	42.76	96.40	0.04	0.30	0.0	0.0	0.0	0.0	1.41	1.79			
190	1.54	0.36	32.17	0.0	0.0	0.0	0.0	41.32	26.18	190	42.76	89.66	0.03	4.27	0.0	0.0	0.0	0.0	1.75	4.29			
191	4.64	0.57	38.72	0.17	0.0	0.0	0.0	26.75	26.75	191	54.76	10.04	0.06	4.27	0.0	0.0	0.0	0.0	1.75	4.29			
194	1.53	0.69	36.29	0.0	0.0	0.0	0.0	23.21	39.81	194	47.83	91.98	0.04	2.08	0.0	0.0	0.0	0.0	3.72	5.90			
195	2.52	0.33	41.62	0.14	0.0	0.0	0.0	30.43	28.48	195	65.28	82.15	0.05	5.65	0.0	0.0	0.0	0.0	4.23	4.56			
195	4.78	0.62	37.01	0.14	0.0	0.0	0.0	43.60	18.63	195	59.26	85.32	0.08	4.58	0.0	0.0	0.0	0.0	7.92	7.92			
196	1.15	1.57	21.14	0.0	0.0	0.0	0.0	38.49	42.80	196	38.26	88.54	0.02	0.22	0.0	0.0	0.0	0.0	4.35	4.61			
197	7.74	0.50	39.18	2.40	0.0	0.0	0.0	35.18	22.73	197	57.41	88.06	0.07	5.14	0.0	0.0	0.0	0.0	4.61	5.96			
198	1.79	0.92	16.32	0.0	0.0	0.0	0.0	28.40	34.34	198	58.19	92.50	0.05	2.03	0.0	0.0	0.0	0.0	1.59	2.82			
199	2.42	0.15	18.42	0.0	0.0	0.0	0.0	25.80	59.64	199	46.56	92.66	0.01	0.66	0.0	0.0	0.0	0.0	1.77	2.97			
201	1.18	0.93	9.10	0.0	0.0	0.0	0.0	40.80	59.16	201	48.08	96.01	0.02	0.43	0.0	0.0	0.0	0.0	0.77	2.97			
204	0.56	0.49	0.0	0.0	0.0	0.0	0.0	31.26	57.28	204	28.17	97.26	0.01	0.0	0.0	0.0	0.0	0.0	0.77	2.02			
204	0.56	0.75	7.60	0.0	0.0	0.0	0.0	38.17	56.41	204	28.17	98.47	0.01	0.08	0.0	0.0	0.0	0.0	0.77	2.02			
206	1.52	0.08	9.48	0.0	0.0	0.0	0.0	28.92	89.92	206	44.41	98.11	0.0	0.05	0.0	0.0	0.0	0.0	0.18	0.65			
207	0.41	1.23	0.0	0.0	0.0	0.0	0.0	28.17	89.92	207	44.41	98.22	0.0	0.0	0.0	0.0	0.0	0.0	0.18	0.65			
208	1.64	1.22	0.0	0.0	0.0	0.0	0.0	28.17	89.92	208	44.41	98.62	0.0	0.0	0.0	0.0	0.0	0.0	0.0	0.38	0.38		
209	1.40	0.0	0.0	0.0	0.0	0.0	0.0	28.17	89.92	209	44.41	99.73	0.0	0.0	0.0	0.0	0.0	0.0	0.0	0.0	1.27		
209	1.40	0.0	0.0	0.0	0.0	0.0	0.0	28.17	89.92	209	44.41	99.99	0.0	0.0	0.0	0.0	0.0	0.0	0.0	0.0	1.00		

TABLE A-2 (Continued)

RUN NO.	YIELD AS PERCENT OF REACTED METHANE										YIELD AS PERCENT OF REACTED OXYGEN									
	CH ₄ CONV. PERCENT	HCOH	MEOH	ETOH	HF(1)	FA(2)	ACAC(3)	CO	CO ₂	H ₂ O	HCOH	MEOH	ETOH	HF(1)	FA(2)	ACAC(3)	CO	CO ₂		
210	0.39	0.0	0.0	0.0	0.0	0.0	0.0	0.0	99.99	210	20.05	99.39	0.0	0.0	0.0	0.0	0.0	0.61		
211	0.10	0.0	0.0	0.0	0.0	0.0	0.0	0.0	99.99	211	11.21	99.77	0.0	0.0	0.0	0.0	0.0	0.23		
212	0.26	0.0	0.0	0.0	0.0	0.0	0.0	0.0	99.99	212	22.60	99.58	0.0	0.0	0.0	0.0	0.0	0.42		
213	0.74	0.0	0.0	0.0	0.0	0.0	0.0	0.0	99.99	213	31.44	99.14	0.0	0.0	0.0	0.0	0.0	0.86		
214	1.03	0.0	0.0	0.0	0.0	0.0	0.0	0.0	99.99	214	48.87	98.86	0.0	0.0	0.0	0.0	0.0	1.14		
215	2.03	0.0	0.0	0.0	0.0	0.0	0.0	0.0	99.99	215	60.25	98.27	0.0	0.0	0.0	0.0	0.0	1.73		
216	0.53	0.0	0.0	0.0	0.0	0.0	0.0	0.0	99.99	216	38.71	98.95	0.0	0.0	0.0	0.0	0.0	1.05		
217	1.20	0.0	0.0	0.0	0.0	0.0	0.0	0.0	99.99	217	55.71	98.52	0.01	0.0	0.0	0.0	0.0	1.47		
218	1.54	0.0	0.0	0.0	0.0	0.0	0.0	0.0	98.59	218	54.67	98.52	0.01	0.0	0.0	0.0	0.0	1.47		
219	0.0	0.0	0.0	0.0	0.0	0.0	0.0	0.0	99.99	219	14.85	99.09	0.0	0.0	0.0	0.0	0.0	0.91		
220	0.17	0.0	0.0	0.0	0.0	0.0	0.0	0.0	99.99	220	28.16	98.11	0.0	0.0	0.0	0.0	0.0	1.89		
221	2.45	1.14	3.01	0.67	0.0	0.0	0.0	0.0	62.11	221	69.00	92.54	0.05	0.0	0.02	0.0	0.0	5.73		
222	1.54	0.19	12.19	0.06	0.0	0.0	0.0	0.0	87.56	222	59.52	94.69	0.01	0.35	0.0	0.0	0.0	4.96		
223	9.36	0.0	0.0	0.0	0.0	0.0	0.0	0.0	99.99	223	45.44	98.67	0.0	0.0	0.0	0.0	0.0	4.33		
224	1.54	0.46	15.80	0.10	0.0	0.0	0.0	0.0	47.11	224	53.57	92.82	0.01	0.77	0.0	0.0	0.0	4.60		
225	1.55	0.22	0.18	0.07	0.0	0.0	0.0	0.0	99.53	225	37.64	92.82	0.0	0.0	0.0	0.0	0.0	1.19		
227	1.43	0.62	32.43	0.13	0.0	0.0	0.0	0.0	45.42	227	60.57	98.60	0.0	0.75	0.0	0.0	0.0	2.50		
229	4.22	0.61	22.14	0.13	0.0	0.0	0.0	0.0	24.89	229	40.57	91.24	0.04	2.64	0.01	0.0	0.0	5.47		
234	2.62	1.38	19.03	0.68	0.0	0.0	0.0	0.0	42.09	234	48.30	91.24	0.09	1.25	0.02	0.0	0.0	5.94		
235	0.14	0.91	0.0	0.0	0.0	0.0	0.0	0.0	42.05	235	44.27	98.13	0.0	0.0	0.0	0.0	0.0	3.02		
236	1.48	1.06	15.66	0.05	0.0	0.0	0.0	0.0	41.16	236	42.43	92.79	0.05	0.80	0.0	0.0	0.0	4.28		
237	1.70	0.61	6.25	0.0	0.0	0.0	0.0	0.0	46.74	237	60.91	91.21	0.04	0.38	0.0	0.0	0.0	2.81		
238	1.73	0.50	16.07	0.0	0.0	0.0	0.0	0.0	48.38	238	40.46	97.40	0.01	0.63	0.0	0.0	0.0	5.57		
239	2.76	0.26	39.86	0.14	0.0	0.0	0.0	0.0	24.66	239	68.50	84.33	0.03	4.63	0.01	0.0	0.0	2.86		
240	4.16	0.28	45.71	0.09	0.0	0.0	0.0	0.0	34.69	240	53.49	89.45	0.02	3.55	0.0	0.0	0.0	8.14		
241	0.63	1.61	45.31	0.12	0.0	0.0	0.0	0.0	17.97	241	39.65	96.52	0.04	1.19	0.0	0.0	0.0	5.59		
242	0.45	1.23	11.57	0.0	0.0	0.0	0.0	0.0	20.37	242	29.77	96.47	0.03	6.23	0.0	0.0	0.0	1.71		
243	3.14	0.15	38.35	0.13	0.0	0.0	0.0	0.0	35.40	243	69.42	79.56	0.02	2.25	0.01	0.0	0.0	2.32		
244	3.67	0.25	16.40	0.14	0.0	0.0	0.0	0.0	25.97	244	65.35	78.81	0.04	3.25	0.01	0.0	0.0	8.90		
247	4.50	0.20	42.46	0.20	0.0	0.0	0.0	0.0	70.40	247	70.40	68.96	0.06	11.71	0.03	0.0	0.0	10.77		
248	4.54	0.25	26.62	0.07	0.0	0.0	0.0	0.0	43.64	248	43.64	90.13	0.02	1.91	0.0	0.0	0.0	7.12		
249	1.61	0.42	21.47	0.66	0.0	0.0	0.0	0.0	58.15	249	58.15	92.26	0.02	1.83	0.0	0.0	0.0	6.99		
250	0.23	1.29	20.54	0.0	0.0	0.0	0.0	0.0	28.22	250	28.22	97.18	0.03	0.44	0.0	0.0	0.0	3.92		
251	0.17	0.78	10.23	0.0	0.0	0.0	0.0	0.0	46.71	251	34.92	96.21	0.02	0.27	0.0	0.0	0.0	1.25		

NOTES
 (1) HF - HYDROFORMATE
 (2) FA - FORMALIC ACID
 (3) ACAC - ACETIC ACID

NOTES
 (1) HF - HYDROFORMATE
 (2) FA - FORMALIC ACID
 (3) ACAC - ACETIC ACID

APPENDIX B

RATES OF CHAIN REACTIONS AND ENERGY CONSIDERATIONS

Since radicals are entities in highly reactive states, they react with other species very rapidly. The average lifetime of radicals taking part in chain reactions rarely exceed one second (66), indicating the ease with which a free radical will react with another material.

This section is designed to review the expressions for reaction rates and the driving forces behind such reactions.

A given reaction,



has a rate given by

$$\text{Rate} = \frac{-1}{a} \frac{d[A]}{dt} = \frac{1}{b} \frac{d[B]}{dt} = kA^n \quad (\text{B-1})$$

where concentration is signified by brackets, k is the reaction rate constant, n is the order of the reaction, t is time, and a and b are the stoichiometric coefficients. In the majority of chain mechanisms, the

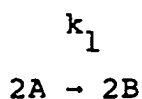
stoichiometric coefficient of compound A is rarely greater than unity and cross-species reactions usually occur. For example



with the rate (with respect to A, for instance) given by:

$$\text{Rate} = \frac{-d[A]}{dt} = k[A]^r[B \cdot]^s \quad (\text{B-2})$$

The coefficients r and s are not necessarily related to the stoichiometric coefficients (which in the case of individual steps in a chain reaction are usually unity). For brevity, however, elementary reactions are often represented by an equation showing both the molecularity (number of molecules or radicals involved) and the rate constant, k; e.g.:



In this manner, the molecularity and the order of reaction are shown simultaneously and the rate is understood to be, where r_A is the rate of accumulation of A:

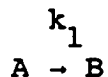
$$\text{Rate} = \frac{-1}{2} r_A = k_1[A]^2$$

and not as

$$\text{Rate} = -r_A = k_1[A]$$

as would be the case if the simplified stoichiometric

coefficients only were shown as:



It is seen from equation B-1 that the rate of disappearance or formation of any species is not necessarily coincident with the definition of the rate of the overall reaction. For instance, consider the reaction



The individual rates measured in terms of components B, D, and P are, respectively:

$$\begin{aligned} -r_B &= k_1' [B] [D]^2 \\ -r_D &= k_1'' [B] [D]^2 \\ r_P &= k_1''' [B] [D]^2 \end{aligned} \quad (\text{B-3})$$

The overall rate, as defined in B-1, is

$$\begin{aligned} \text{Rate} &= \frac{-1}{1} \frac{d[B]}{dt} = -r_B \\ \text{Rate} &= \frac{-1}{2} \frac{d[D]}{dt} = \frac{-1}{2} r_D \\ \text{Rate} &= \frac{1}{3} \frac{d[P]}{dt} = \frac{1}{3} r_P \end{aligned} \quad (\text{B-4})$$

Hence,

$$k_1' = \frac{1}{2} k_1'' = \frac{1}{3} k_1''' \quad (\text{B-5})$$

In chain reactions, termolecular reactions are rare and the avoidance of ambiguity in the failure to specify which component is being considered is usually automatic; however, if one species must be present in pairs of atoms, as in Reaction I, care must be taken in defining the overall rate.

Occasionally, a chain reaction of the form:



has been empirically represented in terms of initial reactants by a rate equation of the form:

$$\text{Rate} = k[A]^n[B]^m \quad (\text{B-6})$$

where n and m have no relationship with the stoichiometric coefficients. The powers to which concentration are raised are referred to as order of the reaction. Thus, the reaction is n th order with respect to A, m th order with respect to B and o th order ($o = m+n$) overall.

Other quantities have been shown to be applicable in place of the concentrations in B-1. With perfect gases partial pressures are often used, in liquid solutions, activities are frequently employed, and at extremes of temperatures and pressure, fugacities can be used. It must be noticed that, although the rate constants are related, they are not necessarily identical in the several forms of the rate equation which can be used to describe a given reaction.

Shtern (66) introduced a convenient shorthand for describing the rates of individual steps in a chain reaction. He accepted the convention of usage of concentration as the driving force variable. He also combined the velocity constant, k , with the concentration of the stable substance taking part in each step. In the case where only free radicals take part in the reaction, the value of the velocity constant coincides with his "kinetic coefficient." For instance with the chain,



he defined kinetic coefficients, a_i , as

$$a_1 = k_1 [A]$$

$$a_2 = k_2$$

The nomenclature comes into use best when describing mathematically the overall appearance of a species. For example:

$$\frac{d[D \cdot]}{dt} = + a_1 [B \cdot] - a_2 [B \cdot][D \cdot] \quad (\text{B-7})$$

In this manner, combined rates can be depicted for chain sequences by only writing the radical species.

By writing such an expression for each of the radicals or intermediates in a process, a set of non-linear

differential equations results. The solution of such a system of equations may or may not be readily obtained, but many features of the overall mechanism can be determined, such as chain length, rate of initiation and overall rate.

In the Russian literature, especially, use is made of the so-called quasi-stationary theory in which the lifetimes of all radicals are assumed to be extremely short, and the rates of formation and depletion of each radical are equal. Then the derivative in the equations of the form (B-7) are all set equal to zero and the set of equations reduces to a set of linear algebraic equations. Standard successive substitutions or matrix methods can then be used for solution. In treating chains with degenerate branching, the lifetime of the intermediate responsible for branching is not so short and the system of equations, by substitution, reduces to a single differential equation describing the chronological history of the intermediate.

In many cases this single equation cannot be solved. However, with intermediates responsible for degenerate branching, concentration goes through a maximum at the maximum rate. The single remaining derivative describing the rate of appearance of the intermediate can then be set equal to zero, resulting in an equation solvable for the maximum concentration of the intermediate.

The amount of energy for a molecule to possess in order to react is called the activation energy, E . Figure B-1

shows the activation energy in relationship to the heat of reaction, ΔH_r , for a given reaction. Thus

$$\Delta H_r = E - E' \quad (\text{B-8})$$

where E is the activation energy of the forward reaction and E' the activation energy of the reverse reaction. From either direction, the reactants must be driven to an energy level which will enable the reaction to proceed toward formation of products. Failure to achieve this intermediate level of energy forces the reactants to remain unchanged. For radical-radical reactions, because the reacting entities already possess

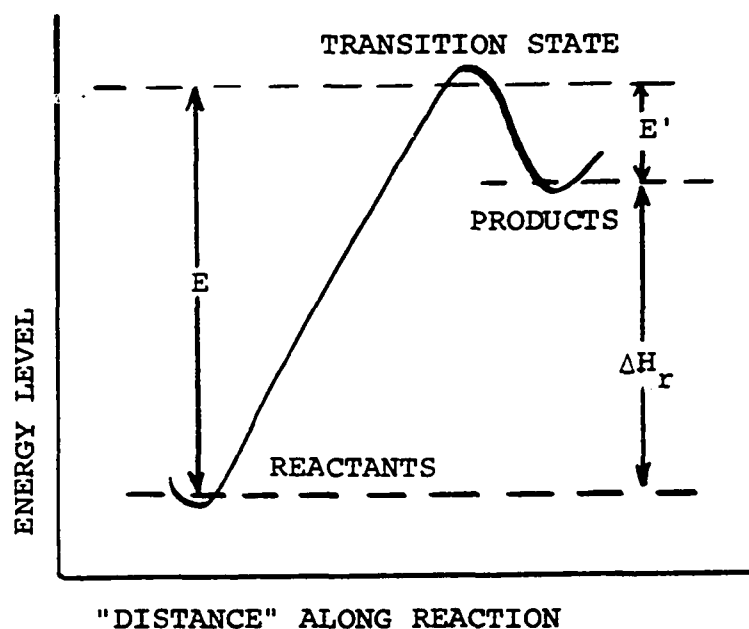


Figure B-1. Activation Energy and Heat of Reaction.

considerable excess energy, very small activation energies are required for completion of reaction.

Several excellent texts in kinetics describe the derivation of equations which express the reaction rate constant as a function of temperature. Derivations based on the activated complex or transition state (the identity of the reactants at the high level of energy) and collision theories lead to expressions of the form:

$$k = k_0 T^m e^{-E/RT} \quad (\text{B-9})$$

where T is absolute temperature, R is the gas constant, and m is a constant. The term k_0 is related to the frequency of collisions occurring between molecules.

The influence of the temperature dependent portion of the pre-exponential term is usually negligible in comparison to the temperature dependency of the exponential term. Considering T^m to be relatively constant, equation B-9 can be simplified to

$$k = Ae^{-E/RT} \quad (\text{B-10})$$

where A is a constant.

For most purposes the simple Arrhenius representation (B-10) adequately describes experimental data if the proper mechanism is selected. Referring to Equation B-10, the pre-exponential term, A , is found for many unimolecular reactions to be about 10^{13}sec^{-1} , and for radical reactions,

about 10^{-10}sec^{-1} . Activation energies are in the order of 60 to 100 kcal/mole for molecular reactions. For reactions between molecules and radicals, values of about 10 kcal/mole or less are common; for reactions involving only radicals, activation energies are nearly zero.

The low activation energies for radicals imply that reaction occurs at all collisions of radicals. However, the highly exothermic bond formation between radicals demands that, unless removal of this energy is caused to occur, free radicals can elastically collide without bond formation unless a third body is present.

The combination of two radicals produces a molecule which will be highly unstable unless the exothermic energy of bond formation is dissipated. For example, consider the combination of two radicals:



where AB^* denotes a molecule in a highly excited state.

Dissipation of energy through a third body can be written as



Using the quasi-stationary state theory described earlier, the rates of appearance of the excited molecule AB^* and the final product AB are given by

$$\frac{d[AB^*]}{dt} = k_1[A\cdot][B\cdot] - k_2[AB^*] - k_3[AB^*][M] \quad (\text{B-11})$$

$$\frac{d[AB]}{dt} = k_3 [AB^*]M \quad (B-12)$$

Because the system is assumed stationary (no accumulation of AB* results after sufficient initiation time has elapsed) the derivative in equation B-11 can be set equal to zero. Solving then for [AB*] and substituting in equation B-12 leads to

$$\frac{d[AB]}{dt} = \frac{k_1 k_3 [A\cdot][B\cdot][M]}{k_2 + k_3[M]} \quad (B-13)$$

At low concentrations of M, the rate of reaction V is much greater than the rate of reaction VI. Thus $k_2 \gg k_3[M]$ and the rate of formation of AB is third order:

$$\frac{d[AB]}{dt} = \frac{k_1 k_3}{k_2} [A\cdot][B\cdot][M] \quad (B-14)$$

At high concentration of M, reaction VI is faster than reaction V ($k_3[M] \gg k_2$) and the rate reduces to:

$$\frac{d[AB]}{dt} = k_1 [A\cdot][B\cdot] \quad (B-15)$$

Equation B-15 means that the rate becomes independent of the concentration of the third body at high concentration of the third body. The third body can be a wall, some type of reactor packing or a third chemical component which can accept the excess bond energy.

APPENDIX C

DETERMINATION OF FACTORS FOR THE BENEDICT-WEBB-RUBIN EQUATION OF STATE

The Benedict-Webb-Rubin (BWR) equation of state is given as:

$$Z = PV/RT = 1 + (B_0 - A_0/RT - C_0/RT^3) (1/V) + (b-a/RT) (1/V^2) + (a \alpha/RT) (1/V^5) + (C/RT^3) [(1+\gamma V^{-2}) V^{-2}] e^{-\gamma V^{-2}} \quad (C-1)$$

where A_0 , B_0 , C_0 , a , b , c , α and γ are constants depending on the compound selected, Z is compressibility factor, P is pressure, V is volume, T is temperature and R is the gas constant. Various forms of the equation can also be used for calculating pure-component and mixture fugacity, enthalpy and entropy. Benedict, Webb and Rubin (8) showed these forms and listed constants for several compounds.

Recent data of Deffet and Ficks (14) showed that at pressures considerably higher than those used for determining the constants in Benedict's original work, the equation was accurate to only about 2 percent at 3000 atm. Similarly,

BWR constants for oxygen determined by Seshadri, Viswanath and Kuloor (65) did not accurately calculate oxygen compressibility at elevated pressures.

It was felt that, in both cases, the constants in general acceptance today were derived with strong bias toward the low pressure regime. With this in mind, the constants were re-evaluated, placing more emphasis on the high-pressure, dense-fluid regimes and minimizing the influence of the lower pressures. The methane data mentioned above were used to modify the existing constants. Similarly, original data of Amagat (4) for oxygen were used for modification of the oxygen constants.

A computer program was available at the University of Oklahoma which, by successive iteration, determined the eight constants. Modification of the constants was done by including only the high pressure data. As a first approximation, the published values for these constants were used. Table C-1 presents the published and new constants as determined in the present program.

The average deviation in calculation of compressibility for methane up to 3000 atm and 150°C was reduced to about 0.3 percent and the deviation for oxygen up to 3000 atm and 200°C was reduced from 13 to 2.5 percent. These values are recommended for use between 1000 and 3000 atm.

TABLE C-1

BWR CONSTANTS FOR METHANE AND OXYGEN
FOR USE AT ELEVATED PRESSURES

	Oxygen		Methane	
	Old	New	Old	New
A_0	0.950851963	0.950851963	1.85500	1.85500
B_0	$0.353285054 \times 10^{-7}$	$0.353285054 \times 10^{-7}$	0.042600	0.042600
C_0	3.26435918×10^4	3.26435918×10^4	0.02257×10^6	0.02257×10^6
a	0.162689940	0.0199761	0.0484	0.0563
b	$0.358834736 \times 10^{-2}$	0.248250×10^{-2}	0.00338004	0.00359708
c	1.2827341×10^4	1.28273741×10^4	0.002545×10^6	0.002545×10^6
α	-3.927058894	0.387408×10^{-4}	0.124359×10^{-3}	0.947228×10^{-4}
γ	0.0301	0.0301	0.6000×10^{-2}	0.00366053

APPENDIX D

METHOD OF REFERENCE CURVES FOR ORDER DETERMINATION

Assume a general rate equation of the form:

$$-\frac{dy}{dt} = k (y)^n \quad (D-1)$$

where y is mole fraction, t is time, k is the rate constant and n is the order with respect to mole fraction. Equation E-1 upon integration, over the time range t_i - t_f , where the subscripts, i and f , refer to initial and final values, gives

$$-y_f^{1-n} + y_i^{1-n} = k(1-n) (t_f - t_i) \quad (D-2)$$

The reaction rate constant, k , can be eliminated in a generalized form by taking the ratio of the time at some conversion point to the time needed to reach full conversion over the reference range of y .

At some time t , conversion results in a concentration, y ; dividing the corresponding equation by (D-2) gives:

$$\frac{y^{1-n} - y_i^{1-n}}{y_f^{1-n} - y_i^{1-n}} = \frac{t - t_i}{t_f - t_i} \quad (D-3)$$

The equation can be rearranged:

$$\frac{(y/y_i)^{1-n-1}}{(y_f/y_i)^{1-n-1}} = \frac{t - t_i}{t_f - t_i} \quad (\text{D-4})$$

The shape of a curve of y/y_i versus $t_f - t_i$ is determined by n . By picking a range of concentration-time data of a given test, thereby selecting y_i , y_f , t_i , and t_f , a calculated reference curve can be superimposed on the actual data. This superposition can be done by solving for t at several y values by:

$$t = (t_f - t_i) \frac{(y/y_i)^{1-n-1}}{(y_f/y_i)^{1-n-1}} \quad (\text{D-5})$$

Proper superposition will indicate the order of reaction over that range.

APPENDIX E

CHROMATOGRAPHIC CALIBRATION CURVES

On the following nine pages, chromatographic calibration curves are presented. The method of acquisition of data for these curves was presented in Chapter VI. The graphs represent the relationship between peak heights (or peak areas) and concentration. With gases, the concentrations are reported as molar ratio of each component to methane; with liquids, concentration is expressed as weight ratio of each component to water.

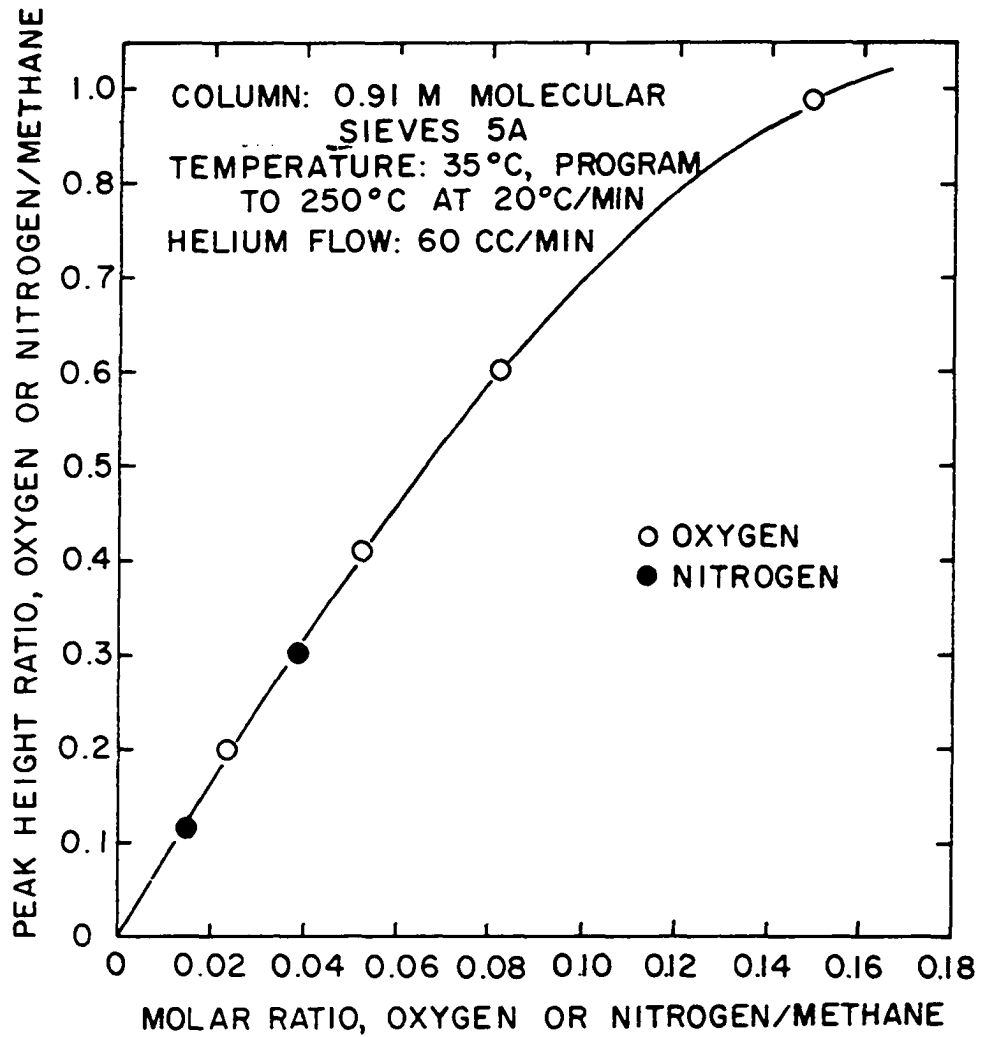


Figure E-1. Chromatographic Calibration Curve for Oxygen and Nitrogen.

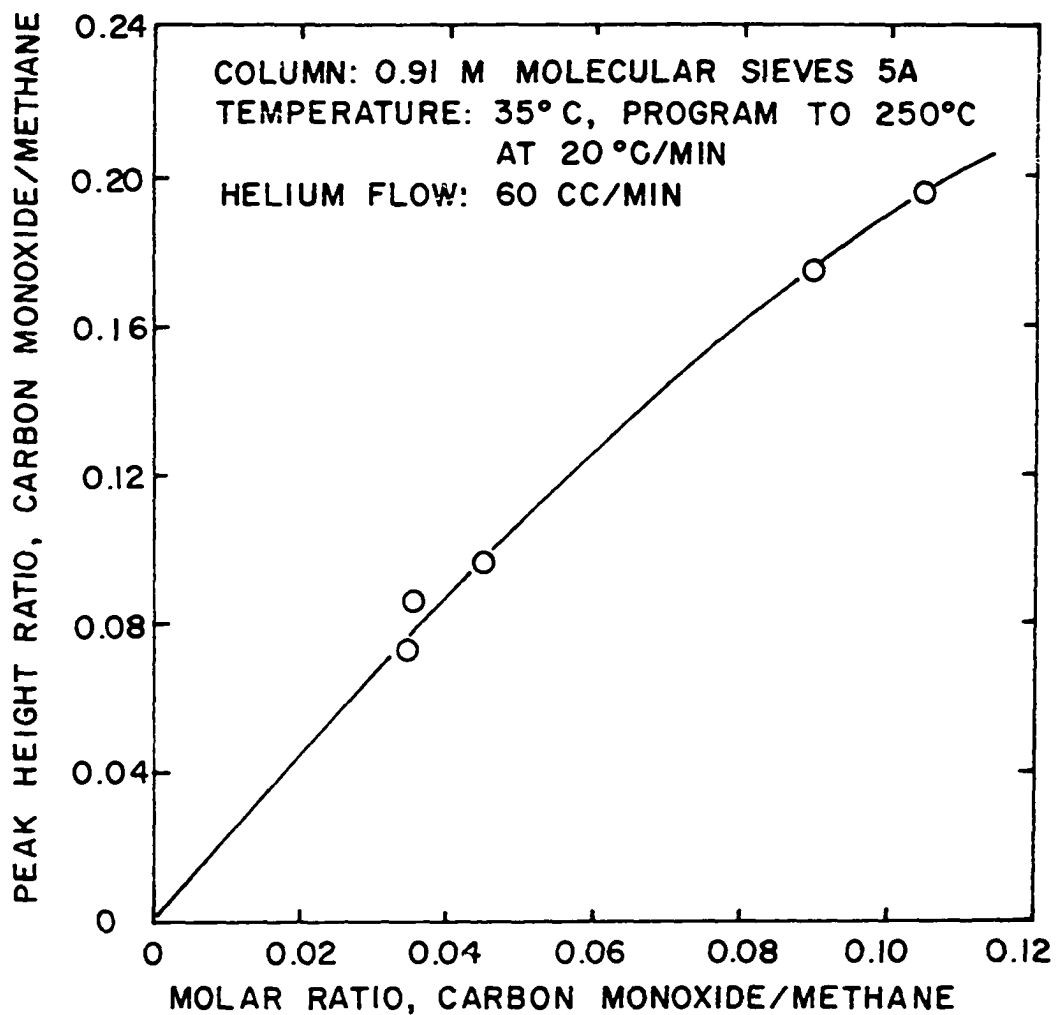


Figure E-2. Chromatographic Calibration Curve for Carbon Monoxide.

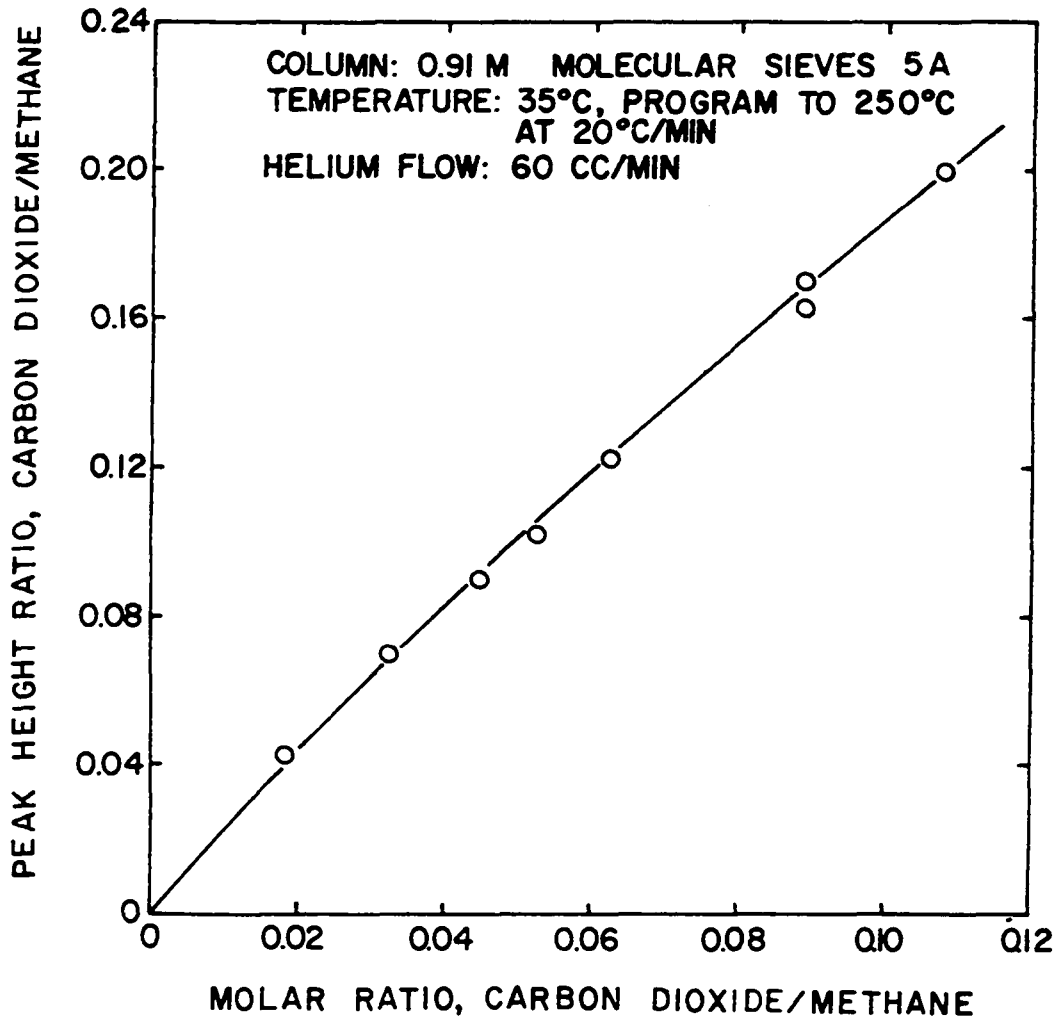


Figure E-3. Chromatographic Calibration Curve for Carbon Dioxide.

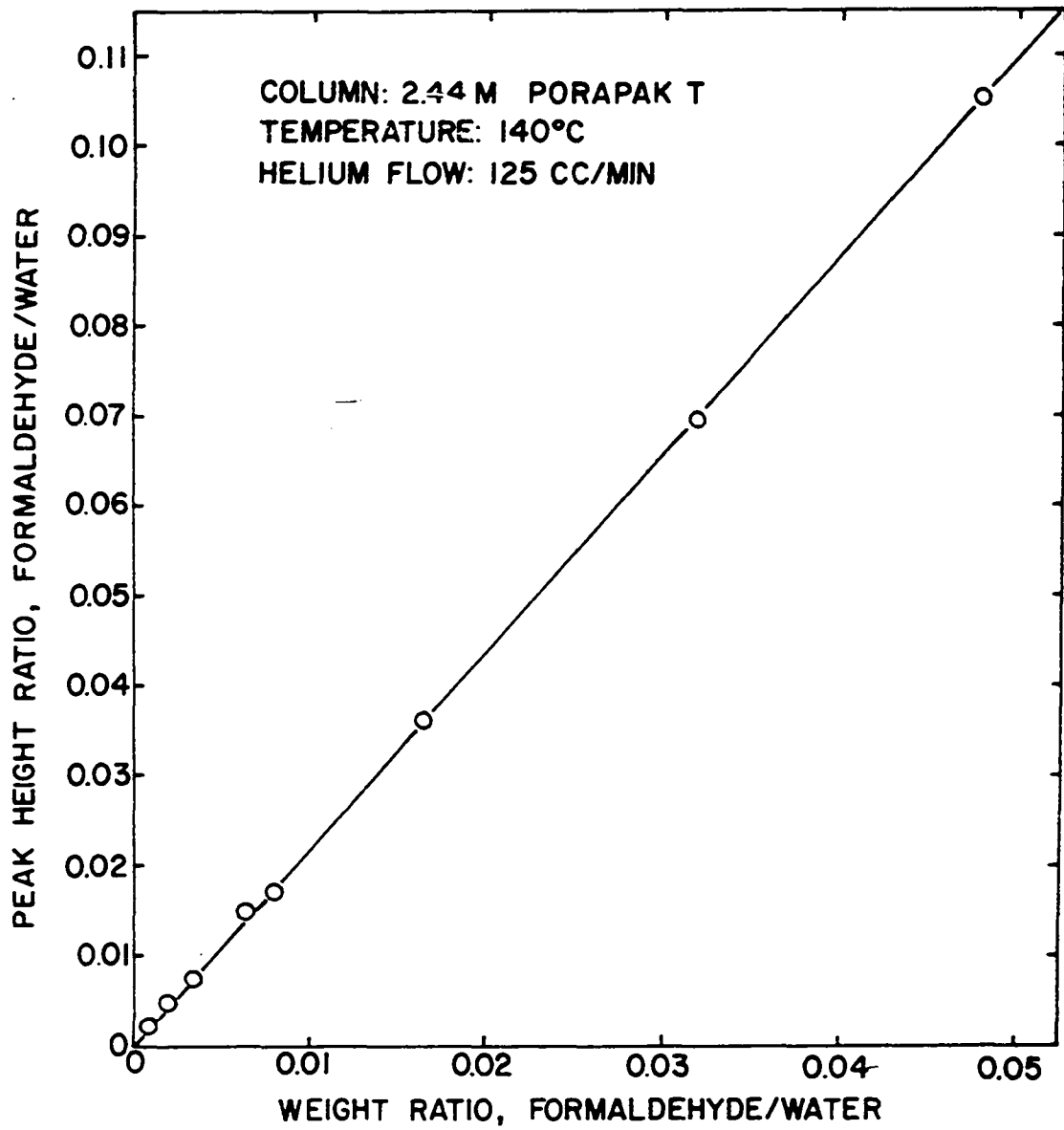


Figure E-4. Chromatographic Calibration Curve for Formaldehyde.

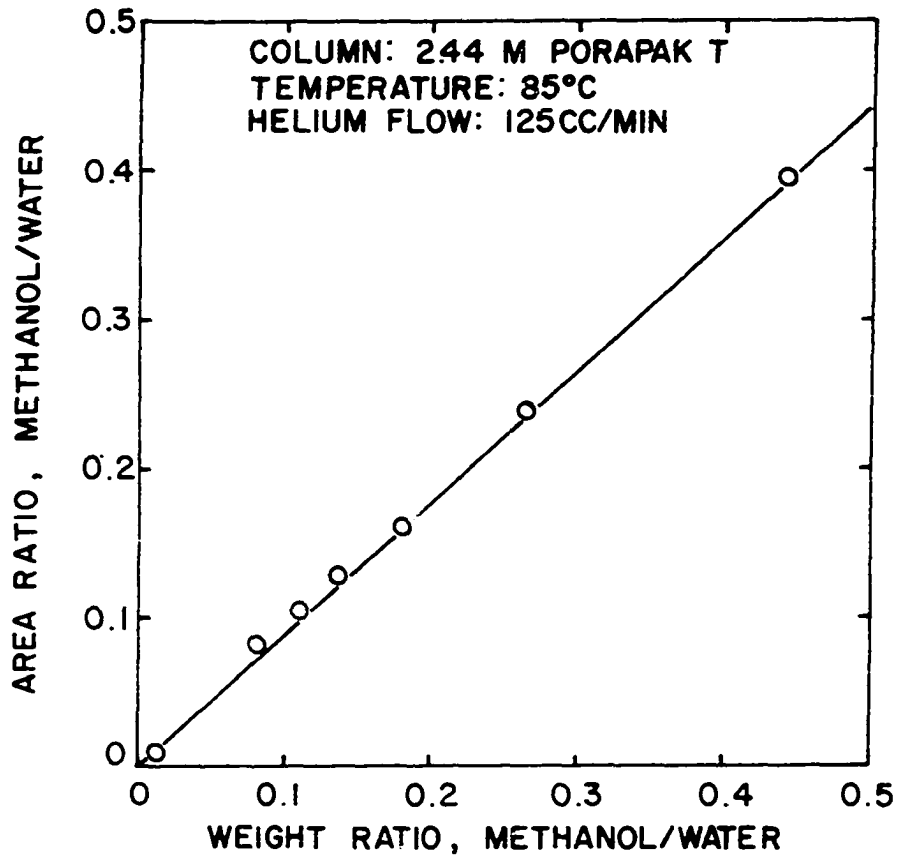


Figure E-5. Chromatographic Calibration Curve for Methanol.

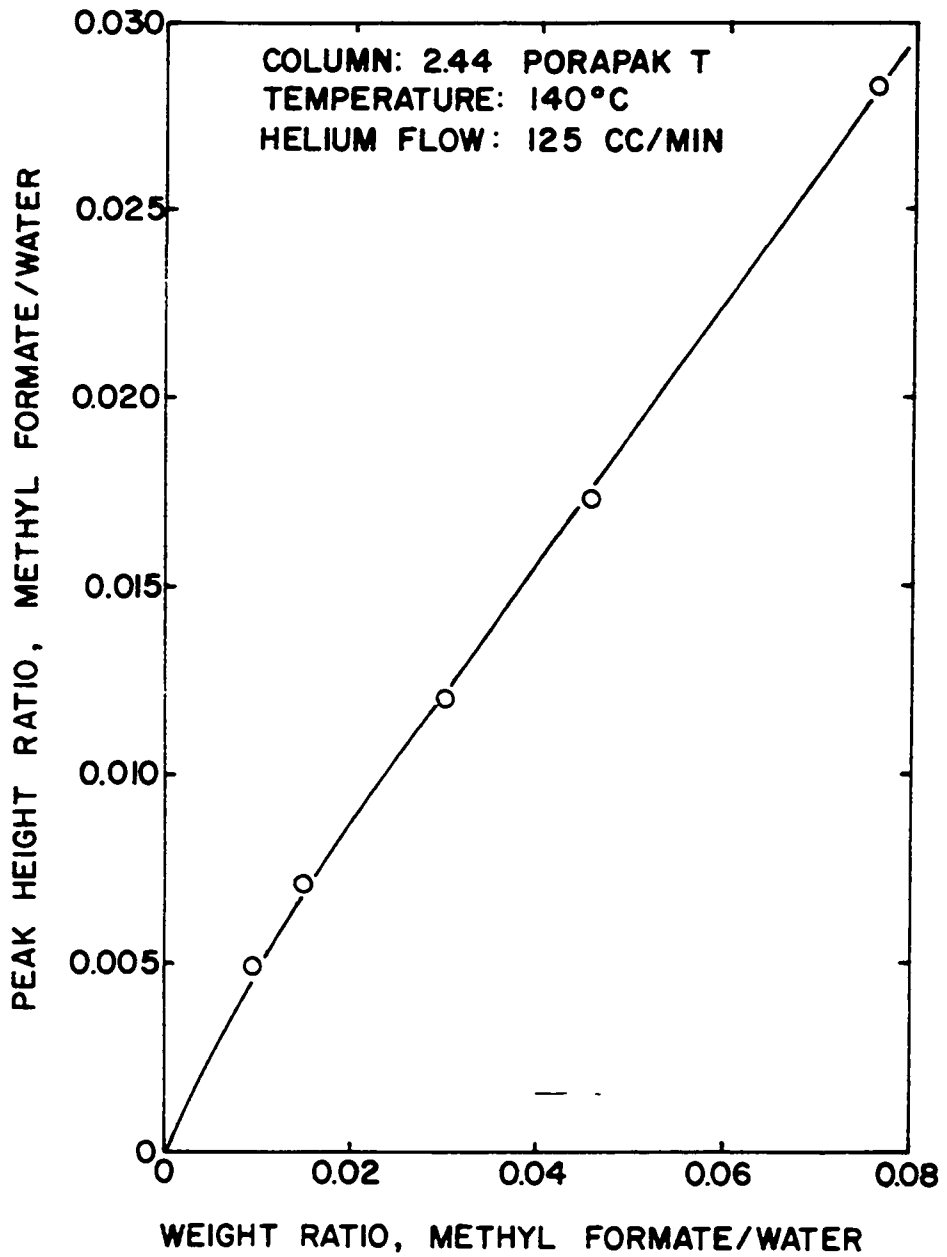


Figure E-6. Chromatographic Calibration Curve for Methyl Formate.

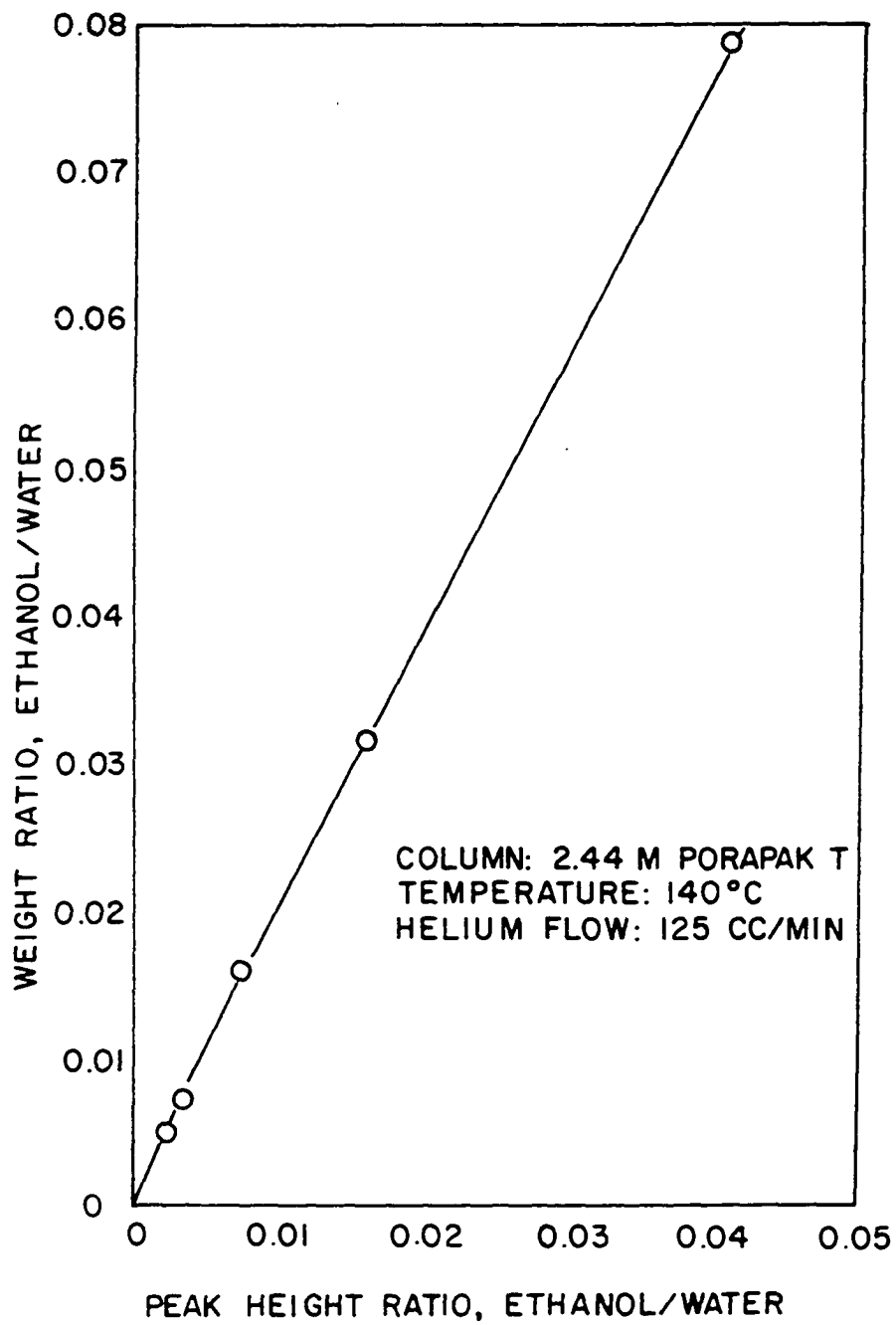


Figure E-7. Chromatographic Calibration Curve for Ethanol.

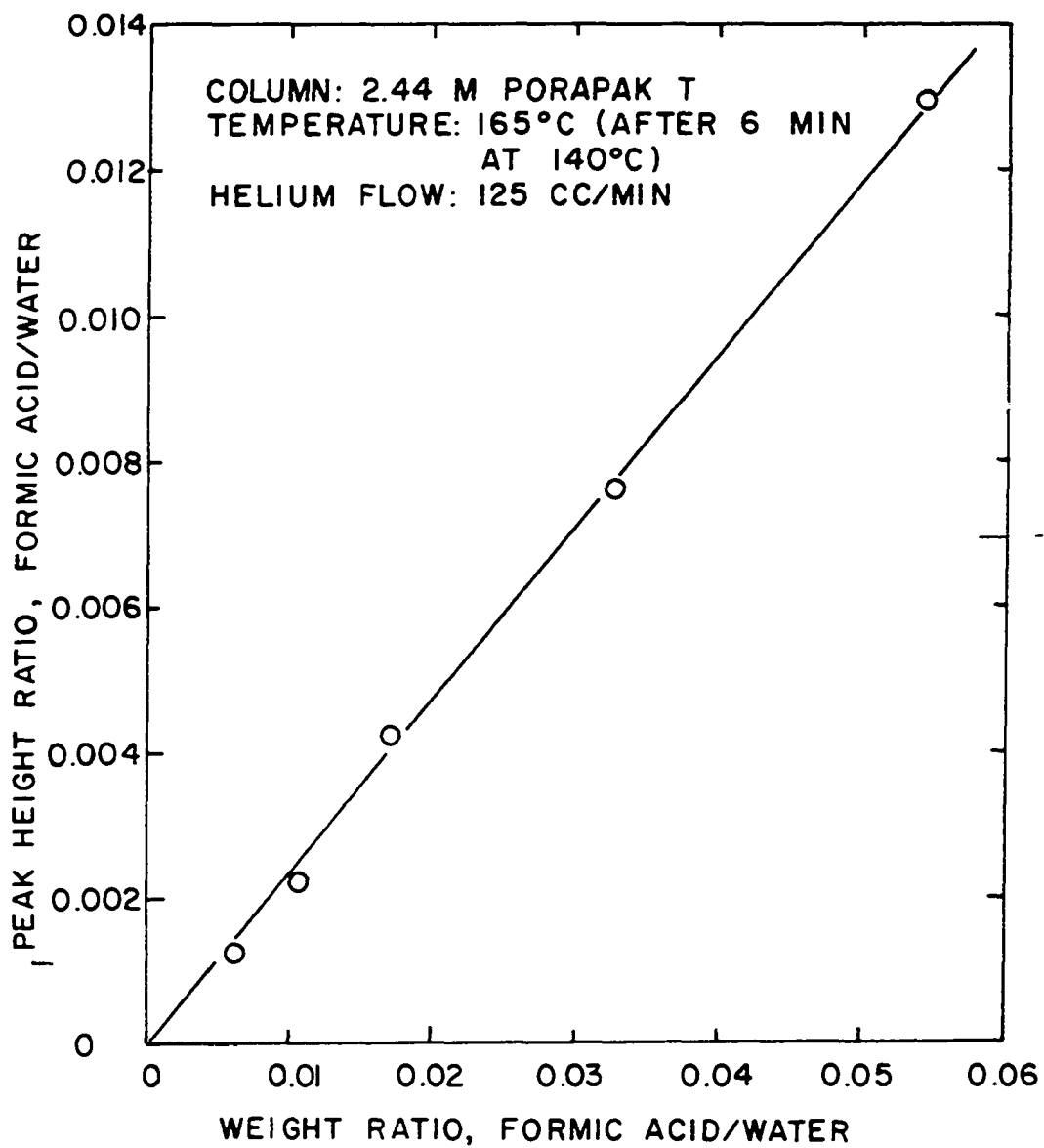


Figure E-8. Chromatographic Calibration Curve for Formic Acid.

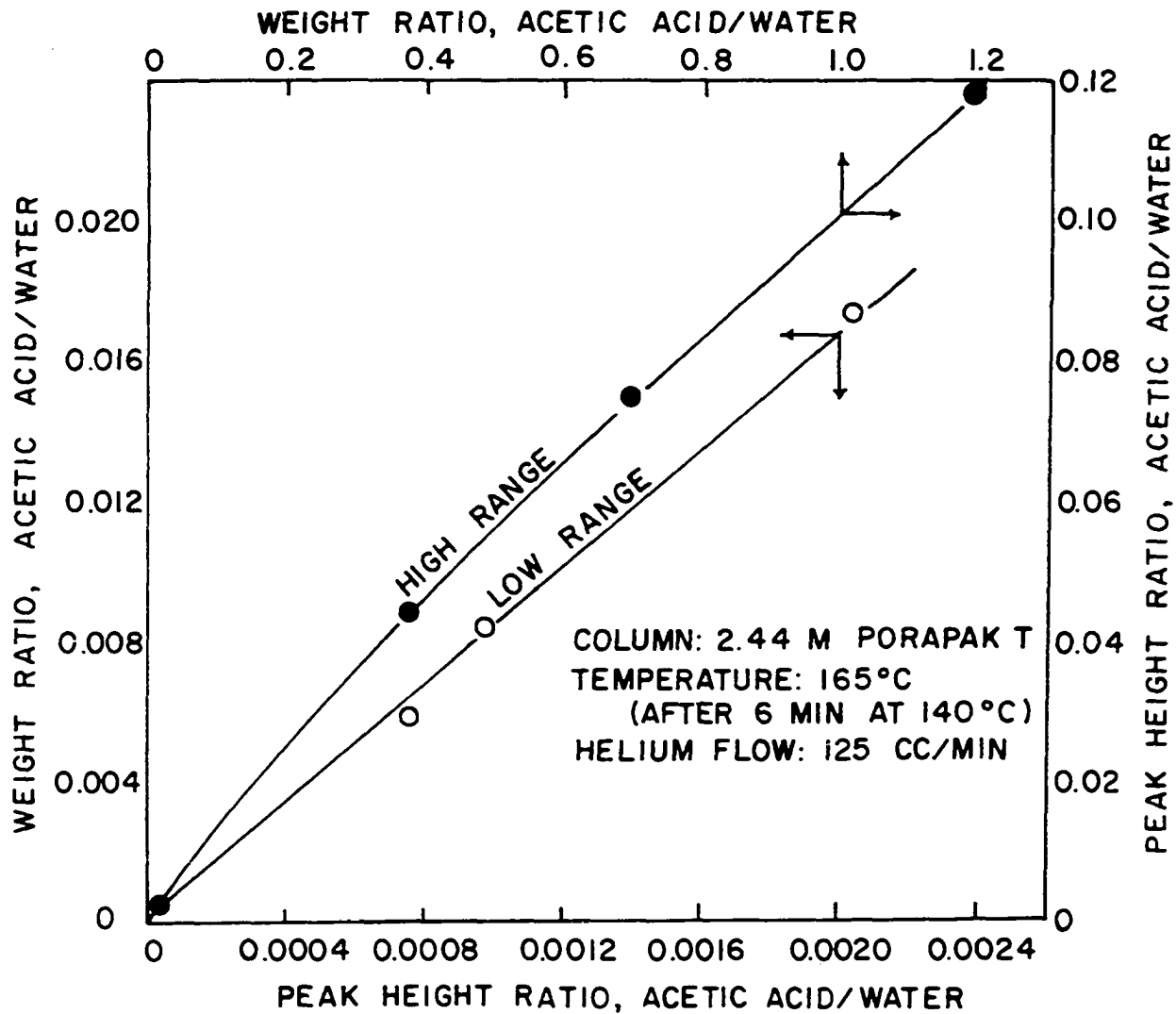


Figure E-9. Chromatographic Calibration Curve for Acetic Acid.